UNCLASSIFIED

AD NUMBER

AD804607

NEW LIMITATION CHANGE

TO

Approved for public release, distribution unlimited

FROM

Distribution authorized to U.S. Gov't. agencies only; Administrative/Operational Use; OCT 1966. Other requests shall be referred to Air Force Materials Lab., Wright-Patterson AFB, OH 45433.

AUTHORITY

AFML ltr, 7 Dec 1972

THIS PAGE IS UNCLASSIFIED

AFML-TR-65-245
Part II

804607

RESEARCH ON ABLATIVE PLASTIC CHARACTERIZATION IN SIMULATED MOTOR EXHAUST

C. S. Mayo
S. L. Ostrow
H. Blaes
J. Shaw
Aeronutronic Division of Philco-Ford Corporation

TECHNICAL REPORT AFML-TR-65-245, Part II

October 1966

Each transmittal of this document outside the agencies of the U. S. Government must have prior approval of the Plastics and Composites Branch, MANC, Nonmetallic Materials Division, Air Force Materials Laboratory, Wright-Patterson AFB, Ohio 45433.

Air Force Materials Laboratory
Research and Technology Division
Air Force Systems Command
Wright-Patterson Air Force Base, Ohio

NOTICES

When Government drawings, specifications, or other data are used for any purpose other than in connection with a definitely related Government procurement operation, the United States Government thereby incurs no responsibility nor any obligation whatsoever; and the fact that the Government may have formulated, furnished, or in any way supplied the said drawings, specifications, or other data, is not to be regarded by implication or otherwise as in any manner licensing the holder or any other person or corporation, or conveying any rights or permission to manufacture, use, or sell any patented invention that may in any way be related thereto.

DDC release to CFSTI not authorized.

Qualified requestors may obtain copies of this report from the Defense Documentation Center (DDC), (formerly ASTIA), Cameron Station, Bldg. 5, 5010 Duke Street, Alexandria 4, Virginia.

Dissemination outside the Department of Defense or to recipients other than Government defense contractors is prohibited.

Copies of this report should not be returned to the Research and Technology Division unless return is required by security considerations, contractual obligations, or notice on a specific document.

RESEARCH ON ABLATIVE PLASTIC CHARACTERIZATION IN SIMULATED MOTOR EXHAUST

C. S. Mayo
S. L. Ostrow
H. Blaes
J. Shaw

FOREWORD

This report was prepared by Aeronutronic, a division of the Philco Corporation, Newport Beach, California under USAF Contract No. AF 33(615)-1632. This contract was initiated under Project No. 7340 "Nonmetallic and Composite Materials", Task No. 734001 "Thermally Protective Plastics and Composites". The work was administered under the direction of the Nonmetallic Materials Division, AF Materials Laboratory, Research and Technology Division, with Mr. Paul F. Pirrung as project engineer.

All research nozzles were furnished by the Nonmetallic Materials Division, Air Force Materials Laboratory, Research and Technology Division. Most of the rocket nozzle inserts were fabricated by the Hughes Aircraft Company under Air Force contract. Further information on the fabrication of these nozzle inserts is in AFML TR 65-94 and AFML TR 66-75, dated April 1965 and April 1966 respectively. Both reports are titled, "New Ablative Plastics and Composites, Their Formulation and Processing."

This report covers work from 1 July 1965 to 1 September 1966.

Manuscript released by authors, 10 October 1966 for publication as an AFML Technical Report.

This technical report has been reviewed and is approved.

R. G. Spain

R. G. SPAIN, Acting Chief
Plastics and Composites Branch
Nonmetallic Materials Division
Air Force Materials Laboratory

ABSTRACT

New chemical compositions and physical constructions of ablative materials were exposed in a small scale, high temperature Aeronutronic solid propellant rocket motor simulator and a liquid propellant (nitrogen tetroxide - 50 percent hydrazine and 50 percent unsymmetrical dimethylhydrazine) combustion gas environment to determine the potential usefulness of these materials for hyperenvironmental conditions associated with current and future solid and liquid propellant motors.

Material erosion and thermal insulation characteristics of the research nozzles were evaluated by comparisons of chamber pressure versus time data, erosion and resin degradation rates, and visual photographic data.

This document is the second yearly summary technical report covering test series four and five, which included forty-nine (49) research nozzle specimens. Thirty (30) research nozzle specimens, comprising test series 4, were exposed to the exhaust environment of a simulated solid propellant having a flame temperature of 5800°F and being highly aluminized. Nineteen (19) nozzles, comprising test series 5, were exposed to the exhaust environment of a storable liquid propellant rocket motor that utilizes nitrogen tetroxide and the 50-50 hydrazine mixture.

Test results and specimen evaluations from test series 4 indicated that the Aeronutronic solid propellant simulator exhaust environment provided the specified exhaust environment with the required repeatable test screening characteristics to enable valid material evaluations.

Test results from test series 5 indicated that the specified nominal test conditions were met and enabled valid material evaluation.

Calculations determining the nozzle throat heat flux for both the liquid and solid propellant exhaust environments are presented for further comparison and evaluation.

CONTENTS

LIST OF ILLUSTRATIONS

LIST OF ILLUSTRATIONS (Continued)

LIST OF ILLUSTRATIONS (Continued)

LIST OF ILLUSTRATIONS (Continued)

LIST OF ILLUSTRATIONS (Continued)

LIST OF ILLUSTRATIONS (Continued)

LIST OF TABLES

LIST OF TABLES (Continued)

INTRODUCTION

A variety of high performance thermally protective materials are being generated on a continuing basis as a result of numerous research programs in this area. Many of these materials, because of their unique properties and characteristics, are intended for use in future solid propellant and liquid motor exhaust environments. Many of the new ablative composites or their components are sensitive to temperature, erosion, and chemical attack by certain rocket exhaust gases.

The object of this program is to determine the material erosion and thermal insulation characteristics of new ablative plastic and composite materials intended for use in current and future rocket nozzle environments. Research materials are exposed in an exhaust environment which will allow comparisons of behavior among different ablative materials and provide reliable information on rocket motor performance characteristics in the throat of a rocket nozzle. Test device capability includes simulation of the chemical composition of current and future solid and liquid propellant exhausts.

The work done during this second twelve month period of the program consisted of testing thirty (30) research nozzles in a solid propellant exhaust environment which had a flame temperature of 5800°F and which was highly aluminized; and testing nineteen (19) additional research nozzles in a liquid propellant motor exhaust environment. The liquid propellants were nitrogen tetroxide (NTO) and a mixture by volume of 50 percent hydrazine and 50 percent unsymmetrical dimethylhydrazine (50-50) at an oxidizer to fuel mixture ratio of 1.6 to 1.0. Nozzle specimens and test data were evaluated and presented in tabulated, graphical, and photographic forms to allow comparisons of behaviour by the Air Force Materials Laboratory.

SOLID PROPELLANT COMBUSTION GAS SIMULATION TESTS

GENERAL DISCUSSION

The solid propellant combustion gas simulation tests conducted in test series 4 were comprised of thirty ablative nozzle test specimens. Tables IA and IB presents the nozzle test specimen material description.

The solid propellant simulators located at the Aeronutronic Aerothermochemical (ATC) laboratory at the Newport Beach location were utilized for these tests. Figure 1 is an overall view of a portion of the ATC complex showing some of these test cells. Figure 2 is an overall view of the test cell control room. Figure 3 shows the rocket motor firing in a test cell.

Check run data calculations resulted in the solid propellant simulator average combustion efficiency being 95.68 percent. This was sufficient indication that simulation was being achieved.

The Aeronutronic Solid Propellant Combustion Gas Simulator

Simulation Procedure

The rocket engine exhaust gas generator used for this program is a sophisticated device for identically reproducing the combustion products composition and temperature of a solid propellant by use of a propellant system employing only liquids, gases, or slurries. This Aeronutronic developed device has been perfected over the past six years, so that it is now operating on a routine basis as a highly successful research tool.

A given solid propellant can be exactly duplicated by any of a large number of combinations of liquid, gaseous, and/or slurry systems. The duplications are achieved with respect to both chamber temperature and chamber combustion products.

The composition and thermodynamic properties of the equilibrium products of a combustion process are uniquely determined by the atomic composition, the temperature, and the pressure. Pressure, as an independent variable, is usually specified in advance. The adiabatic flame temperature is determined by the heats of formation of the reacting propellant ingredients and their products.

Thus, in order to simulate a solid propellant with a liquid or gaseous system, the important parameters are atomic composition and enthalpy change. For example, if the solid propellant to be simulated contains six atomic species, it is possible to select six chemicals which contain the desired elements. Then, by a simple mass-balance process, the composition can be precisely determined. If an additional chemical is added, the heat balance equation can also be satisfied, such that not only the atomic composition, but also the temperature of the combustion products is reproduced. In the completely general case, n + 1 ingredients are needed, where n is the number of elements in the solid propellant. In practice, however, fluid propellants can usually be found which combine several of the requisite elements, and then fewer than n + 1 ingredients are required.

As a control on the simulation procedure, every proposed simulator composition is checked on the Aeronutronic computer before firing to assure that the flame temperature and gas composition are identical to the solid propellant being simulated. Further comparison and evaluation calculations determining the nozzle throat heat flux for the solid propellant exhaust environments are presented in Appendix I.

The exhaust gas composition for the highly aluminized 5800°F solid propellant used in this program is shown on the following page.

ALUMINIZED SOLID PROPELLANT SIMULATION

Species	Molecular Weight	Moles/100 Grams	Weight %
$AlCl$ (g)	62.44	0.0113	0.71
$AlCl_2$ (g)	97.89	0.0209	2.04
CO (g)	28.01	0.7857	22.01
CO_2 (g)	44.01	0.0787	3.46
Cl (g)	35.46	0.0588	2.08
HCl (g)	36.47	0.5081	18.53
HO (g)	17.00	0.0551	0.94
H_2 (g)	2.02	0.8845	1.78
H_2O (g)	18.02	0.6992	12.60
N_2 (g)	28.02	0.3101	8.68
Al_2O_3 (c)	101.96	0.2613	26.64
Other (minor species)			0.53
			100.00%

Note: Simulation is at 500 psia chamber pressure and 3425°K chamber temperature

Solid Propellant Simulator, Propellant Feed Systems, Controls and Instrumentation

Aeronutronic has designed the solid propellant simulator especially for material testing. In achieving this goal, the simulator system has been designed to provide a constant flow of propellants independent of variations in chamber pressure. The simulator rocket motor hardware consists of a combustion chamber, a propellant feed injector, a nozzle holder, and the ablative nozzle test specimen. During the past five years the design of a representative solid propellant simulator has evolved into its present configuration.

The combustion chamber is a water cooled copper lined combustion chamber with an inside diameter of 3 inches at the injector end and 2.56 inches at the nozzle specimen end, with an overall length of 22-5/8 inches.

The propellant feed injector is made of copper. The injectants for the specified simulation were gaseous oxygen, gaseous nitrogen, gaseous hydrogen, and an aluminized slurry. Criteria pertinent to heat transfer, pressure drop, and impingement patterns were carefully employed in the design of the injector. The chamber and nozzle holder were designed to accept the test nozzle specimens which were furnished to Aeronutronic for this test evaluation program. These test specimens consist of an assembly comprising of a nozzle housing insert mold of refrasil phenolic into which the test ablative nozzle materials are inserted. Figure 4 presents a schematic of the injector. Figure 5 is a photo of the injector, chamber, and nozzle holder assembly. Figure 6 is a schematic of a typical test nozzle specimen.

The propellant feed systems are designed to provide constant flow independent of chamber pressure. The flow of each gas and the slurry propellant is independent of chamber pressure and each of the other propellants. Each of the gaseous oxygen, hydrogen, and nitrogen propellants feed systems includes a block valve, regulator, sonic nozzle, firing valve, bleed valve, pressure transducers, and thermocouples. The gases flow rate is controlled and measured by setting and recording the pressure upstream of the sonic nozzle. The setting of the flows are made under the exact flow conditions as during the run thus assuring reproducibility of the desired propellant flow rates. The slurry propellant is prepared in a mixer under carefully controlled conditions and then transferred into a run tank containing a floating piston. The slurry is expelled from the run tank during a test run by displacing the slurry with RP-1 fluid. Metering of the slurry is provided by controlling the volumetric amount of RP-1 which is used to displace the slurry. The metering of the RP-1 is provided by the setting of the RP-1 tank pressure and the use of a cavitating venturi. The flow rate through the cavitating venturi is determined by the area of the venturi, the upstream pressure, and the vapor pressure of the RP-1 fluid.

The system employed during these tests provides a differential (ΔP) pressure in the order of 1200 psi., thus the small variations in tank pressure results in minute changes in slurry flow rate. Figure 7 presents a test schematic of Aeronutronic's solid propellant simulator system.

In order to achieve the desired starting transients which are representative of a solid propellant motor, extreme care has to be observed in the timing of the firing valves. The timing of the control valves are controlled through a sequenced timer. During this test sequence, two shutdown criteria were used -- one was time, the other pressure, whichever occurred first. The pressure shutdown was accomplished by the use of an automatic pressure control electronic circuit. The actual shutdown occurred approximately 1 second after the initiation of the shutdown circuit, thus allowing the shutdown to be accomplished with the sequence timer.

The instrumentation used during this sequence of tests is as follows: Dynisco "direct current" transducers were employed for all pressure measurements. The combined linearity and hysteresis of these transducers were held to better than 0.25 percent. Individual 10 volt excitation is provided to each transducer using Systems Research range and balance units. All temperatures were recorded using thermocouples conditioned for recording, utilizing a Pace thermocouple control unit. Gaseous flows were determined by measuring sonic nozzle upstream pressure and by the configuration of the sonic nozzle. The flow rate is then calculated by the appropriate flow equation and a series of correction graphs which compensates for temperature, upstream pressure, and gas medium. These formulas and corrections were developed through a computer program especially designed for determining propellant flow using high pressure sonic nozzles in the appropriate size range. The verification of this method of measuring flow has been documented using turbine type flow meters which were calibrated at the University of Colorado. RP-1 flow is measured using a Waugh turbine type flow meter. All data recorded during this test series were on a CEC oscillograph. The overall system accuracy achieved during this test series is better than ± 1.5 percent.

Propellant System Characterization

The solid propellant which was simulated is characterized by its combustion temperature, characteristic velocity, and its exhaust species. The theoretical values were then calculated based upon the ingredients which make up the propellant and the chamber pressure at which the system is to operate (i.e., 500 psia).

When the selected chemical ingredients are introduced into the combustion chamber and are allowed to react, the system is treated as a conventional rocket motor, which it is, wherein the combustion performance can be evaluated in accordance with accepted techniques. Utilizing the relationships among pressure, mass flow rates, and geometry to determine characteristic velocity (C^*); if the experimental value approaches the theoretical C^*, then this is sufficient indication that simulation has been achieved.

Prior to testing any ablative nozzle specimens, short check runs were conducted on basically noneroding (graphite) nozzles. This permitted accurate definition of the throat area for simulation efficiency evaluation. Measurements made during each check firing are chamber pressure, propellant flow rates, and initial and final throat areas. From these measurements the experimental characteristic velocity is determined and combustion efficiency calculated.

Chamber pressure is obtained in a straightforward manner, employing a pressure transducer to sense pressure at a tap in the combustion chamber. The output from this transducer is converted to an oscillogram. Two transducers are utilized to provide redundancy for this parameter.

Flow rates are measured by methods best suited to each propellant. Gas flows are determined by measuring temperature and pressure upstream of sonic nozzles with known effective flow areas.

By virtue of the displacement technique employed to transfer the aluminized slurry (which contains solids in suspension), slurry flow rates are determined by measuring the volumetric flow rate of the displacement fluid.

Reproducibility of experimental or test conditions to ensure a common comparative base is largely dependent on the measurement of propellant flow meter outputs, pressures, and system temperatures.

Current technology for measurement of slurry flow rates in the Aeronutronic solid propellant simulator is based on measuring the flow rate of the transfer medium which displaces a known volume within a zero-leakage cylinder. A turbine type flow-meter is utilized to measure this flow rate. Overall accuracy of the measurement is dependent primarily on dynamic fluid correction, basic flow meter calibration, and instrumentation system accuracies.

Preset flow rates, monitored by means of pulse counting techniques (electronic counter), provides a system accuracy of better than ± 0.5 percent, while flow measurement conducted during the run via analog recording provides an overall accuracy of ± 1.5 percent.

Gaseous flow rates are measured by utilizing critical flow venturis designed according to classic principles and flow calibration techniques. Here again the accuracy is primarily dependent on the following good design and fabrication techniques and verification of discharge characteristics. Measurement of flow-associated pressures and temperatures by pressure transducers and thermocouples provide the remaining basis for computation of the flow rates. Overall accuracy of this flow measurement and recorded data is +1.5 percent.

Measurement of all pressure parameters is made utilizing high-frequency bonded strain-gage pressure transducers, associated conditioning equipment, and galvanometer oscillographic recorders. Transfer function of each transducer channel is periodically verified with pressure standards and derived electrical equivalents. System accuracy is better than 1.5 percent.

Test Conditions

All simulator testing was conducted utilizing a solid propellant simulation specified by the Nonmetallic Materials Division, Air Force Materials Laboratory, Research and Technology Division. The specified propellant had an equilibrium characteristic velocity (C*) of 5212 ft/sec and a flame temperature of 5800°F.

The weight flows "desired" for each propellant system were as follows:

GO_2	=	0.215 pps
GN_2	=	0.051 pps
GH_2	=	0.014 pps
Slurry	=	0.313 pps
Total		0.593 pps

Slurry Composition (% of Total Propellant)	
Al	10.68
Al_2O_3	8.04
Trichlorethane	27.67
RP-1	5.28
Jelling Agent	1.00

Test firing standard parameters for all nozzle specimen runs were as follows:

Initial Chamber Pressure: 500 psia (as determined by checkrun graphite nozzles)

Run Duration: 60 seconds or chamber pressure reduction to 150 psia, whichever occurred first.

Check Run Performance

Check runs were completed prior to the actual specimen nozzle firings in each group. Check runs were performed for the following reasons:

(1) To demonstrate proper simulation.

(2) To optimize start transients of the various propellants.

(3) To optimize simulator propellant flows, rocket motor performance, and demonstrate repeatability.

(4) To experimentally verify a constant C* value for the simulator, to enable calculations for the equivalent erosion rate based on chamber pressure.

Test Evaluation Techniques

Chamber Pressure versus Time Curves

For each motor firing, a chamber pressure versus time graph has been prepared.

These graphs have been plotted so that a minimum of six points were used to define the curve and that no point is more than 4 seconds from an adjacent point. The graphs also note the pertinent research nozzle material.

Figures 8 through 37 present these data from Test Series 4.

Erosion and Resin Degradation Rate Evaluation

Erosion rates were based on calculated nozzle specimen throat areas for the fired nozzles at rocket motor combustion chamber pressures of 350, 300, 250, 200, and 150 (or final) psia. The following standard formula was used:

$$A_t = \frac{W\ C^*}{g\ P_c}$$

where

A_t = throat area (inch^2)

W = total weight flow (pounds per second)

C^* = (equilibrium C^*) x (average combustion efficienty) feet/second

g = constant (32.2 feet/second^2)

P_c = chamber pressure (pounds per square inch absolute)

Resin degradation rates were calculated by adding the erosion rate at the end of the test run to the similar char depth rate. The char depth was measured on the post test sectioned nozzle at the resultant throat location.

The erosion rates per nozzle were plotted graphically to evaluate individual nozzles and nozzle groupings by materials. The resin degradation rates are tabulated for similar evaluations.

The above data are presented as follows:

(1) Table III presents the tabulated, calculated, and measured values used in erosion property analysis.

(2) Table IV presents the tabulated char depths and resin degradation rates.

(3) Figure 38 presents the erosion rate versus nozzle number at the five specified combustion chamber pressures.

(4) Figure 39 presents erosion rate comparisons per nozzle grouping based on similar resin content.

<u>Nozzle Post Test Sectioning and Photographic Methods</u>

Each of the ablative nozzles were sectioned and polished. All of the nozzles were sectioned with relation to the "12 O'clock" position of the simulator and so marked. The photographed section of each nozzle has been returned to the Nonmetallics Material Division.

Two different types of post test photographs were taken of each nozzle: an axial photograph of the complete nozzle, and a profile photograph of a bisected nozzle.

A cross section throat area axial photograph was taken of the complete nozzle. The throat image was projected on a negative utilizing a point light source on the ceiling in the high bay photographic laboratory. A new nozzle was used to cast the original throat shape on a then reproduced negative. The negative was then aligned in a plexiglass fixture which also held the outside diameter of the phenolic nozzle holder, thus aligning the centers. A nozzle number and an injector orientation mark was also photographed through the plexiglass.

Profile photographs of the sectioned nozzles were taken utilizing a grid overlay, which consisted of a five-lines-per-inch grid around the perimeter of the overlay and an original nozzle outline to emphasize and indicate erosion. The photographs emphasize the background highlights of the nozzles as well as the sanded nozzle plane for a more complete visual description of the post-fired nozzle section. For visual clarity only a perimeter grid was used. Both the grid and the outline were drawn with white ink on a clear mylar sheet. The grid was aligned to the bisected nozzle utilizing the exit e. ' of the insert and the 2.56 inch phenolic holder diameter. White chalk was placed on the nozzle contour for clarification.

Figures 40 through 54 present the photographic data for Test Series 4.

Table V presents a brief tabulated post test nozzle visual evaluation.

Check Run Performance

Three checkruns were completed before the Test Series specimen nozzle firings. These tests were performed for the following reasons:

(1) To optimize start transients of the various propellants.

(2) To obtain repeatable simulator propellant flows and rocket motor performance.

(3) To experimentally verify a constant C* value for the simulator so that later calculations could be made for the equivalent erosion rate based on chamber pressure.

The solid propellant simulator checkrun performance is presented in Table II. Checkruns were all conducted utilizing graphite nozzles with 0.500-inch nominal throats. Following checkrun No. 3, the nozzle specimen test series was started.

As part of the checkruns that were made, a realistic value of characteristic velocity (C*) was obtained which was subsequently used for area calculation. The solid propellant simulator efficiency was calculated at the end of each run, utilizing the final nozzle throat diameter. Due to the short test durations, the graphite check nozzle throat had eroded very slightly and was easily accurately measurable. The following data were taken for characteristic velocity determination (Reference Table II).

Check Run No.	Efficiency
1	95.50%
2	95.50%
3	96.05%
Average Efficiency	95.68%

After half of the test nozzles were tested, another checkrun was made to document the efficiency of the solid propellant simulation (Reference Table II).

Check Run No.	Efficiency
4	95.0%

Nozzle 532 was prematurely shut down at 16 seconds by the automatic shut off switch. It was restarted and the test completed.

Nozzles were restarted in order to obtain some data that could be evaluated, even though possibly compromised by the ignition effects.

Table V covers the post-test visual analysis of each nozzle specimen. Table IV tabulates the specimen char depth and resin degradation. The material description of each test specimen is presented in Table IA and Table IB. Photographs of the post test nozzle, showing the bisected profile section and the axial throat view, are presented in Figures 40 through 54. Figure 55 presents the average control nozzle chamber pressure versus time curve based on Nozzles 508, 529 and 530. This curve is based on averages of constant pressure points. A transparency of this curve is enclosed in the envelope attached to the rear of this report. This transparency can be overlayed on pertinent curves for evaluation purposes.

Test Operation Conditions

The solid propellant simulator flowrate performance is tabulated in Table VI and the test-to-test variation from the nominal is shown in Figures 56, 57, and 58. The slurry flowrate was within ±1 percent from the nominal value in 87 percent (26 tests) of the tests and the other 13 percent of the tests were within -1.4 percent. The total propellant flowrate variation is between ±1.2 percent and -2 percent. Oxygen, hydrogen and nitrogen were affected quite extensively by the ambient 20°F temperature variations during the tests and, due to the inability to make the correction for the exact gaseous propellant run temperature, a larger variation from the nominal values was experienced than in previous test series. Oxygen had only 53.5 percent of the runs within ±1 percent of the nominal value and 33.3 percent within ±2 percent. Only on two occasions did the oxygen run 3 percent or more from the nominal values (±3 percent and -3.9 percent). Hydrogen had 80 percent of the runs within ±2 percent of the nominal value. Nitrogen had 60 percent (18 runs) within ±1 percent of the nominal value. The remaining 40 percent varied between +1 percent and -3.2 percent of the nominal values.

Nozzle Specimen Tests

An automatic cutoff relay was used in conjunction with a timer to obtain more consistent test pressure cut off at 150 psia chamber pressure. This allowed a more standardized evaluation of material degradation and char formation. This circuit was successful in holding minimum chamber pressure shutdown to 150 ± 4 psia in 22 of the thirty nozzles run.

Nozzle 458 experienced a shutdown at 156 psia due to an incorrectly wired circuit. This was remedied and nozzles 469 and 508 were run. During these two runs the timing circuit had to be set. Nozzle 508 was run and experienced a shutdown at 138 psia. Nozzle 469 experienced a shutdown at 143 psia. The following 14 nozzles were run with minimum chamber pressures falling within the 150 ± 4 psia tolerance stated above.

During the running of Nozzle 534, the timer circuit failed and a manual shutdown was not accomplished until 63.1 seconds, resulting in a minimum chamber pressure of 101 psia. The circuit was repaired but the timing component failed completely during the testing of Nozzle 537 resulting in a minimum chamber pressure of 137 psia.

The only other deviation noted in minimum chamber pressure occurred on Nozzle 545 and was attributed to the short run duration with the accompanying steeper slope of the pressure versus time curve.

There were three other deviations to be noted during the testing of the 30 nozzles. The circumstances were as follows:

(1) Nozzle 506 was shut down at 44 seconds due to insufficient slurry. The slurry tank was refilled and the unit fired again. The slight discontinuity in the chamber pressure versus time curve attests this fact.

(2) Nozzle 513 was fired and immediately shut down due to lack of slurry flow. A subsequent restart was made. This accounts for the 0.593 initial throat diameter occurring on Table III.

Materials Evaluation

A comparison of nozzle performance can be made with some tests of Series 1, reported in Reference 1, as well as a comparison within this Test Series.

Carbon Cloth (CCA-1) - 91LD Phenolic Resin Series

A comparison of the erosion rate data of specimens 529 and 530 indicate that there is little, if any, discernible effect of molding pressure on the erosion performance under these test conditions. Specimens 529 and 530 of this report, and 400 and 421 of Reference 1, were all fabricated under the same conditions except for a shorter post-cure cycle for Specimen 400. The erosion rate data indicate that all data lie within the spread for identical parts 429 and 430. The residual contour of tested throats show similar delamination patterns for Specimens 429, 430 and 421. There is less delamination of Specimen 400. The only reason considered at the present time for the lesser amount of delamination of Specimen 400 is the lower hardness which may allow pyrolysis products to be released and a char layer to develop without a more rigid delaminating structure. It has been noted on other work, however, that very low hardness composites in general appear to exhibit poor erosion resistance and/or plastic deformation. As a consequence, there may be an optimum hardness or other characteristic reflected in hardness which will result in minimum delamination and surface recession.

Specimen 423 containing a low alkaline content in the reinforcement does not appear to influence performance when compared to Specimens 400, 421, 429, or 430.

Carbon Cloth (CCA-1) - 2,2 BIS (p-hydroxyphenyl) propane-phenolformaldehyde Resin Series

This resin system with CCA-1 reinforcement was tested as Specimen 394 (Reference 1) and Specimens 546 and 547 in the current series. The erosion rates of the specimens showed some variation; the lowest erosion rate being exhibited by the specimen of the prior test series.

Carbon Cloth (CCA-1) - 2,7 Dihydroxynapthalene phenol formaldehyde Series

The specimens tested during this series were identical to No. 463 in prior tests. Specimens 431 and 457 from the previous series were from a different resin batch; however, the erosion rate of Specimens 464 and 431 were very similar, while 457 and 463 were also very similar. This would indicate that processing and testing present greater variables to measured performance than batch-to-batch variation of the resin system. The post-test photographs of the tested nozzles all exhibit characteristic large local gaps between laminations. These gaps extend in some cases to near the backface of the specimens.

Carbon Cloth (CCA-1) - P-polyphenol phenol formaldehyde Series

One specimen with this resin system was tested. It appears to be a companion part to No. 490, tested previously, and is possibly different than Nos. 455 and 456 which have a higher resin content in the composite. The erosion rate data is analogous to that of the 2,7 Dihydroxynaphalene phenol formaldehyde discussed above (there is greater similarity of erosion between "nonidentical" specimens). Some delamination and separation can be observed, although not as severe as that of the (2,7 Dpf) composites. One specimen (455) tested previously did exhibit "chunking" or loss of char during test as the modified surface contour is also that of the char-virgin insulator surface.

Carbon Cloth (CCA-1) - Polyphenylene Series

The polyphenylenes which have been tested include varying post-cure as well as mold pressure and cure temperature. The various composites exhibited surface erosion rates comparable to those of the CTL 91LD control comparison along with slightly lower charring rates. Typically, the ablated surfaces have a rough texture after test. The polyphenylenes, as a group, exhibited less surface recession and char penetration during this series of test than those reported for the first two series (Reference 1).

Carbon Cloth (CCA-1) - Polybenzimidazole Series

The polybenzimidazole containing composites were of two subtypes. One group (Spec. 510, 511, 512, 513) were processed with Imidite 4834. These specimens were subsequently impregnated with other resin systems. The other group of specimens were fabricated with Imidite 2803 as the resin matrix phase.

Reimpregnated Imidite 4834

Specimens 510 and 513 exhibited relatively high surface recession rates as well as high charring rates. It would, therefore, appear that this performance is due to the two infiltrating resin systems, Sylgard 182 and 0-28-0903 (cyclic silicone - epoxy). However, it is not known at the present time that the extent of infiltration of the four specimens is identical. The erosion and charring behavior of Specimens 511 and 512 (infiltrated with R-1746 resin and epoxy novalac) was lower than that of specimens 510 and 513. The degradation rates of the latter two specimens was similar to 91LD reinforced with carbon cloth. Assuming the four specimens of this group are of common infiltrant resin concentration and therefore of identical structure except for the infiltrant resin composition, the epoxy novalac and R1746 exhibit superior performance. This behavior is consistent with that of specimens composed of carbon cloth and R1748, DEN 438 or the Sylgard resin systems. The silicone-epoxy resin system had not been tested as a single resin bearing composite.

Imidite 2803

Two Imidite 2803 - carbon cloth specimens were tested. Specimen 533 behaved in a manner similar to the reimpregnated samples. The erosion of this sample was slightly superior to that of 91LD - carbon cloth. Sample 534 exhibited charring and erosion performance superior to other specimens in either group of polybenzimidazole bearing composites. The performance was, in fact, superior to that of the standard 91LD phenolic - with carbon cloth CCA-1 reinforcement specimens.

91LD Phenolic with G1550 for Reinforcement Series

The performance of the high mold pressure graphite fiber reinforced composited (536 and 537) appear to be superior to the carbon reinforced analogs. The char penetration was comparable to the better insulators, while the erosion rate was unquestionably the lowest of all composites in the Test Series. Both test specimens had smooth textured ablation surfaces after the test.

Carbon Cloth (CCA-1) - PH990 Resin Series

Specimens 538 and 539 containing PH990 as the resin phase of the composite eroded and charred at a high rate. The erosion was high, but the char penetration depth was the highest of all groups tested in this series.

Carbon Cloth (CCA-1) - Epoxy Novolac Series

The Epoxy Novolac specimens (540 and 544) experienced moderate thermal penetration (comparable to or slightly higher than the CTL91LD analog). However, the surface recession was almost as low as that of the high pressure molded graphite reinforced 91LD-phenolic. It appears that the specimen may delaminate into relatively thin plates which then char, preserving a strong surface char which erodes at the edge.

Carbon Cloth (CCA-1) Skygard 700 Series

This composite (Specimen 545) eroded at a very rapid rate (19 mils/sec). Due to the rapid rate of surface removed, the char penetration was high, although the residual char thickness was not great.

General Comments

It appears then that the 91LD resin incorporating Graphite cloth was equivalent or superior in performance (low surface recession, low char penetration and preservation of smooth surface texture) to other materials, with the exception of some of the polyphenylenes, although the heat penetration rate of the p-phenylphenol phenol formaldehyde reinforced with carbon cloth is slightly higher. This resin might then be expected to perform well; is a strong ablating composite, can be fabricated utilizing a graphite reinforcing phase.

Aeronutronic's evaluation is considering at the same time thermal degradation and erosion resistance. Obviously, dependent on the application, one or the other of these characteristics can be of little importance. As an example, the performance of the Epoxy Novolacs is such that there is surface erosion but little thermal degradation. A possible use for this material could be in high area ration nozzle entrance sections.

LIQUID PROPELLANT COMBUSTION GAS TESTS

GENERAL DISCUSSION

The liquid propellant combustion gas nozzle specimen tests were conducted in one grouping of nineteen nozzles. Table VII presents the test specimen description. The liquid propellants were nitrogen tetroxide (NTO) and a 50 percent hydrazine and 50 percent unsymmetrical dimethyl hydrazine (50-50) mixture by volume at an oxidizer to fuel mixture ratio of 1.6 to 1.

The liquid propellant testing was conducted at the Aeronutronic Remote Test Site located about 15 miles from the main plant. Figure 59 is an overall view of the test cell - control room arrangement. Figure 60 is a view of the control room instrumentation area. Figure 61 shows the liquid propellant motor in Test Cell B during a test firing.

A series of five check runs were made utilizing the identical rocket motor hardware from test series 3 (Reference I). These check runs indicate that the very good nozzle erosion patterns and combustion efficiency were almost identical to that obtained during test series 3.

Check runs were completed prior to the actual specimen nozzle firings and after any significant rocket motor or system modification. Check runs were performed for the following reasons:

(1) To demonstrate proper mixture ratio, chamber pressure, and uniform combustion.

(2) To demonstrate reliable and repeatable hardware performance.

(3) To optimize starting and stopping transients.

The liquid propellant check runs are presented in Table VIII. All check runs were conducted utilizing graphite nozzles with 0.500-inch nominal throats.

For further comparison and evaluation of the rocket motor performance, calculations determining the nozzle throat heat flux for the liquid propellant exhaust environment is presented in Appendix I.

Liquid Propellant Rocket Motor, Propellant Feed Systems, Controls and Instrumentation

Aeronutronic also designed the liquid propellant rocket motor (N_2O_4 - 50/50) especially for material testing. In achieving this goal, extreme care was utilized to get even nozzle erosion characteristics from the rocket engine. The liquid rocket motor hardware consists of a combustion chamber, a propellant feed injector, ablative-nozzle holder, and the test specimen.

All testing hardware was identical to the final configuration used during Test Series 3. The combustion chamber used during this test sequence was identical as that utilized for the solid propellant simulator tests. The injector is a stainless steel, water cooled unit shown in Figure 62, which shows the configuration of the eight injection doublets.

The propellant fuel systems are of a constant flow design. The flow of each liquid propellant is "set" by utilizing a specially designed cavitating venturi having a pressure drop of approximately 700 psi. This large drop results in the flow rates being very constant and repeatable.

Each of the two propellant systems includes a nitrogen pressurized propellant tank, block valve, cavitating venturi, firing valve, purge systems, pressure transducers, and thermocouples. Two purge systems are utilized: gaseous nitrogen and water. The nitrogen purge is automatic at the start and finish of each run. The water purge is a post-test operation conducted to efficiently purge and clean the system. Figure 63 presents a test schematic of the Aeronutronic liquid propellant NTO/50-50 system.

The instrumentation system employed during the liquid propellant tests is basically the same as that employed during simulator tests with the exception that the data are recorded using an analog to digital recorder in addition to the oscillograph recording. The analog to digital recorder is a paper tape, three digit system which an accuracy of better than 0.2 percent. This system is manufactured by Applied Development Corporation. By use of the digital recorder, the overall system accuracy will be better than $\pm$1/2 percent.

The data were obtained by recording thirty channels of test pressure information per second in a sequential manner. each channel being recorded in sequence every two-thirds (2/3) of a second. Ten chamber pressure channels per each two-thirds (2/3) second scan were employed to enable data analysts to more easily "pick out" desired data points and to ensure that these points were consistent with the pressure values within a range as short as one-tenth (1/10) second from the selected data point.

Test Conditions

All NTO/50-50 testing was conducted at an oxidizer to fuel mixture ratio of 1.6 to 1.0 as specified by the Nonmetallic Materials Division, Air Force Materials Laboratory, Research and Technology Division.

At the desired initial chamber pressure of 300 psia at the specified mixture ratio, the theoretical equilibrium characteristic velocity (C*) was 5627 feet/second; and the flame temperature was approximately 5300°F (reference Figure 64, Theoretical C* versus Mixture Ratio).

The weight flows "desired" for each propellant system were as follows:

NTO = 0.2164 pps

50-50 = 0.1352 pps

Total 0.3516 pps

The firing standard parameters for all nozzle specimen runs were as follows:

Initial Chamber Pressure: 300 psia (as determined by check run graphite nozzles).

Run Duration: 240 seconds or chamber pressure reduction to 100 psia, whichever occurred first.

Test Evaluation Techniques

Test evaluation for the specimen nozzles subjected to the liquid propellant environment were the same as for those exposed to the solid propellant simulator exhaust (refer to page 10). Erosion rates were based on calculated nozzle specimen throat areas for the fired nozzles at rocket motor combustion chamber pressures of 250, 200, 150, and 100 (or final) psia.

Data are presented as follows:

(1) Chamber pressure versus time curves as shown in Figures 65 through 83.

(2) Table IX presents the tabulated, calculated, and measured values used in erosion property analysis.

(3) Figure 84 presents the erosion rate versus nozzle member at the four specified combustion chamber pressures.

(4) Figure 85 presents erosion rates, at the four specified combustion chamber pressures, in relation to like resins and reinforcements.

(5) Figures 86 through 95 present the photographic data.

(6) Table X presents liquid propellant motor performance data.

(7) Table XI presents the post test nozzle erosion evaluation consisting of char depth and resin degradation rates.

(8) Table XII is the post test nozzle visual evaluation.

(9) Figure 96 is the test-to-test propellant flow-rate variation from nominal conditions.

Test Operation Conditions

The test-to-test propellant flowrates and mixture ratio is presented in Table 10. The associated test-to-test propellant flowrate and mixture ratio variation from nominal conditions is shown in Figure 96.

The nitrogen tetroxide (NTO) flowrate was within ±1.0 percent from the nominal value in 16 of the 19 tests. The other three were within -1.52 percent of the nominal value. The 50/50 fuel flowrate was within ±1.0 percent from the nominal value in 18 of the 19 tests. One test had a fuel variation of -1.18 percent from the nominal value. The total propellant flowrate was within ±1.0 percent of the nominal value on all of the tests. Propellant mixture ratios for 16 of the 19 tests were within ±1.0 percent of the nominal value. The other tests were within ±1.5 percent of the nominal.

The planned run duration for each nozzle test was 240 seconds or if 100 psia chamber pressure is reached. Six (6) nozzle tests were terminated early due to nozzle material characteristics. Material flow into the throat caused an increasingly higher chamber pressure. The nozzle specimens were 549, 552, 553, 556, 557, and 567. During testing of nozzles 549 and 552, the nozzle specimens completely blew out of the nozzle holder. Nozzle specimen 570 was the only nozzle to go the full programmed 240 second duration.

On nine (9) of the nozzle specimen tests erosion "streaking" (a unique erosion pattern) was apparent. The nozzle specimens were 548, 550, 551, 553, 554, 558, 559, 566, and 571. As a possible cause of this condition, the rocket motor injector and chamber design was reviewed. Injector impingement -- if not perfect -- over long runs could possibly lend itself to localized mixture ratio variances. However, chamber design utilized a L^* of 700 to ensure excellent propellant mixing and burning at the nozzle entrance. Although it would therefore appear that the facility system was not a contributing factor, it cannot be theoretically entirely ruled out. Therefore, prior to the next liquid propellant test series, the injector impingement patterns will be analyzed for further optimization, the propellant facility will be recleaned to eliminate chance particle contamination, and the use of a "soft" ablative check nozzle will be considered as a check on uniformity of combustion.

Representation of corrected data of nozzle specimen 409 which was exposed to the liquid propellant exhaust as part of Test Series 3 is shown in Table IX and Figure 97.

Materials Evaluation

All of the specimens tested during this series consisted of composites with a high SiO_2 content reinforcement phase. The single exception to this was a filament wound composite with boron reinforcement. In all seven, different matrices were evaluated.

This test series differs from the one reported in Reference 1 in one respect. During this test series, runs were not terminated at 120 seconds but were continued 240 seconds or until chamber pressure decreased to 100 psi. The longer duration tests can have two effects upon composite performance. The longer duration would accentuate non-uniform surface recession due to slight variations in heat transfer or chemical attack. The very minor variations in chemistry and the effect would be additive throughout the run. In addition, grooves which develop can lead to variations in throat location and the development of shock interactions from the grooves aft of the throat which result in complex erosion patterns which are not due to test material or propellant distribution variations. This type of performance would be expected when testing materials with high char strength and stiffness. This type of performance is believed to be typical of specimen 553, Figure 89.

Materials which exhibit plasticity in the char bulk would be expected to show a different mode of material loss than that discussed above. Reinforcement - char combinations which allow lower viscosity melt phases or macroplasticity within the char would be expected to loosen material by molten flow of reinforcement from the convergent section through the throat, causing restriction and less material loss downstream due to reduced heat transfer through the molten layer. This material loss method is typical of Specimens 556 and 557, Figures 90 and 91.

Material Comparison

Silica - Phenolic. Specimens 552, 553, 554, 556, 557, 570, 580

The first three numbered specimens contained leached glass, high silica, reinforcement while the latter four specimens contained modifications of amorphous Silica or quartz fiber containing various proprietary addition for viscosity control.

The three specimens all exhibit similar decreases in chamber pressure with respect to time up to greater than 160 seconds of test time. Towards the end of the tests, the chamber pressure increases due to liquid flow through the throat and therefore throat area restriction. Specimens 553 and 554 which remained intact after the run can be seen in Figures 89 and 90. Specimen 553 is believed to be slightly grooved during the test. The groove in the throat establishing a shock wave which reacts with the opposite wall downstream, as discussed in the previous section. It also appears that bulk movement of the composite has taken place. It is believed that bulk movement is caused during these relative long runs by

heating of the silica reinforcement in the char to the extent that the SiO_2 viscosity decreases to a point where bulk plastic deformation of the insert can take place; the driving force for plastic deformation being the axial combustion pressure gradient applied to the insert.

Specimen 554 shows evidence of the loss of material by spalling or other methods of gross char removal. This is supported as an occurrence during the run by the charring of the local underlying insulator. However, the chamber pressure trace does not reflect this occurrence.

A comparison of the chamber pressure traces for the three refrasil-phenolic specimens with their analogs in the first series of N_2O_4/N_2H_4 tests indicate that the shape of the curves are similar to 120 seconds of run time (the maximum test time during Series 1).(1) This would indicate the reproducibility of tests conducted at large time intervals.

The four silica reinforced specimens, utilizing two proprietary compositions of amorphous silica and quartz with additives all exhibited varying behavior. Specimens 566 and 571 had chamber pressure curves similar to the Refrasil-phenolic although all specimen tests were terminated due to throat enlargement before the Refrasil-phenolic. Both specimens, Figures 93 and 95 exhibited quite uniform erosion. Both specimens were coated with a layer of reinforcement phase. The char structure of both specimens appear to be relatively free of delamination during test.

Specimens 567 and 570 both exhibited "blunting" of the forward edge and plastic movement of the char. The plastic motion and a loss of small segments of the char may be the cause of the relatively erratic chamber pressure traces. Figures 81 and 82. As can be seen in the section photograph, Figure 94, very little of insert No. 570 remains after the test. The reason for the over pressure during the first two to four seconds of tests for Specimens 466, 467, 470 and 471 is not known. It is indicative of a temporary throat restriction and may be caused by loss of the forward edge of the specimen by mechanical breakup, which would result in "blunting" of the specimens.

The composite compositions of specimens 556, 567, 570 and 571 were not evaluated during the first test series and as a consequence the effect of test duration extension cannot be assessed.

Silica-Imidite

Two specimens of this composition were tested; Specimens 549 and 550. One specimen was ejected from the holder during test. Both specimens were tested for time periods longer than the Silica-phenolic composites. The erosion as indicated by the chamber pressure trace is common for the first 120 seconds of test. After this time period the chamber pressure during the test of Specimen 549 remained constant for 90 seconds. This is believed

to be due to the molten flow of reinforcement phase, possibly accompanied by bulk plastic deformation. After 210 seconds of test it is felt that plastic flow increases due to additional heating. The plastic flow causes throat restriction and an increase in chamber pressure until test specimen ejection occurred.

The other matched specimen (550) exhibited continual and slow throat enlargement after 120 seconds. The sectioned photograph of this specimen, Figure 88, shows some delamination and greater erosion on one side than the other. Evidence of some molten oxide and gas flow through the char fissure can be seen. It also appears that the forward edge of the specimen is about to be lost by plastic flow. This may be the cause of throat restriction and failure of Specimen 549.

Silica-Epoxy Novolac

Two identical specimens were tested, Specimens 556 and 557. The test durations of both specimens were very short. The chamber pressure traces were virtually identical and the same as that of Specimen 526 reported in Reference (1) on the first N_2O_4/N_2H_4 test series. An examination of the cross section photographs for these nozzles indicates some delamination and apparent flow of the hot or pyrolizing resin system which causes the throat restriction.

Boron Fiber - Epoxy Novolac

This single test specimen (566A) was fabricated by a low angle filament winding. The test duration was very short. It appears that the test material performance was probably limited by the reinforcement orientation rather than the reinforcement or resin composition. This is further substantiated by the loss of fibers or groups of fibers as shown in the section photograph, Figure 93.

Silica-Polyimide (I-8)

The polyimide matrix system was tested as a single insert. The erosin rate was about twice as high as the phenolic analogs. The erosion (chamber pressure decrease) was uniform. The tested insert showed that throat enlargement was uniform with no plastic flow, probably due to the short duration and the rapid erosion rate.

Silica-Polyphenylene

The single test of this composition indicated a chamber pressure decrease similar in shape to silica-phenolic. However, the throat increase was more rapid for the polyphenylene resin containing composite. Post test examination of the specimen revealed some delamination. This is not usual for low conductivity silica reinforced composites since thinner char

layers result and less pyrolysis gas pressure occurs. A relatively thin layer of silica was found on the specimen surface. This may be due to in situ reaction of SiO_2 with the char to form SiC. The SiC - carbon composite char would then be lost by erosion with somewhat a limited silica surface layer. This occurrence necessitates relatively high temperatures within the char however, which is not necessarily consistent with the delamination possibility discussed above. A further resolution would require a detailed analysis of the char composition and morphology to propose a more consistent mechanism.

Silica - 2,2 - Bis (p-hydroxyphenyl) propane - phenolformaldehyde

The test durations of this composition was in the range of that of Silica-phenolic; however, erosion of these composites was not uniform. A burn-through of the insert No. 548 was experienced on one side and two pieces of char appear to have been lost during the test. The apparent burn-through could be due to the mechanical loss of a segment of material with subsequent heating, molten flow and erosion obscurring the details of the local discontinuity.

The chamber pressure trace of this test indicates a limited chamber pressure increase at 160 seconds, followed by rapid throat area increase. It is felt that this may have occurred during the loss of the two pieces of char.

The second specimen of this composition exhibited a chamber pressure decrease without a subsequent increase. The tested nozzle did not, however, indicate the loss of char segments. The difference in performance in the latter stages may be due to minor differences in material performance over this very long test duration.

Silica-Polyphenylene

Three specimens of this nominal composition were tested. Specimens 558 and 559 were molded at 3500 psi. Specimen 562 was molded at higher pressure, 10000 psi. Other than molding pressure, specimen preparation was the same.

A comparison of the chamber pressure time curves indicates much more rapid throat enlargement for the high pressure molded test insert, Specimen 562. It is not known by what mechanism the high pressure consolidation could result in more rapid erosion. Post test examination of Specimen 562 indicates that erosion was not uniform. Pieces of char appear to have been removed. After test, some small local broken pieces of composite were observed within the specimen. At the present time, it is felt that this composition may form in a more brittle char and at high temperatures when reinforcement softening occurs, brittle fractures of the char phase results.

The low pressure molded inserts were run for longer time periods. The throat enlargement was similar for the first 110 seconds. At that time, Specimen 559 experienced a decrease in throat enlargement, followed by throat restriction.

Examination of the specimens after test indicates that the molten oxide film was thick in both cases and that surface discontinuity typical of char loss had occurred.

General Results

The apparent variable material performance observed in some groups of test specimens in general occurred late in the test (after 100 seconds). It is believed that test durations of this length are very long for inserts of this size and heat capacity. As a result, after two to three minutes of test bulk material movement and changes are occurring. The bulk movement and plugging for identical specimens occurring at say 20 seconds time differential appears at first glance to be a large difference. However, when this occurs after 200 seconds, the variation in performance is then only 10 percent and in general in the range of performance for shorter test durations.

The longer tests conducted in this series result in massive changes in material rather than primarily thin char and surface effects as encountered during prior test series.

The longer test durations also make post test analysis difficult because changes which occur in the test specimen can, on additional exposure, be subject to additional general erosion and ablation and as a consequence be more difficult to define.

TABLE IA
DESCRIPTION OF TEST SPECIMENS
ABLATIVE NOZZLE CHARACTERIZATION

DATA SHEET**	NOZZLE NUMBER	RESIN CHEMICAL TYPE	REINFORCEMENT AGENT	RESIN CONTENT (percent)	MOLDING CONDITIONS PRESSURE (psi)	MOLDING CONDITIONS TEMPERATURE (°F)	MOLDING CONDITIONS TIME (Min.)	POST CURE CYCLE*	BARCOL HARDNESS	DENSITY gm/cc
—	458	2, 7-dipydroxynaphthalene phenol formaldehyde (B2353-36)	Carbon Cloth CCA-1	44.4	300	300	120	III	N.A.	N.A.
303	464	2, 7-dihydroxynaphthalene phenol formaldehyde (B2353-41)	Carbon Cloth CCA-1	39.7	300	300	120	III	75	1.45
311	469	Polyphenylene (B2353-42) 1000-1500 MW	Carbon Cloth CCA-1	39.9	300	425	180	X	N.A.	1.28
311	470	Polyphenylene (B2353-42) 1000-1500 MW	Carbon Cloth CCA-1	40.2	300	425	180	X	N.A.	1.28
325	491	P-phenylphenol phenol formaldehyde (B2353-40)	Carbon Cloth CCA-1	40.4	300	300	120	III	63	1.43
323	506	Phenolic (CTL 91LD)	Graphite Cloth G1550 (Uncoated)	41.2	300	300	120	III	54	1.34
329	508	Phenolic (CTL 91LD)	Carbon Cloth CCA-1	42.7	300	300	120	III	75	1.41
340	510	Polybenzimidazole (Imidite 4834) Impregnated with Sylgard 182	Imidite 4834	30.8	200	700	180	I	46	1.24
343	511	Polybenzimidazole (Imidite 4834) Impregnated with Silicone (R-7146)	Imidite 4834	30.8	200	700	180	I	46	1.24
346	512	Polybenzimidazole (Imidite 4834) Impregnated with epoxy novolac (DEN 438)	Imidite 4834	30.8	200	700	180	I	46	1.24
349	513	Polybenzimidazole (Imidite 4834) Impregnated with cyclic silicone epoxy (OZ 8-0903)	Imidite 4834	30.8	200	700	180	I	46	1.24
366	521	Polyphenylene (ABCHAR 413) 1000-1500 MW	Carbon Cloth CCA-1	40.0	3,000	400	120	II	30	1.38
359	523	Phenolic (CTL 91LD)	Carbon Cloth Low Alkalinity (SS-1641)	42.8	10,000	300	120	III	65	1.41
3[illegible]9a	529	Phenolic (CTL 91LD)	Carbon Cloth CCA-1	42.0	10,000	200 - 300	60	III	80	1.40
3[illegible]9a	530	Phenolic (91-LD)	Carbon Cloth CCA-1	41.4	10,000	300	120	III	75	1.41
406	531	Polyphenylene (ABCHAR 412)	Carbon Cloth CCA-1	38.0	10,000	380	120	IV	40	1.31
406	532	Polyphenylene (ABCHAR 412)	Carbon Cloth CCA-1	36.2	10,000	380	120	IV	40	1.31
392	533	PBI Polybenzimidazole AFR-151 (Imidite 2803)	Carbon Cloth CCA-1	38.0	10,000	600 - 700	60 - 120	V	78	1.35
392	534	PBI Polybenzimidazole AFR-151 (Imidite 2803)	Carbon Cloth CCA-1	41.0	10,000	600 - 700	60 - 120	V	80	1.29
400	536	Phenolic (91-LD)	Graphite Cloth G1550 (Uncoated)	40.3	10,000	300	120	III	53	1.35
400	537	Phenolic (91-LD)	Graphite Cloth G1550 (Uncoated)	39.7	10,000	300	120	III	45	1.35
410	538	Phosphonitrilic (PH 990)	Carbon Cloth CCA-1	40.4	10,000	450	60	IX	59	1.33
410	539	Phosphonitrilic (PH 990)	Carbon Cloth CCA-1	39.9	10,000	450	60	IX	60	1.39
402a	540	Epoxy novolac (DEN 438)	Carbon Cloth CCA-1	30.3	10,000	300	120	VII	75	1.36
372	542	Polyphenylene (ABCHAR 413)	Carbon Cloth CCA-1	37.6	10,000	400	120	VI	55	1.36
372	543	Polyphenylene (ABCHAR 413)	Carbon Cloth CCA-1	38.3	10,000	400	120	VI	55	1.34
402c	544	Epoxy novolac (DEN 438)	Carbon Cloth CCA-1	28.8	10,000	300	120	VII	60	1.34
403a	545	Skygard 700	Carbon Cloth CCA-1	41.2	10,000	600	180	VIII	51	1.25
423	546	2, 2-Bis (p-hydroxyphenyl) propane-phenolformaldehyde	Carbon Cloth CCA-1	40.5	10,000	300	120	III	78	1.34
423	547	2, 2-Bis (p-hydroxyphenyl) propane-phenolformaldehyde	Carbon Cloth CCA-1	40.8	10,000	300	120	III	81	1.36

*See Table IB
**Hughes Aircraft data sheet numbers are from reports shown in the "Foreword."

TABLE IB

DETAILS OF POST-CURE CYCLES AS ENUMERATED IN TABLE OF TEST SPECIMENS DESCRIPTION

I. 600°F for 24 hours, 650°F for 24 hours, 700°F for 24 hours, 750°F for 24 hours, 800°F for 8 hours. Parts were post-cured in a helium atmosphere.

II. 18 hours at 275°F, 114 hours from 275° to 600°F, 6 hours cooling to below 200°F. Post-cured under helium atmosphere.

III. 18 hours at 275°F, 72 hours from 275° to 400°F, 4 hours at 400°F, 7 hours cooling to below 200°F.

IV. 18 hours at 275°F, 72 hours from 275° to 400°F, 39 hours from 400°F to 550°F, 7 hours cooling to below 200°F. Parts were post-cured under helium atmosphere.

V. 24 hours at 600°F, 24 hours at 650°F, 24 hours at 700°F, 6 hours at 750°F, 6 hours at 800°F, 6 hours at 850°F, 1½ hours between temperatures, 18 hours cooling to room temperature.

VI. 18 hours at 275°F, 108 hours from 275°F to 550°F, 6 hours at 550°F, 7 hours cooling to below 200°F, parts were post-cured in Argon atmosphere.

VII. 17 hours at 275°F, 6 hours from 275°F to 400°F, 1 hour at 400°F. 7 hours cooling to below 200°F.

VIII. 24 hours at 375°F, 24 hours at 475°F, 24 hours at 575°F (6 hours between temperatures), 7 hours cooling to below 200°F.

IX. 18 hours at 275°F, 72 hours from 275° to 400°F, 4 hours at 400°F, 4 hours at 425°F, 7 hours cooling to below 200°F.

X. 18 hours at 275°F, 72 hours from 275° to 450°F, 6 hours at 450°F, cool to below 200°F. Parts post-cured in a nitrogen atmosphere.

XI. 16 hours room temperature to 275°F, 17 hours at 275°F, 6 hours from 275° to 400°F, 1 hour at 400°F, 7 hours cooling to below 200°F.

TABLE II

SOLID PROPELLANT SIMULATOR CHECK RUN PERFORMANCE

ABLATIVE NOZZLE CHARACTERIZATION

SIMULATOR CHECKOUT NUMBER	TEST DURATION (sec)	TOTAL FLOW RATE (lb/sec)	MAXIMUM CHAMBER PRESSURE (psia)	FINAL CHAMBER PRESSURE (psia)	INITIAL THROAT DIAMETER (in.)	FINAL THROAT DIAMETER (in.)	CALCULATED C* (ft/sec)	EFFICIENCY %	OXYGEN FLOW RATE (lb/sec)	HYDROGEN FLOW RATE (lb/sec)	NITROGEN FLOW RATE (lb/sec)	SLURRY FLOW RATE (lb/sec)	REMARKS
1	9.0	.5955	534	448.3	.5010	.5090	4972	95.50	.2152	.0145	.0522	.3136	Performance Checkrun
2	7.1	.5947	562	462.6	.5015	.5030	4977	95.50	.2160	.0143	.0513	.3131	Performance Checkrun
3	7.0	.5923	558	468.0	.5010	.5010	5006	96.05	.2148	.0140	.0513	.3132	Performance Checkrun
4	7.0	.5999	566	469.0	.5000	.5000	4941	95.00	.2200	.0144	.0520	[illegible]	Performance Checkrun made midway through the Wright Field tests.

CALCULATED AND M
SOLI

NOZZLE NUMBER	TIME (sec.)	MAXIMUM CHAMBER PRESSURE (psia)	ORIGINAL THROAT DIAMETER (inch)	MINIMUM CHAMBER PRESSURE (psia)	TOTAL FLOW RATE (lb/sec)	TIME 350 psia (sec)	CALC. THROAT AREA 350 psia (in^2)	CALC. THROAT RADIUS 350 psia (inch)	CALC. EROSION RATE 350 psia (mils/sec)	TIME 300 psia (sec)	CALC. THROAT AREA 300 psia (in^2)	CALC. THRO RADI 300 (in
458	54.2	570	.500	156	.5902	9.4	.2611	.2885	4.10	14.5	.3047	.31
464	53.2	563	.500	149	.5918	11.4	.2618	.2887	3.39	17.1	.3055	.31
469	52.8	594	.500	143	.5822	10.2	.2576	.2864	3.57	15.3	.3006	.30
470	55.2	595	.500	149	.5953	11.6	.2634	.2896	3.41	17.4	.3073	.31
491	54.9	598	.502	[illegible]	.5868	10.3	.2596	.2875	3.54	16.3	.3029	.310
506	50.5	613	.498	150	.5932	14.7	.2624	.2891	2.73	21.2	.3062	.31
508	52.8	547	.500	138	.5801	9.9	.2567	.2858	3.62	15.0	.2995	.308
510	36.6	584	.500	148	.5924	9.9	.2621	.2890	3.94	14.0	.3058	.31
511	50.4	619	.500	151	.5913	12.3	.2616	.2886	3.14	17.3	.3052	.31
512	43.3	606	.503	151	.5924	10.0	.2621	.2890	3.75	14.2	.3058	.31
513	32.0	428	.593	149	.5994	1.0	.2652	.2906	5.90	2.6	.3094	.314
521	48.8	493	.500	153	.5966	10.6	.2640	.2899	3.76	16.2	.3080	.313
523	48.7	574	.500	150	.6000	10.5	.2655	.2907	3.88	14.7	.3097	.314
529	43.1	596	.499	149	.5913	9.7	.2616	.2886	4.03	14.7	.3052	.31
530	47.3	606	.500	150	.5941	10.8	.2628	.2893	3.64	15.2	.3067	.31
531	40.1	561	.500	150	.5883	7.6	.2603	.2879	4.99	11.8	.3037	.310
532	42.2	572	.500	152	.5934	8.6	.2626	.2893	4.57	13.6	.3063	.31
533	36.3	561	.500	145	.5961	8.8	.2637	.2898	4.52	12.6	.3077	.313
534	63.1	581	.500	101	.5966	9.3	.2640	.2899	4.29	13.3	.3080	.313
536	56.6	511	.500	149	.5916	13.6	.2618	.2886	2.84	19.6	.3054	.31
537	58.0	587	.500	137	.5875	14.2	.2599	.2877	2.65	19.9	.3033	.310
538	35.3	590	.500	150	.5929	7.1	.2623	.2890	5.49	11.8	.3061	.312
539	36.0	584	.500	148	.5914	7.6	.2616	.2886	5.08	11.4	.3053	.31
540	54.6	584	.500	154	.5950	11.7	.2632	.2895	3.38	17.8	.3071	.31
542	50.8	567	.500	152	.5902	9.8	.2611	.2883	3.90	16.0	.3047	.311
543	51.3	583	.500	150	.5906	9.9	.2613	.2885	3.89	16.0	.3049	.311
544	53.0	613	.499	152	.6037	13.3	.2671	.2916	3.17	19.0	.3116	.315
545	23.8	566	.499	140	.5940	6.7	.2628	.2893	5.94	9.8	.3065	.312
546	44.0	566	.499	150	.5997	7.7	.2654	.2906	5.34	12.8	.3096	.313
547	44.3	566	.499	150	.5916	9.2	.2618	.2886	4.25	13.2	.3054	.311

A

TABLE III

CALCULATED AND MEASURED VALUES USED IN EROSION PROPERTY ANALYSIS

SOLID PROPELLANT SIMULATOR

CALC. THROAT AREA 300 psia (in^2)	CALC. THROAT RADIUS 300 psia (inch)	CALC. EROSION RATE 300 psia (mils/sec)	TIME 250 psia (sec)	CALC. THROAT AREA 250 psia (in^2)	CALC. THROAT RADIUS 250 psia (inch)	CALC. EROSION RATE 250 psia (mils/sec)	TIME 200 psia (sec)	CALC. THROAT AREA 200 psia (in^2)	CALC. THROAT RADIUS 200 psia (inch)	CALC. EROSION RATE 200 psia (mils/sec)	TIME 150 psia (sec)	CALC. THROAT AREA 150 psia (in^2)
.3047	.3115	4.24	22.0	.3656	.3410	4.14	32.5	.4570	.3815	4.05	54.2*	.6093*
.3055	.3119	3.62	24.4	.3666	.3417	3.76	35.3	.4582	.3819	3.73	52.3	.6110
.3006	.3094	3.88	22.2	.3607	.3388	4.00	32.4	.4508	.3789	3.98	51.6	.6011
.3073	.3128	3.61	23.6	.3688	.3427	3.93	33.9	.4610	.3831	3.93	54.0	.6146
.3029	.3106	3.66	24.0	.3635	.3401	3.71	35.8	.4544	.3803	3.61	54.[illegible]	.6058
.3062	.3122	2.98	28.8	.3674	.3420	3.23	41.4	.4593	.3825	3.22	49.7	.6124
.2995	.3086	3.92	21.4	.3594	.3384	4.13	30.2	.4492	.3763	4.18	48.3	.5989
.3058	.3120	4.43	17.7	.3670	.3418	5.19	23.3	.4587	.3822	5.67	34.8	.6116
.3052	.3118	3.57	23.6	.2663	.3415	3.88	34.6	.4578	.3817	3.81	50.4*	.6105*
.3058	.3120	4.26	20.2	.3670	.3418	4.47	27.3	.4587	.3822	4.79	43.3*	.6116*
.3094	.3140	6.73	10.9	.3713	.3438	4.34	19.8	.464[illegible]	.3845	4.44	32.0	.6188
.3080	.3131	3.90	22.8	.3696	.3430	4.08	33.2	.4620	.3835	4.02	48.8*	.6159*
.3097	.3140	4.35	20.8	.3717	.3440	4.52	31.1	.4646	.3846	4.33	48.7	.6195
.3052	.3118	4.24	20.4	.3663	.3415	4.51	28.5	.4578	.3817	4.64	42.8	.6105
.3067	.3125	4.11	21.2	.3680	.3423	4.35	30.1	.4600	.3827	4.41	47.0	.6133
.3037	.3109	5.16	16.8	.3644	.3406	5.39	24.8	.4555	.3808	5.27	39.0	.6073
.3063	.3123	4.58	20.7	.3676	.3421	4.49	27.7	.4595	.3825	4.82	42.4*	.6127*
.3077	.3130	5.00	17.0	.3692	.3430	5.47	24.1	.4616	.3832	5.53	34.9	.6154
.3080	.3131	4.74	17.8	.3696	.3430	5.22	24.1	.4620	.3835	5.54	37.2	.6159
.3054	.3118	3.15	28.8	.3665	.3415	3.18	41.2	.4581	.3817	3.20	56.0	.6108
.3033	.3107	3.05	26.1	.3639	.3401	3.45	34.7	.4549	.3806	3.76	51.6	.6065
.3061	.3121	5.75	15.9	.3673	.3419	5.79	23.5	.4591	.3823	5.63	35.2	.6121
.3053	.3118	5.42	16.1	.3663	.3415	5.68	23.0	.4579	.3817	5.73	33.7	.6105
.3071	.3127	3.52	25.9	.3686	.3426	3.58	38.0	.4607	.3830	3.50	54.7*	.6143*
.3047	.3115	3.84	23.3	.3656	.3410	3.91	34.7	.4570	.3815	3.79	50.9*	.6093*
.3049	.3115	3.84	24.4	.3658	.3413	3.74	35.4	.4573	.3817	3.72	51.3	.6097
.3116	.3150	3.39	26.4	.3740	.3450	3.62	37.5	.4674	.3856	3.63	53.1*	.6233*
.3066	.3124	6.42	12.5	.3680	.3423	7.38	16.3	.4600	.3826	8.17	22.5	.6133
.3096	.3139	5.03	18.6	.3715	.3439	5.08	25.9	.4644	.3845	5.21	41.3	.6192
.3054	.3116	4.72	19.6	.3665	.3415	4.69	29.0	.4581	.3817	4.56	44.3	.6108

*Calculated at chamber pressure at term

\LC. IROAT EA) psia in²)	CALC. THROAT RADIUS 150 psia (inch)	CALC. EROSION RATE 150 psia (mils/sec)	NOZZLE NUMBER	MATERIAL RESIN/REINFORCEMENT
6093*	.4405*	3.51*	458	2, 7-dihydroxynaphthalene phenol formaldehyde (B2353-36) 44.4% Carbon Cloth (CCA-1)
.6110	.4411	3.65	464	2, 7-dihydroxynaphthalene phenol formaldehyde (B2353-41) 39.7% Carbon Cloth (CCA-1)
.6011	.4375	3.63	469	Polyphenylene (B2353-42) 1000-1500 MW, 39.9%/Carbon Cloth (CCA-1)
6146	.4425	3.56	470	Polyphenylene (B2353-42) 1000-1500 MW, 40.2%/Carbon Cloth (CCA-1)
6058	.4391	3.46	491	P-phenylphenol phenol formaldehyde (B2353-40) 40.4%/Carbon Cloth (CCA-1)
6124	.4416	3.83	506	Phenolic (CTL 91LD) 41.2%/Graphite Cloth G1550 (uncoated)
5989	.4365	3.86	508	Phenolic (CTL 91LD) 42.7%/Carbon Cloth (CCA-1)
6116	.4412	5.49	510	Polybenzimidazole (Imidite 4834) (1) 30.8%/Carbon Cloth (CCA-1)
.6105*	.4408*	3.79*	511	Polybenzimidazole (Imidite 4834) (2) 30.8%/Carbon Cloth (CCA-1)
.6116*	.4412*	4.38*	512	Polybenzimidazole (Imidite 4834) (3) 30.8%/Carbon Cloth (CCA-1)
188	.4438	4.60	513	Polybenzimidazole (Imidite 4834) (4) 30.8%/Carbon Cloth (CCA-1)
159*	.4427*	3.95*	521	Polyphenylene (ABCHAR 413) 1000-1500 MW 40%/Carbon Cloth (CCA-1)
195	.4441	3.99	523	Phenolic (CTL 91LD) 42.8%/Carbon Cloth (CCA-1), low alkalinity (SS-1641)
105	.4408	4.47	529	Phenolic (91-LD) 42.0%/Carbon Cloth (CCA-1)
133	.4419	4.08	530	Phenolic (91-LD) 41.4%/Carbon Cloth (CCA-1)
073	.4397	4.86	531	Polyphenylene (ABCHAR 412) 38%/Carbon Cloth (CCA-1)
127	.4416*	4.52*	532	Polyphenylene (ABCHAR 412) 38.5%/Carbon Cloth (CCA-1)
154	.4426	5.52	533	PBI Polybenzimidazole AFR-151 (Imidite 2803) 38.0%/Carbon Cloth (CCA-1)
159	.4427	5.18	534	PBI Polybenzimidazole AFR-151 (Imidite 2803) 38.0%/Carbon Cloth (CCA-1)
108	.4408	3.41	536	Phenolic (91-LD) 40.3%/Graphite Cloth G1550 (uncoated)
6065	.4395	3.67	537	Phenolic (91-LD) 39.7%/Graphite Cloth G1550 (uncoated)
.6121	.4414	5.44	538	Phosphonitrilic (PH 990) 40.4%/Carbon Cloth (CCA-1)
6105	.4408	5.66	539	Phosphonitrilic (PH 990) 39.9%/Carbon Cloth (CCA-1)
6143*	.4423*	3.52*	540	Epoxy novolac (DEN 438) 30.3%/Carbon Cloth (CCA-1)
6093*	.4405*	3.74*	542	Polyphenylene (ABCHAR 413) 37.6%/Carbon Cloth (CCA-1)
6097	.4406	3.72	543	Polyphenylene (ABCHAR 413) 38.3%/Carbon Cloth (CCA-1)
6233*	.4454*	3.70*	544	Epoxy novolac (DEN 438) 28.8%/Carbon Cloth (CCA-1)
6133	.4418	8.55	545	Skygard 700 41.2%/Carbon Cloth (CCA-1)
.6192	.4439	4.71	546	2,2-Bis (p-hydroxyphenyl) propane-phenolformaldehyde 40.5%/Carbon Cloth (CCA-1)
.6108	.4410	4.31	547	2,2-Bid (p-hydroxyphenyl) propane-phenolformaldehyde 40.8%/Carbon Cloth (CCA-1)

re at termination of test.

(1) Impregnated with Sylgard 182.
(2) Impregnated with Silicone (R-7146).
(3) Impregnated with epoxy novolac (DEN 438).
(4) Impregnated with cyclic silicone epoxy (OZ 8-0903).

L

TABLE IV

POST TEST NOZZLE EROSION EVALUATION
ABLATIVE NOZZLE CHARACTERIZATION

Nozzle Number	(1) Char Depth (in.)	(2) Resin Degradation Rate (mils/sec)
*453	0.45	12.01
*464	0.47 to 0.54	12.52 to 13.85
*469	0.50	13.01
*470	0.50 to 0.52	12.70 to 13.05
*491	0.45	11.66
*506	0.45 to 0.50	12.79 to 13.78
*508	0.48	12.96
*510	0.40	16.41
*511	0.47 to 0.53	13.12 to 14.30
*512	0.45	14.73
513	0.42	17.72
*521	0.45 to 0.50	13.17 to 14.20
*523	0.46	13.43
*529	0.42 to 0.45	14.21 to 14.90
*530	0.45	13.59
*531	0.35 to 0.40	13.58 to 14.82
532	0.40	14.01
533	0.40	16.53
*534	0.40 to 0.45	11.52 to 12.30
*536	0.57	13.47
*537	0.45 to 0.55	11.43 to 13.16
538	0.38 to 0.44	16.19 to 17.89
539	0.37 to 0.43	15.94 to 17.60
*540	0.49	12.50
*542	0.51 to 0.54	13.78 to 14.36
*543	0.52	13.78
*544	0.55	14.09
545	0.25	19.05
546	0.40	13.[illegible]1
*547	0.3 to 0.5	11.09 to 15.61

Notes:

(1) Char depth measured at resultant throat with 6 inch scale.

(2) Resin degradation rate (d) calculated by adding calculated erosion rate and char depth rate.

(3)* Nozzles so marked experienced degradation extending past insert and into phenolic.

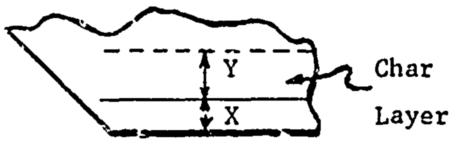

$$d = \frac{x}{t} + \frac{y}{t}$$

where

x = erosion

y = char depth

t = run time

TABLE V

POST TEST NOZZLE VISUAL EVALUATION
ABLATIVE NOZZLE CHARACTERIZATION

Nozzle	Evaluation
458	Bore rough, even erosion, cylindrical cracks, slight spalling
464	Bore rough, uneven erosion, cylindrical cracks, slight spalling
469	Bore rough, even erosion, slight cylindrical cracks
470	Bore rough, even erosion, slight cylindrical cracking, slight spalling
491	Bore rough, even erosion, slight cylindrical cracks
506	Bore smooth, uneven erosion, slight spalling
508	Bore rough, even erosion, cylindrical cracks
510	Bore smooth, even erosion, laminations
511	Bore smooth, even erosion, slight spalling
512	Bore smooth, even erosion, slight spalling
513	Bore rough, even erosion, cylindrical cracks and slight spalling
521	Bore rough, even erosion, cylindrical cracks
523	Bore smooth, even erosion, 2 cylindrical cracks
529	Bore rough, even erosion, slight cylindrical cracks, slight spalling
530	Bore rough, even erosion, slight cylindrical cracks
531	Bore smooth, even erosion, several cylindrical cracks, slight spalling
532	Bore rough, even erosion, slight cylindrical cracks, slight spalling
533	Bore rough, even erosion, slight cylindrical cracks and slight spalling
534	Bore smooth, even erosion
536	Bore smooth, uneven erosion, heavy spalling
537	Bore smooth, uneven erosion, slight spalling
538	Bore smooth, even erosion, slight cylindrical cracks
539	Bore smooth, even erosion, slight cylindrical cracks, slight spalling
540	Bore rough, even erosion, and cylindrical cracks
542	Bore rough, even erosion, wide cylindrical cracks
543	Bore rough, uneven erosion, cylindrical cracks
544	Bore rough, uneven erosion, cylindrical cracks and spalling
545	Rough bore, uneven erosion, laminations, and slight spalling
546	Bore smooth, uneven erosion, slight cylindrical cracks
547	Bore smooth, even erosion

TABLE VI

SOLID PROPELLANT SIMULATOR PERFORMANCE DATA
ABLATIVE NOZZLE CHARACTERIZATION

Nozzle Number	Total Flow Rate (lb/sec)	Oxygen Flow Rate (lb/sec)	Hydrogen Flow Rate (lb/sec)	Nitrogen Flow Rate (lb/sec)	Slurry Flow Rate (lb/sec)
458	.5902	.2124	.0142	.0514	.3122
464	.5918	.2127	.0139	.0526	.3126
469	.5822	.2091	.0139	.0504	.3088
470	.5952	.2169	.0143	.0522	.3118
491	.5868	.2107	.0138	.0507	.3116
506	.5932	.2142	.0145	.0520	.3125
508	.5801	.2066	.0136	.0511	.3088
510	.5924	.2164	.0144	.0526	.3091
511	.5913	.2142	.0141	.0513	.3116
512	.5924	.2135	.0141	.0513	.3137
513	.5994	.2191	.0137	.0520	.3146
521	.5966	.2169	.0146	.0516	.3135
523	.6000	.2181	.0144	.0521	.3154
529	.5913	.2147	.0138	.0515	.3113
530	.5941	.2130	.0144	.0517	.3150
531	.5883	.2136	.0142	.0517	.3088
532	.5934	.2162	.0143	.0517	.3112
533	.5961	.2182	.0141	.0510	.3128
534	.5966	.2172	.0142	.0514	.3138
536	.5916	.2152	.0142	.0506	.3116
537	.5875	.2110	.0142	.0507	.3116
538	.5929	.2150	.0139	.0504	.3136
539	.5914	.2142	.0139	.0511	.3122
540	.5950	.2176	.0142	.0516	.3116
542	.5902	.2141	.0139	.0506	.3116
543	.5906	.2116	.0142	.0515	.3135
544	.6037	.2214	.0141	.0519	.3163
545	.5940	.2157	.0139	.0508	.3136
546	.5997	.2193	.0139	.0511	.3154
547	.5916	.2116	.0138	.0508	.3154

TABLE VII

LIQUID PROPELLANT TEST SERIES TEST SPECIMEN DESCRIPTION ABLATIVE NOZZLE CHARACTERIZATION

DATA SHEET**	NOZZLE NUMBER	RESIN CHEMICAL TYPE	REINFORCEMENT AGENT	RESIN CONTENT (PERCENT)	MOLDING CONDITIONS PRESSURE (PSI)	MOLDING CONDITIONS TEMPERATURE (°F)	MOLDING CONDITIONS TIME (MINUTES)	POST CURE CYCLE	BARCOL HARDNESS	DENSITY gm./cc
275	454	Polyimide I-8 N.A.	Refrasil Cloth C100-48	N.A.	4,000	710	120	II	N.A.	1.55
313	474	Polyphenylene (B2353-42)	Refrasil Cloth C100-48	41.0	300	425	180	X	30	1.42
424A	548	2,2-Bis (p-hydroxyphenyl) propane-phenolformaldehyde	Refrasil Cloth C100-48	42.2	10,000	300	120	III	68	1.52
393	549	Polybenzimidazole AFR-151 (Imidite 2803)	Refrasil Cloth C100-48	40.4	10,000	700	180	V	50	1.60
393	550	Polybenzimidazole AFR-151 (Imidite 2803)	Refrasil Cloth C100-48	39.8	10,000	700	180	V	50	1.59
424B	551	2,2-Bis (p-hydroxyphenyl) propane-phenolformaldehyde	Refrasil Cloth C100-48	39.4	10,000	300	120	III	65	1.59
401	552	Phenolic (91LD)	Refrasil Cloth C100-48	41.1	10,000	300	120	III	75	1.63
401	553	Phenolic (91LD)	Refrasil Cloth C100-48	40.3	10,000	300	120	III	76	1.61
401	554	Phenolic (91LD)	Refrasil Cloth C100-48	38.4	10,000	300	120	III	75	1.62
405	555	Epoxy novolac (DEN 438)	Refrasil Cloth C100-48	32.1	4,823	300	120	VII	N.A.	1.60
405	557	Epoxy novolac (DEN 438)	Refrasil Cloth C100-48	31.9	4,823	300	120	VII	N.A.	1.63
433	558	Polyphenylene (ABCHAR 413)*	Refrasil Cloth C100-48	N.A.	3,500	400	120	VI	N.A.	1.49
433	559	Polyphenylene (ABCHAR 413)*	Refrasil Cloth C100-48	N.A.	3,500	400	120	VI	N.A.	1.53
466A	561	Epoxy novolac (DEN 438)	Boron Fibers	21.8 - 32.0	500	300	120	XI	N.A.	2.03
433B	562	Polyphenylene (ABCHAR 413)*	Refrasil Cloth C100-48	N.A.	10,000	400	120	VI	N.A.	1.42
489	566	Phenolic (91LD)	Astroquartz #570	36.0	10,000	300	120	III	75	1.67
489	567	Phenolic (91LD)	Astroquartz #570	36.6	10,000	300	120	III	75	1.70
490	570	Phenolic (91LD)	Astrosil 11341-B	36.5	10,000	300	120	III	80	1.60
490	571	Phenolic (91LD)	Astrosil 11341-B	35.0	10,000	300	120	III	80	1.60

*Includes Para-polyphenylene (ABCHAR 503) Filler. See Table IB.
**Hughes Aircraft data sheet numbers are from reports shown in the "Foreword."

TABLE VIII

LIQUID PROPELLANT MOTOR CHECKRUN PERFORMANCE DATA

ABLATIVE NOZZLE CHARACTERIZATION

SIMULATOR CHECKRUN NUMBER	TOTAL FLOW RATE (LB/SEC)	INITIAL STABILIZED CHAMBER PRESSURE (PSIA)	CALCULATED C* (FT/SEC)	EFFICIENCY (PERCENT)	MIXTURE RATIO (O/F)
1	0.3551	304.0	5399	96.9	1.598
2	0.3582	306.8	5397	96.9	1.598
3	0.3586	304.6	5360	96.3	1.602
4	0.3584	304.6	5368	96.4	1.612
5	0.3500	297.6	5406	96.1	1.608

NOZZLE NUMBER	TIME (SEC)	MAXIMUM CHAMBER PRESSURE (PSIA)	ORIGINAL THROAT DIAMETER (IN.)	MINIMUM CHAMBER PRESSURE (PSIA)	TOTAL FLOWRATE (LB/SEC)	TIME 250 PSIA (SEC)	CALCULATED THROAT AREA 250 PSIA (IN^2)	CALCULATED THROAT RADIUS 250 PSIA (IN)	CALCULATED EROSION RATE 250 PSIA (MILS/SEC)	TIME 200 PS[illegible] (SEC)
454	84.40	360	0.5012	100	0.3503	20.6	0.2363	0.2742	1.15	34.[illegible]
474	177.10	364	0.5002	101	[illegible].3493	29.0	0.2356	0.2738	0.82	54[illegible]
548	184.0	361	0.5007	100	0.3518	32.0	0.2373	0.2748	0.76	57.[illegible]
549	233.5	373	0.4924	132	0.3529	39.5	0.2381	0.2753	0.74	65.[illegible]
550	229.8	343	0.5004	100	0.3484	47.0	0.2351	0.2736	0.50	73.[illegible]
551	171.6	330	0.5005	100	0.3510	36.3	0.2368	0.2746	0.67	68.[illegible]
552	182.3	315	0.5007	136	0.3502	30.5	0.2363	0.2742	0.78	52.[illegible]
553	212.8	309	0.5008	152	0.3438	71.5	0.2353	0.2737	0.33	105[illegible]
554	213.8	315	0.5012	100	0.3480	48.6	0.2348	0.2734	0.47	83[illegible]
555	41.0	320	0.5009	310	0.3508					
557	38.0	397	0.5066	310	0.3497					
558	150.0	348	0.5017	100	0.3486	25.3	0.2352	0.2736	0.90	50[illegible]
559	188.3	340	0.5023	100	0.3496	29.0	0.2359	0.2740	0.79	59[illegible]
561	12.3	320	0.5034	114	0.3514	4.0	0.2371	0.2747	5.76	[illegible]
562	65.5	342	0.5080	100	0.3518	23.0	0.2373	0.2748	0.91	33[illegible]
566	185.8	338	0.5038	100	0.3515	65.3	0.2371	0.2747	0.35	97[illegible]
567	124.0	37[illegible]	0.5032	208	0.3509	83.0	0.2367	0.2745	0.28	[illegible]
570	239.6	335	0.5019	109	0.3501	56.5	0.2362	0.2742	0.41	11[illegible]
571	190.9	337	0.5022	100	0.3459	40.5	0.2361	0.2741	0.57	8[illegible]
400	30.4	384	0.5025	100	0.3507	8.3	0.2346	0.2733	2.65	1[illegible]

A

TABLE IX

CALCULATED AND MEASURED VALUES USED IN EROSION PROPERTY ANALYSIS
LIQUID PROPELLANT TEST SERIES

...TED ...RATE ...IA ...EC)	TIME 200 PSIA (SEC)	CALCULATED THROAT AREA 200 PSIA (IN^2)	CALCULATED THROAT RADIUS 200 PSIA (IN)	CALCULATED EROSION RATE 200 PSIA (MILS/SEC)	TIME 150 PSIA (SEC)	CALCULATED THROAT AREA 150 PSIA (IN^2)	CALCULATED THROAT RADIUS 150 PSIA (IN)	CALCULATED EROSION RATE 150 PSIA (MILS/SEC)	TIME 100 PSIA (SEC)	CALCULATED THROAT AREA 100 PSIA (IN^2)
	34.8	0.2954	0.3066	1.61	55.0	0.3939	0.3540	1.88	84.4	0.5908
	54.3	0.2945	0.3062	1.03	94.0	0.3926	0.3535	1.10	177.1*	0.5768*
	57.0	0.2967	0.3073	0.99	104.5	0.3956	0.3548	1.00	184.0	0.5934
	65.5	0.2976	0.3078	0.94	102.5	0.3968	0.3553	1.06	233.3*	0.1596*
	73.0	0.2938	0.3058	0.76	117.3	0.3918	0.3531	0.85	229.8	0.5876
	68.2	0.2960	0.3070	0.83	102.5	0.3947	0.3543	1.02	171.6	0.5920
	52.3	0.2953	0.3066	1.08	94.0	0.3938	0.3540	1.10	182.3*	0.3175*
	105.5	0.2942	0.3060	0.53					212.8*	0.2775*
	83.2	0.2935	0.3056	0.66	164.0	0.3913	0.3529	0.62	213.8	0.5870
									41.0*	0.0954*
									38.0*	0.1486*
	50.0	0.2940	0.3059	1.10	83.5	0.3920	0.3532	1.23	150.0	0.5880
	59.2	0.2948	0.3063	0.93	104.8	0.3931	0.3536	0.98	188.8	0.5897
	5.5	0.2963	0.3071	10.07	8.3	0.3951	0.3546	12.40	12.3*	0.5217*
	31.5	0.2967	0.3073	1.69	41.2	0.3956	0.3548	2.45	65.5	0.5934
	97.0	0.2964	0.3072	0.57	124.0	0.3952	0.3546	0.83	185.8	0.5929
									134.0*	0.1879*
	119.3	0.2952	0.3065	0.47	199.5	0.3937	0.3539	0.52	239.6*	0.5437*
	83.0	0.2951	0.3065	0.67	125.0	0.3934	0.3538	0.82	190.9	0.5902
	13.2	0.2932	0.3055	4.11	18.7	0.3910	0.3526	5.42	30.4	0.5865

CALCULATED THROAT AREA 100 PSIA (IN^2)	CALCULATED THROAT RADIUS 100 PSIA (IN)	CALCULATED EROSION RATE 100 PSIA (MILS/SEC)	NOZZLE NUMBER	MATERIAL RESIN/REINFORCEMENT
0.5908	0.4337	2.17	454	Polyimide I-8 N.A./Refrasil Cloth (C100-48)
0.5768*	0.4284*	1.01*	474	Polyphenylene (B2353-42) 41%/Refrasil Cloth (C100-48)
0.5934	0.4346	1.00	548	2,2-Bis (p-hydroxyphenyl) propane-phenolformaldehyde, 42.2%/Refrasil Cloth (C100-48)
0.1596*	0.2254*	-0.09*	549	Polybenzimidazole AFR-151 (Imidite 2803) 40.4%/Refrasil Cloth (C100-48)
0.5876	0.4324	0.79	550	Polybenzimidazole AFR-151 (Imidite 2803) 39.8%/Refrasil Cloth (C100-48)
0.5920	0.4340	1.07	551	2,2-Bis (p-hydroxyphenyl) propane-phenolformaldehyde, 39.4%/Refrasil Cloth (C100-48)
0.3175*	0.3179*	0.37*	552	Phenolic (91LD) 41.1%/Refrasil Cloth (C100-48)
0.2775*	0.2972*	0.22*	553	Phenolic (91LD) 40.3%/Refrasil Cloth (C100-48)
0.5870	0.4322	0.85	554	Phenolic (91LD) 38.4%/Refrasil Cloth (C100-48)
0.0954*	0.1743*	-1.86*	556	Epoxy novolac (DEN 438) 32.1%/Refrasil Cloth (C100-48)
0.1486*	0.2175*	-0.94*	557	Epoxy novolac (DEN 438) 31.9%/Refrasil Cloth (C100-48)
0.5880	0.4326	1.21	558	Polyphenylene (ABCHAR 413) (1) N.A./Refrasil Cloth (C100-48)
0.5897	0.43	0.96	559	Polyphenylene (ABCHAR 413) (1) N.A./Refrasil Cloth (C100-48)
0.5217*	0.407	12.67*	561	Epoxy novolac (DEN 438) 21.8-32.0%/Boron fibers
0.5934	0.4346	2.76	562	Polyphenylene (ABCHAR 413) (1) N.A./Refrasil Cloth (C100-48)
0.5929	0.4355	0.99	566	Phenolic (91LD) 36.0%/Astroquartz #570
0.1879*	0.2446*	-0.05*	567	Phenolic (91LD) 36.6%/Astroquartz #570
0.5437*	0.4160*	0.69*	570	Phenolic (91LD) 36.5%/Astrosil 11341-B
0.5902	0.4334	0.96	571	Phenolic (91LD) 35.0%/Astrosil 11341-B
0.5865	0.4359	6.07	409	CCA-1/Polybenzimidazole (Imidite)

*Calculated at chamber pressure at termination of test
(1)Includes Para-polyphenylene (ABCHAR 600) filler. See Table IB.

TABLE X

MOTOR PERFORMANCE DATA

ABLATIVE NOZZLE CHARACTERIZATION

Liquid Propellant Test Series

NOZZLE NUMBER	TOTAL FLOW RATE (lb./sec.)	NTO FLOW RATE (lb./sec.)	50/50 FLOW RATE (lb./sec.)	MIXTURE RATIO
454	0.3503	0.2156	0.1347	1.6006
474	0.3492	0.2156	0.1336	1.6138
548	0.3518	0.2166	0.1352	1.6021
549	0.3529	0.2169	0.1360	1.5948
550	0.3484	0.2144	0.1340	1.6000
551	0.3510	0.2171	0.1339	1.6214
552	0.3502	0.2154	0.1348	1.5979
553	0.3488	0.2140	0.1348	1.5875
554	0.3480	0.2131	0.1349	1.5797
556	0.3508	0.2166	0.1342	1.6140
557	0.3497	0.2148	0.1349	1.5923
558	0.3486	0.2139	0.1347	1.5880
559	0.3496	0.2147	0.1349	1.5915
561	0.3514	0.2168	0.1346	1.6107
562	0.3518	0.2162	0.1356	1.5944
566	0.3515	0.2174	0.1341	1.6218
567	0.3509	0.2161	0.1348	1.6031
570	0.3501	0.2161	0.1340	1.6127
571	0.3499	0.2159	0.1340	1.6112

TABLE XI

POST TEST NOZZLE EROSION EVALUATION
ABLATIVE NOZZLE CHARACTERIZATION

Liquid Propellant Test Series

NOZZLE NUMBER	CHAR[(1)] DEPTH (in.)	RESIN[(2)] DEGRADATION RATE (mils/sec.)
454	0.20	0.00455
474	0.50 (0.15)*	0.00383
548	0.70 (0.20)*	0.00481
549	Not Measurable	
550	0.50 (0.15)*	0.00297
551	0.45 (0.10)*	0.00370
552	Not Measurable	
553	0.65 (0.20)*	0.00328
554	0.55 (0.20)*	0.00389
556	0.35	0.00669
557	0.25	0.00572
558	0.60 (0.10)*	0.00522
559	0.60 (0.20)*	0.00414
561	0.15	0.02500
562	0.40	0.00893
566	0.50 (0.15)*	0.00369
567	0.50	0.00369
570	0.70 (0.25)*	0.00361
571	0.35 (0.05)*	0.00279

NOTES:

(1) Char depth measured at resultant throat.

(2) Resin degradation rate (d) calculated by adding calculated erosion rate and char depth rate.

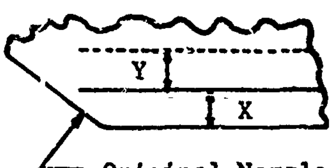

Original Nozzle Profile

$$d = \frac{x}{t} + \frac{y}{t}$$

Where:

x = Erosion
y = Char Depth
t = Run Time

* ( ) Amount of char depth in specimen holder.

TABLE XII

POST TEST SPECIMEN VISUAL EVALUATION
ABLATIVE NOZZLE CHARACTERIZATION

Liquid Propellant Test Series

NOZZLE	EVALUATION
454	Smooth, even erosion with a thick molten resin coating covering throat, laminations visible.
474	Smooth, even erosion with a slight molten resin coating.
548	Molten leading edge that has started to collapse unevenly; molten resin coating on throat with a 20° sector streak at 1 o'clock position.
549	Test specimen completely washed out.
550	Smooth, even erosion with a slight molten resin coating.
551	Smooth, even erosion with a slight molten resin coating.
552	Test specimen completely washed out.
553	Smooth, even erosion with a slight molten resin coating; some uneven erosion due to a 20° sector streak at the 5 o'clock position.
554	Smooth, even erosion with a slight molten resin coating; some uneven erosion due to a 15° sector streak at the 5 o'clock position.
556	Molten leading edge collapsed toward the throat; a thick coating of molten resin in throat.
557	Leading edge undercut, molten, and partially collapsed toward throat, slight spalling.
558	Smooth, even erosion except for 15° sector streak at 5 o'clock position, molten resin coated.
559	Molten leading edge with slight collapsing toward throat, light molten resin on throat with one deep spall.
561	Slight spalling, laminations visible with no resin coating.
562	Medium spalling with a slight molten resin coating.
566	Smooth, even erosion with a molten resin coating.

TABLE XII (CONTINUED)

POST TEST SPECIMEN VISUAL EVALUATION
ABLATIVE NOZZLE CHARACTERIZATION

Liquid Propellant Test Series

NOZZLE	EVALUATION
567	Molten leading edge with slight collapsing toward throat, smooth molten resin coating.
570	Leading edge undercut deeply and partially washed away; surface smooth with a thin molten resin coating.
571	Smooth, even erosion with a molten resin coating.

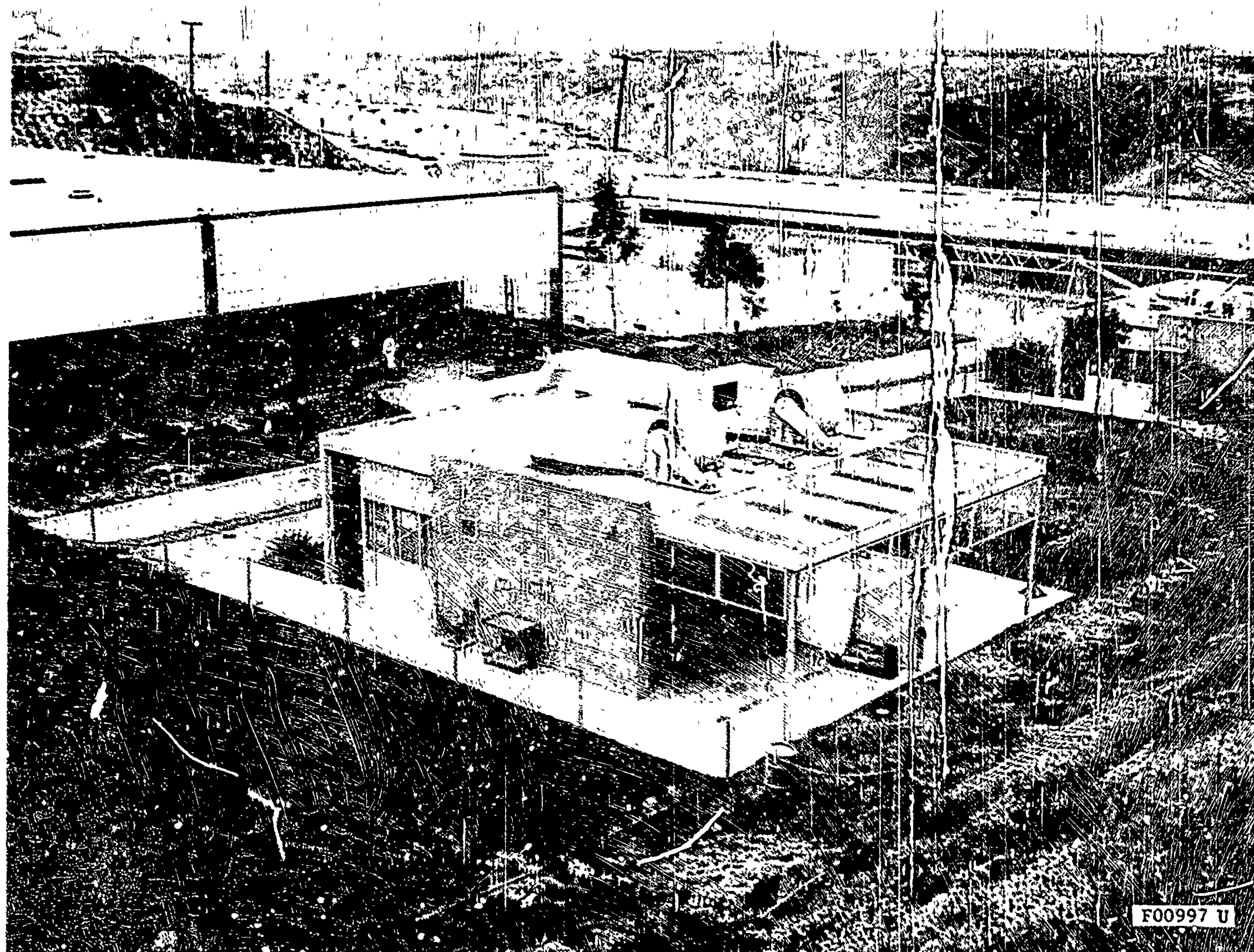

FIGURE 1. AEROTHERMOCHEMICAL LABORATORY TEST CELLS 6 AND 7

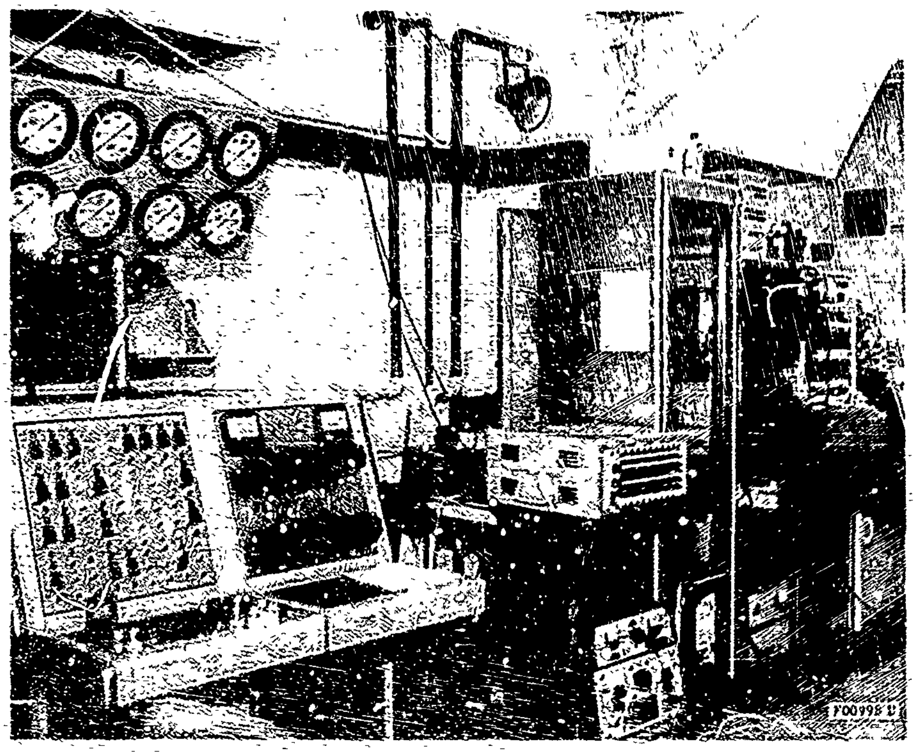

FIGURE 2. ATC TEST CELL 6 CONTROL ROOM

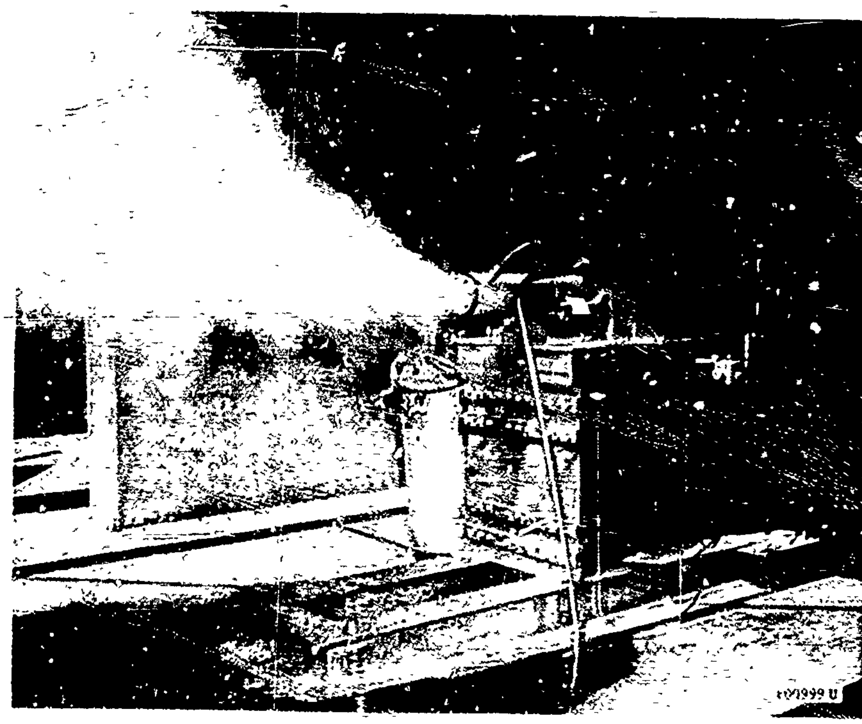

FIGURE 3. TEST SIMULATOR FIRING

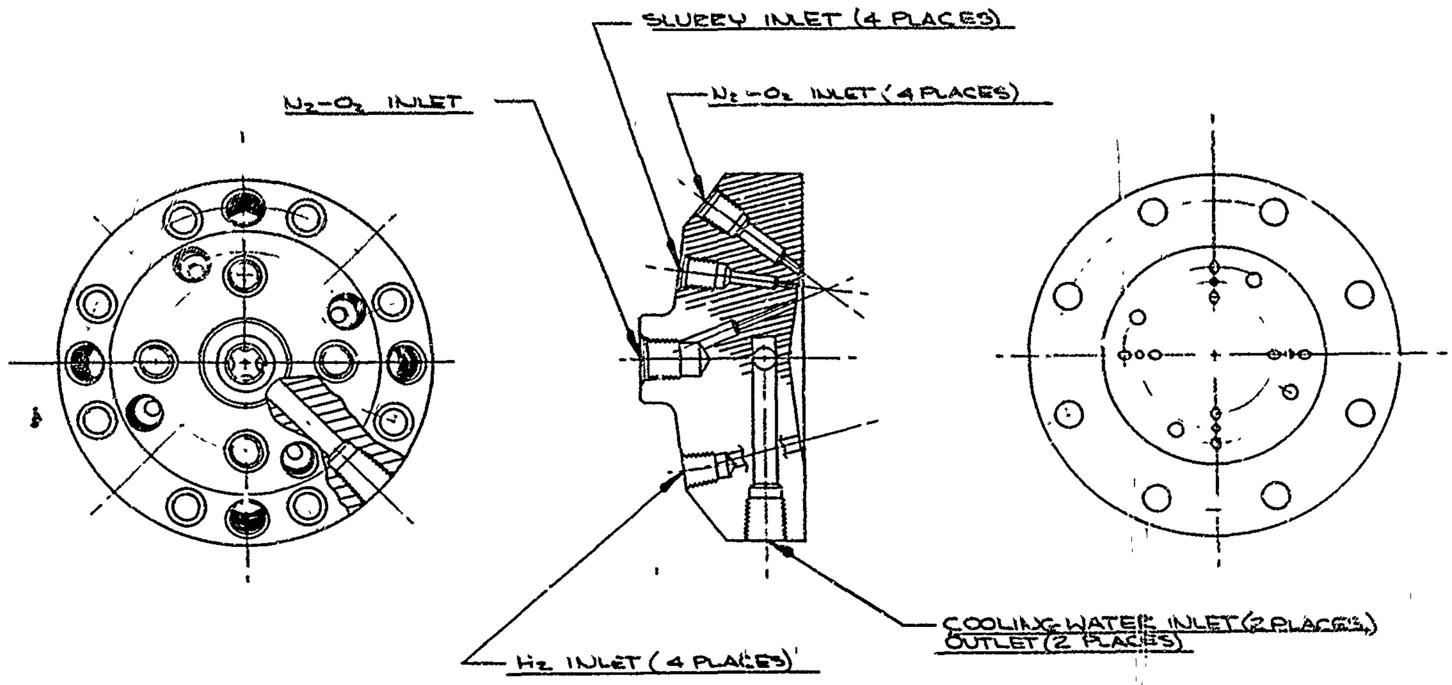

F01000 U

FIGURE 4. SOLID PROPELLANT SIMULATOR ROCKET MOTOR INJECTOR - WRIGHT FIELD NOZZLE TEST (COPPER)

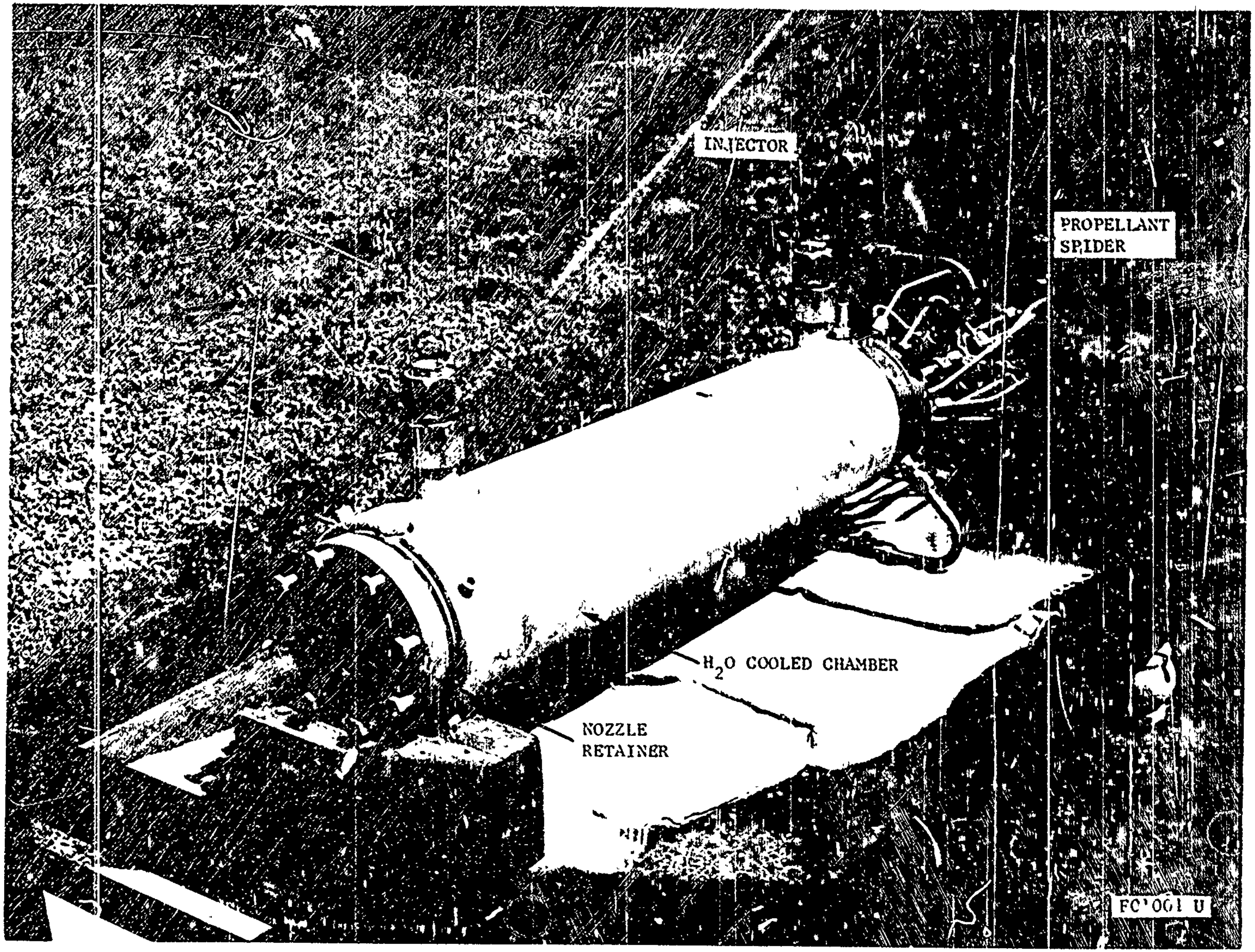

FIGURE 5. SOLID PROPELLANT SIMULATOR ROCKET MOTOR HARDWARE

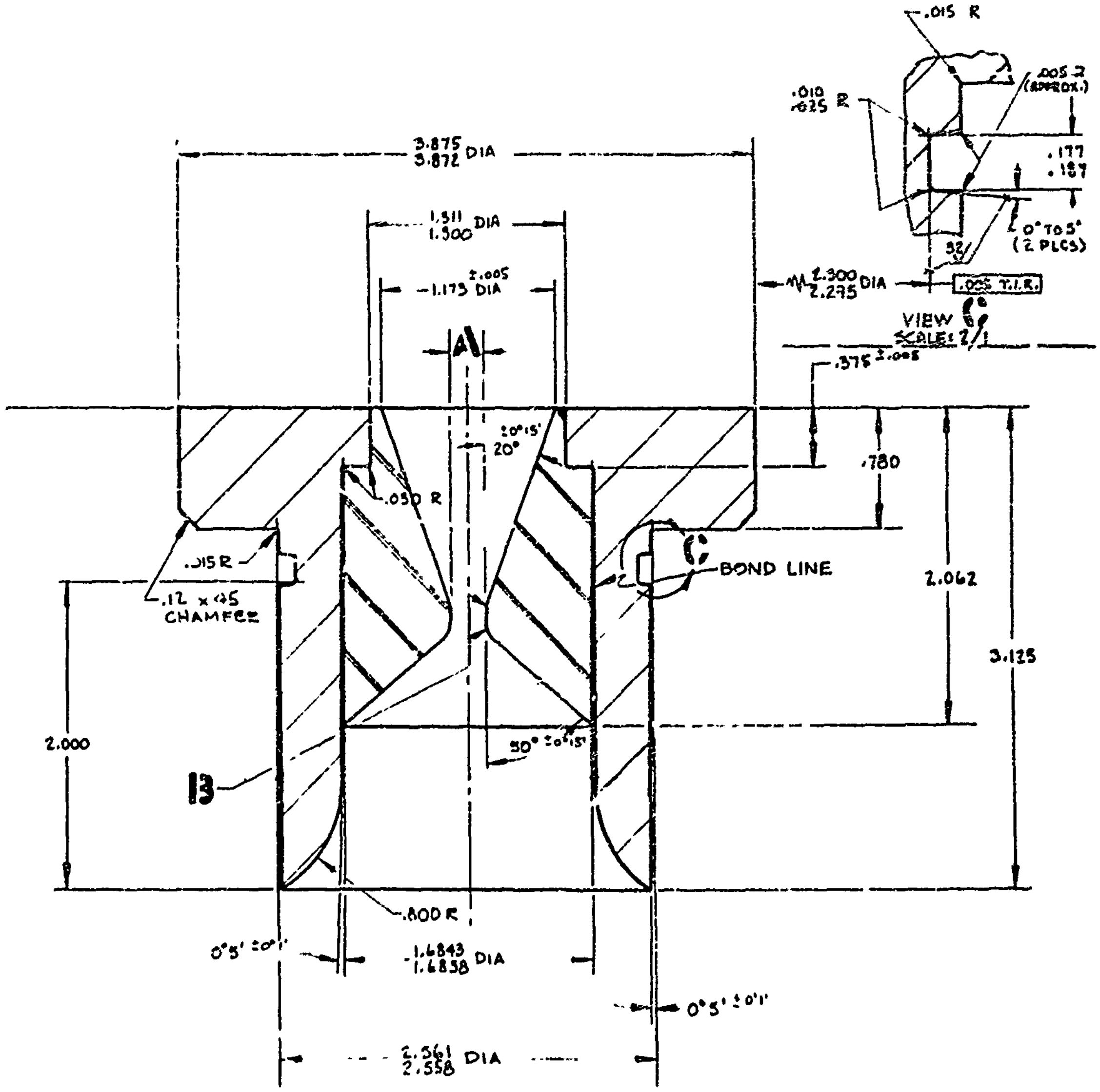

NOTE: A SHRINK FACTOR OF .001 IN/IN HAS BEEN ADDED TO THE PART DIMENSIONS TO PRODUCE THE DIMENSIONS SHOWN

	A	B
-1	.500	.38

F01002 U

FIGURE 6. TYPICAL TEST NOZZLE SPECIMEN SCHEMATIC

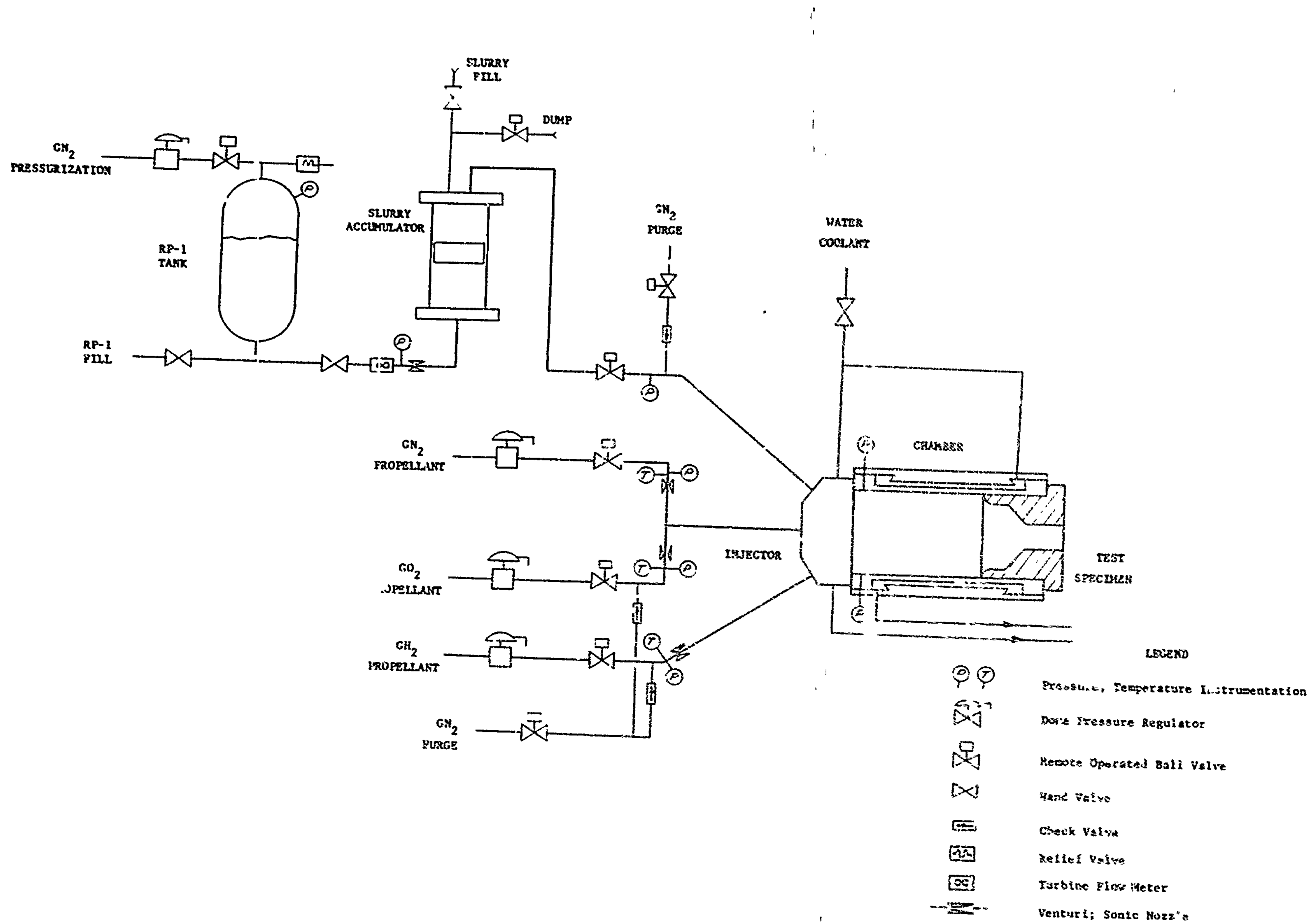

FIGURE 7. SOLID PROPELLANT SIMULATED ROCKET MOTOR TEST CELL SCHEMATIC

F01003 U

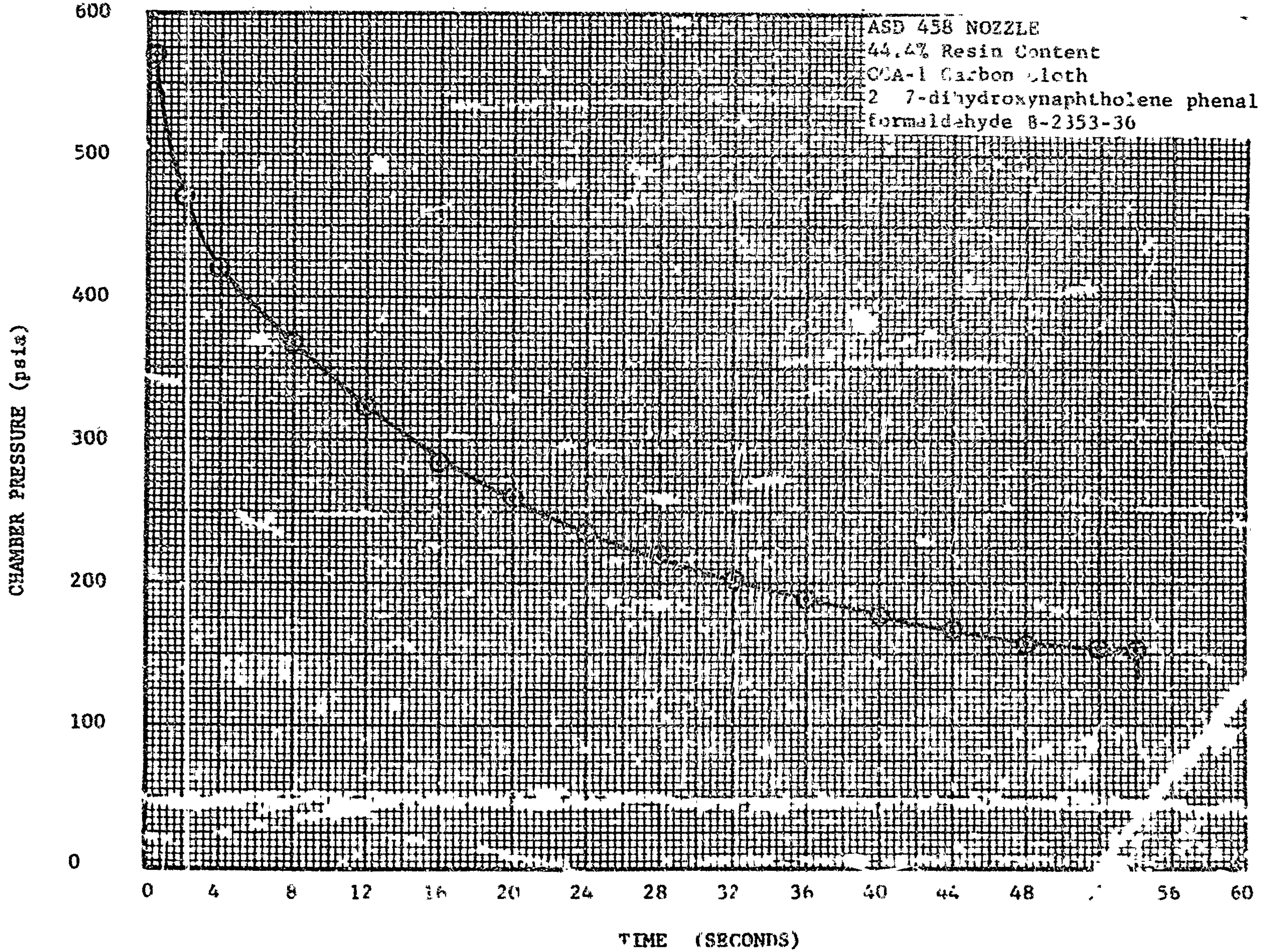

FIGURE 8. ASD NOZZLE 458 - CHAMBER PRESSURE VS. TIME

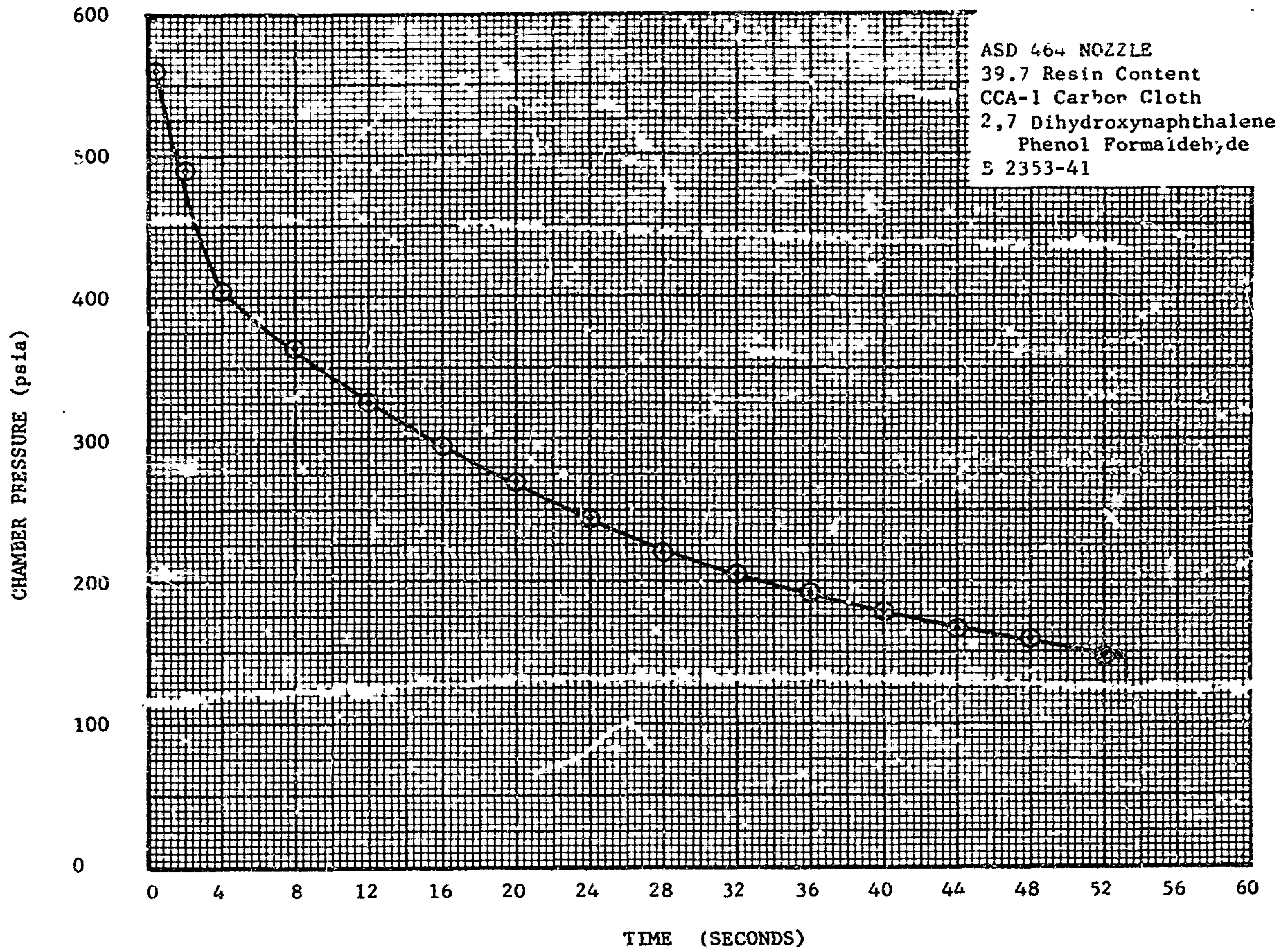

FIGURE 9. ASD NOZZLE 464 - CHAMBER PRESSURE VS. TIME

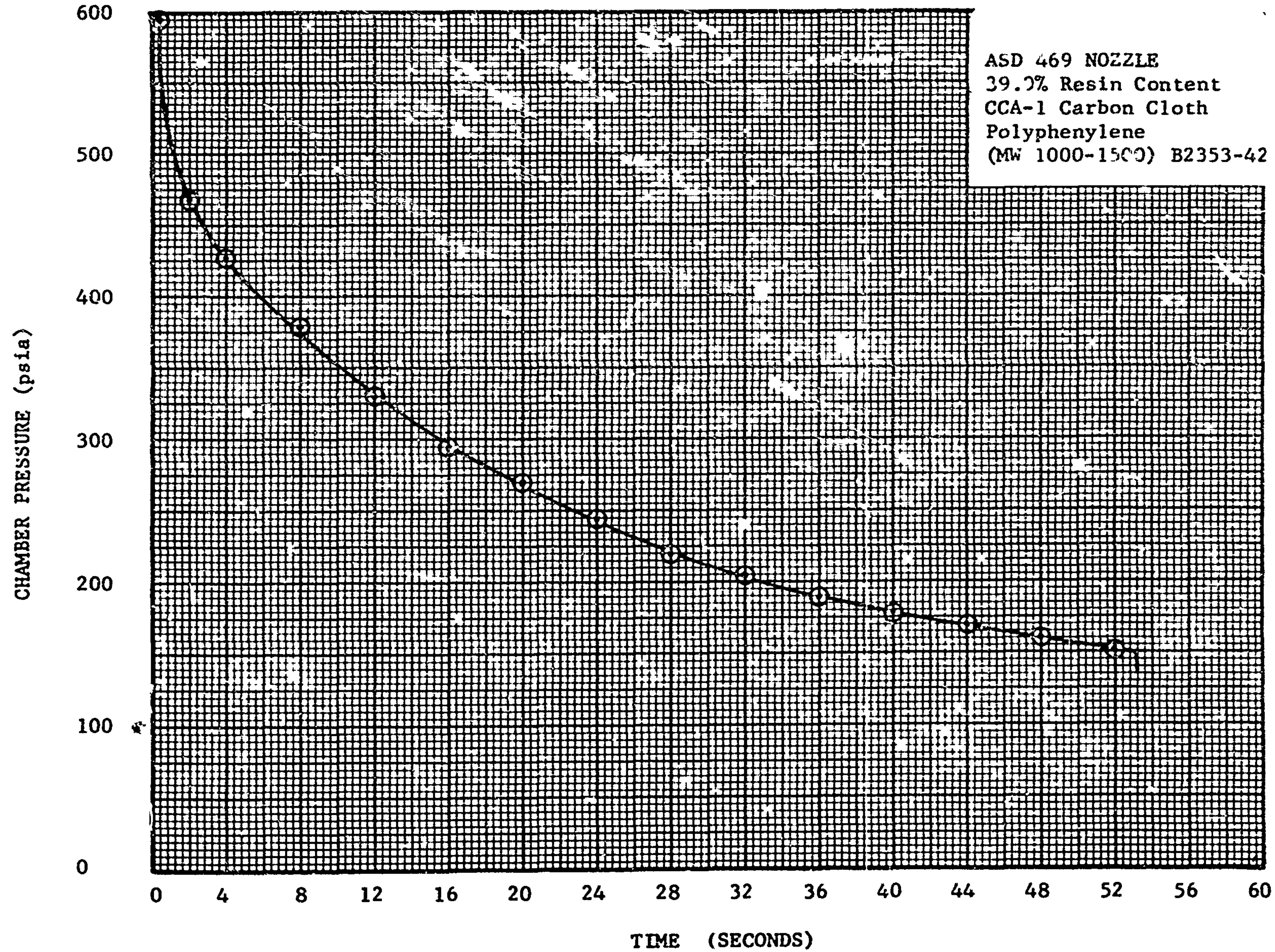

FIGURE 10. ASD NOZZLE 469 - CHAMBER PRESSURE VS. TIME

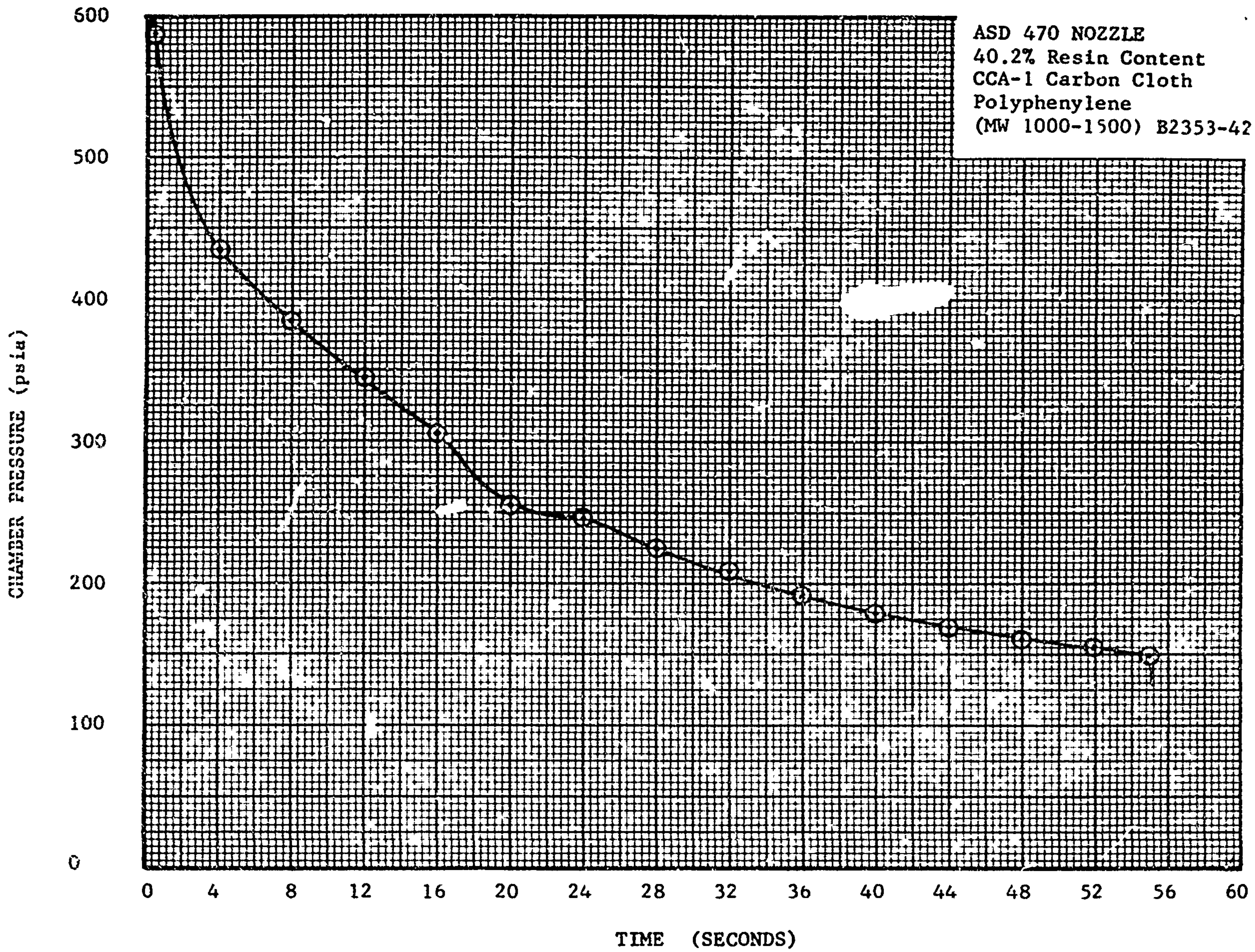

FIGURE 11. ASD NOZZLE 470 - CHAMBER PRESSURE VS. TIME

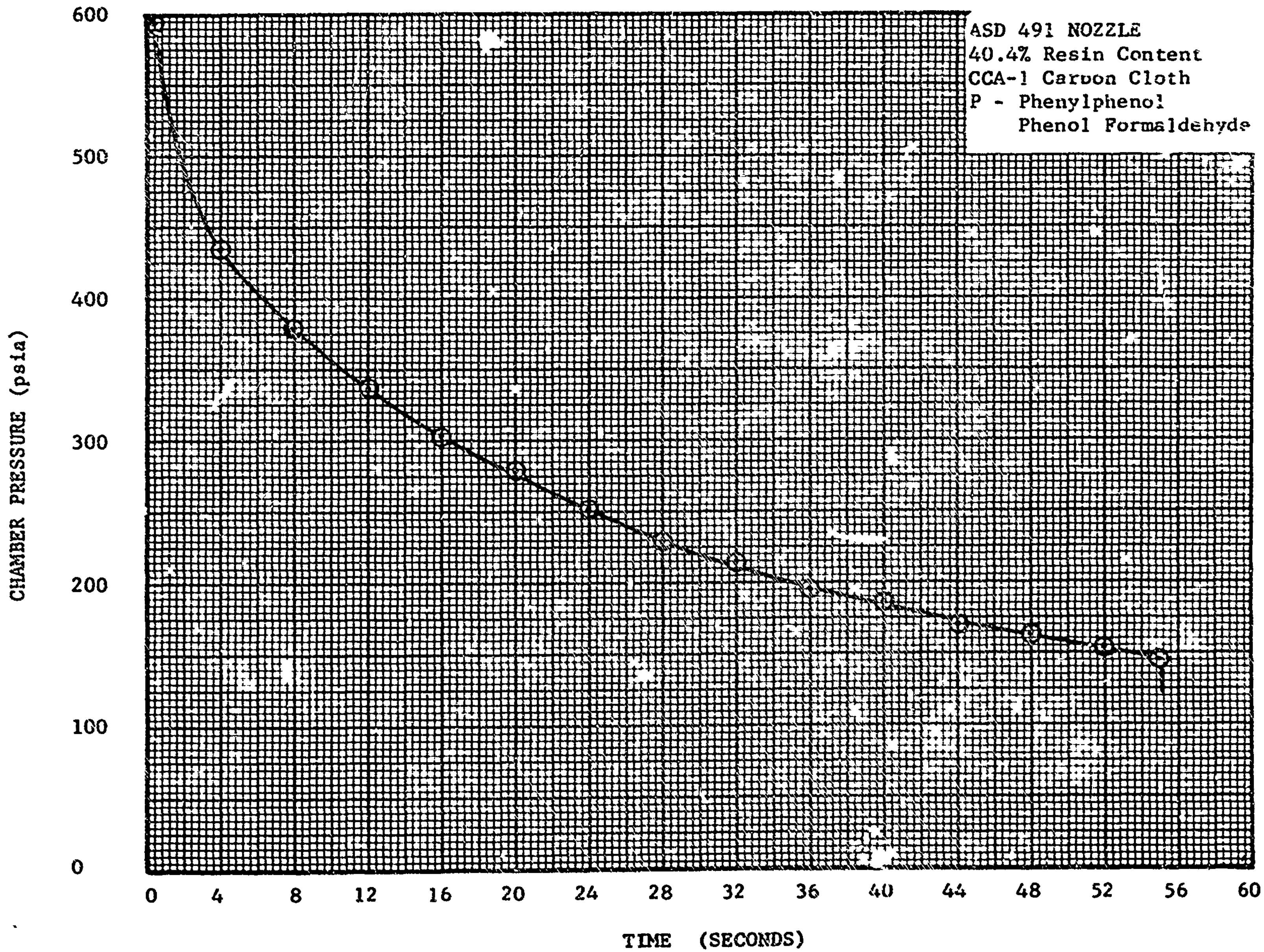

FIGURE 12. ASD NOZZLE 491 - CHAMBER PRESSURE VS. TIME

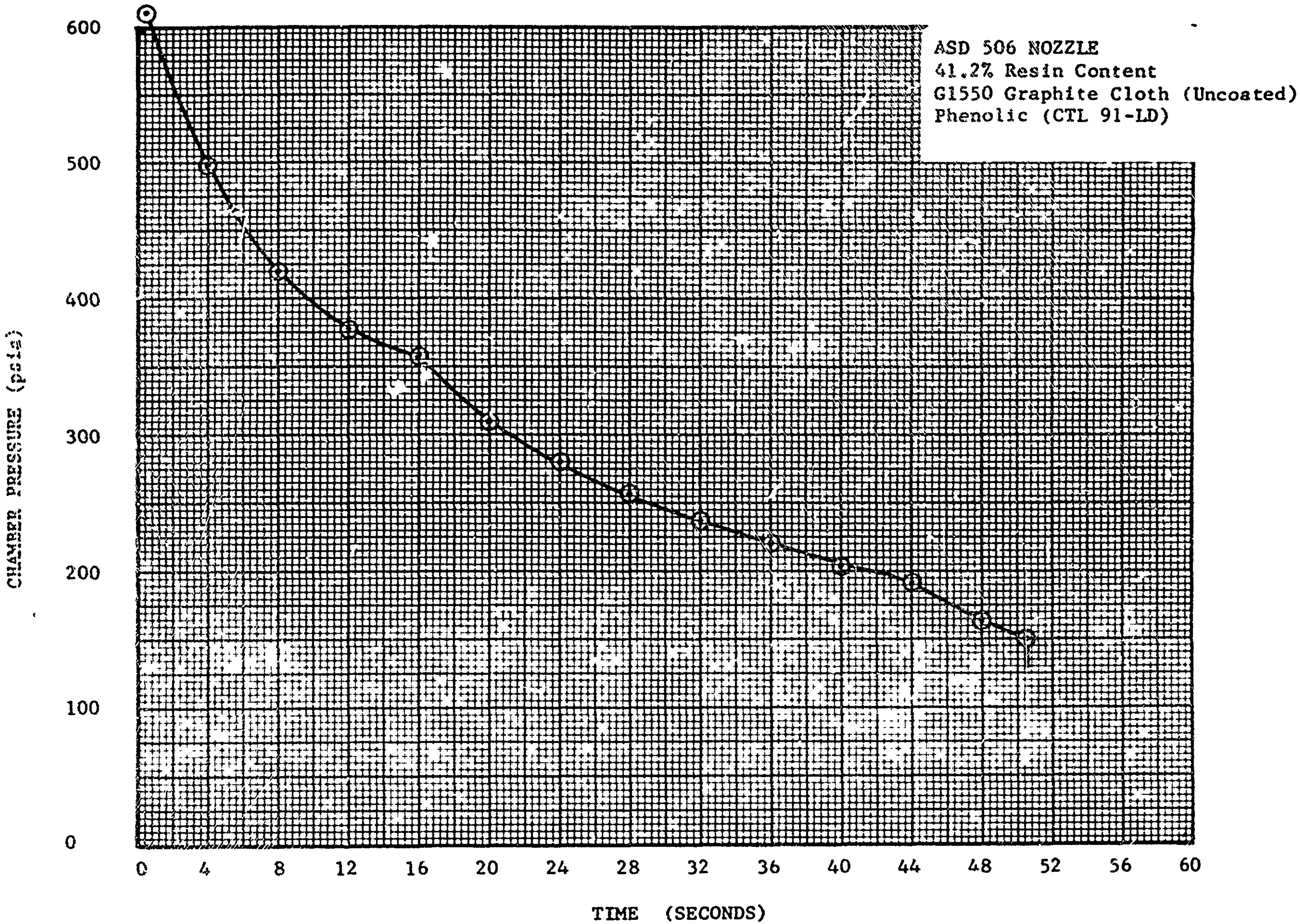

FIGURE 13. ASD NOZZLE 506 - CHAMBER PRESSURE VS. TIME

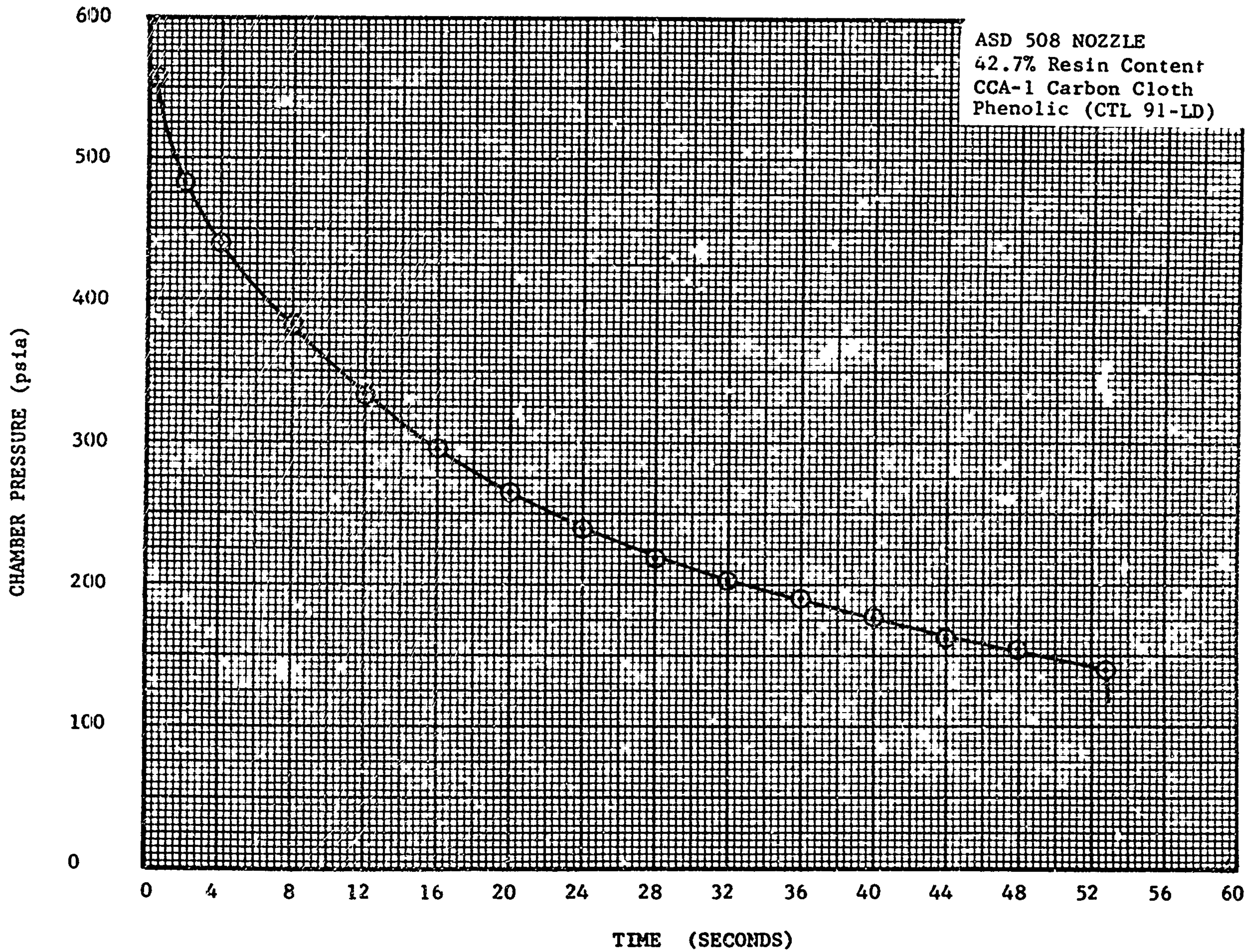

FIGURE 14. ASD NOZZLE 508 - CHAMBER PRESSURE VS. TIME

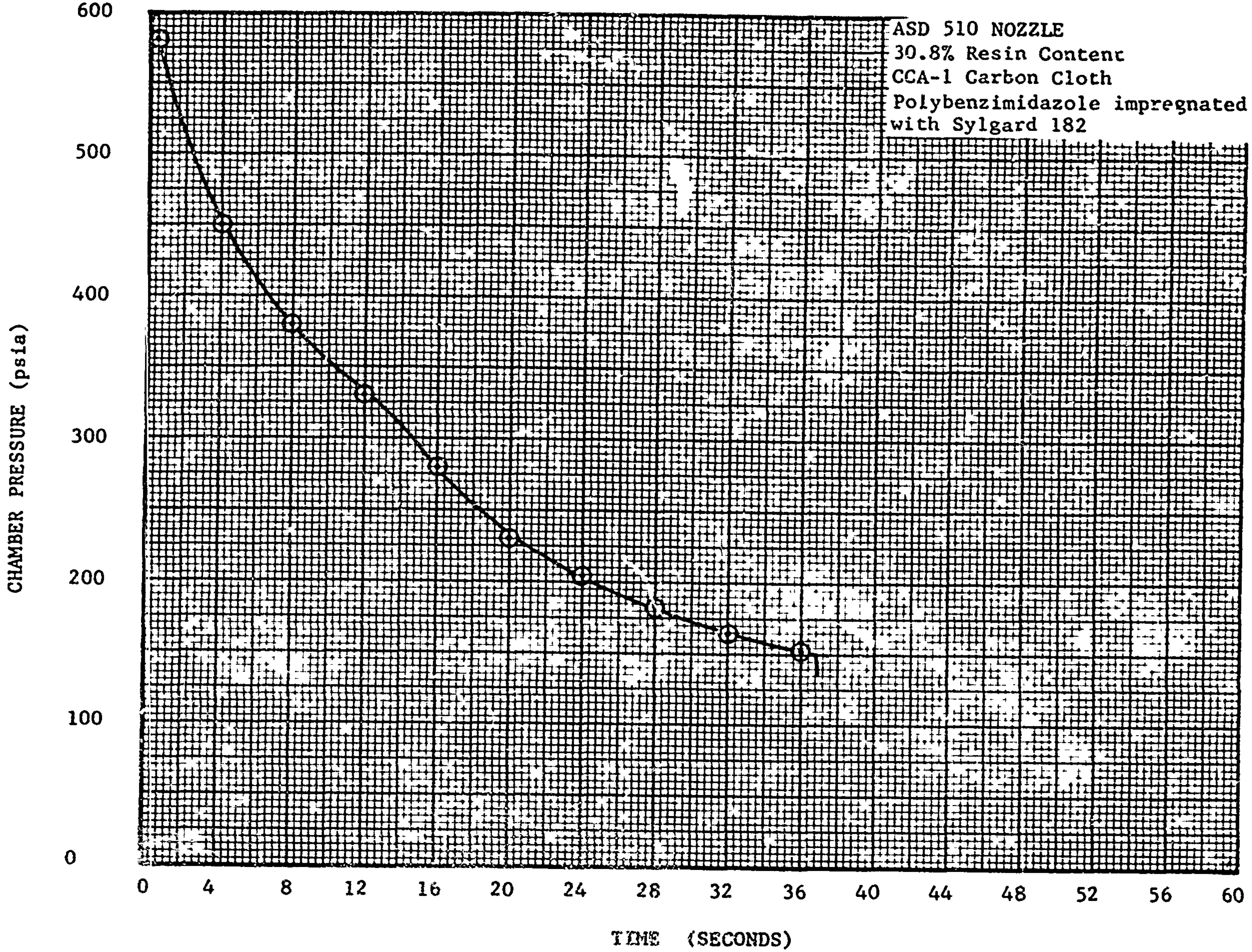

FIGURE 15. ASD NOZZLE 510 - CHAMBER PRESSURE VS. TIME

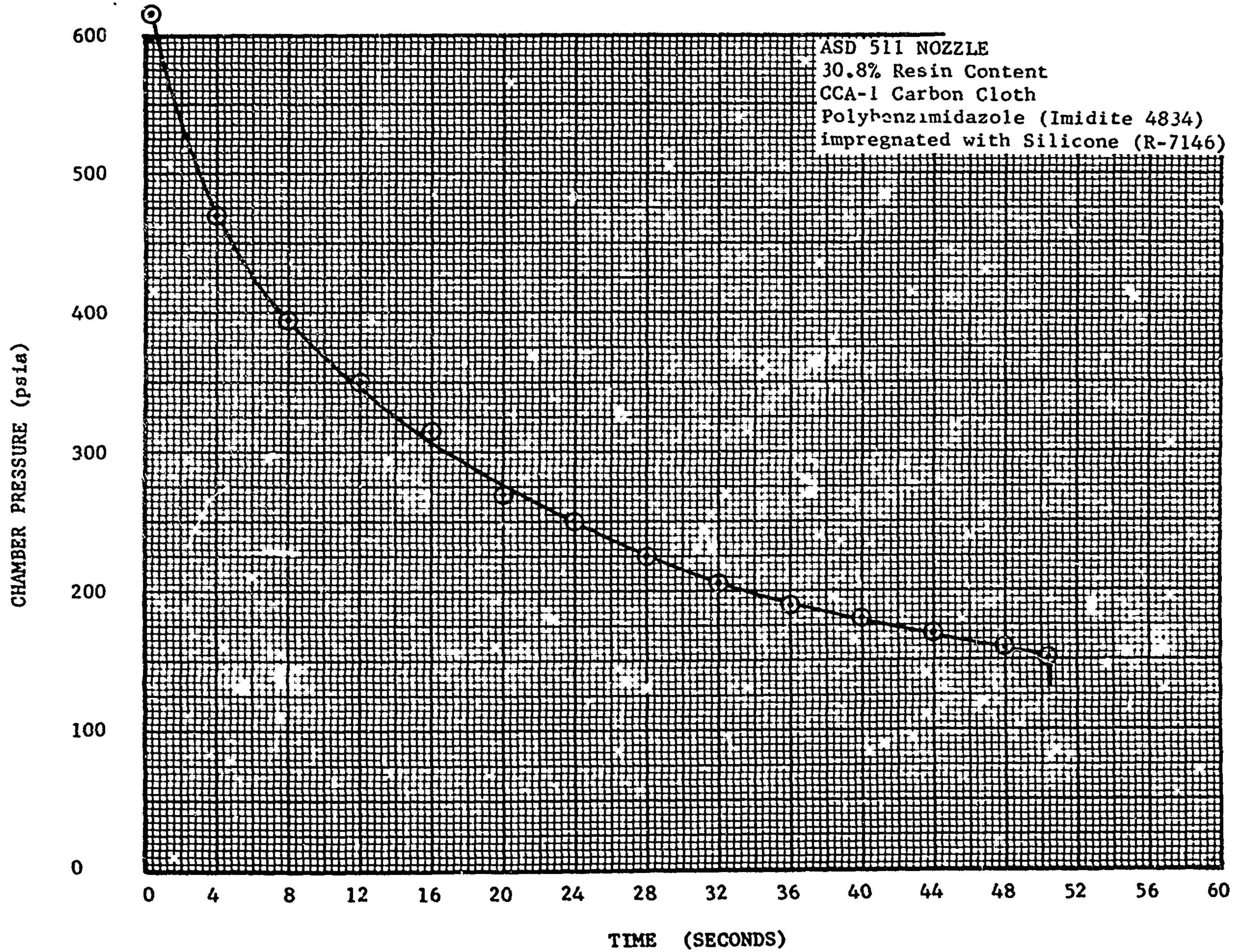

FIGURE 16. ASD NOZZLE 511 - CHAMBER PRESSURE VS. TIME

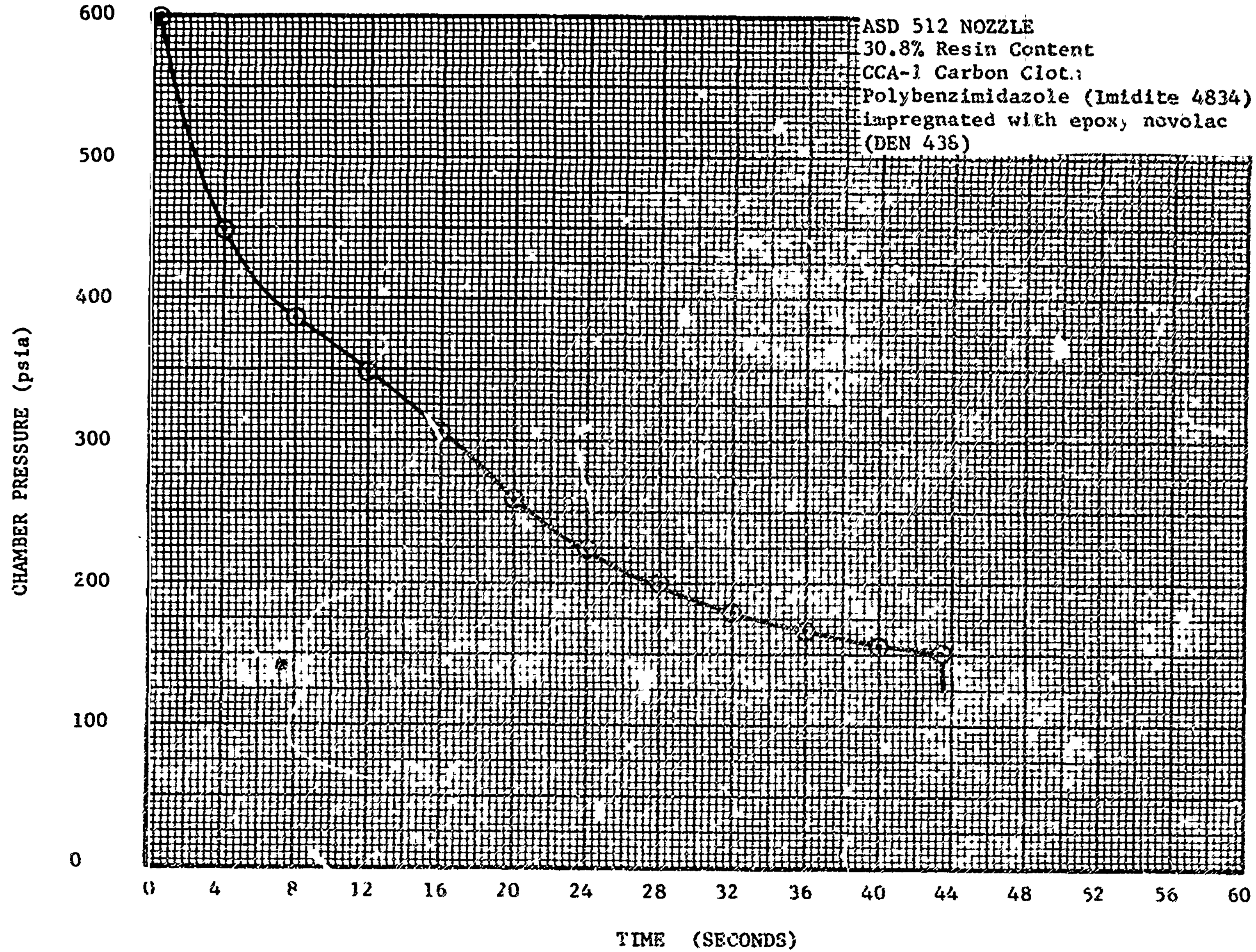

FIGURE 17. ASD NOZZLE 512 - CHAMBER PRESSURE VS. TIME

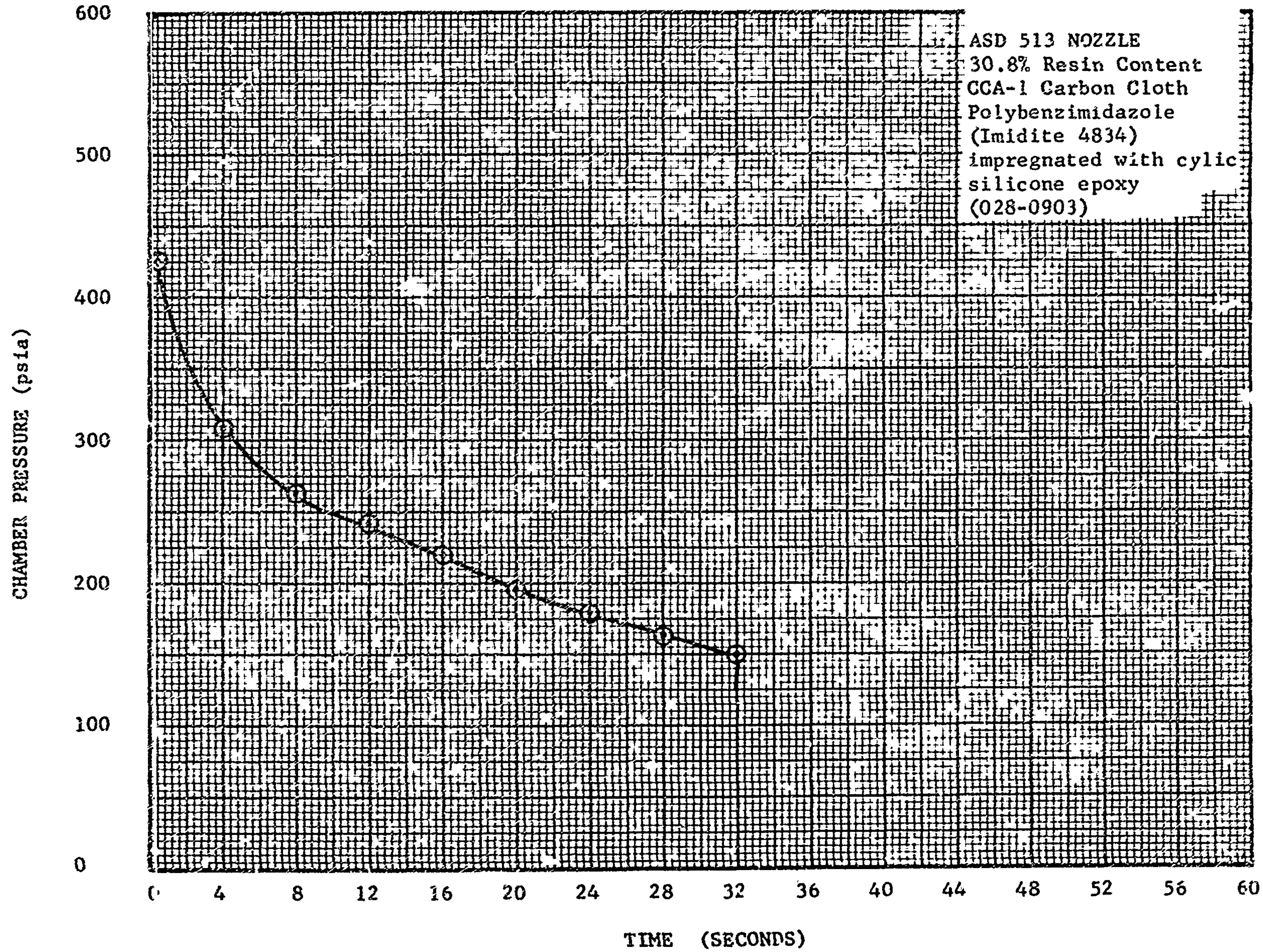

FIGURE 18. ASD NOZZLE 513 - CHAMBER PRESSURE VS. TIME

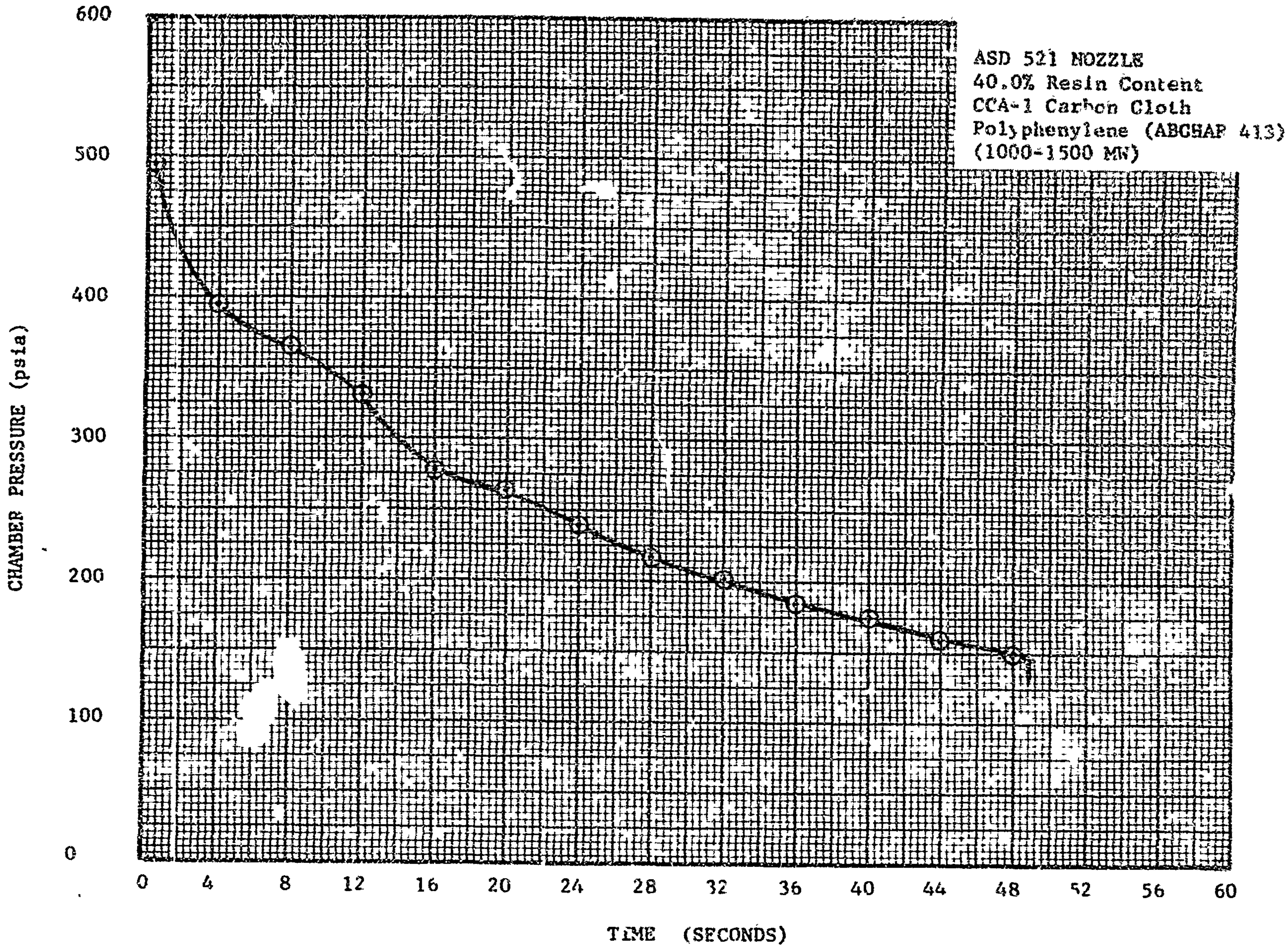

FIGURE 1?. ASD NOZZLE 521 - CHAMBER PRESSURE VS. TIME

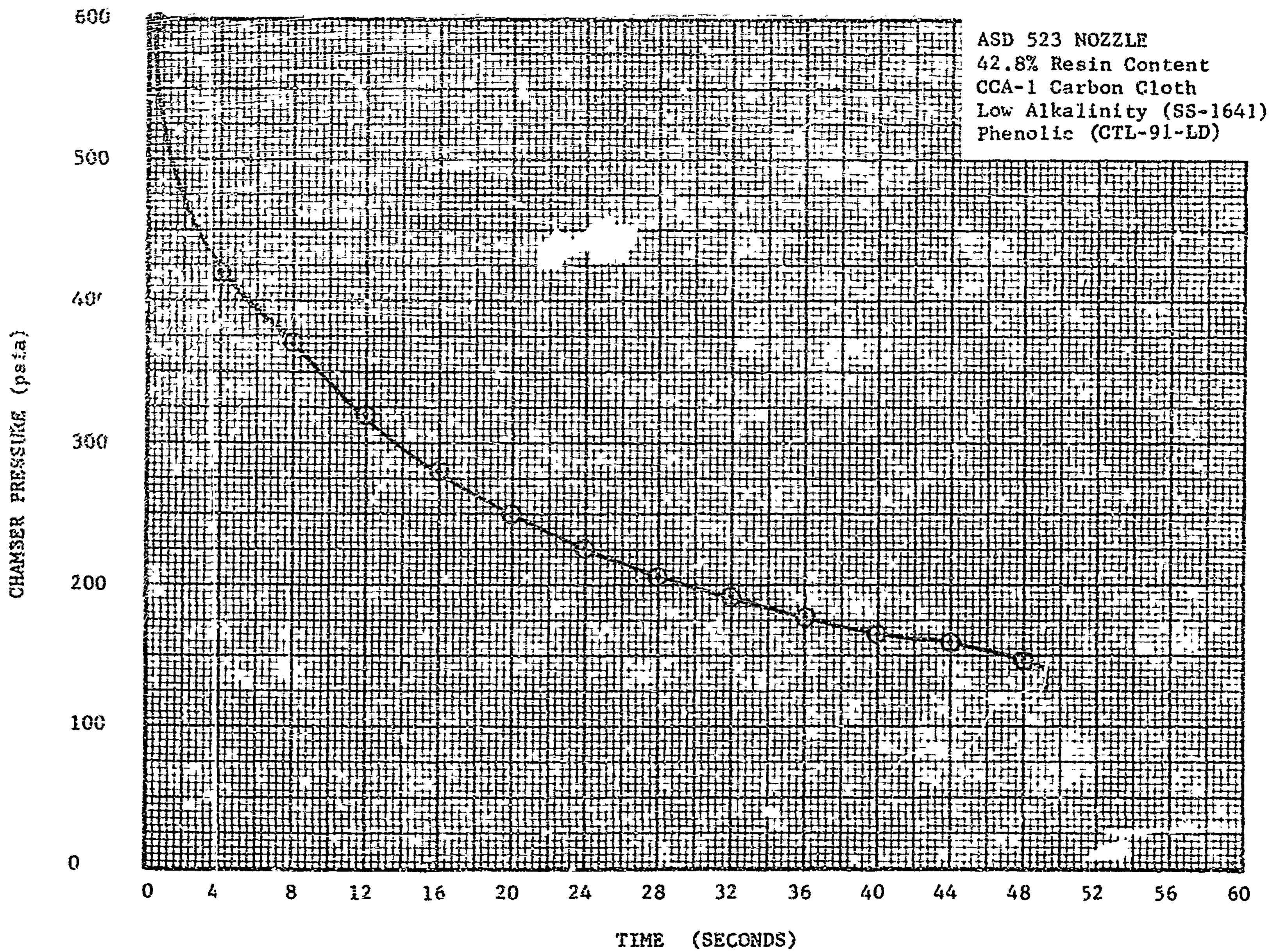

FIGURE 20. ASD NOZZLE 523 - CHAMBER PRESSURE VS. TIME

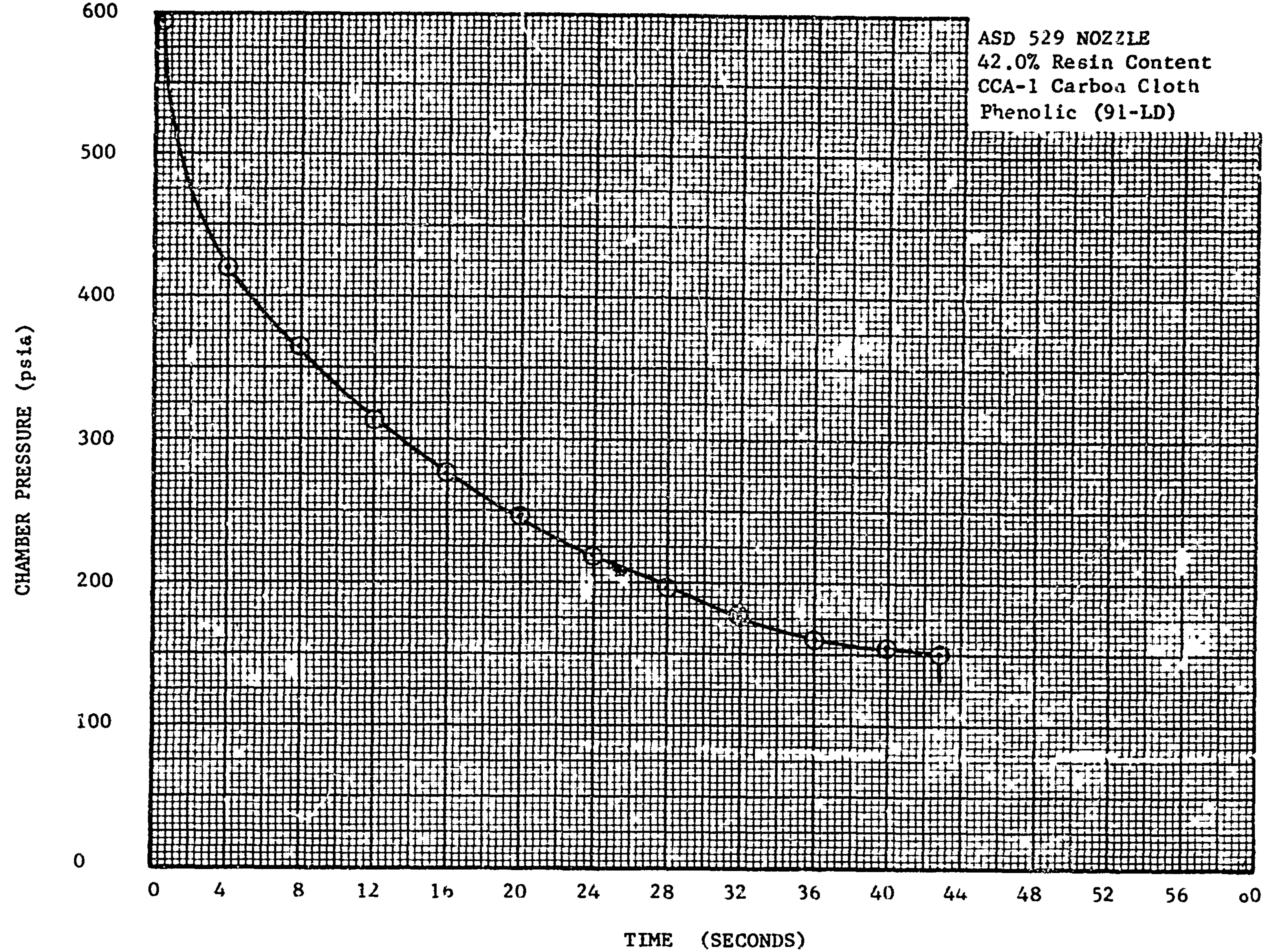

FIGURE 21. ASD NOZZLE 529 - CHAMBER PRESSURE VS. TIME

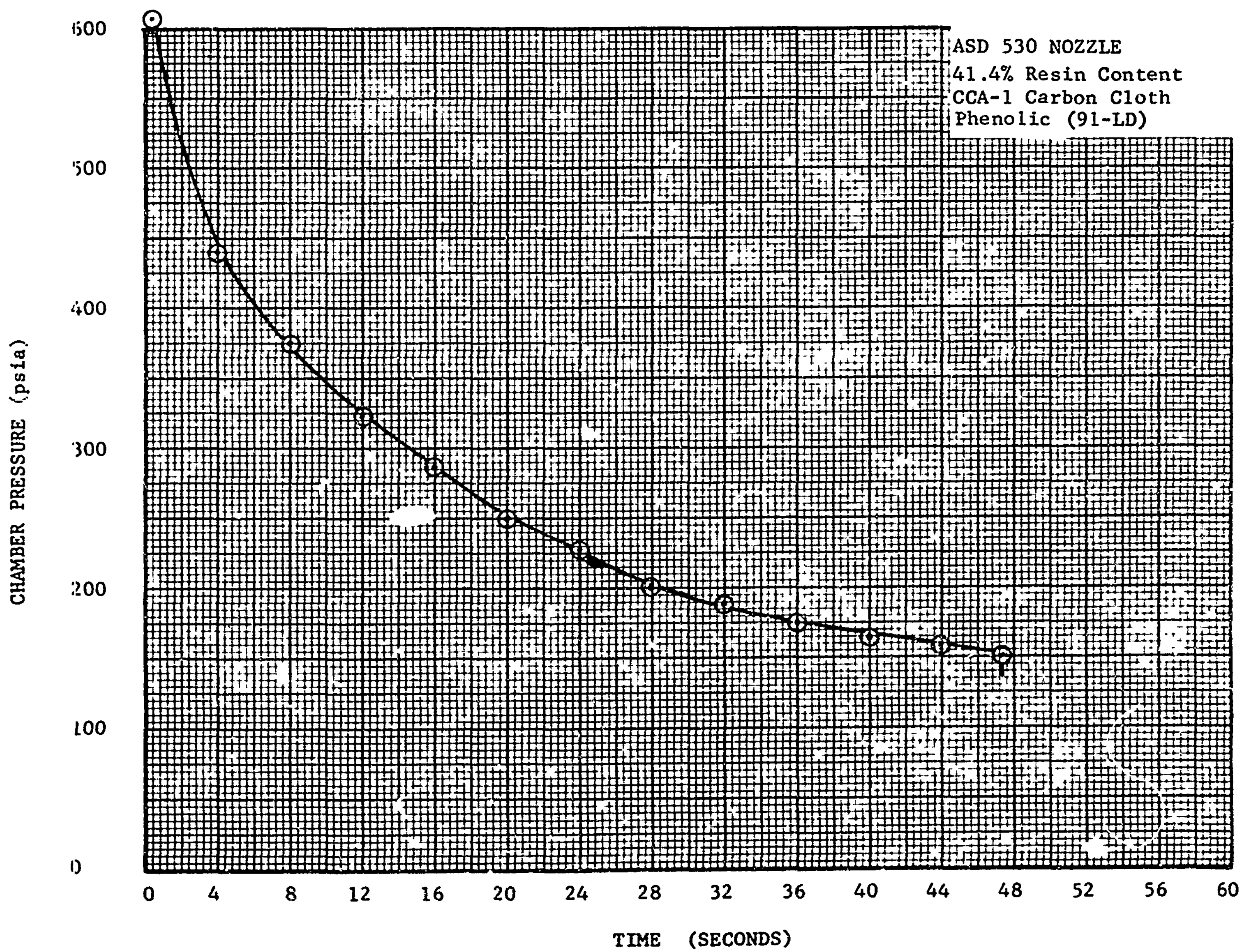

FIGURE 22. ASD NOZZLE 530 - CHAMBER PRESSURE VS. TIME

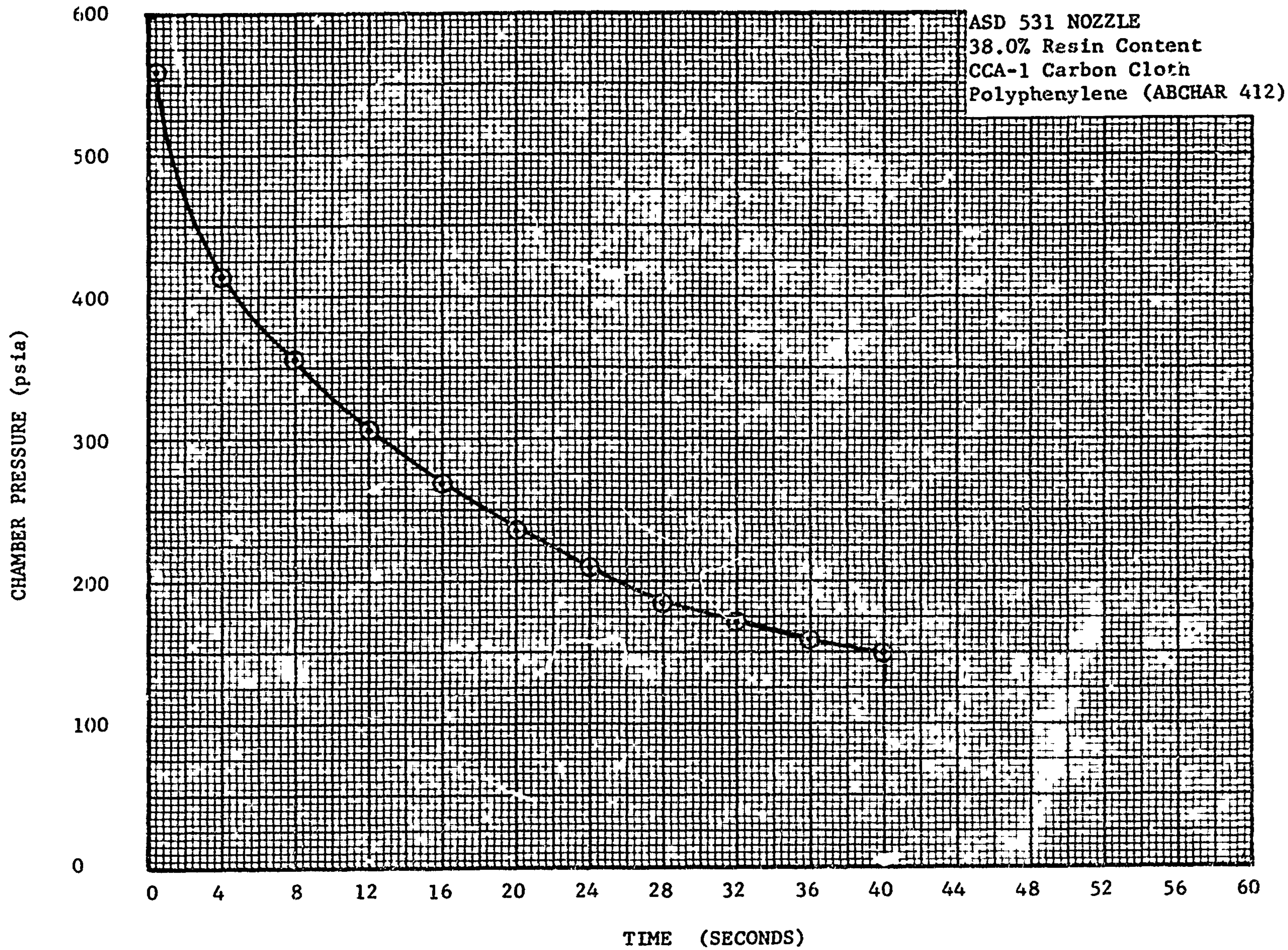

FIGURE 23. ASD NOZZLE 531 - CHAMBER PRESSURE VS. TIME

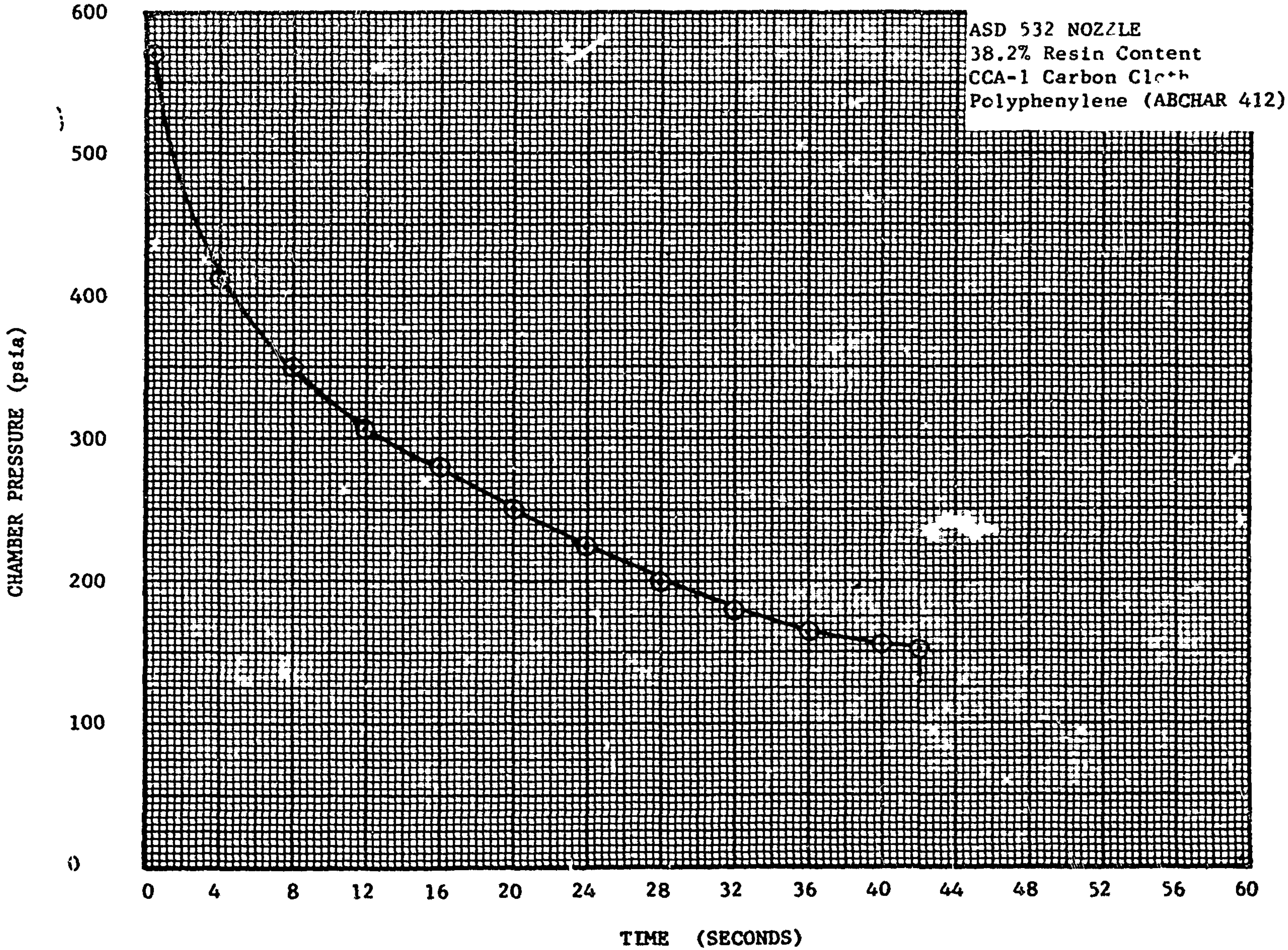

FIGURE 24. ASD NOZZLE 532 - CHAMBER PRESSURE VS. TIME

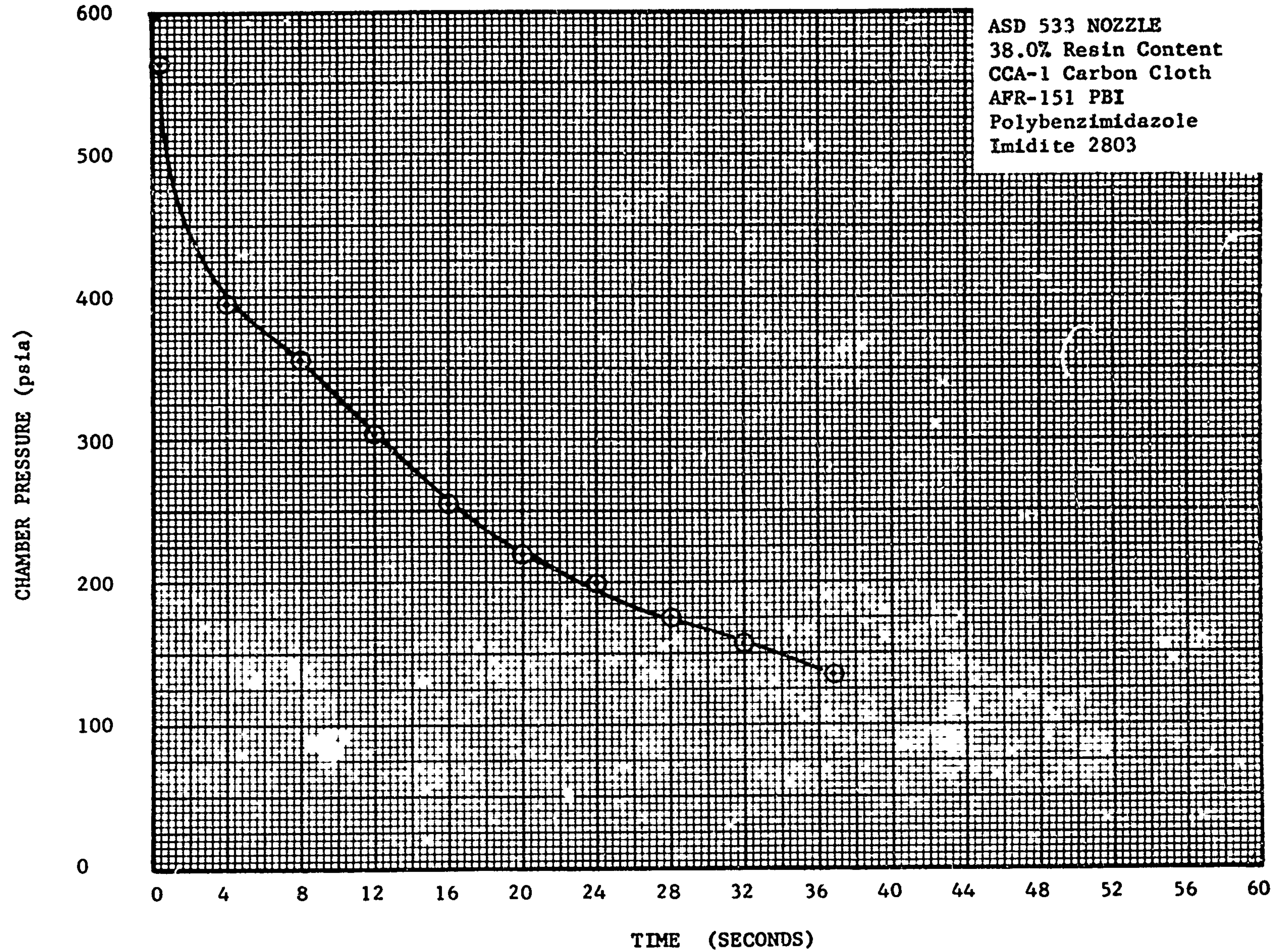

FIGURE 25. ASD NOZZLE 533 - CHAMBER PRESSURE VS. TIME

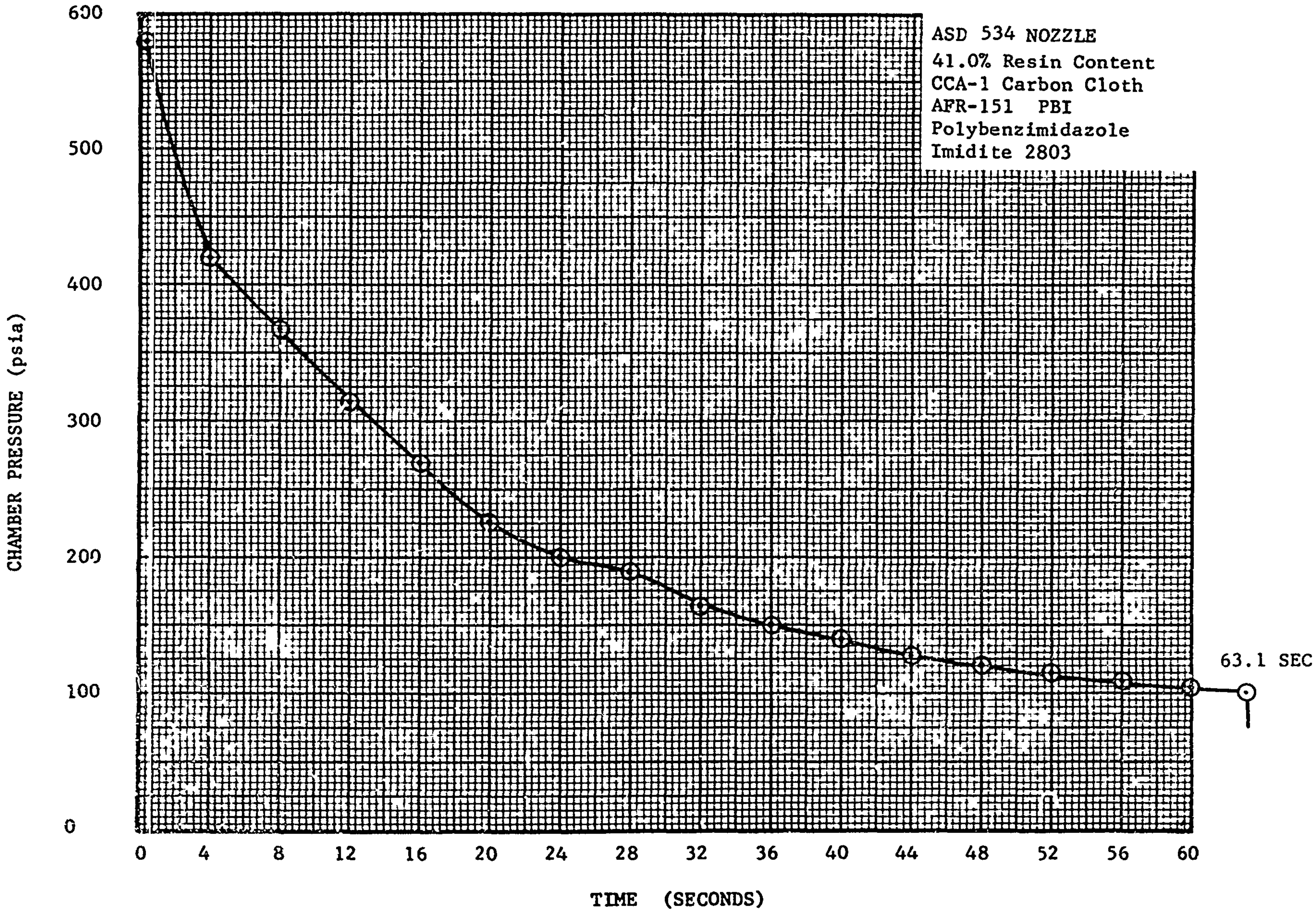

FIGURE 26. ASD NOZZLE 534 - CHAMBER PRESSURE VS. TIME

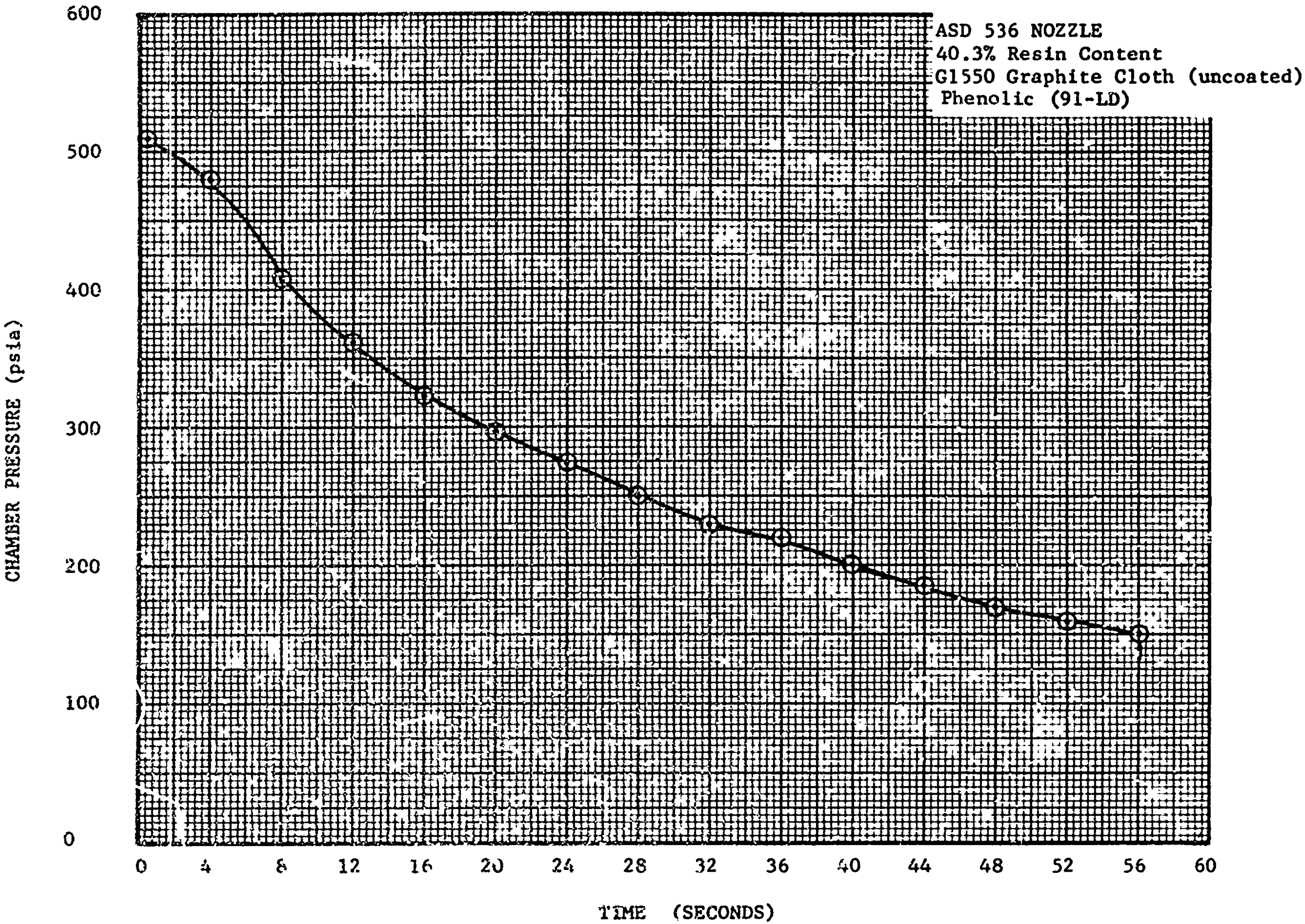

FIGURE 27. ASD NOZZLE 536 - CHAMBER PRESSURE VS. TIME

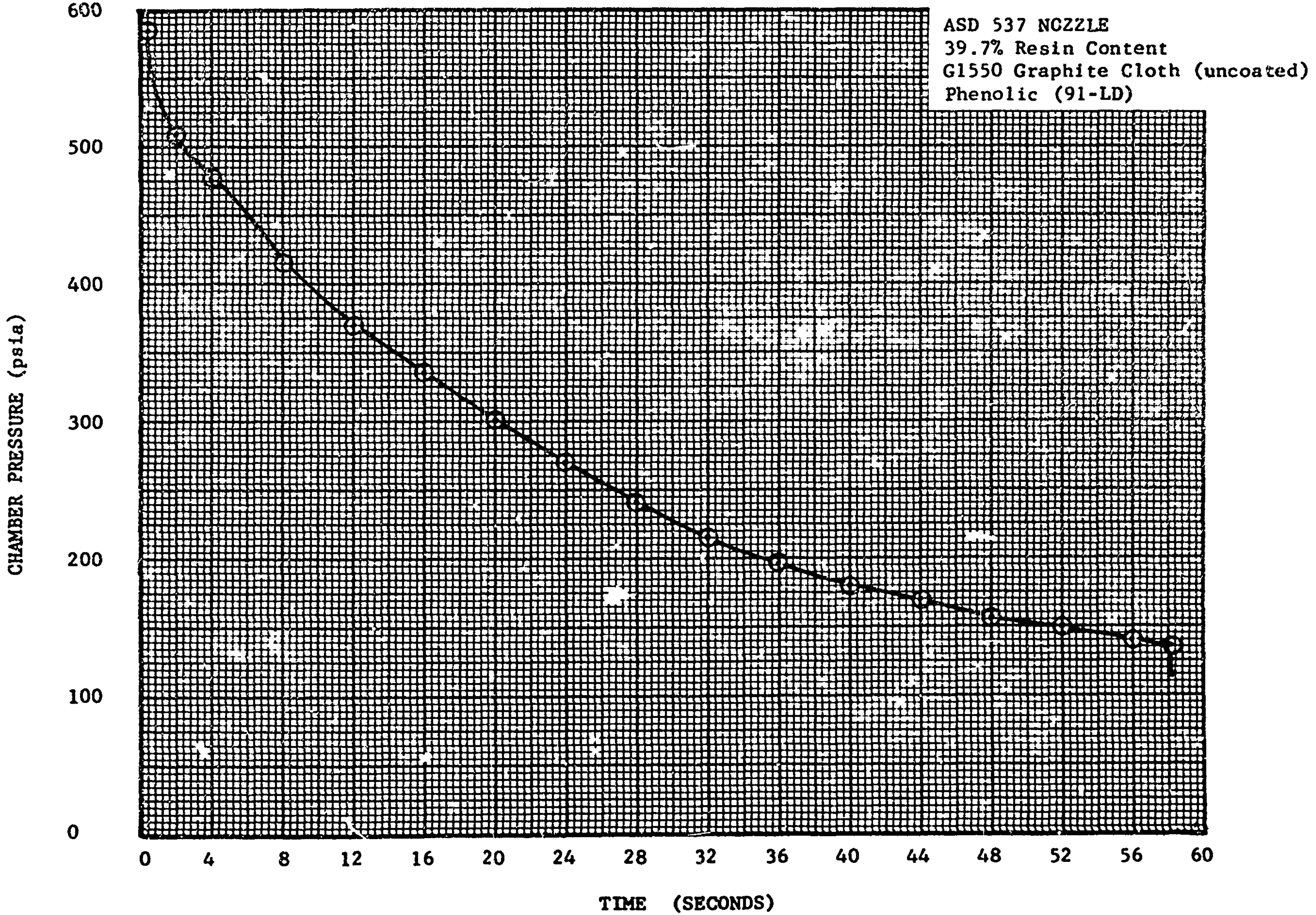

FIGURE 28. ASD NOZZLE 537 - CHAMBER PRESSURE VS. TIME

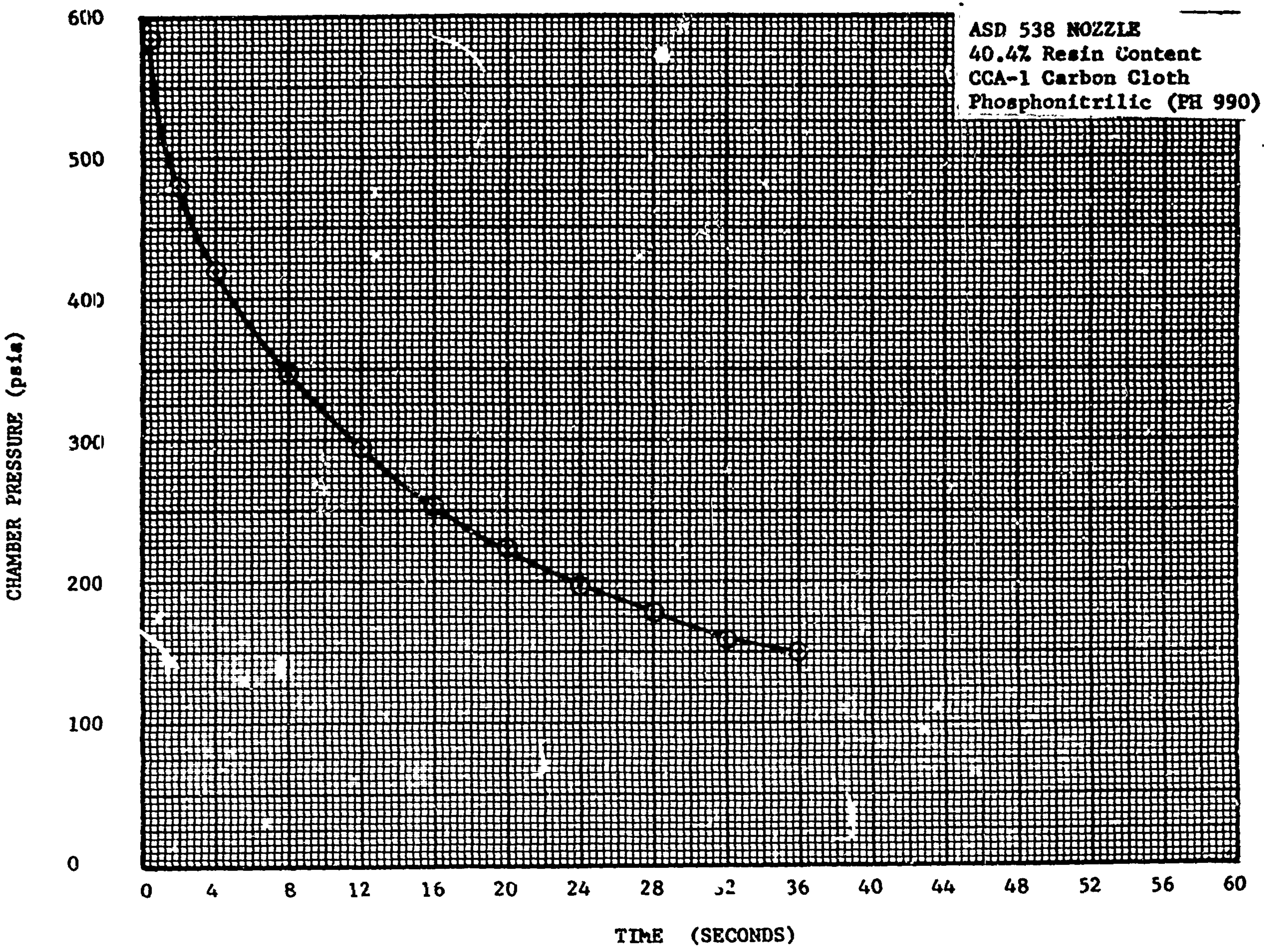

FIGURE 29. ASD NOZZLE 538 - CHAMBER PRESSURE VS. TIME

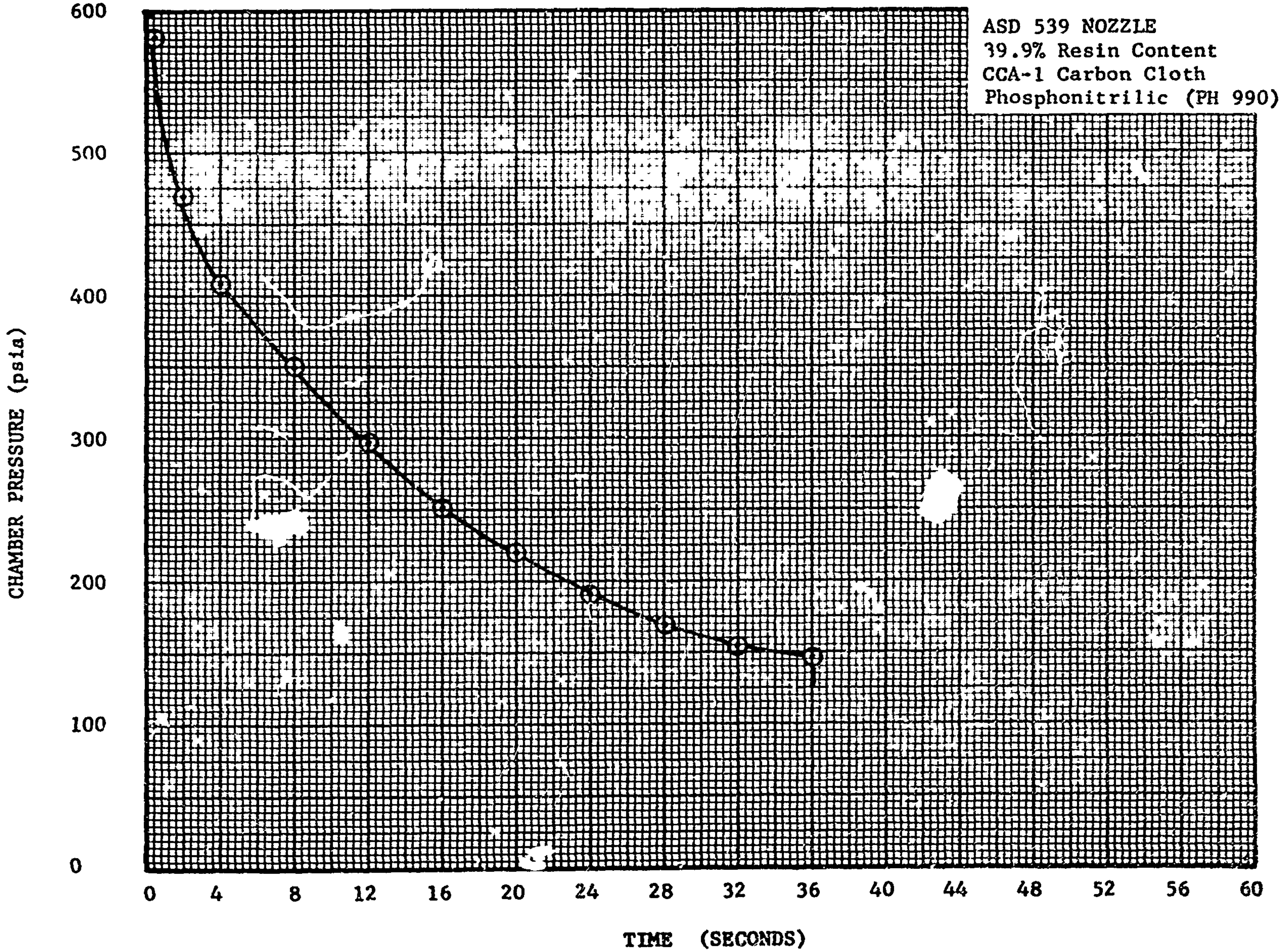

FIGURE 30. ASD NOZZLE 539 - CHAMBER PRESSURE VS. TIME

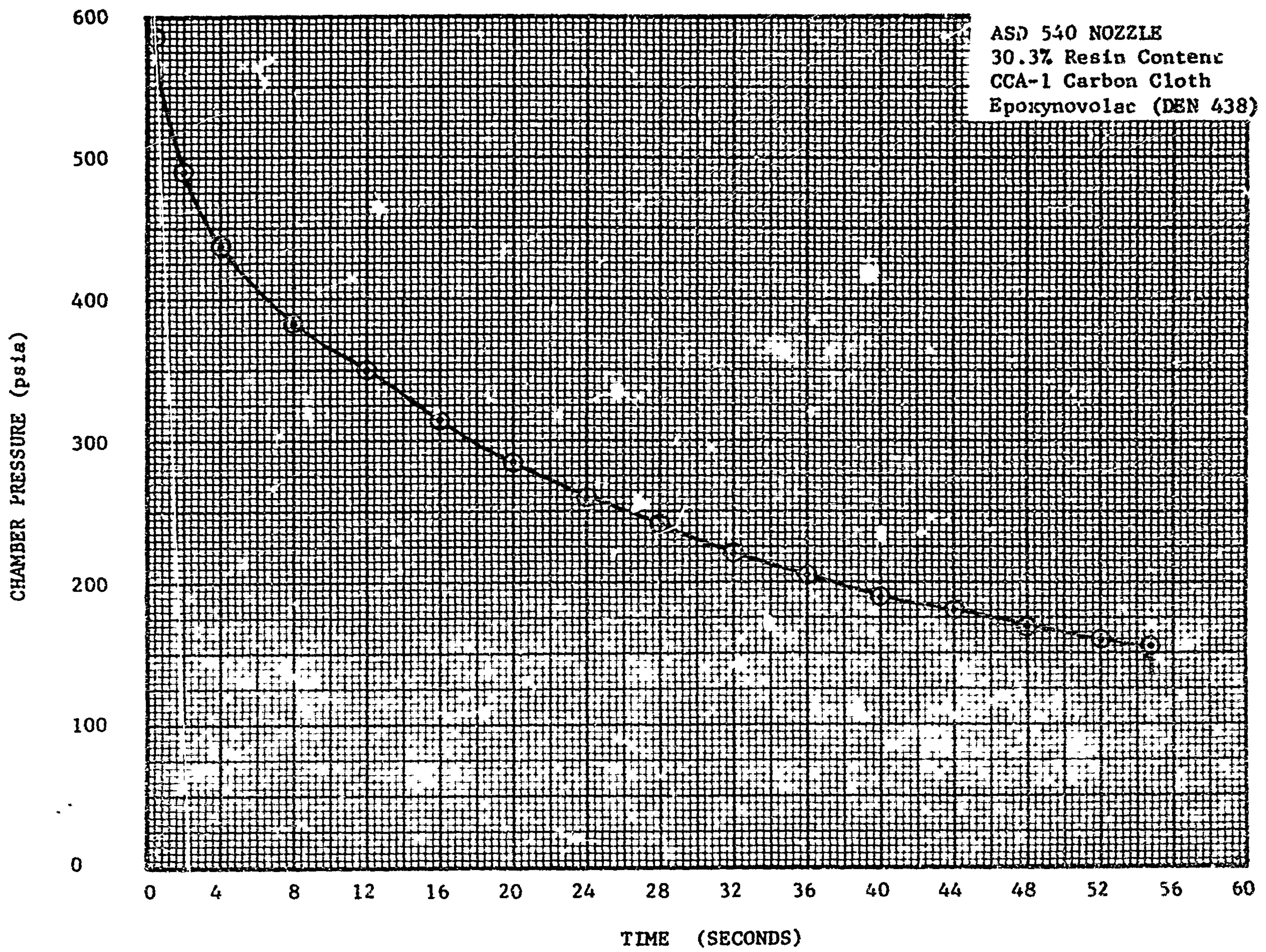

FIGURE 31. ASD NOZZLE 540 - CHAMBER PRESSURE VS. TIME

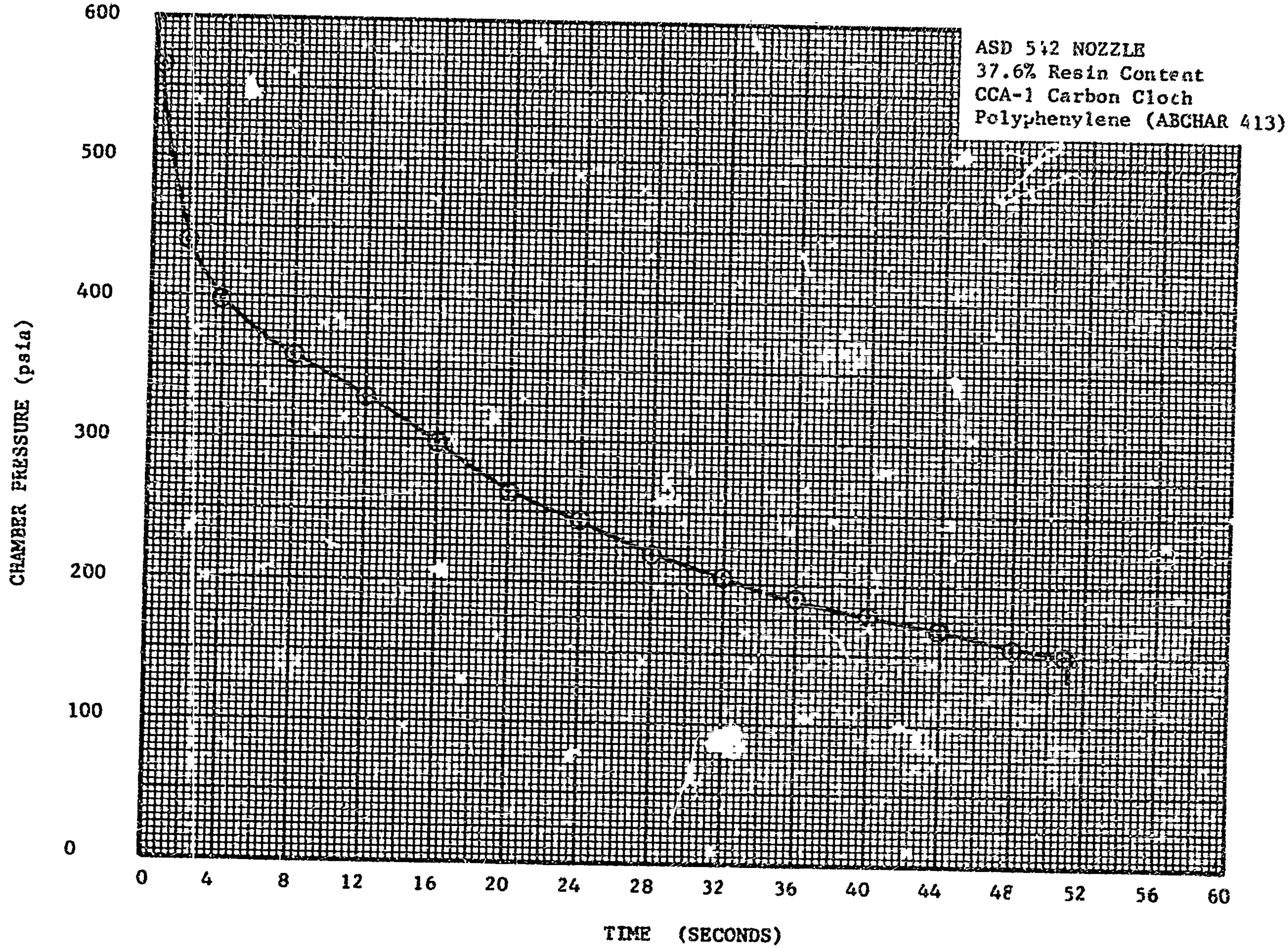

FIGURE 32. ASD NOZZLE 542 - CHAMBER PRESSURE VS. TIME

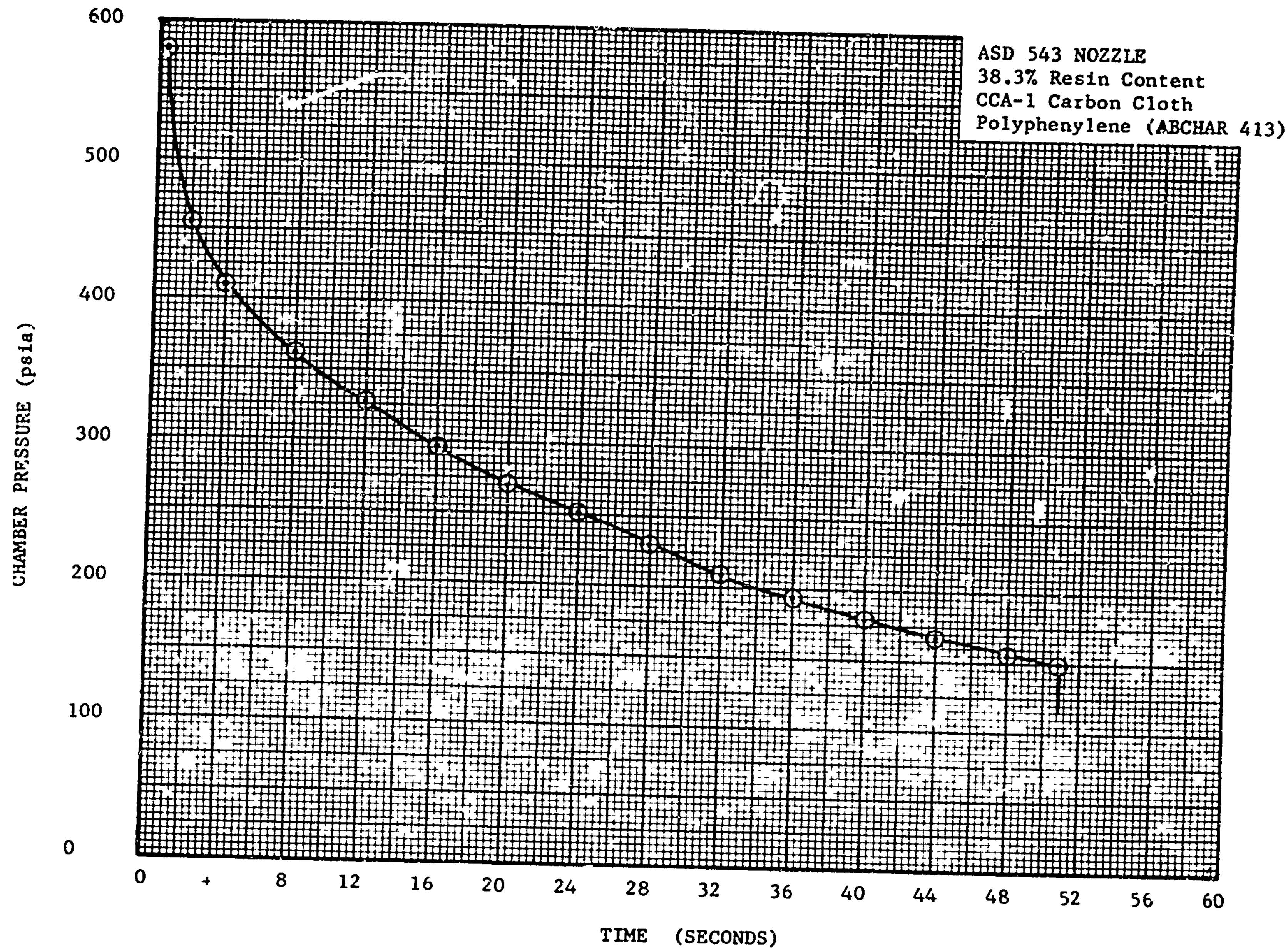

FIGURE 33. ASD NOZZLE 543 - CHAMBER PRESSURE VS. TIME

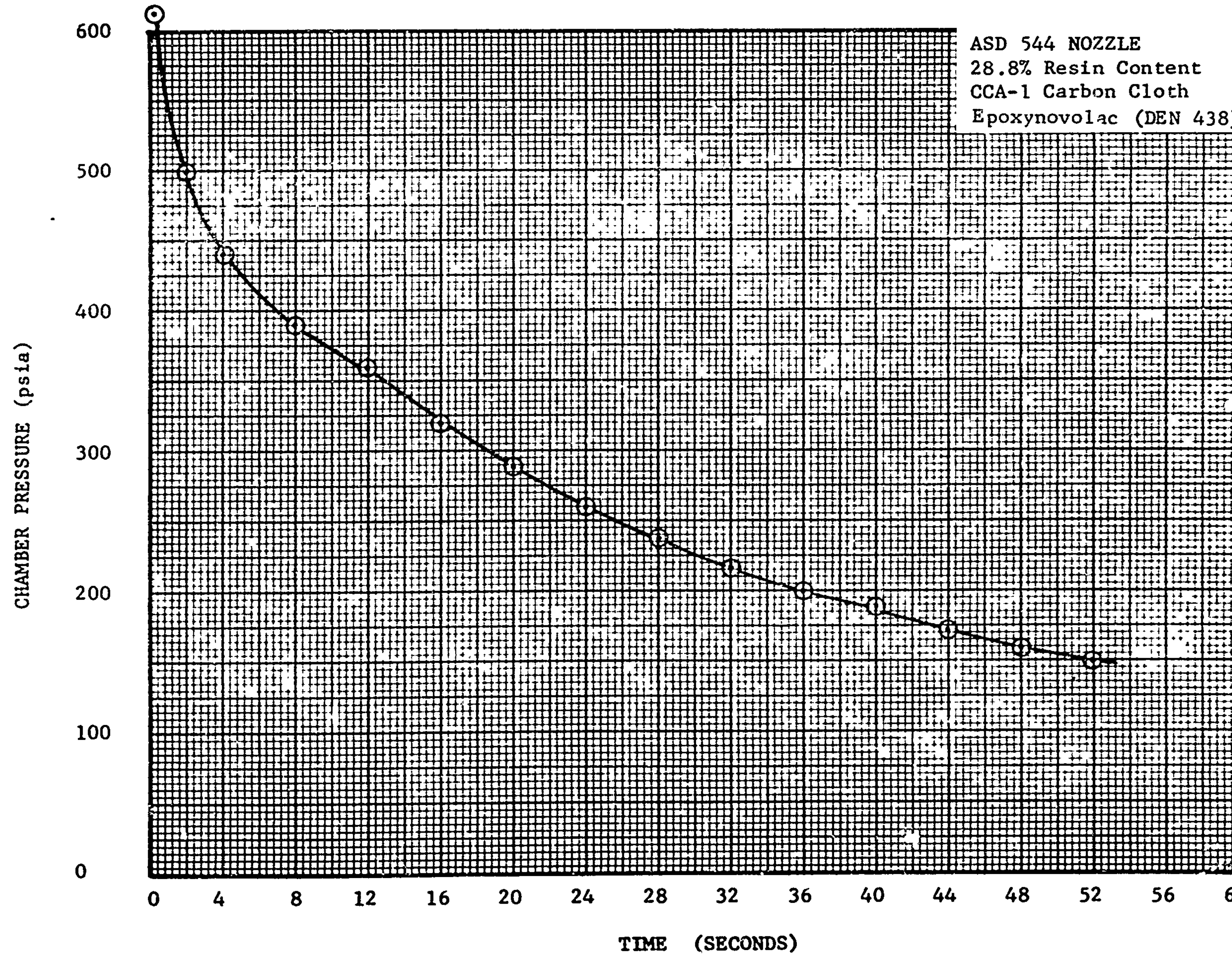

FIGURE 34. ASD NOZZLE 544 - CHAMBER PRESSURE VS. TIME

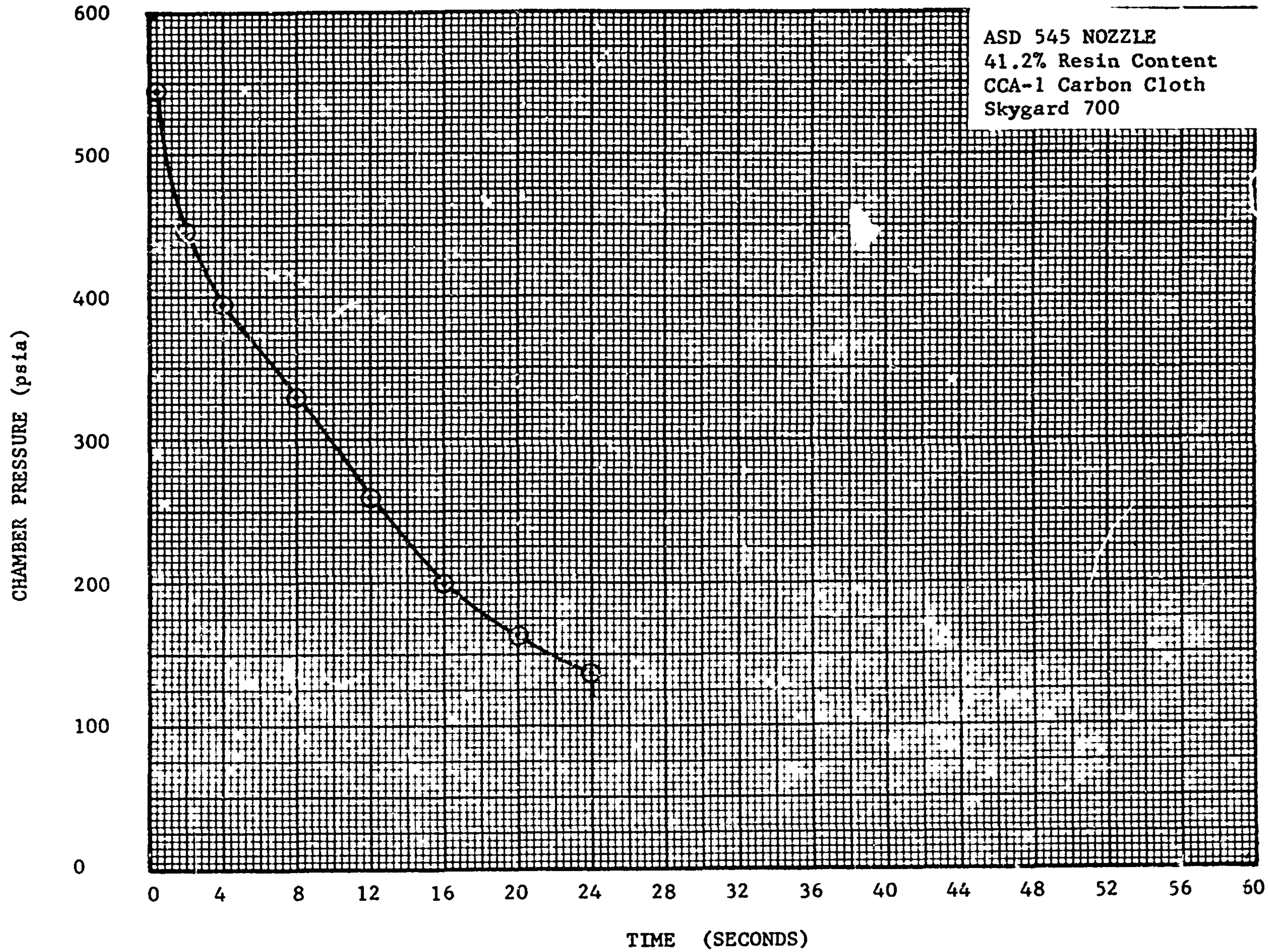

FIGURE 35. ASD NOZZLE 545 - CHAMBER PRESSURE VS. TIME

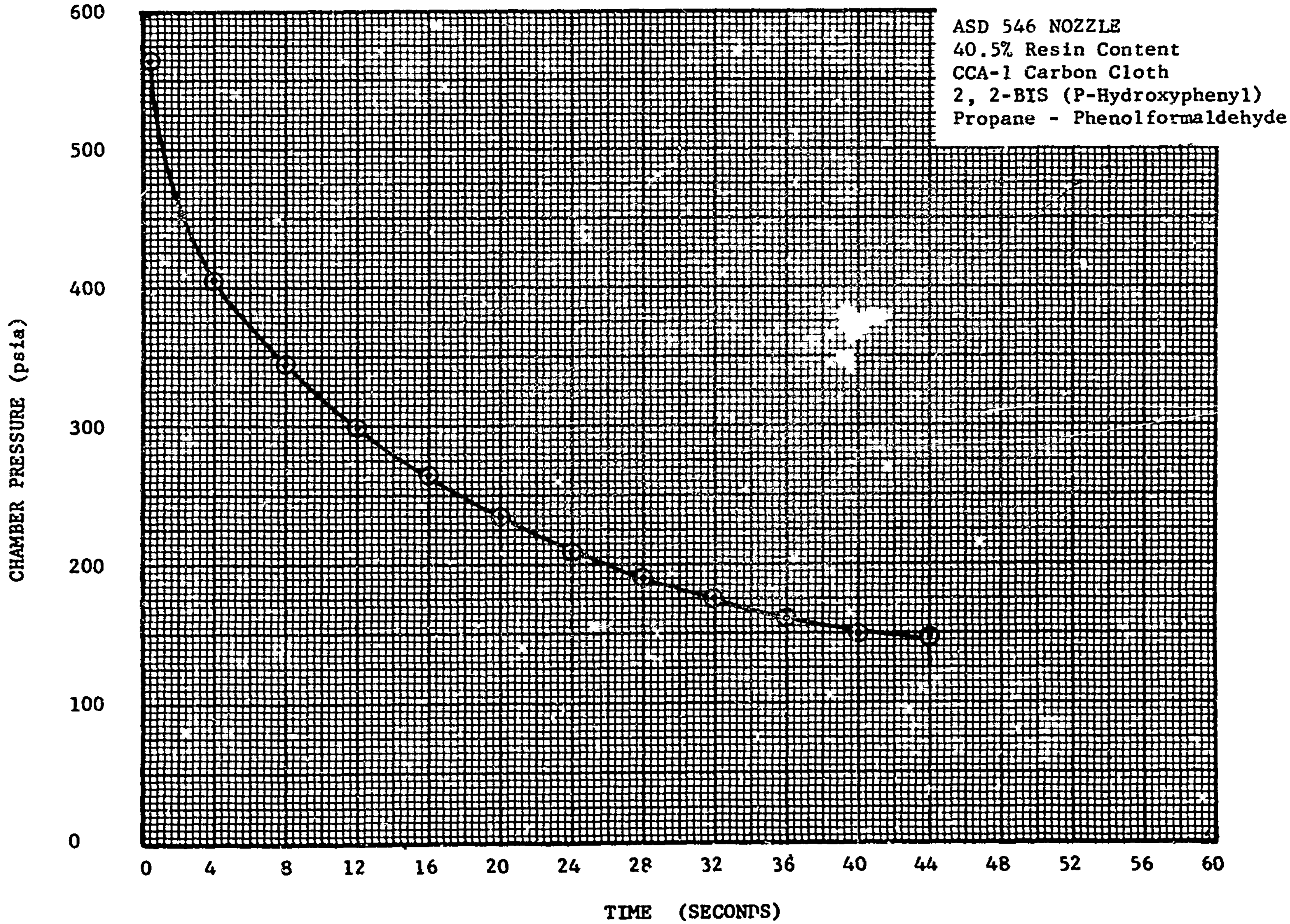

FIGURE 36. ASD NOZZLE 546 - CHAMBER PRESSURE VS. TIME

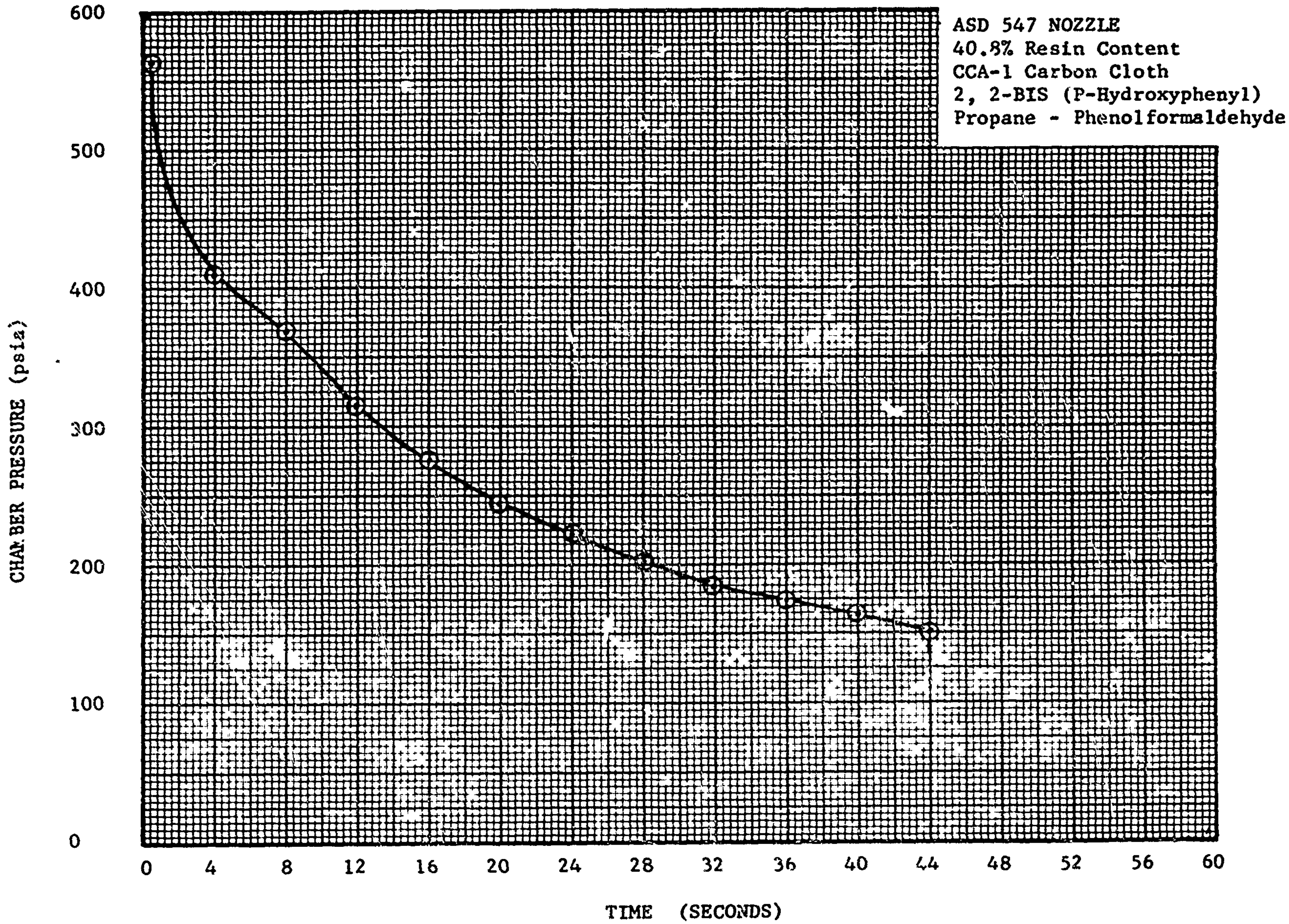

FIGURE 37. ASD NOZZLE 547 - CHAMBER PRESSURE VS. TIME

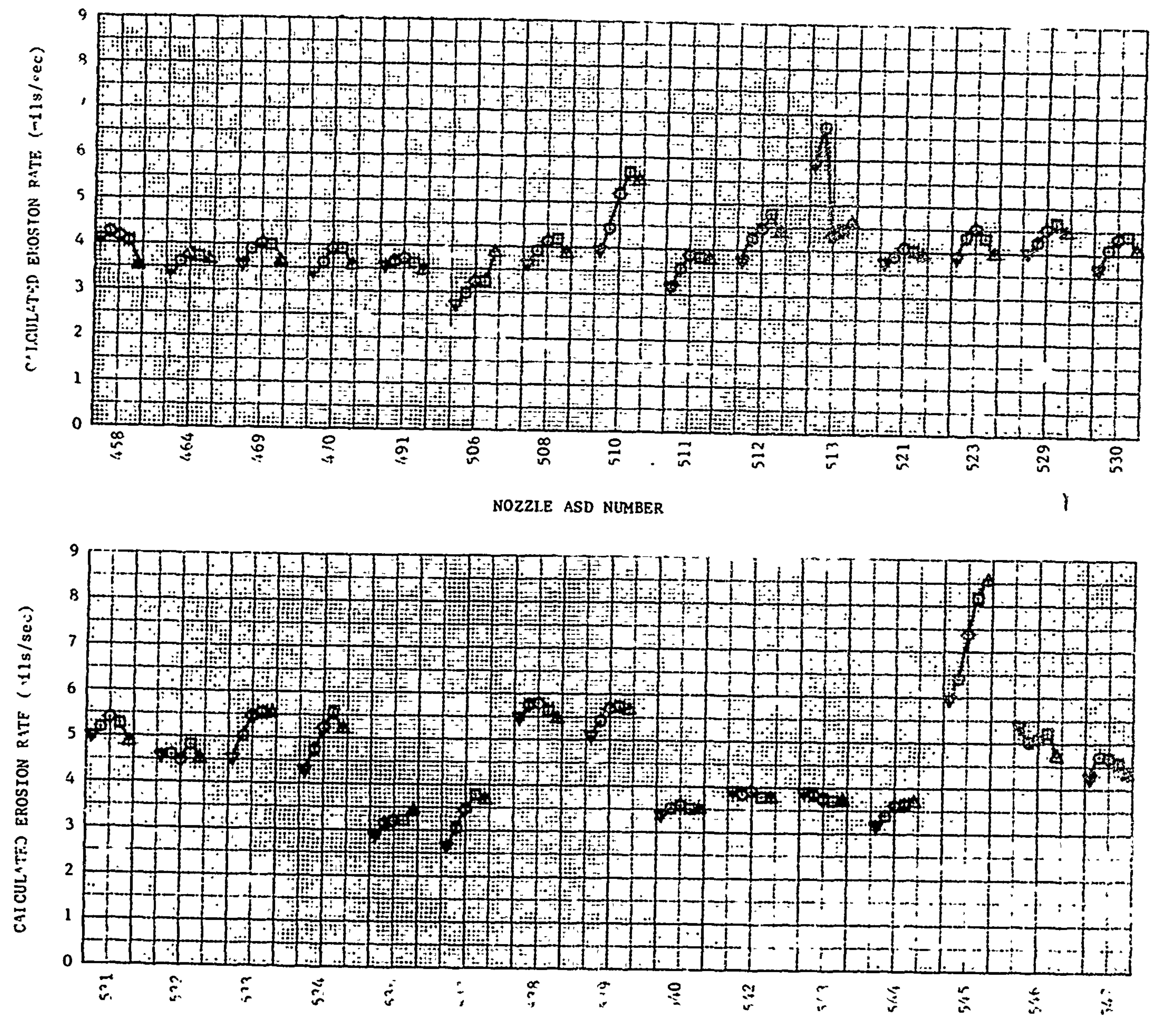

LEGEND FOR EROSION RATES

- ▽ at 350 psia
- ○ at 300 psia
- ◇ at 250 psia
- ☐ at 200 psia
- △ at 150 psia or final chamber

Pressure	Noz #
156	458
151	511
[illegible]	512
153	521
152	532
154	540
152	542
152	544

FIGURE 38. EROSION RATE VERSUS NOZZLE NUMBER, TEST SERIES NO.
SOLID PROPELLANT SIMULATOR

RESIN: POLYPHENYLENE

REINFORCEMENT: CCA-1

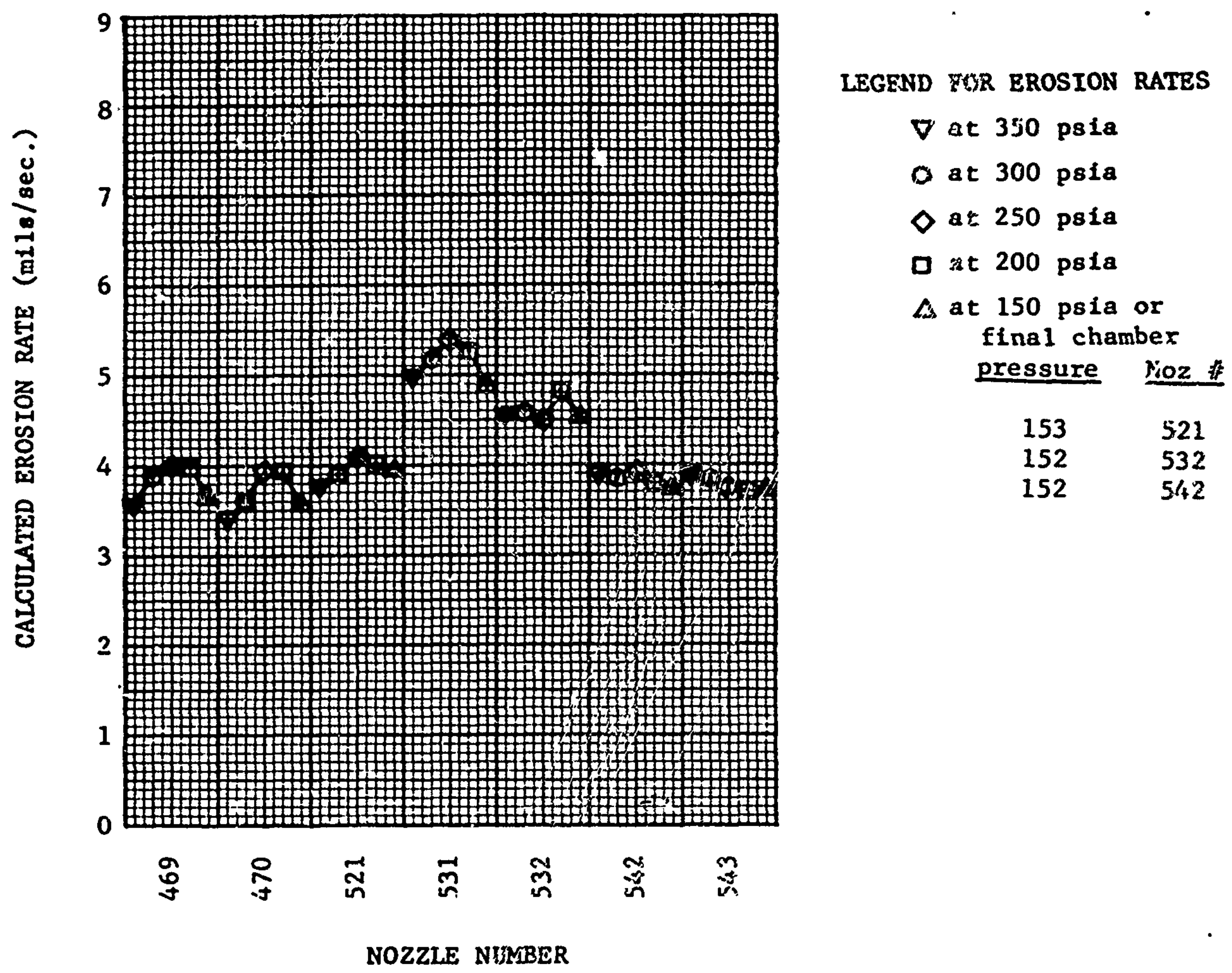

FIGURE 39. EROSION RATE COMPARISON, TEST SERIES 4
SOLID PROPELLANT SIMULATOR

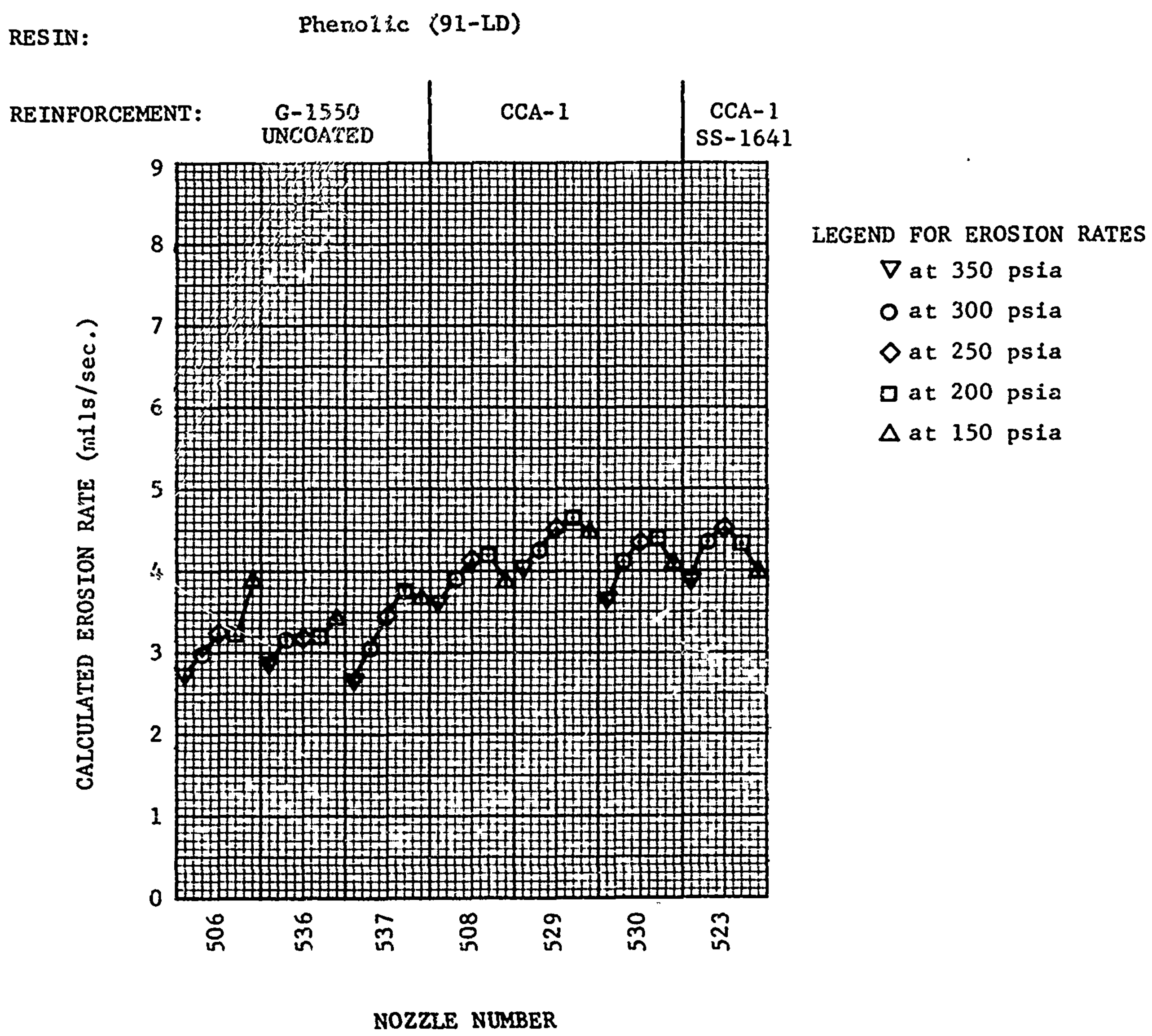

FIGURE 39.(CONT.) EROSION RATE COMPARISON, TEST SERIES 4
SOLID PROPELLANT SIMULATOR

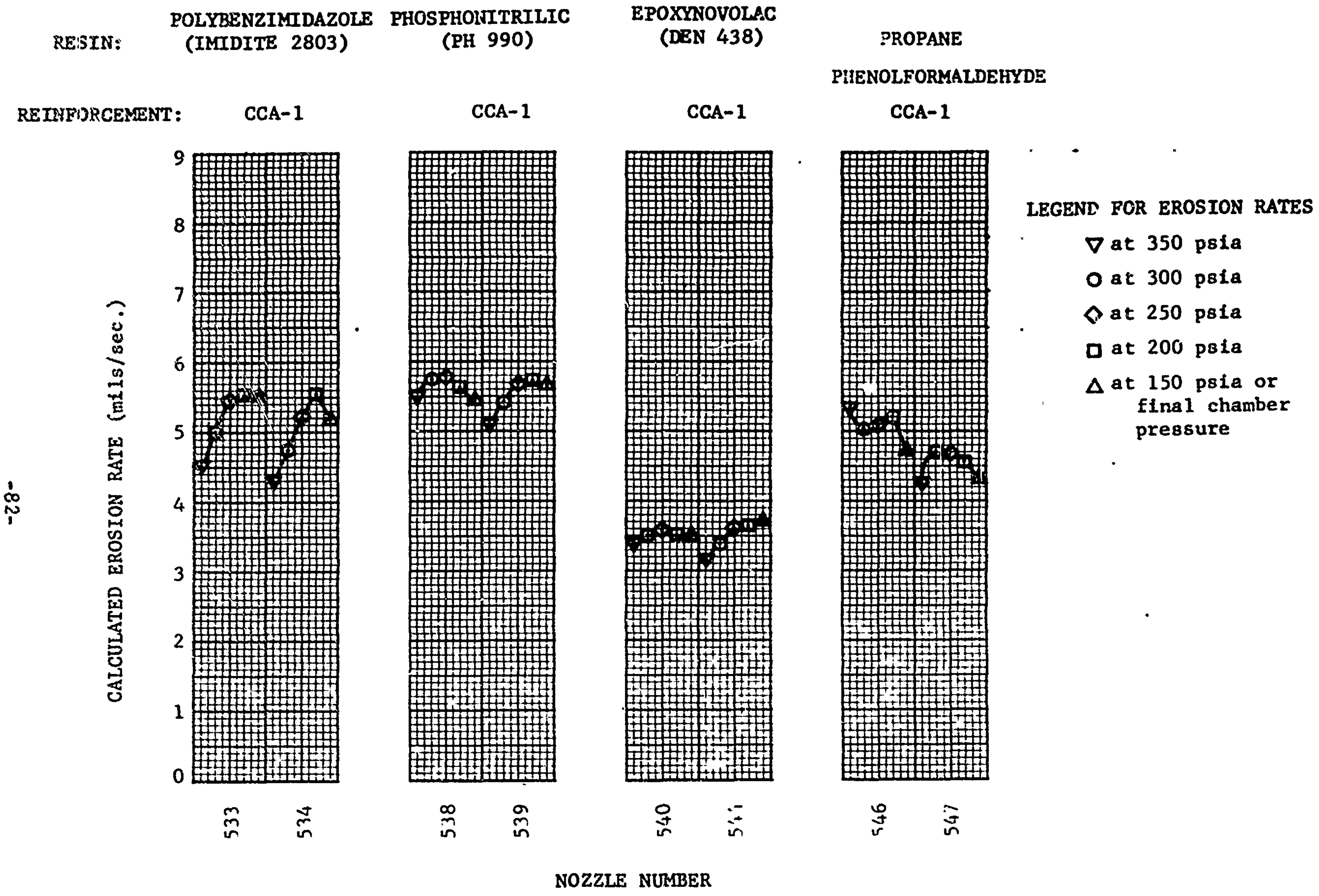

FIGURE 39. (CONT.) EROSION RATE COMPARISON, TEST SERIES 4
SOLID PROPELLANT SIMULATOR

NOZZLE NO. ASD-458

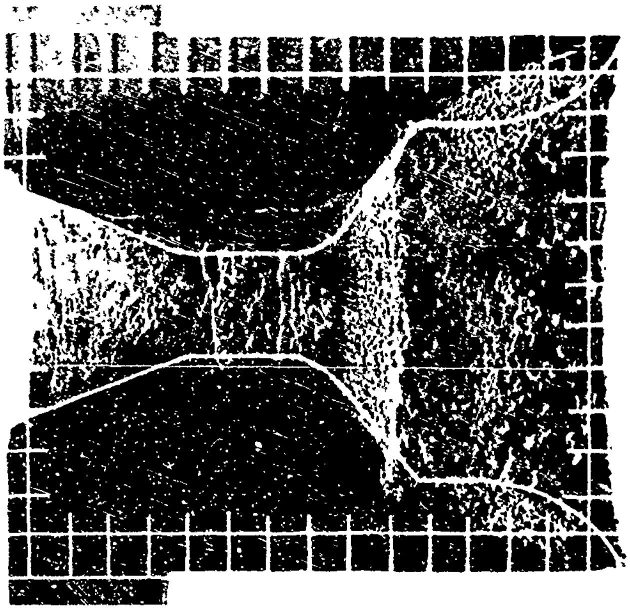

12 O'CLOCK

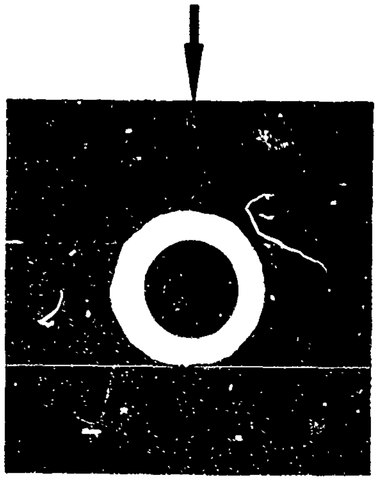

NOZZLE NO. ASD-464

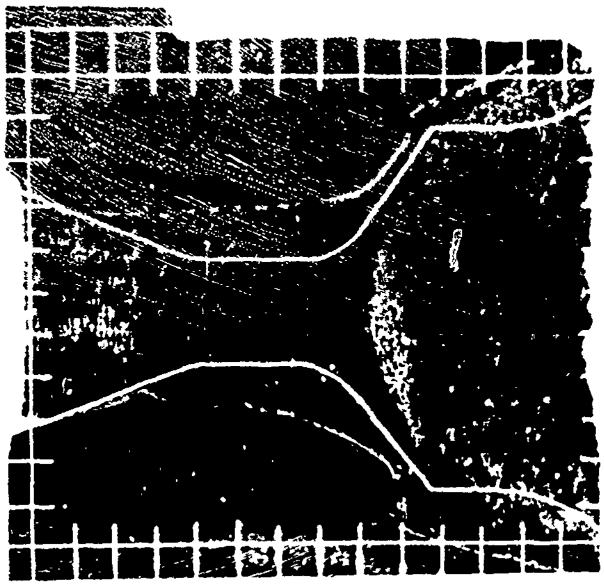

12 O'CLOCK

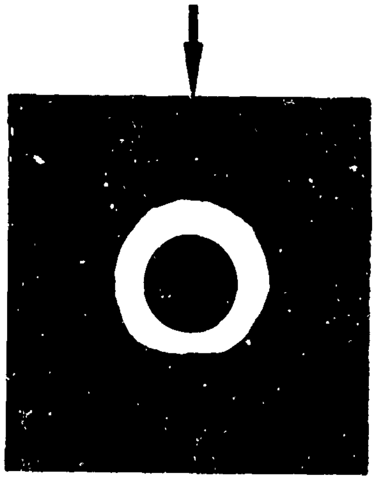

GRID SCALE
0.20 INCH

FIGURE 40. PROFILE AND AXIAL NOZZLE PHOTOGRAPHS

NOZZLE NO. ASD-469

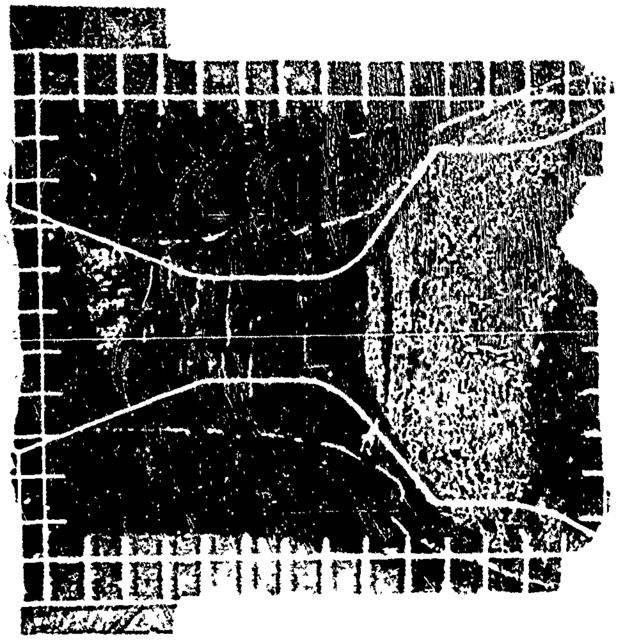

12 O'CLOCK

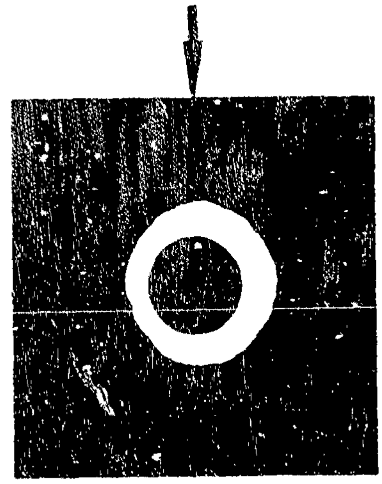

NOZZLE NO. ASD-470

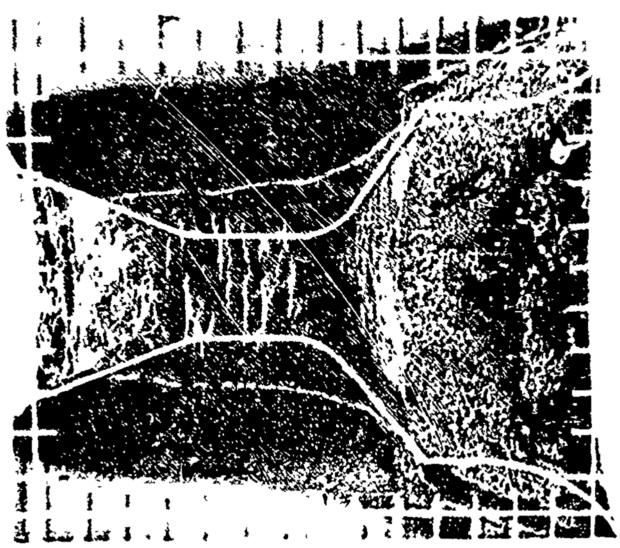

12 O'CLOCK

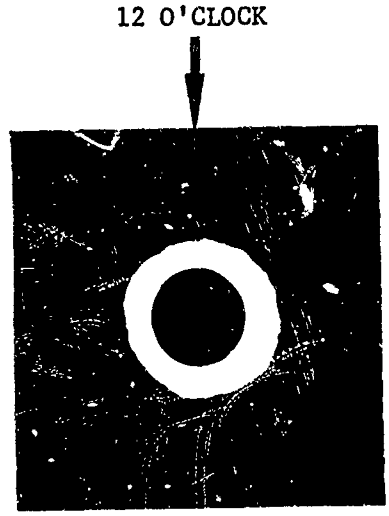

GRID SCALE
0.20 INCH

FIGURE 41. PROFILE AND AXIAL NOZZLE PHOTOGRAPHS

NOZZLE NO. ASD-491

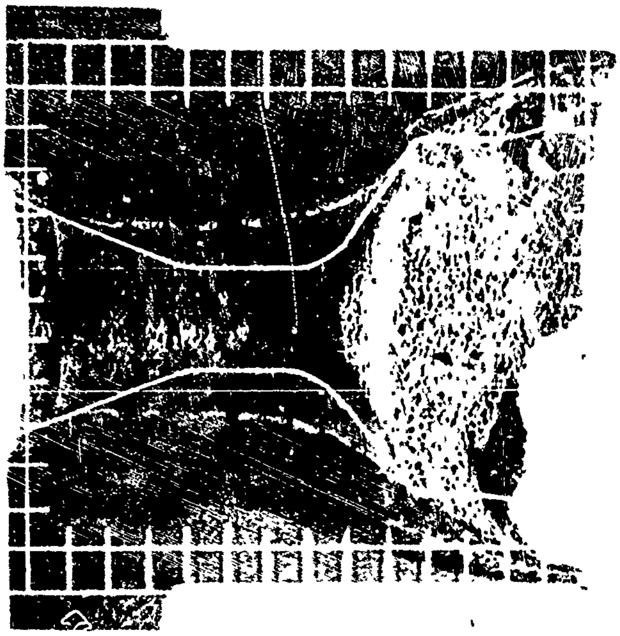

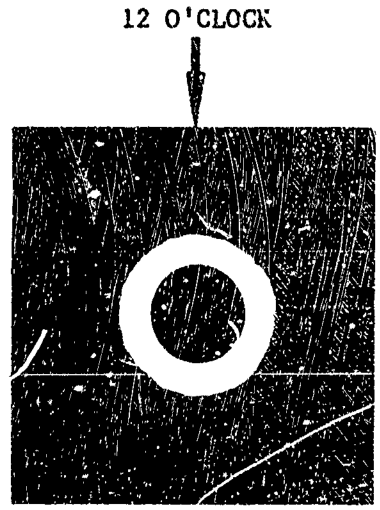

NOZZLE NO. ASD-506

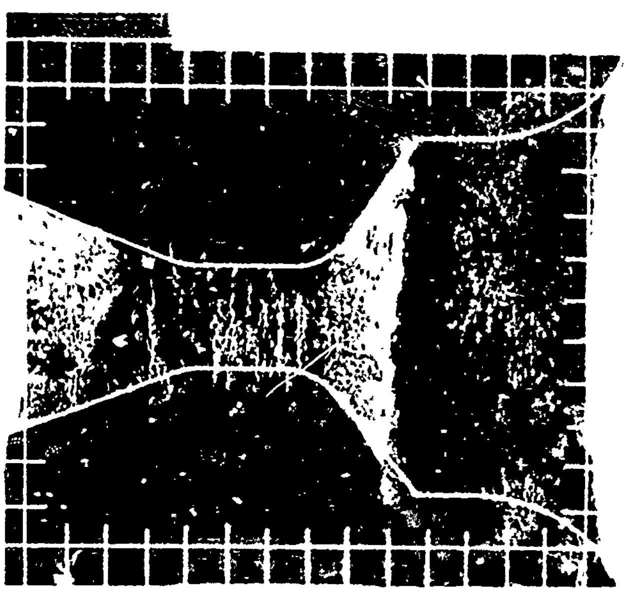

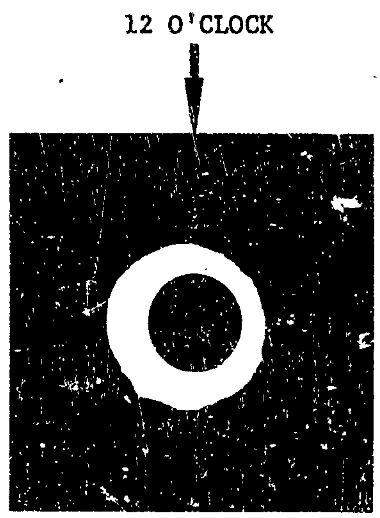

GRID SCALE
0.20 INCH

FIGURE 42. PROFILE AND AXIAL NOZZLE PHOTOGRAPHS

NOZZLE NO. ASD-508

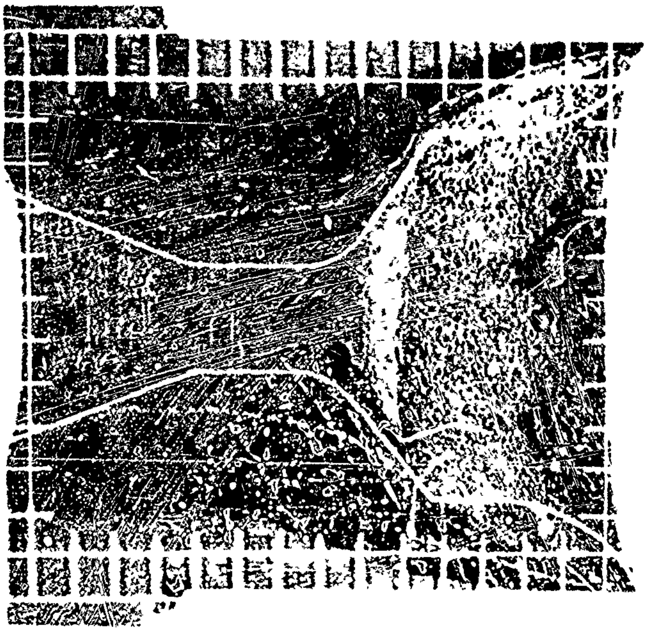

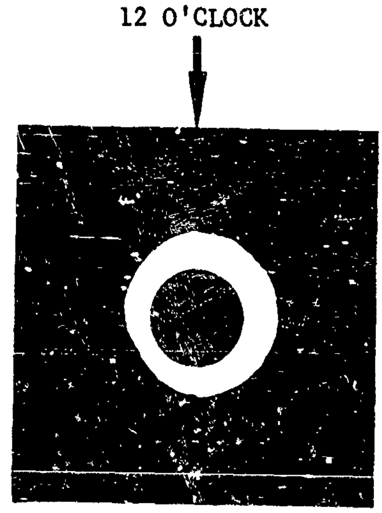

NOZZLE NO. ASD-510

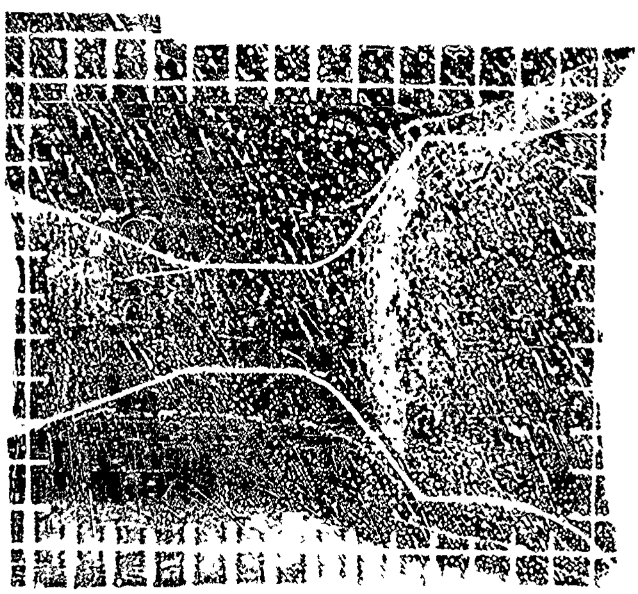

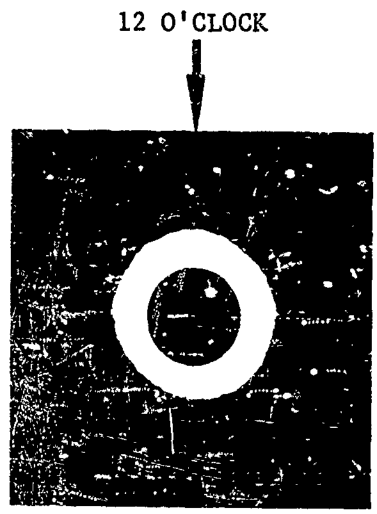

GRID SCALE
0.20 INCH

FIGURE 43. PROFILE AND AXIAL NOZZLE PHOTOGRAPHS

NOZZLE NO. ASD-511

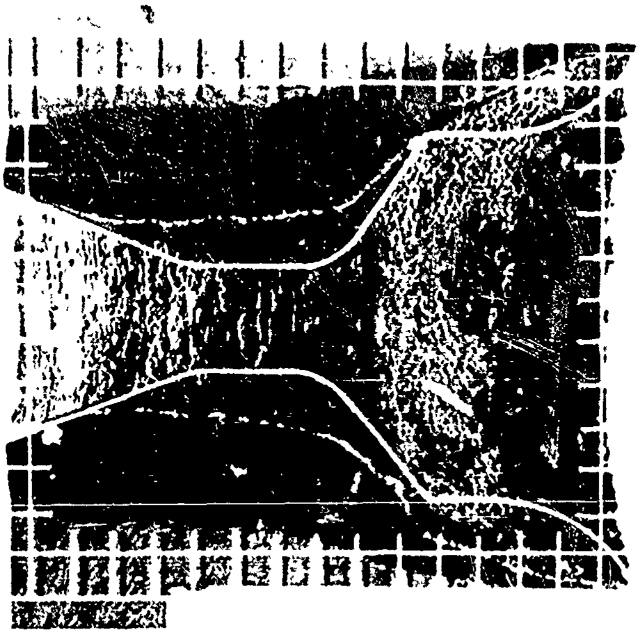

12 O'CLOCK

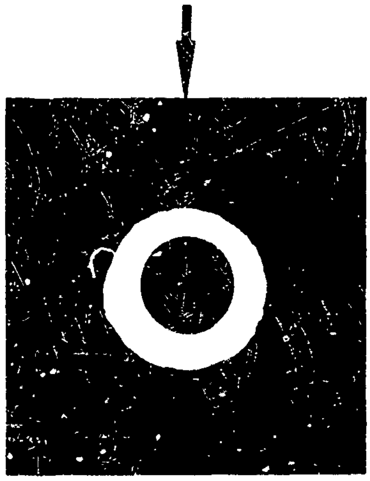

NOZZLE NO. ASD-512

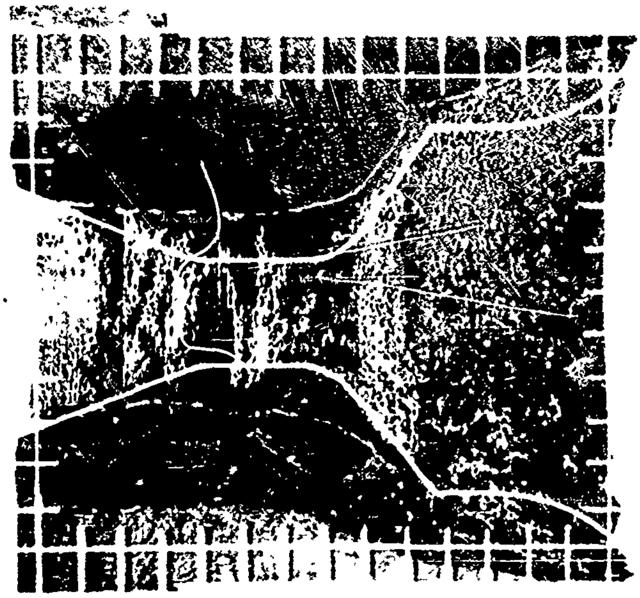

12 O'CLOCK

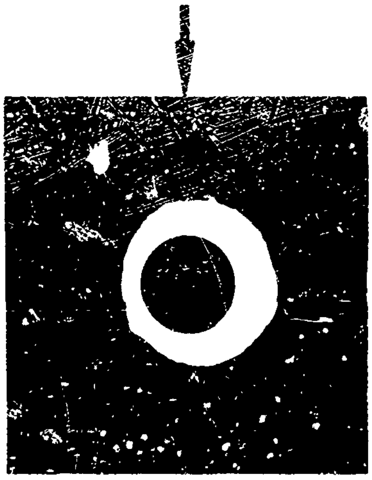

GRID SCALE
0.20 INCH

FIGURE 44. PROFILE AND AXIAL NOZZLE PHOTOGRAPHS

NOZZLE NO. ASD-513

12 O'CLOCK

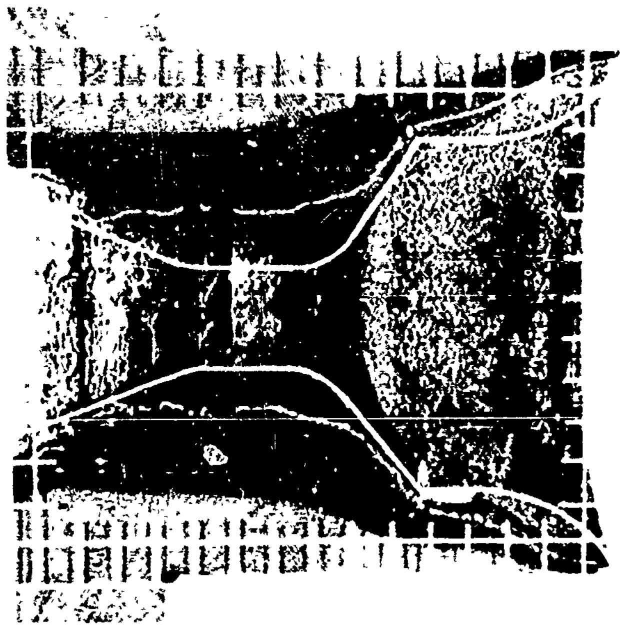

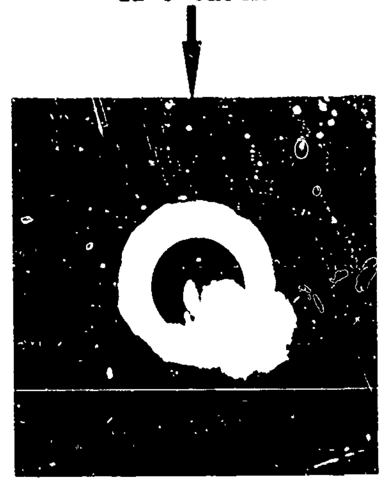

NOZZLE NO. ASD-521

12 O'CLOCK

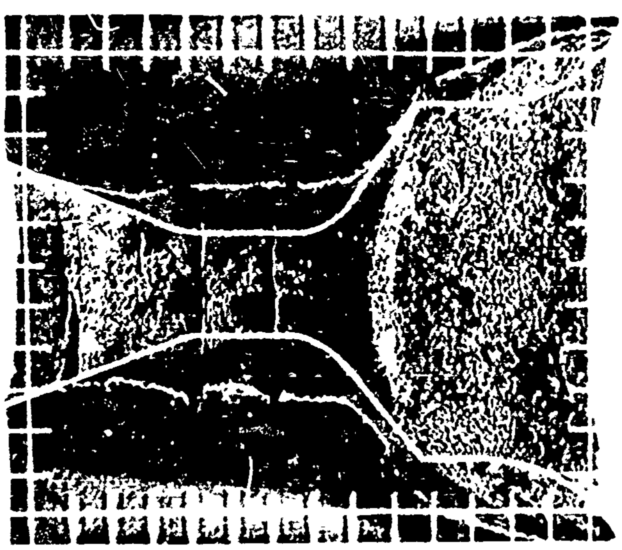

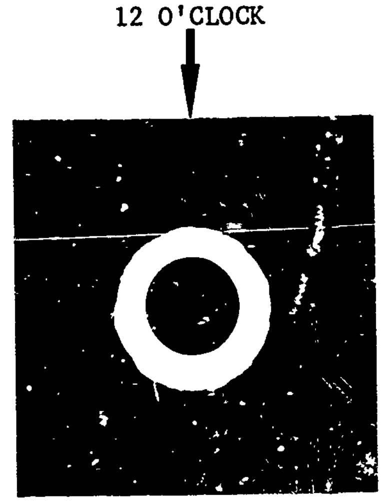

GRID SCALE
0.20 INCH

FIGURE 45. PROFILE AND AXIAL NOZZLE PHOTOGRAPHS

NOZZLE NO. ASD-523

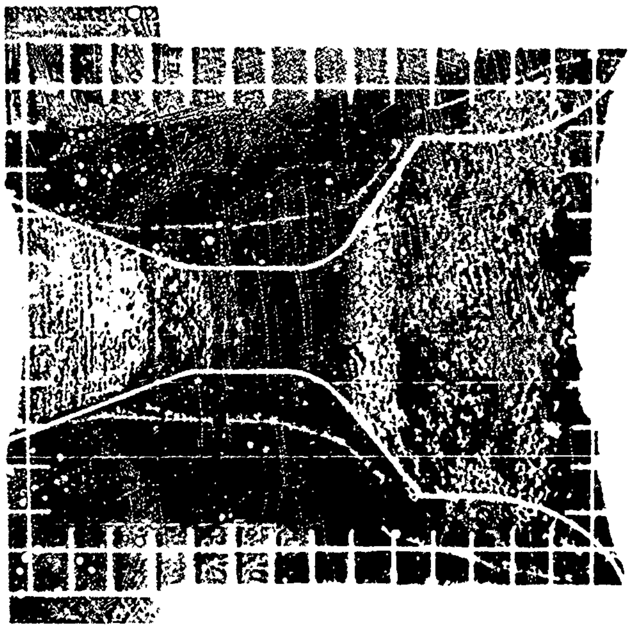

12 O'CLOCK

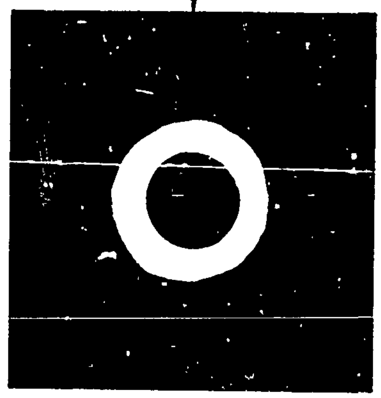

NOZZLE NO. ASD-529

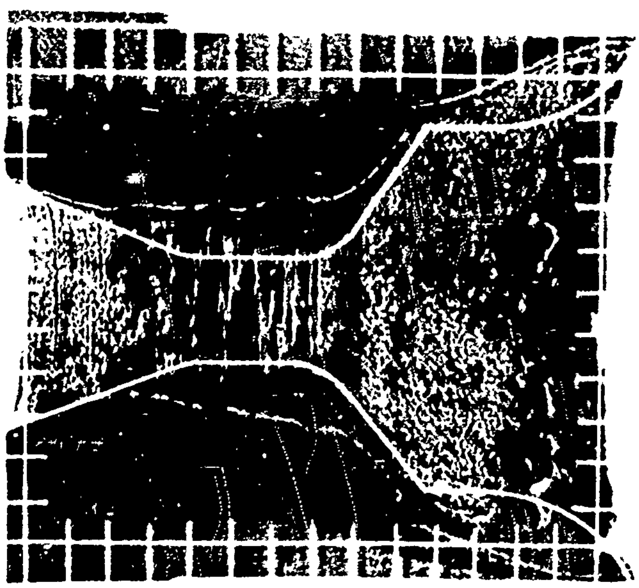

12 O'CLOCK

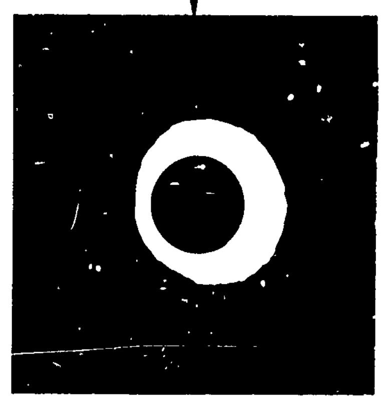

GRID SCALE
0.20 INCH

FIGURE 46. PROFILE AND AXIAL NOZZLE PHOTOGRAPHS

NOZZLE NO. ASD-530

12 O'CLOCK

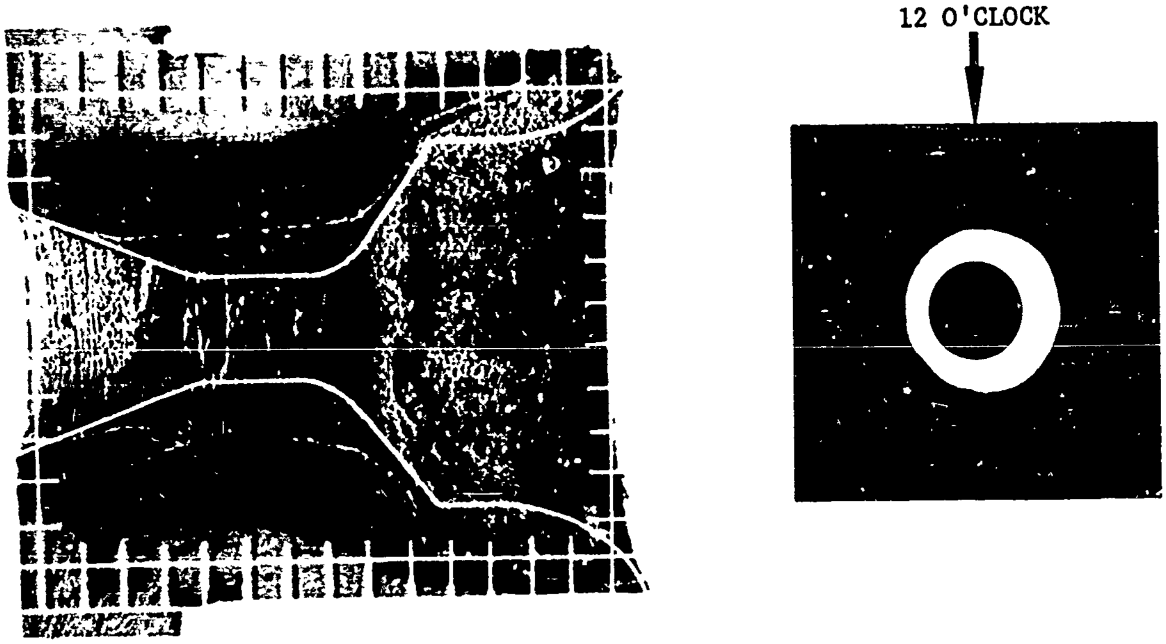

NOZZLE NO. ASD-531

12 O'CLOCK

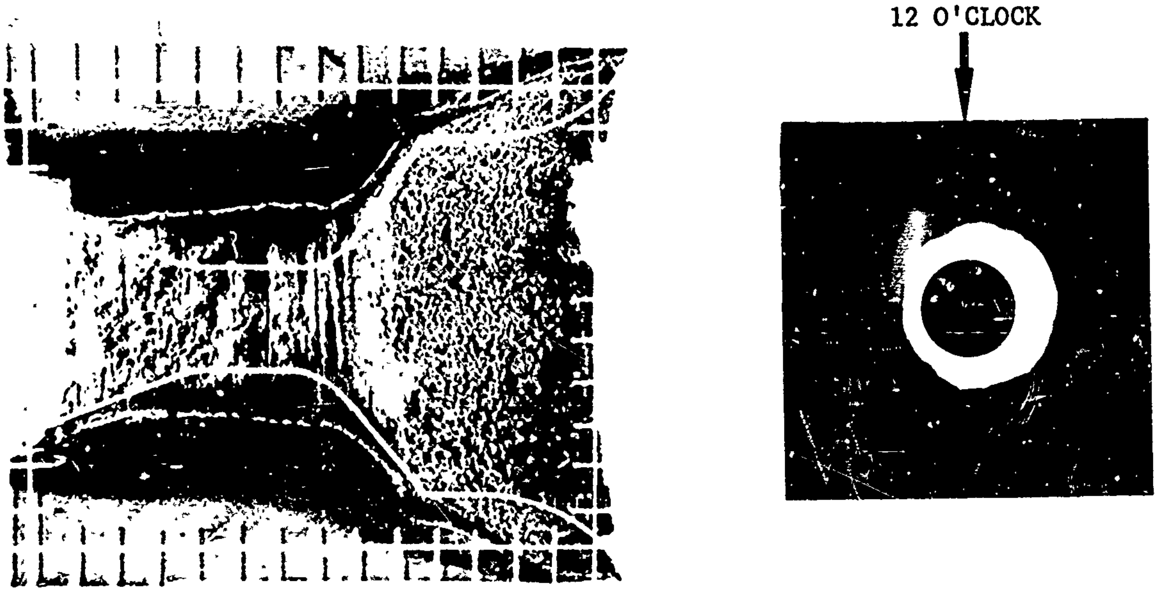

GRID SCALE
0.20 INCH

FIGURE 47. PROFILE AND AXIAL NOZZLE PHOTOGRAPHS

NOZZLE NO. ASD-532

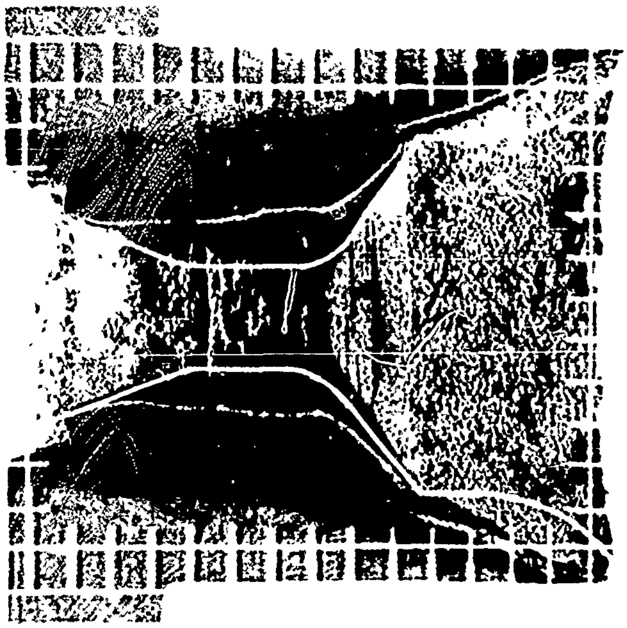

12 O'CLOCK

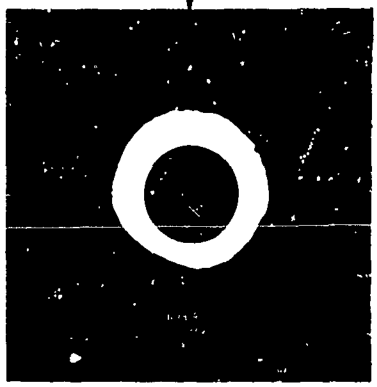

NOZZLE NO. ASD-533

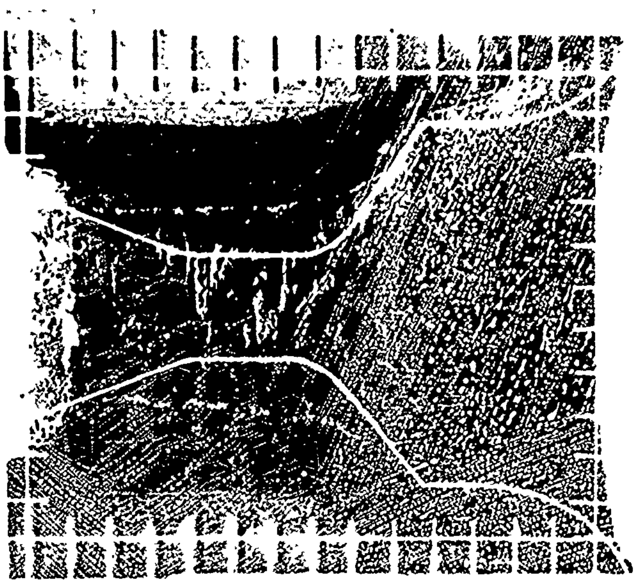

12 O'CLOCK

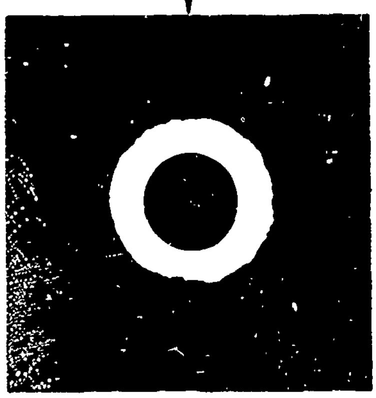

GRID SCALE
0.20 INCH

FIGURE 48. PROFILE AND AXIAL NOZZLE PHOTOGRAPHS

NOZZLE NO. ASD 534

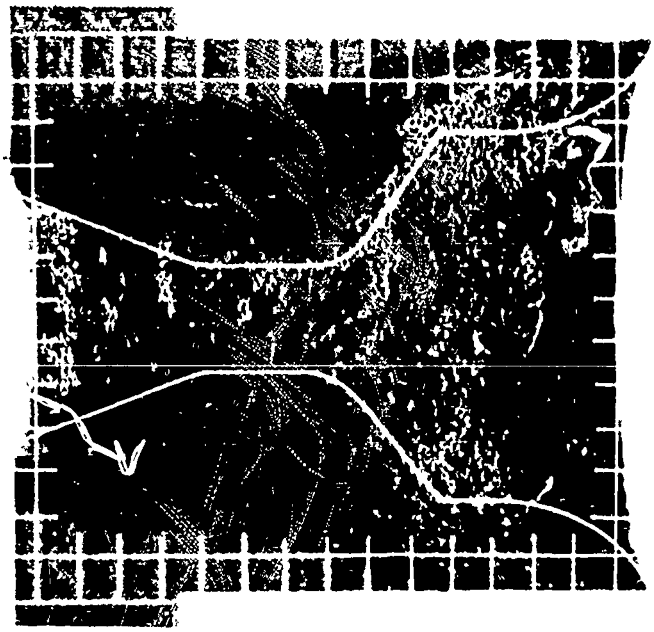

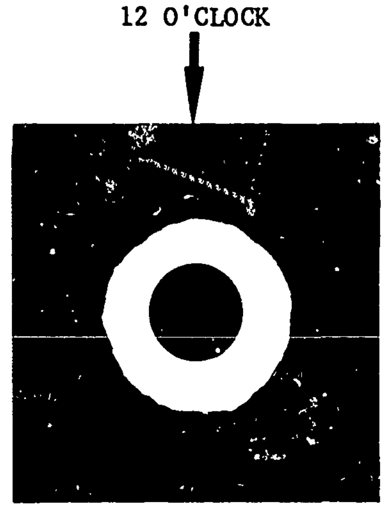

NOZZLE NO. ASD-536

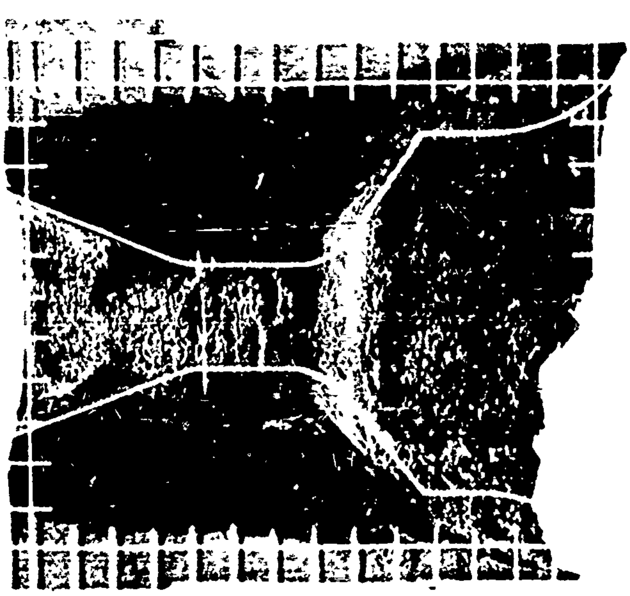

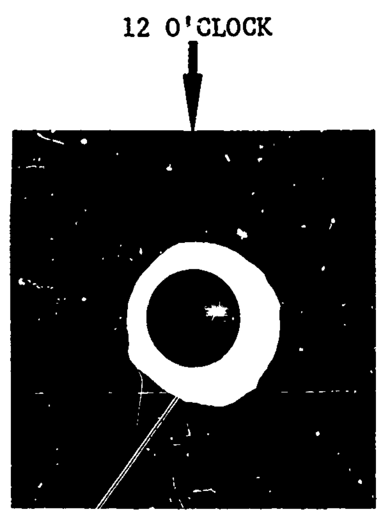

GRID SCALE
0.20 INCH

FIGURE 49. PROFILE AND AXIAL NOZZLE PHOTOGRAPHS

NOZZLE NO. ASD-537

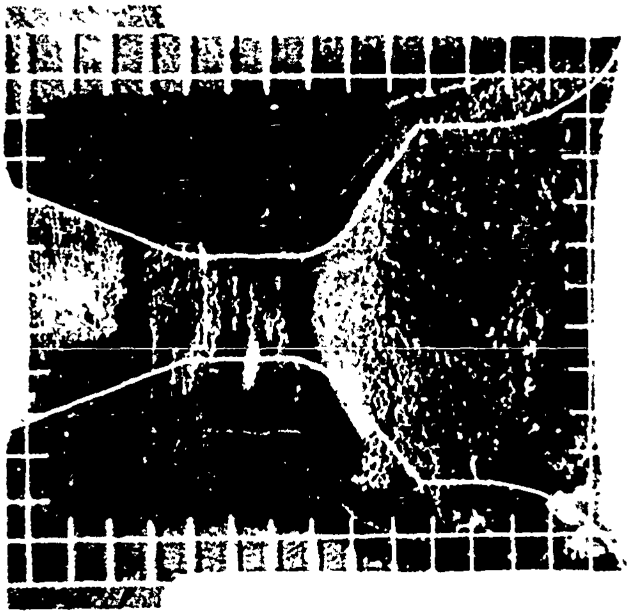

12 O'CLOCK

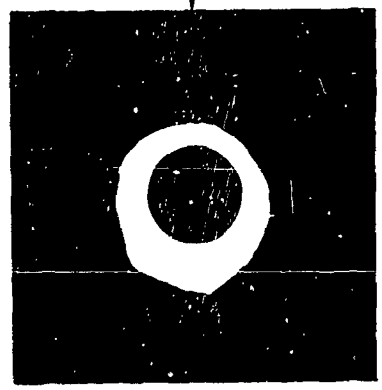

NOZZLE NO. ASD-538

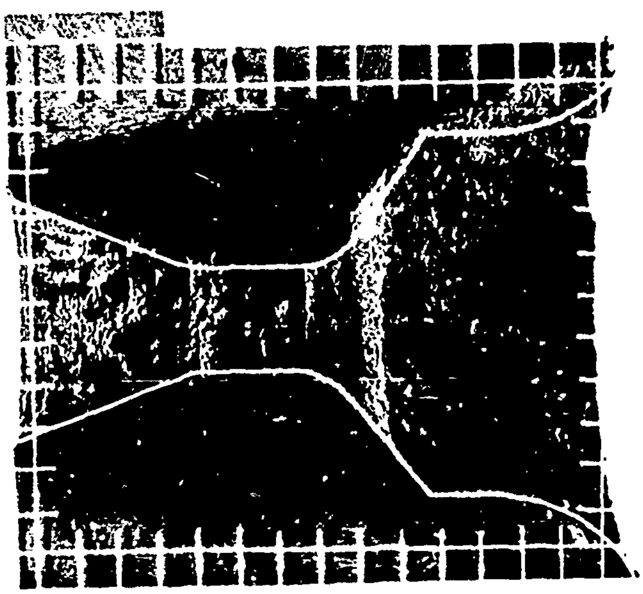

12 O'CLOCK

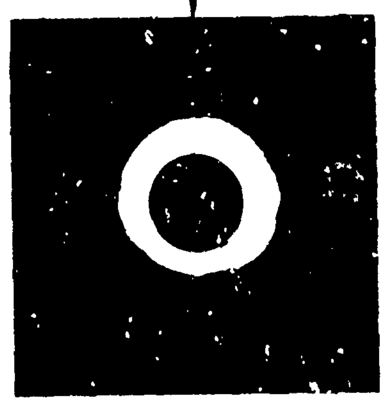

GRID SCALE
0.20 INCH

FIGURE 50. PROFILE AND AXIAL NOZZLE PHOTOGRAPHS

NOZZLE NO. ASD-539

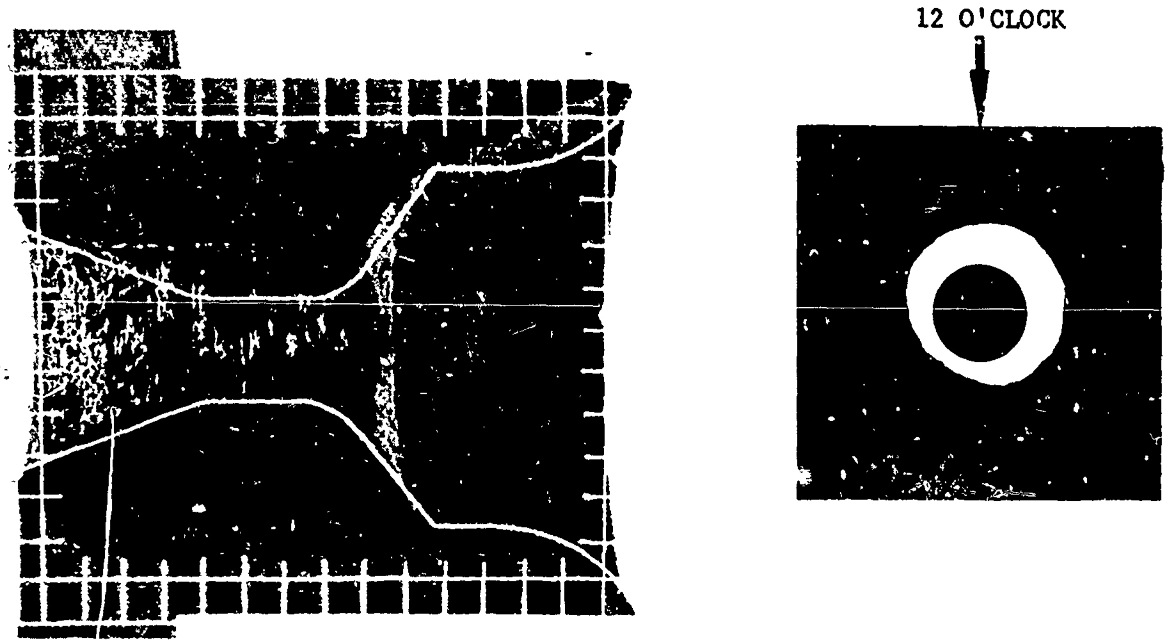

NOZZLE NO. ASD-540

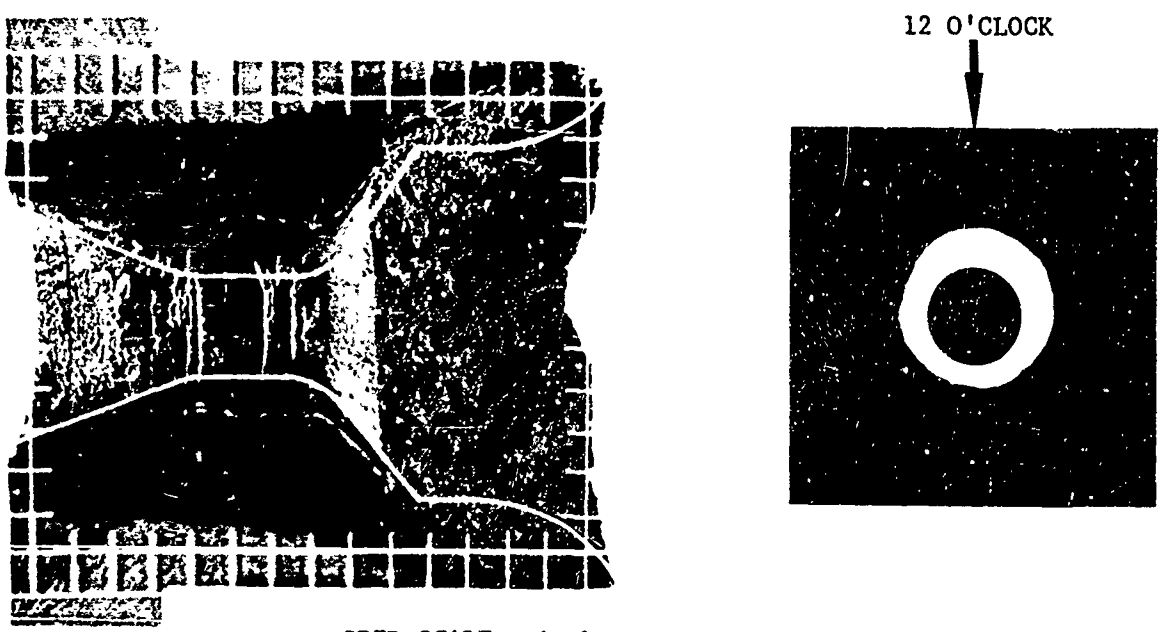

GRID SCALE
0.20 INCH

FIGURE 51. PROFILE AND AXIAL NOZZLE PHOTOGRAPHS

NOZZLE NO. ASD-542

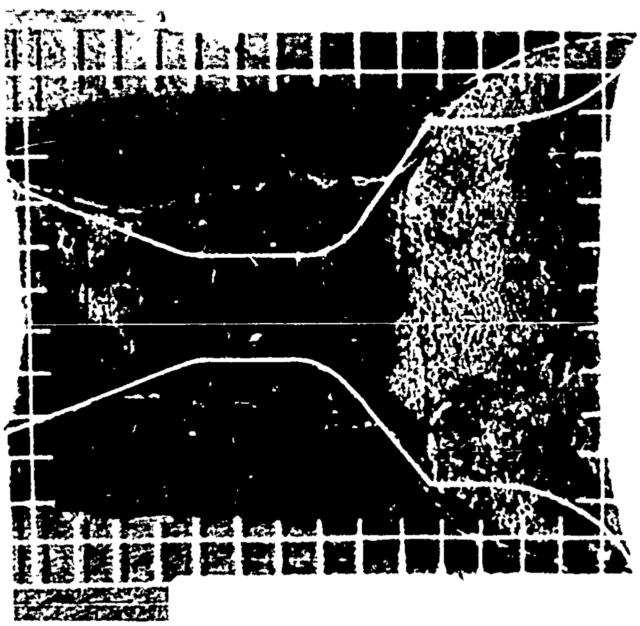

12 O'CLOCK

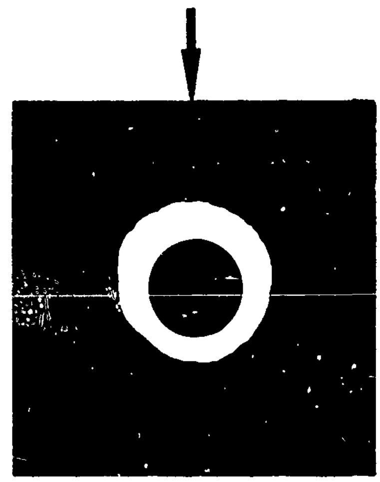

NOZZLE NO. ASD-543

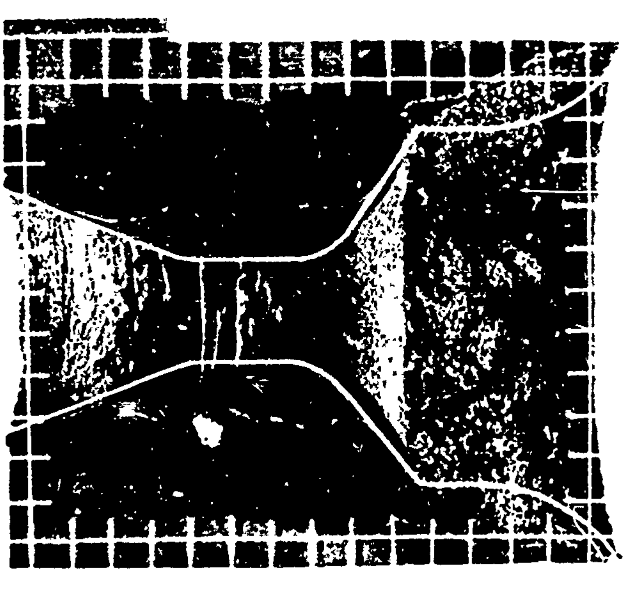

12 O'CLOCK

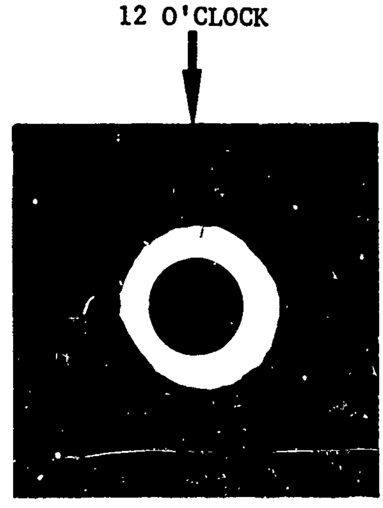

GRID SCALE
0.20 INCH

FIGURE 52. PROFILE AND AXIAL NOZZLE PHOTOGRAPHS

NOZZLE NO. ASD-544

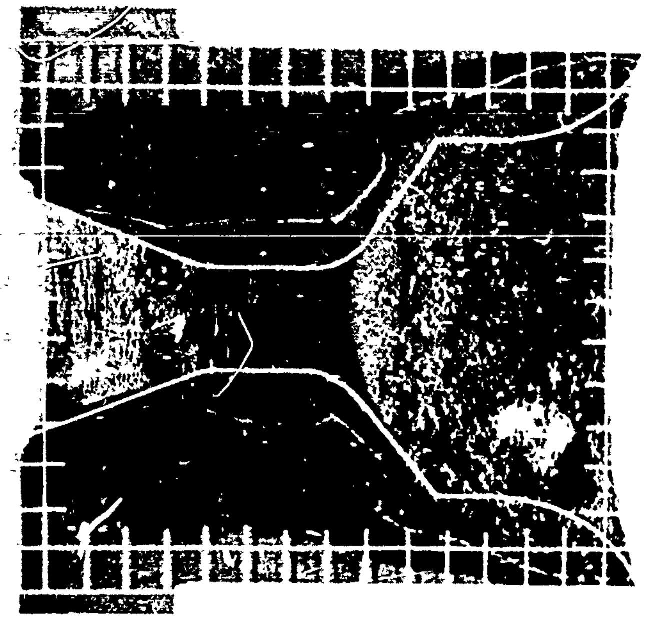

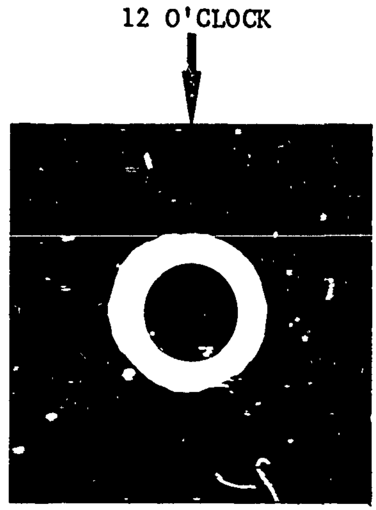

NOZZLE NO. ASD-545

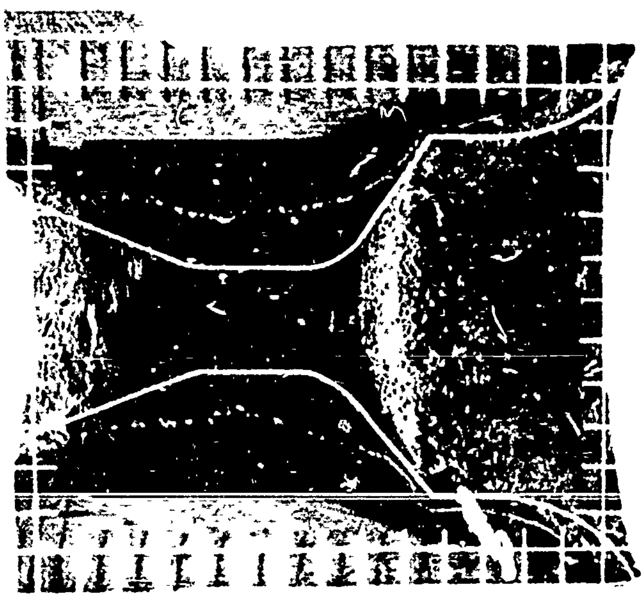

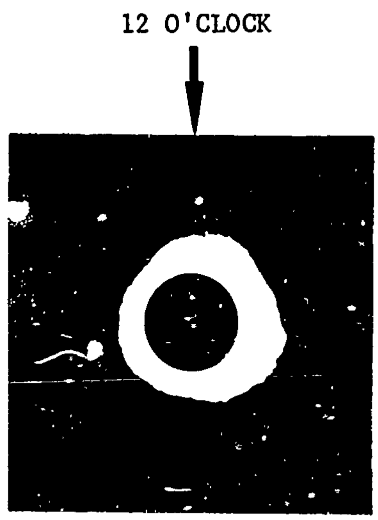

GRID SCALE
0.20 INCH

FIGURE 53. PROFILE AND AXIAL NOZZLE PHOTOGRAPHS

NOZZLE NO. ASD-546

12 O'CLOCK

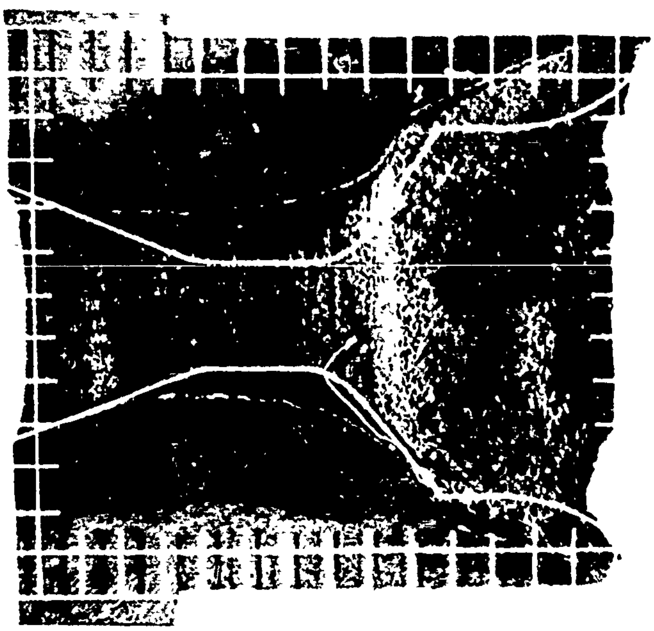

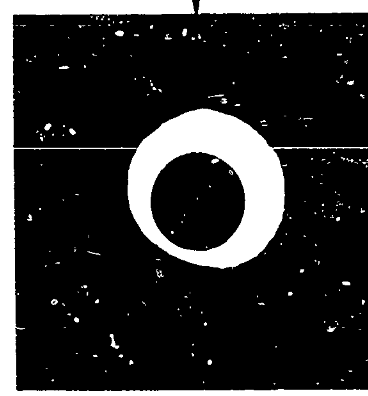

NOZZLE NO. ASD-547

12 O'CLOCK

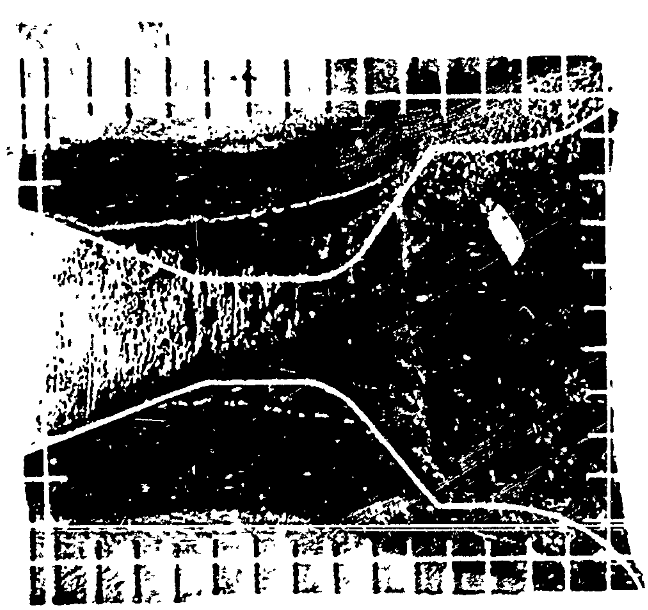

GRID SCALE
0.20 INCH

FIGURE 54. PROFILE AND AXIAL NOZZLE PHOTOGRAPHS

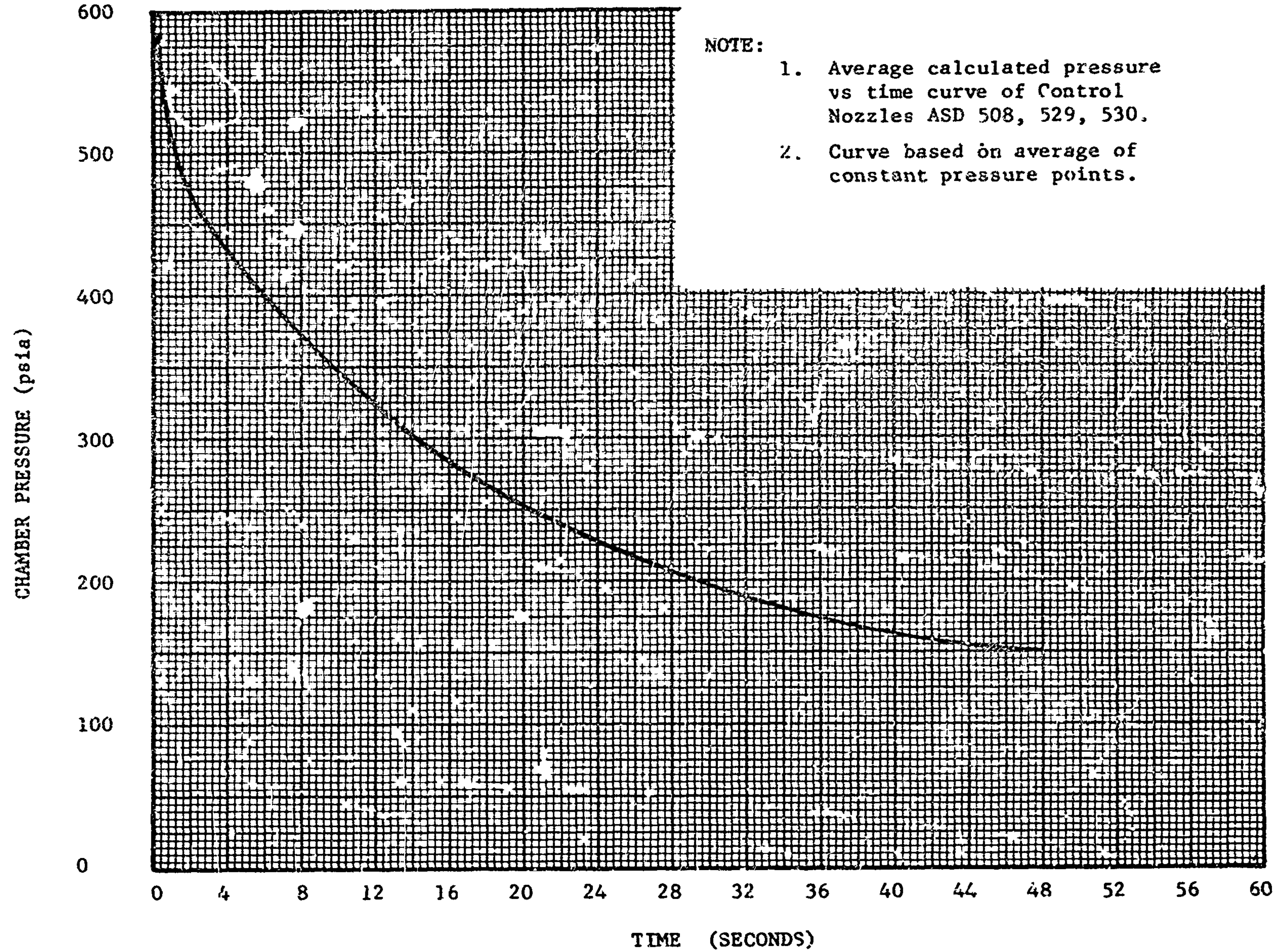

FIGURE 55. AVERAGE CONTROL NOZZLE CHAMBER PRESSURE VS. TIME

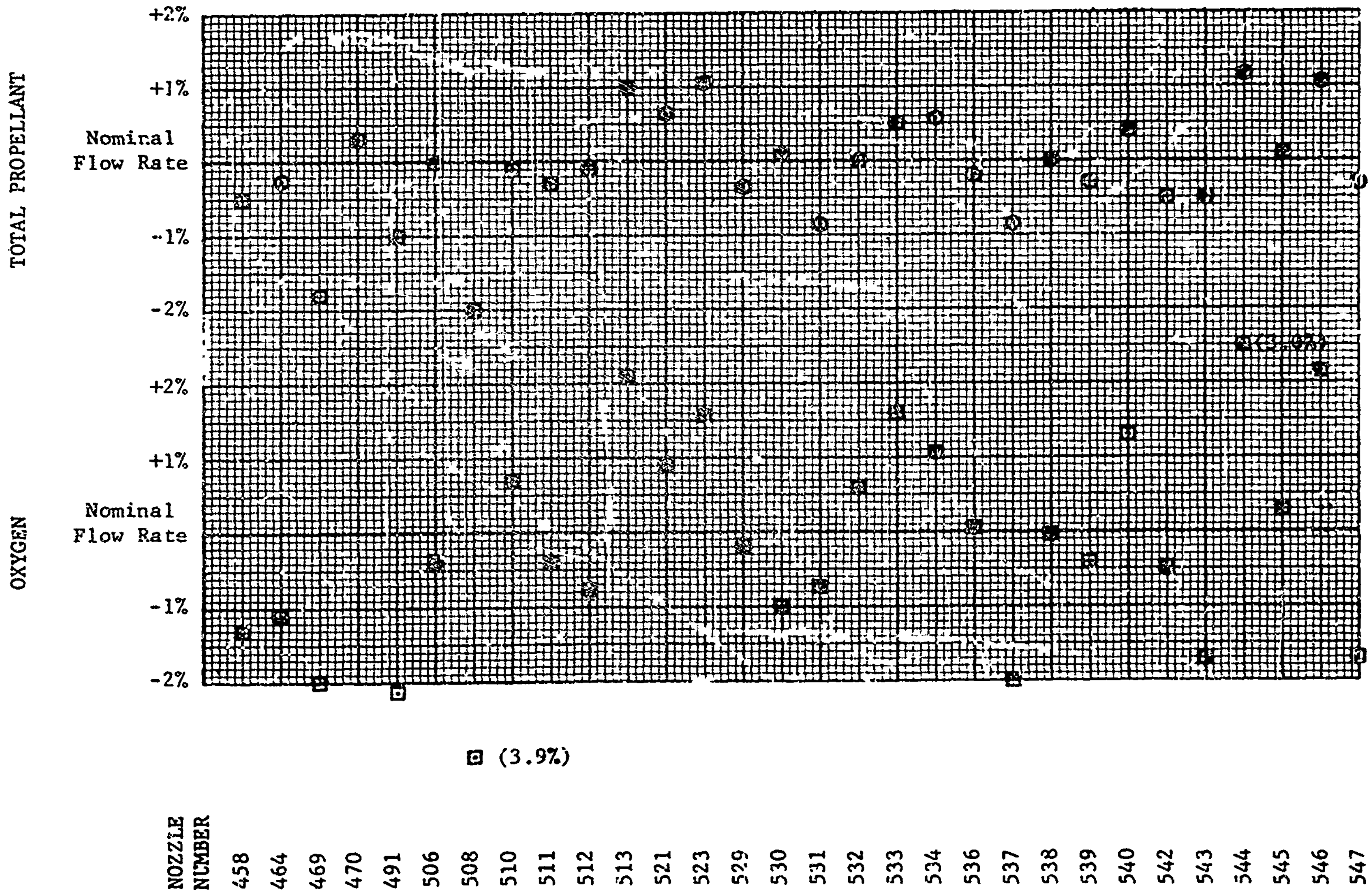

FIGURE 56. TEST - TO - TEST PROPELLANT FLOWRATE VARIATION FROM NOMINAL CONDITICN

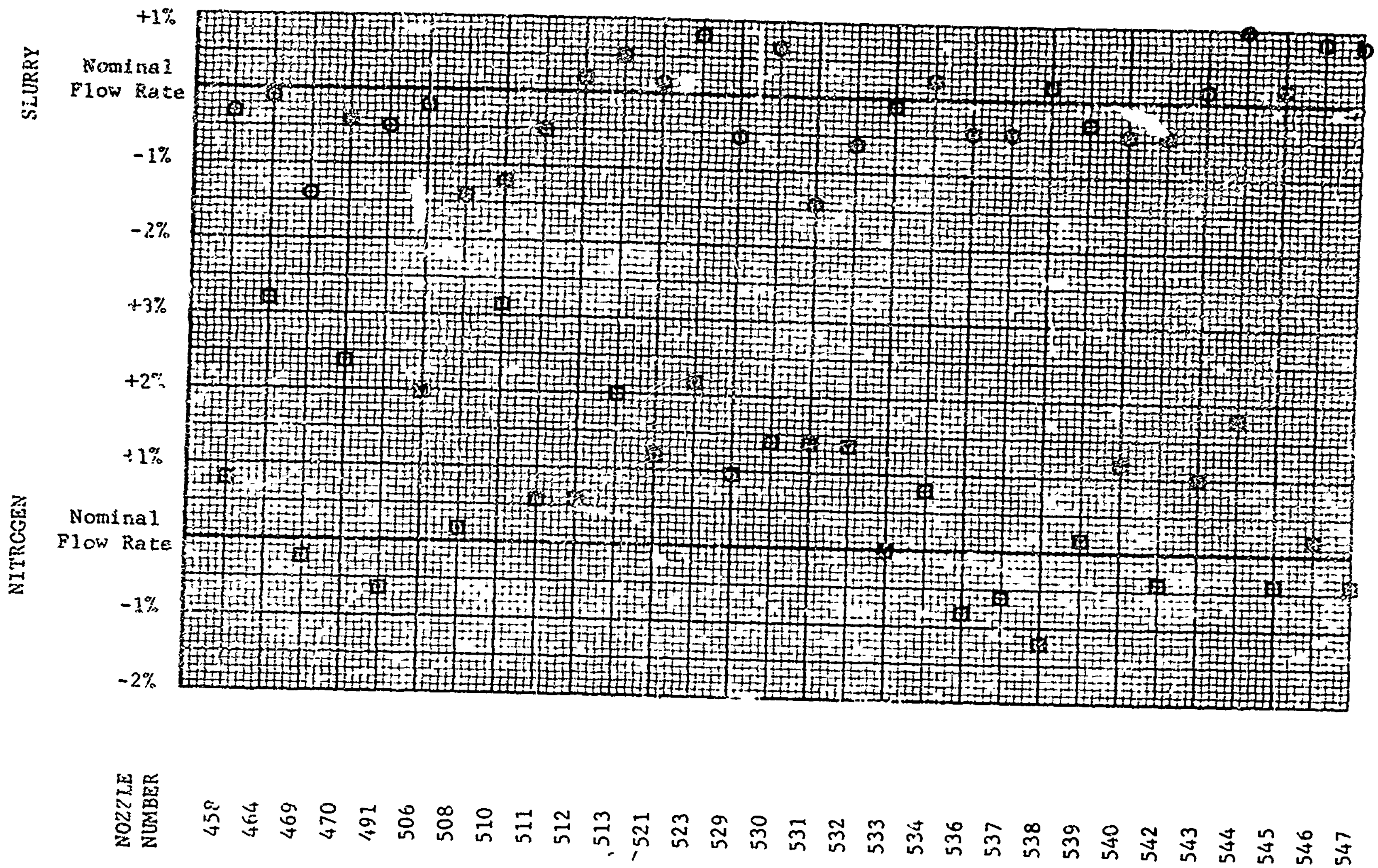

FIGURE 57. TEST-TO-TEST PROPELLANT FLOWRATE VARIATION FROM NOMINAL CONDITION

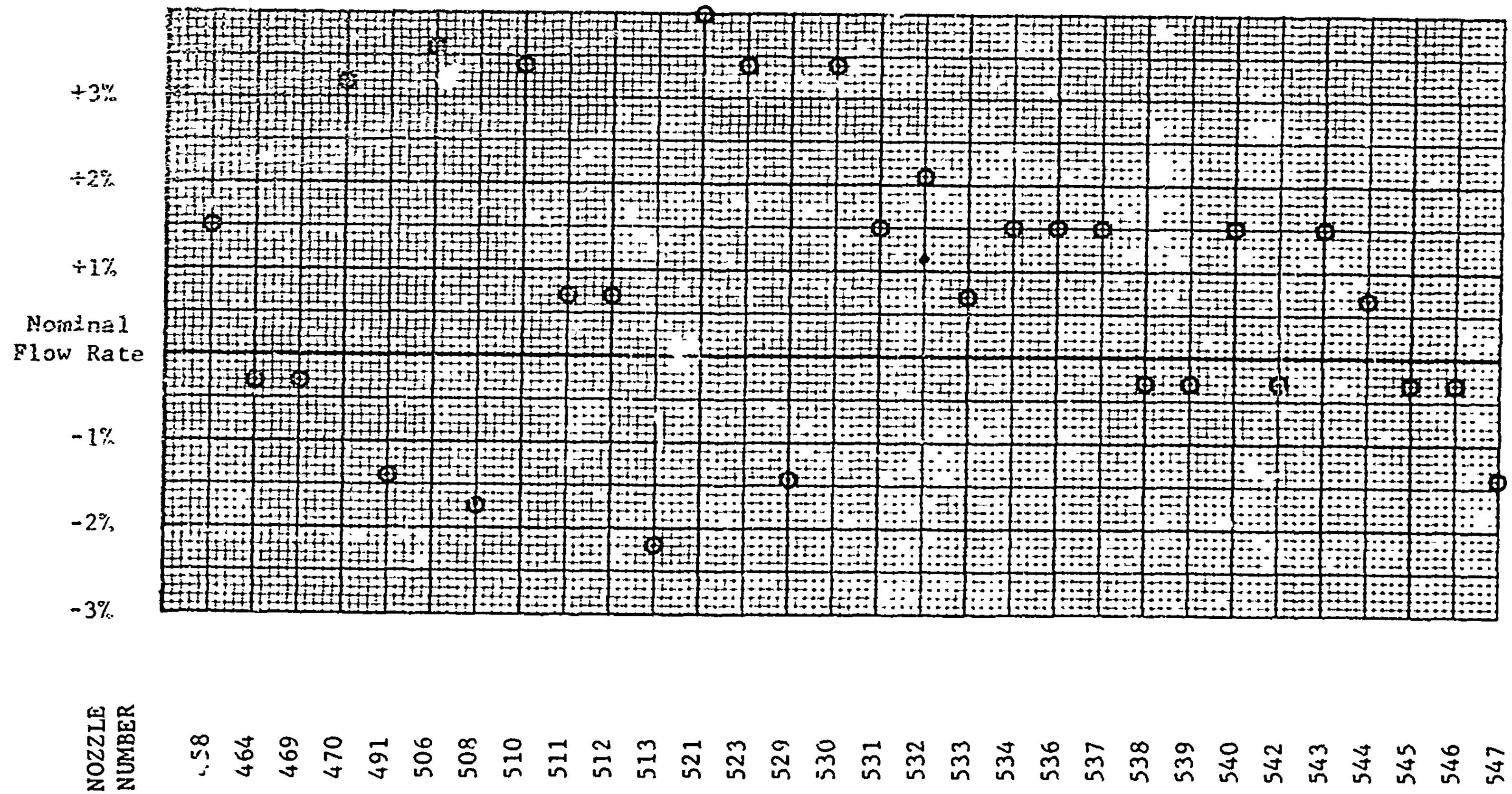

FIGURE 58. TEST-TO-TEST PROPELLANT FLOWRATE VARIATION FROM NOMINAL CONDITION

HYDROGEN

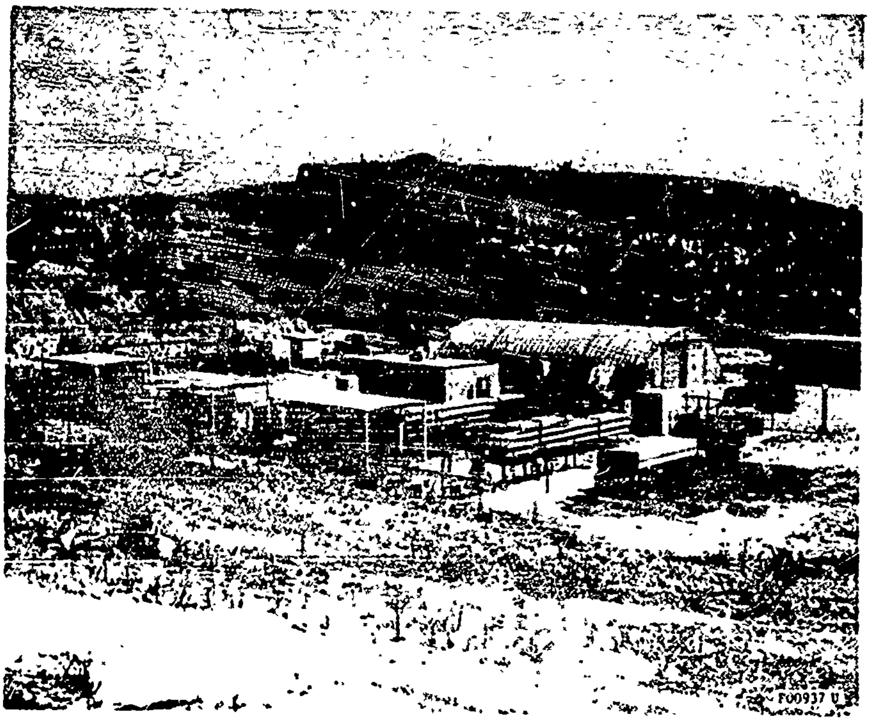

FIGURE 59. AERONUTRONIC EL TORO TEST SITE

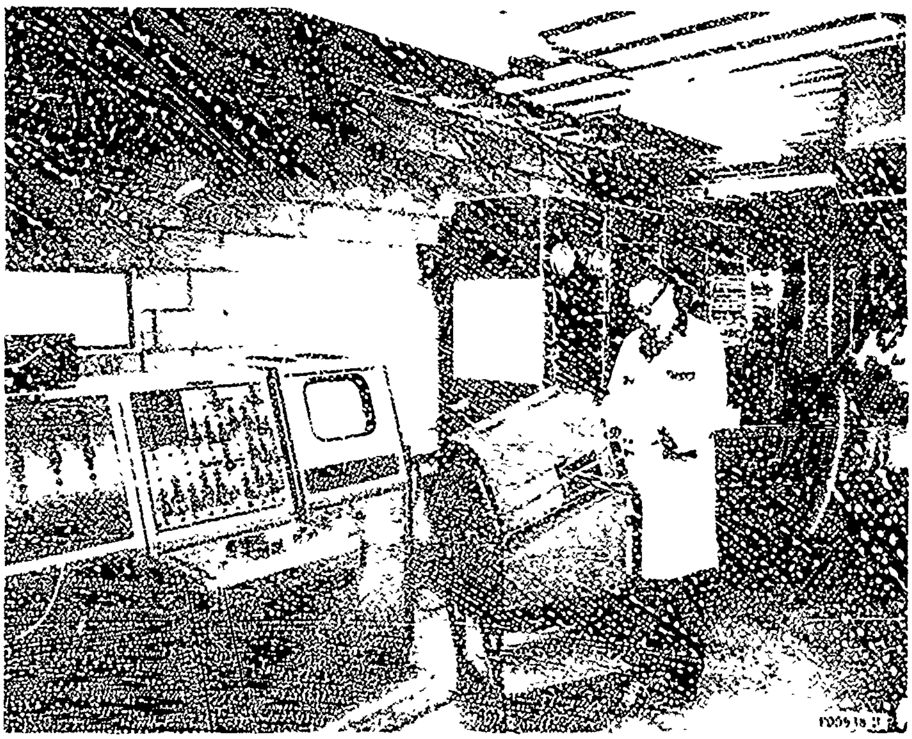

FIGURE 60. CONTROL COMPLEX AT EL TORO

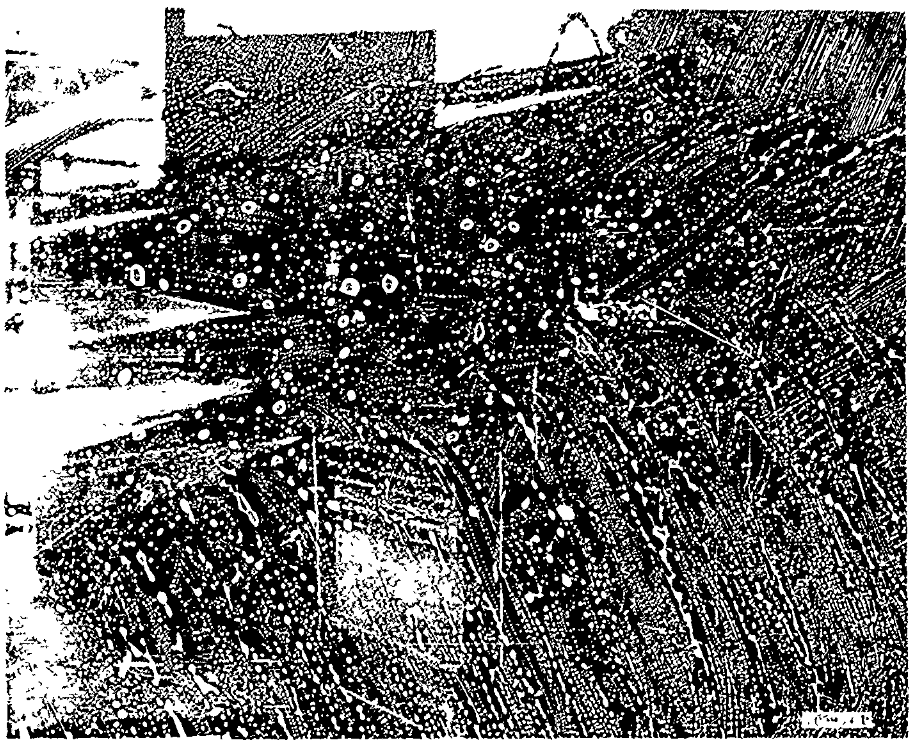

FIGURE 61. AERONUTRONIC REMOTE TEST SITE - TEST CELL B - NTO/50-50 ABLATIVE NOZZLE TEST FIRING

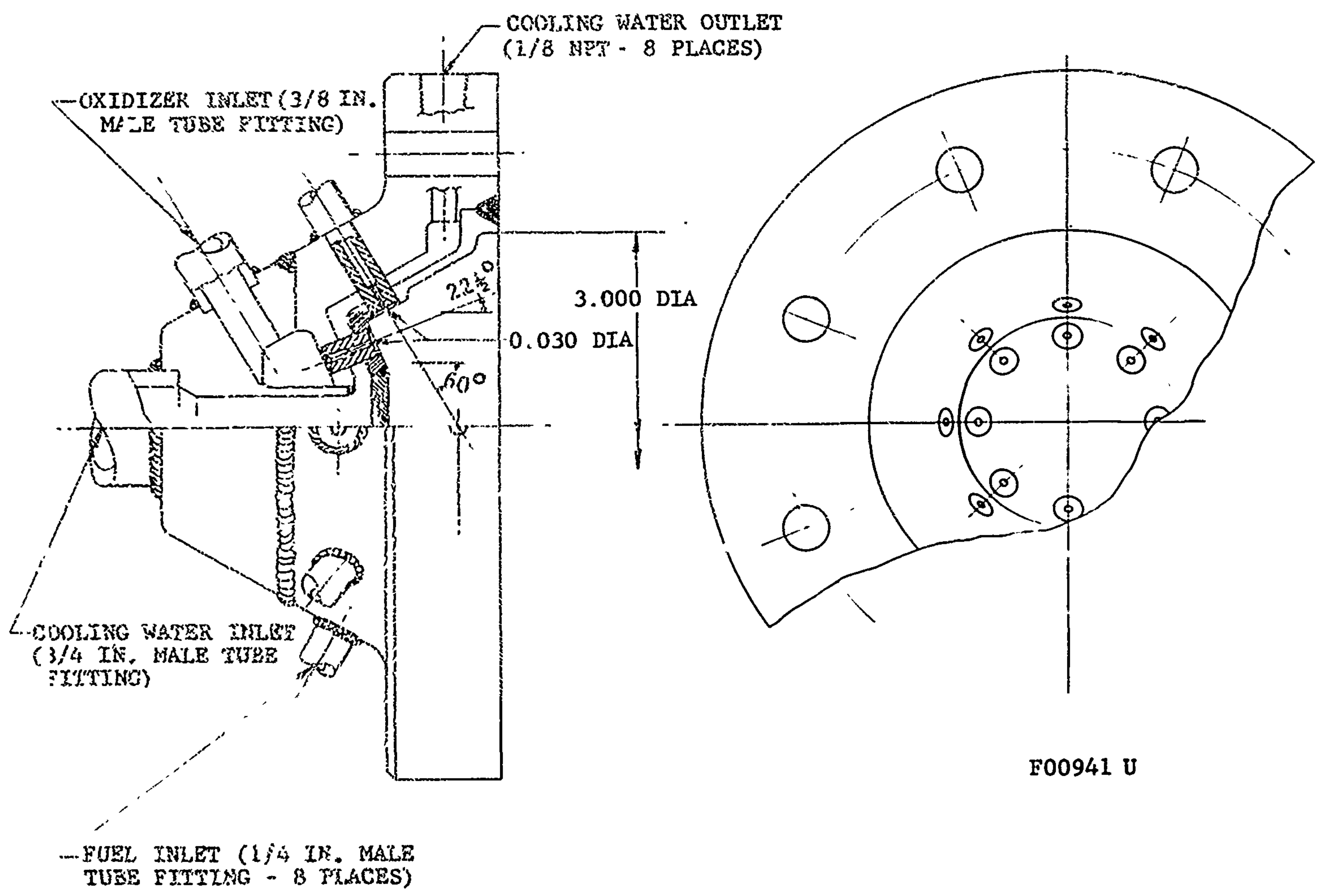

FIGURE 62. N_2O_4 - AEROZINE INJECTOR - WRIGHT FIELD NOZZLE TEST (STAINLESS)

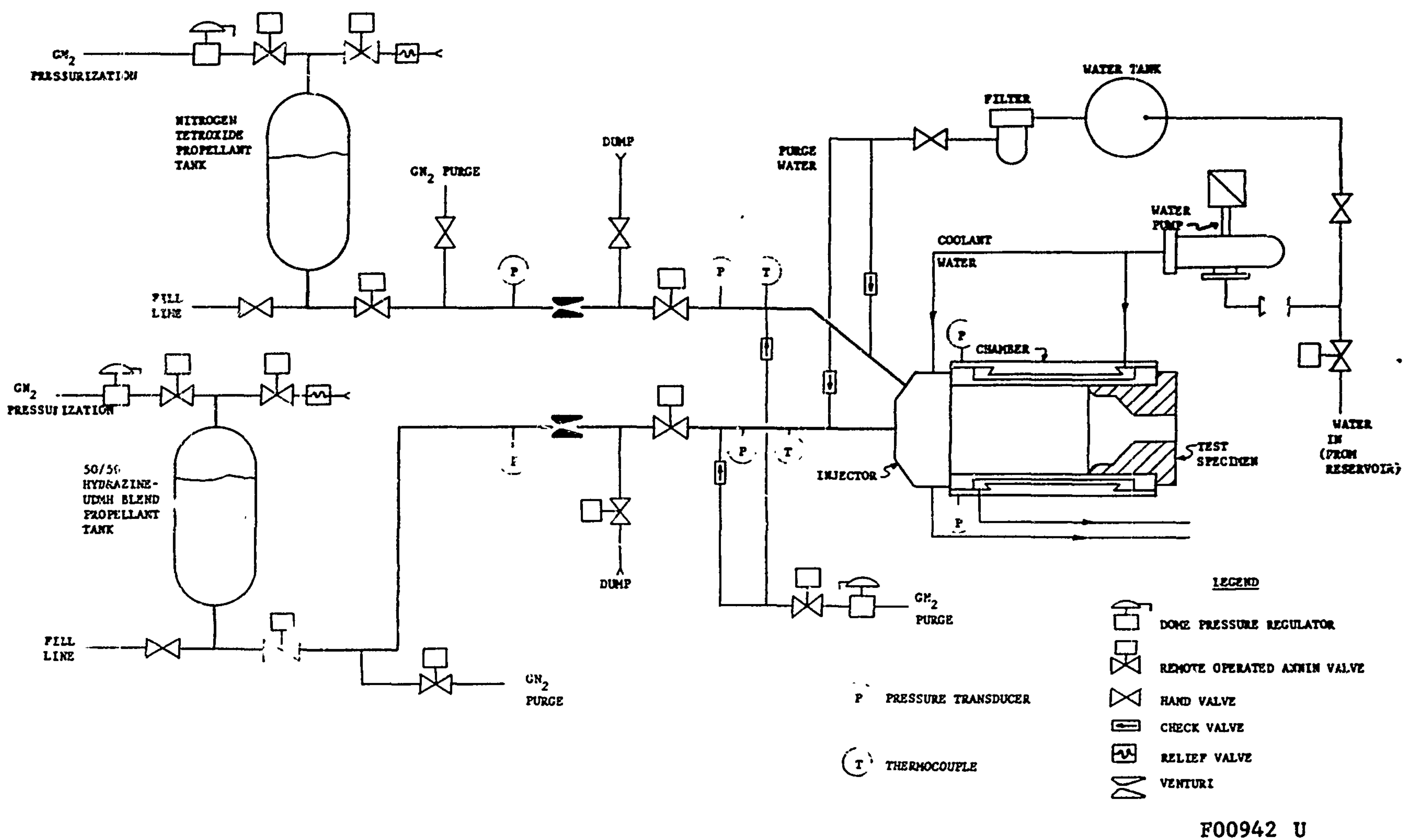

FIGURE 63. EL TORO CELL B SCHEMATIC - WRIGHT FIELD ABLATIVE NOZZLE TEST SERIES

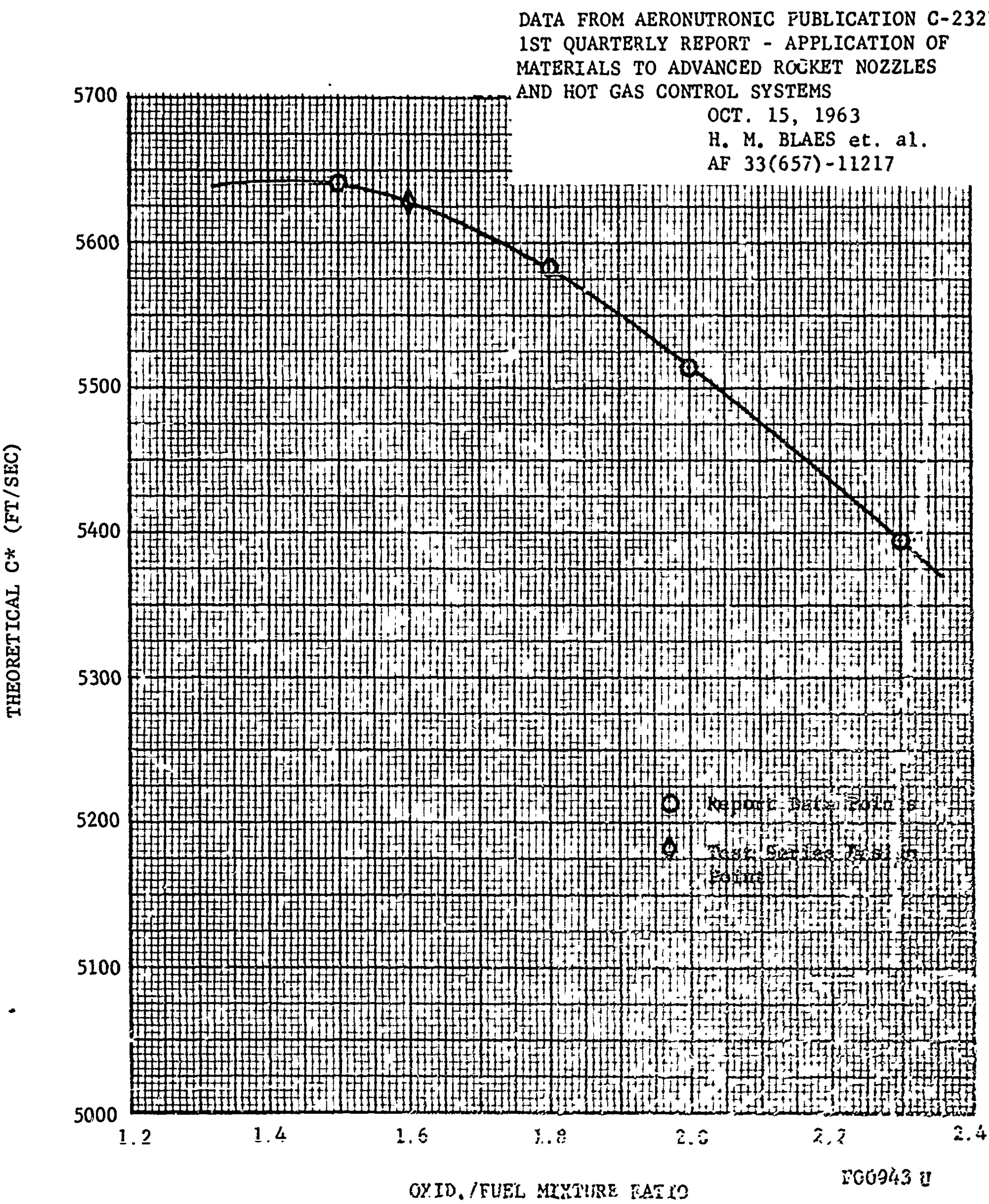

FIGURE 64. THEORETICAL C* VERSUS MIXTURE RATIO N_2O_4/50% N_2H_4-50% UDMH PROPELLANT AT 300 PSIA CHAMBER PRESSURE

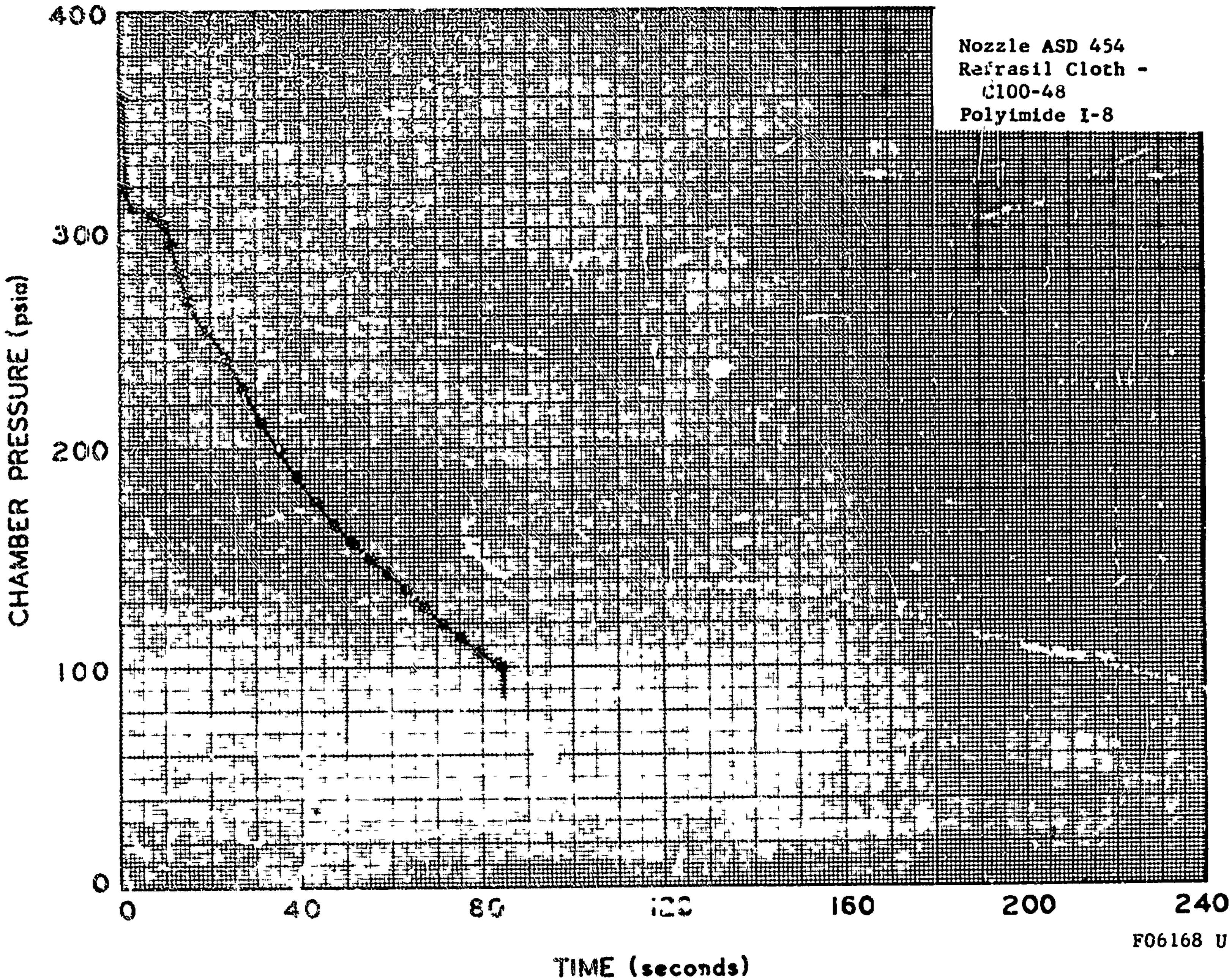

FIGURE 6.. NOZZLE ASD 454, CHAMBER PRESSURE VERSUS TIME

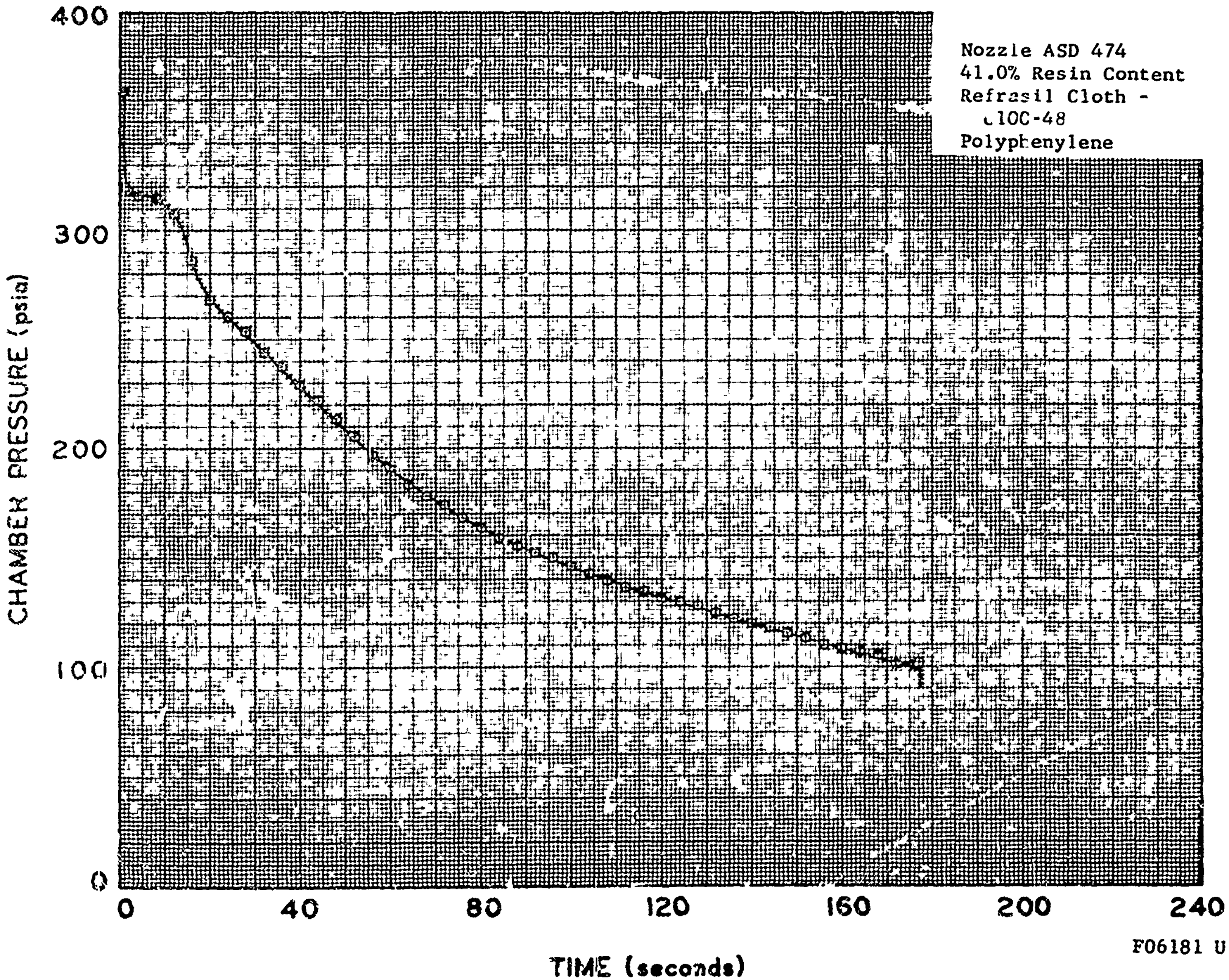

FIGURE 66. NOZZLE ASD 474; CHAMBER PRESSURE VERSUS TIME

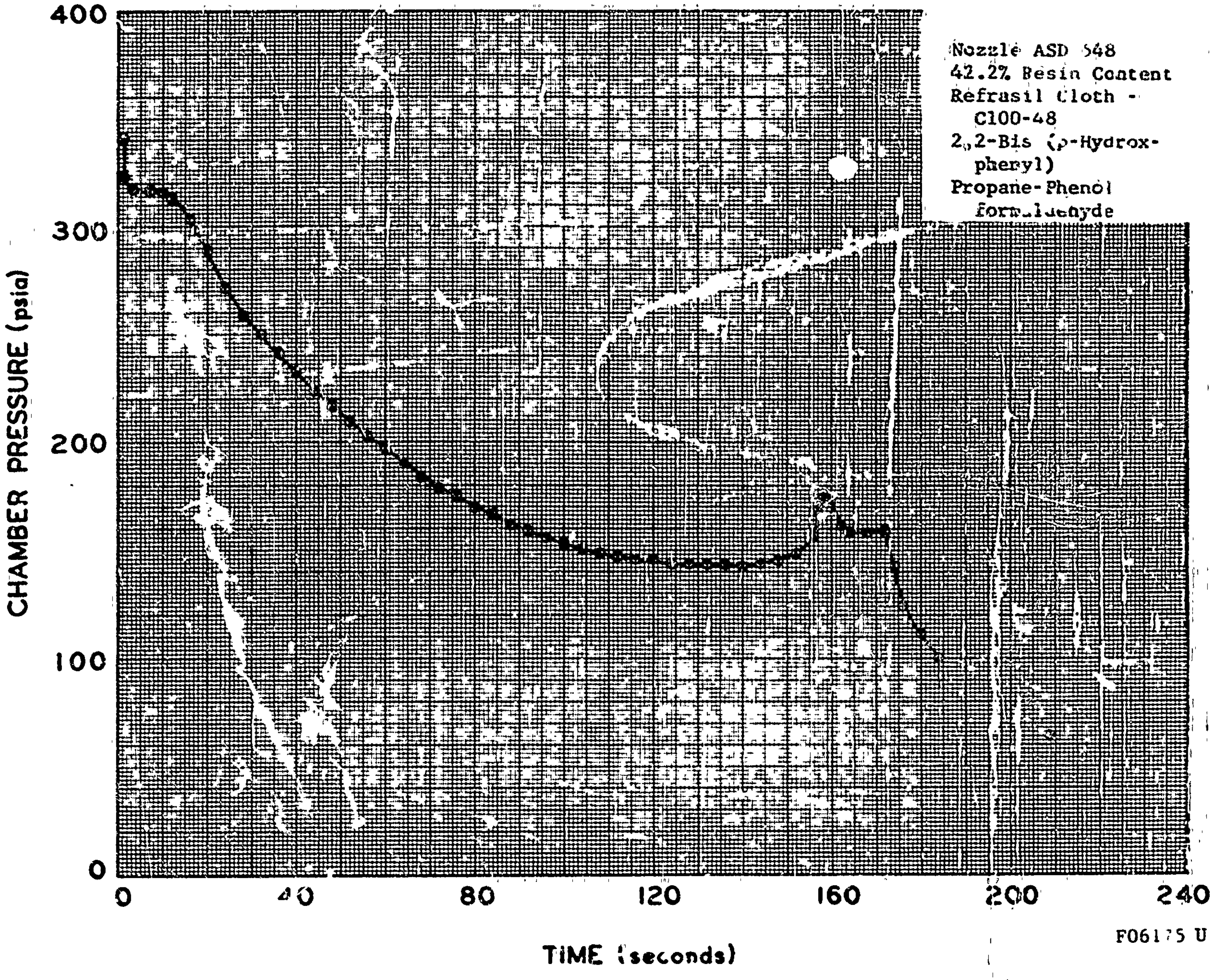

FIGURE 67. NOZZLE ASD 548; CHAMBER PRESSURE VERSUS TIME

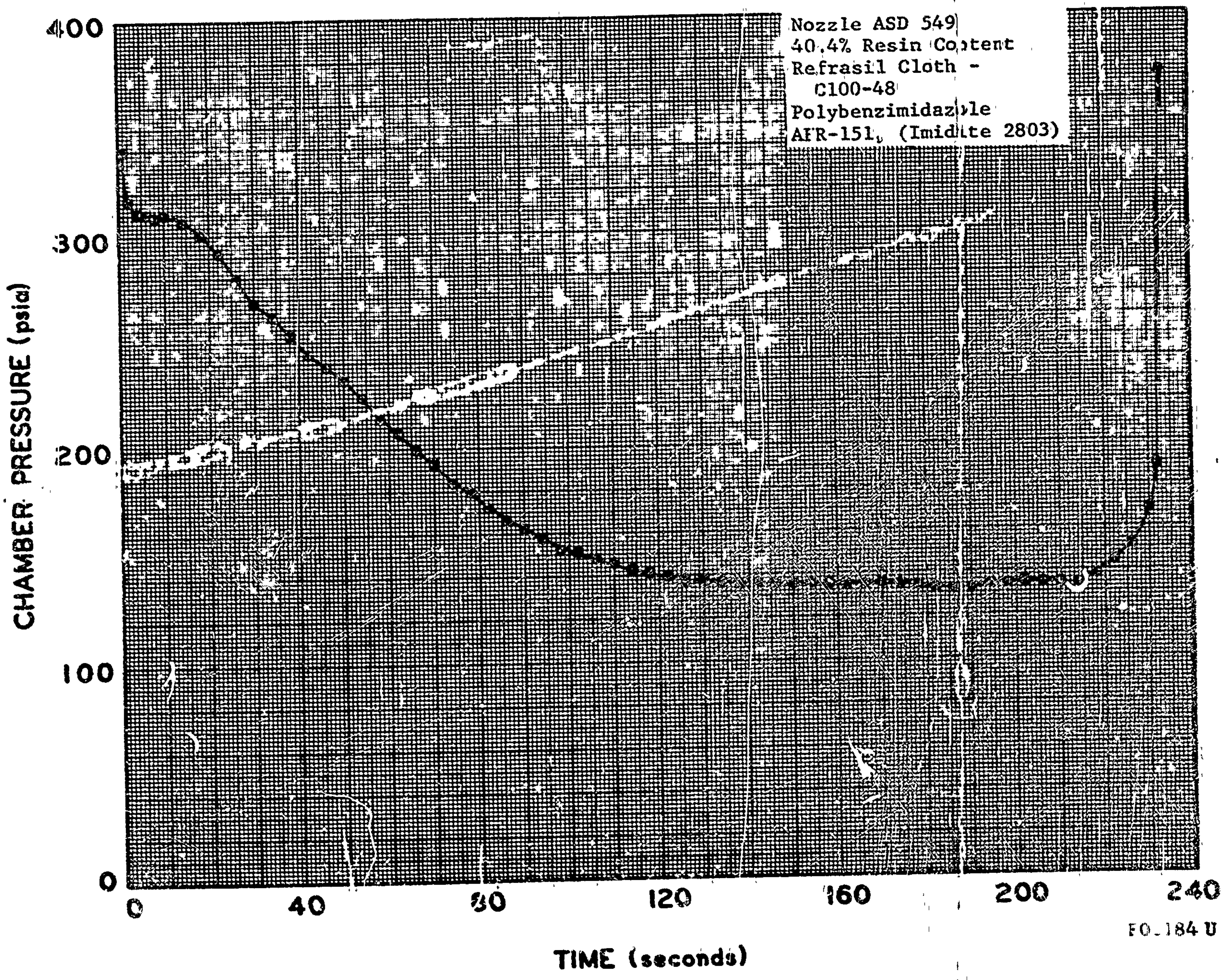

FIGURE 68. NOZZLE ASD 549; CHAMBER PRESSURE VERSUS TIME

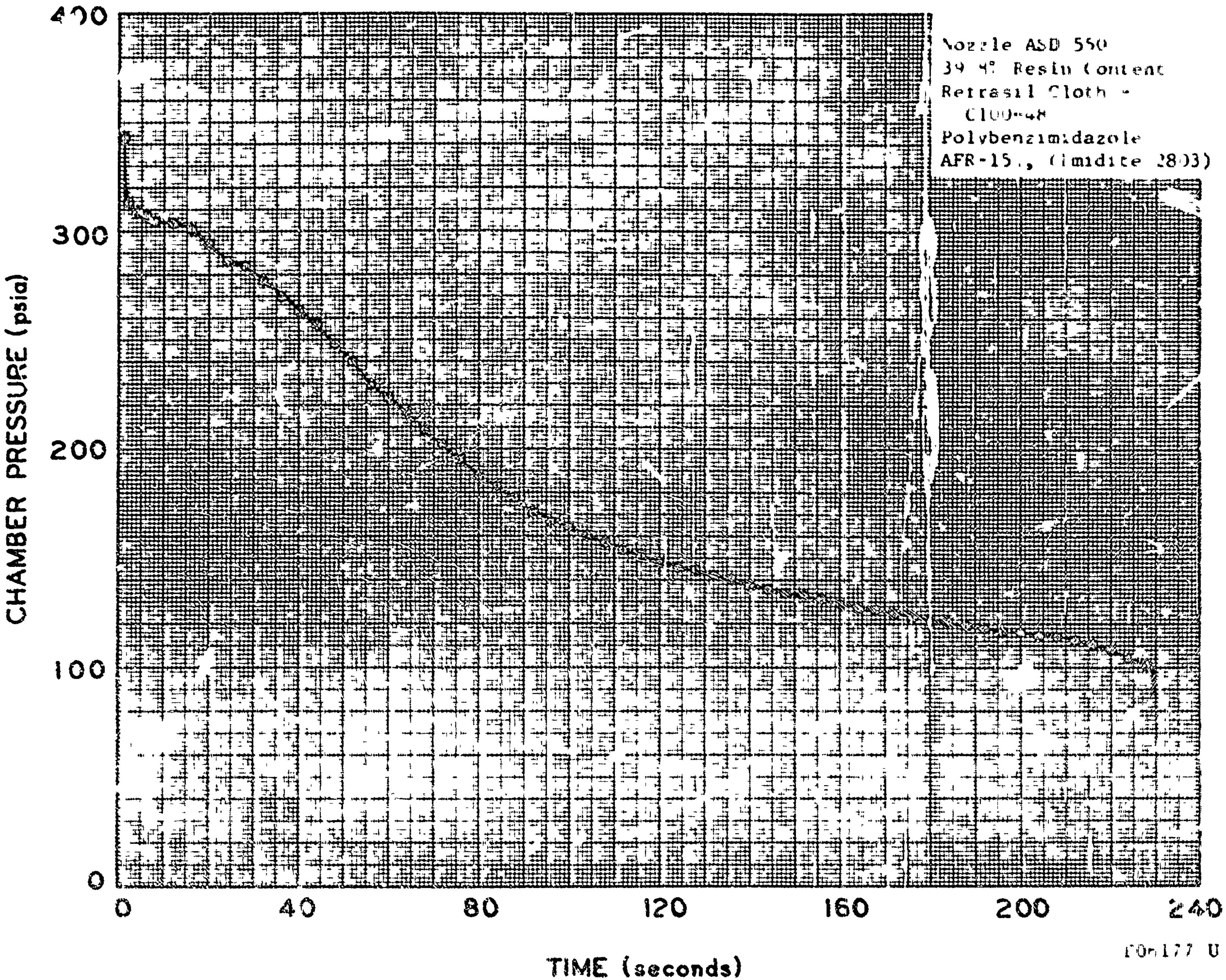

FIGURE 6[illegible]. [illegible]E ASD 550; CHAMBER PRESSURE VERSUS TIME

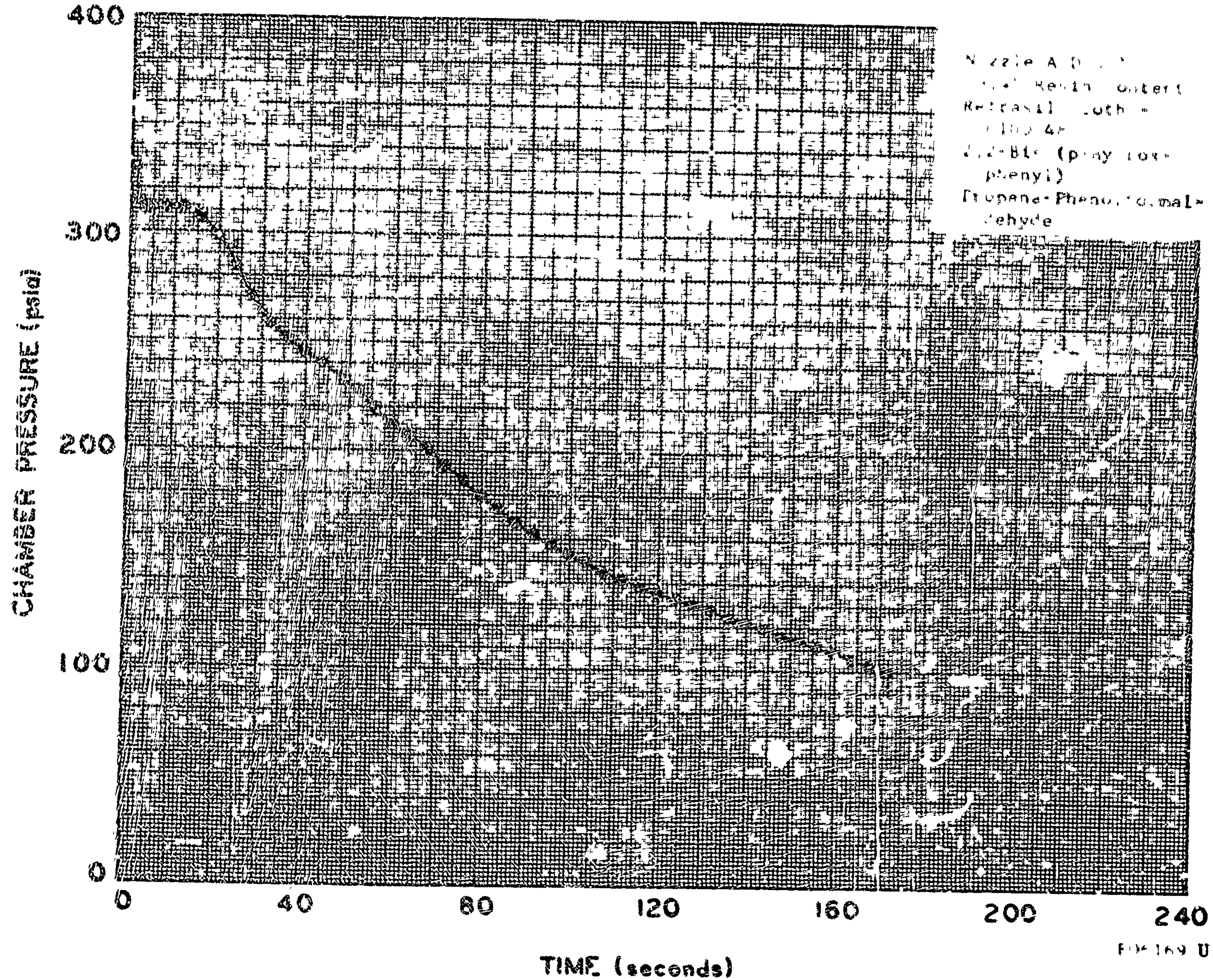

FIGURE 70. NOZZLE ASD 551, CHAMBER PRESSURE VERSUS TIME

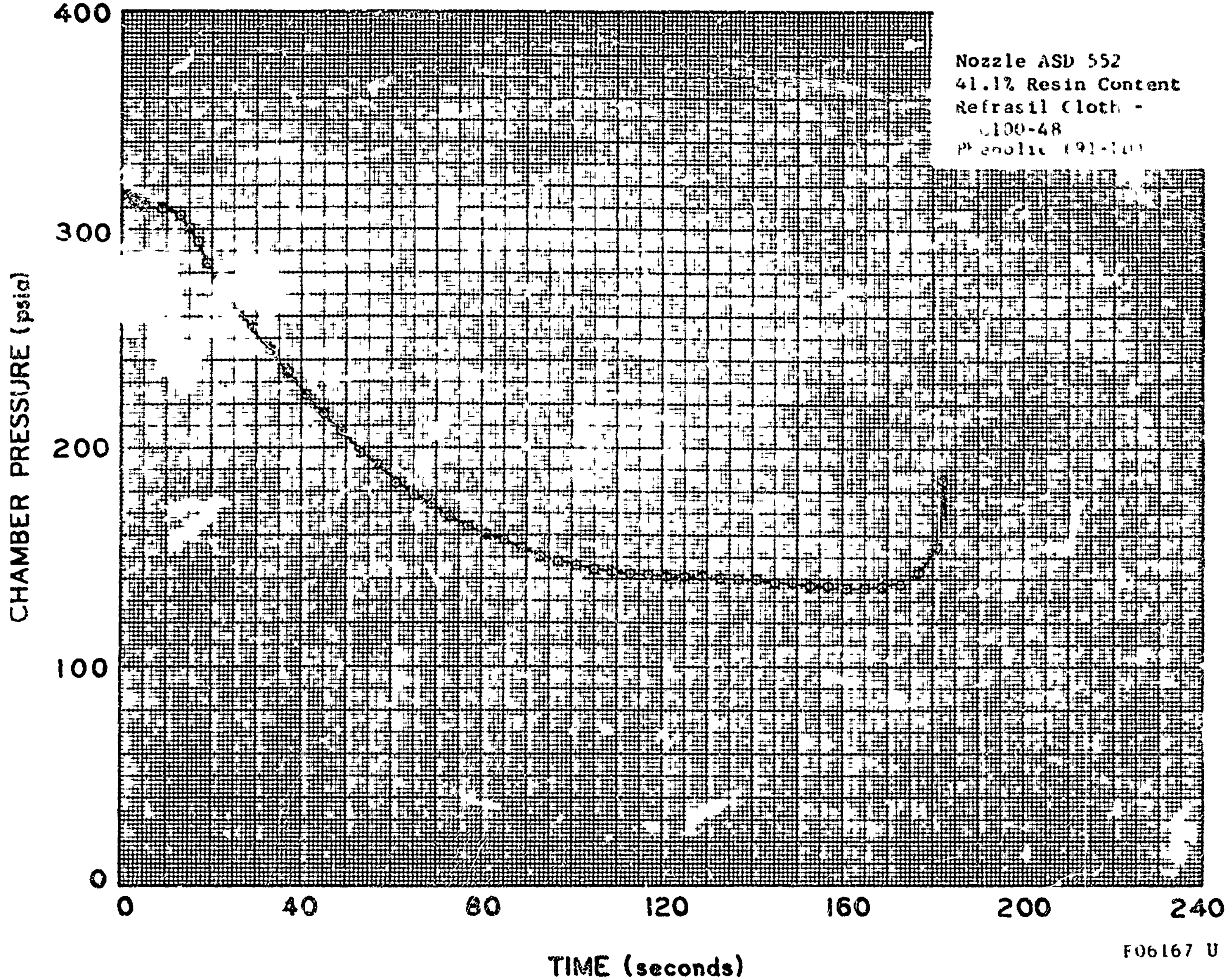

FIGURE 71. NOZZLE ASD 552; CHAMBER PRESSURE VERSUS TIME

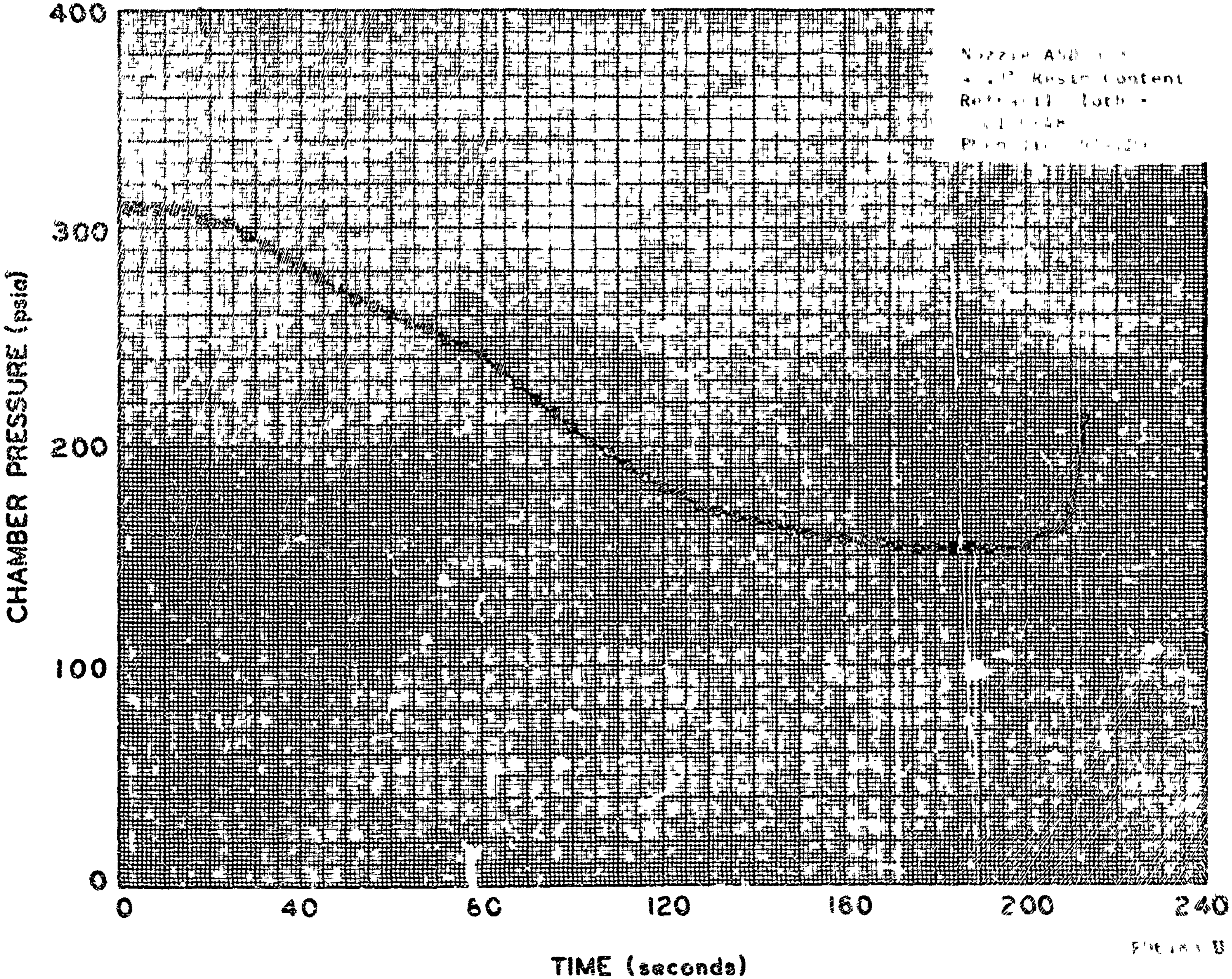
CHAMBER PRESSURE (psia)
400
300
200
100
0
0
40
60
120
160
200
240
TIME (seconds)

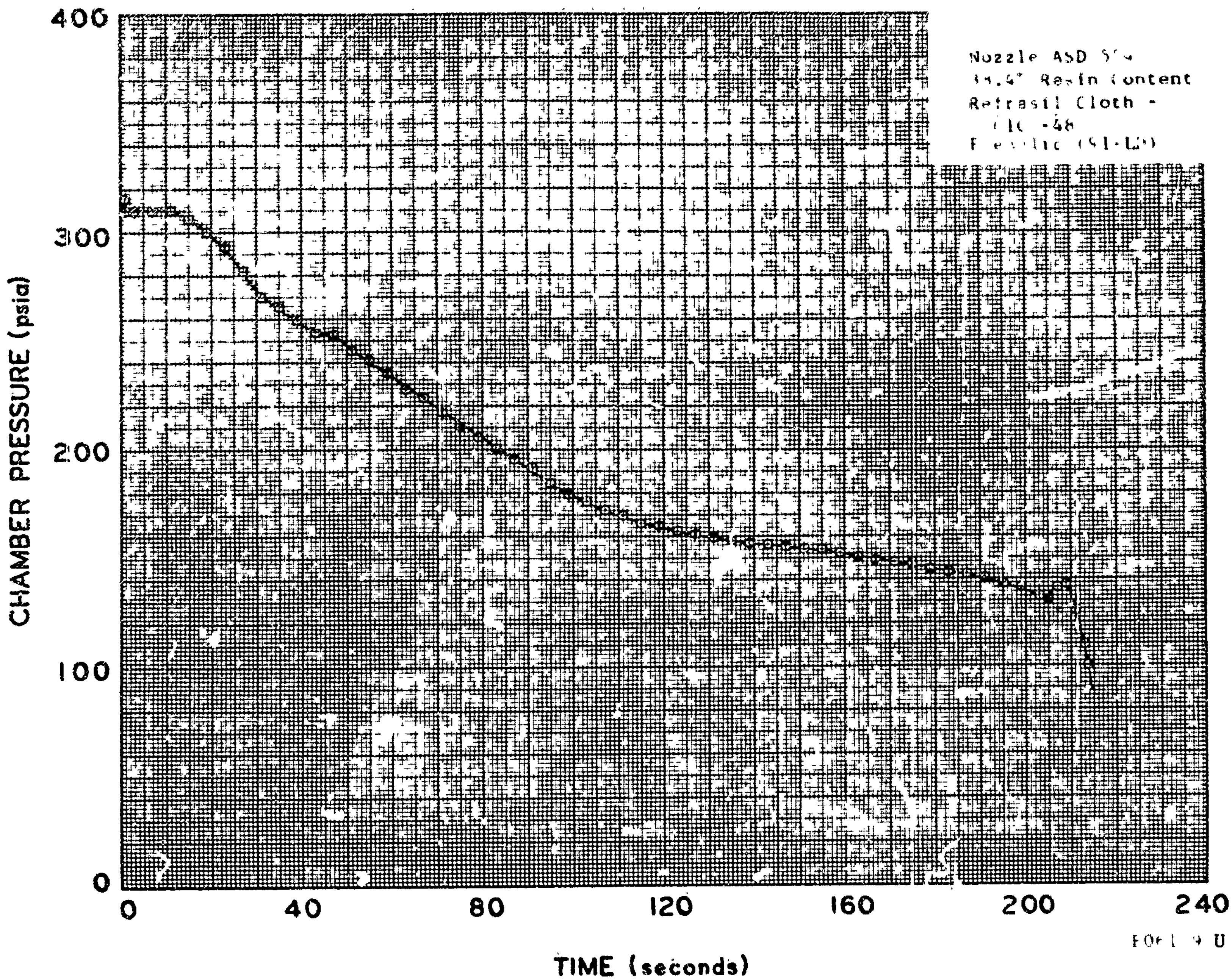

FIGURE 7?, NOZZLE ASD 5?4, CHAMBER PRE...

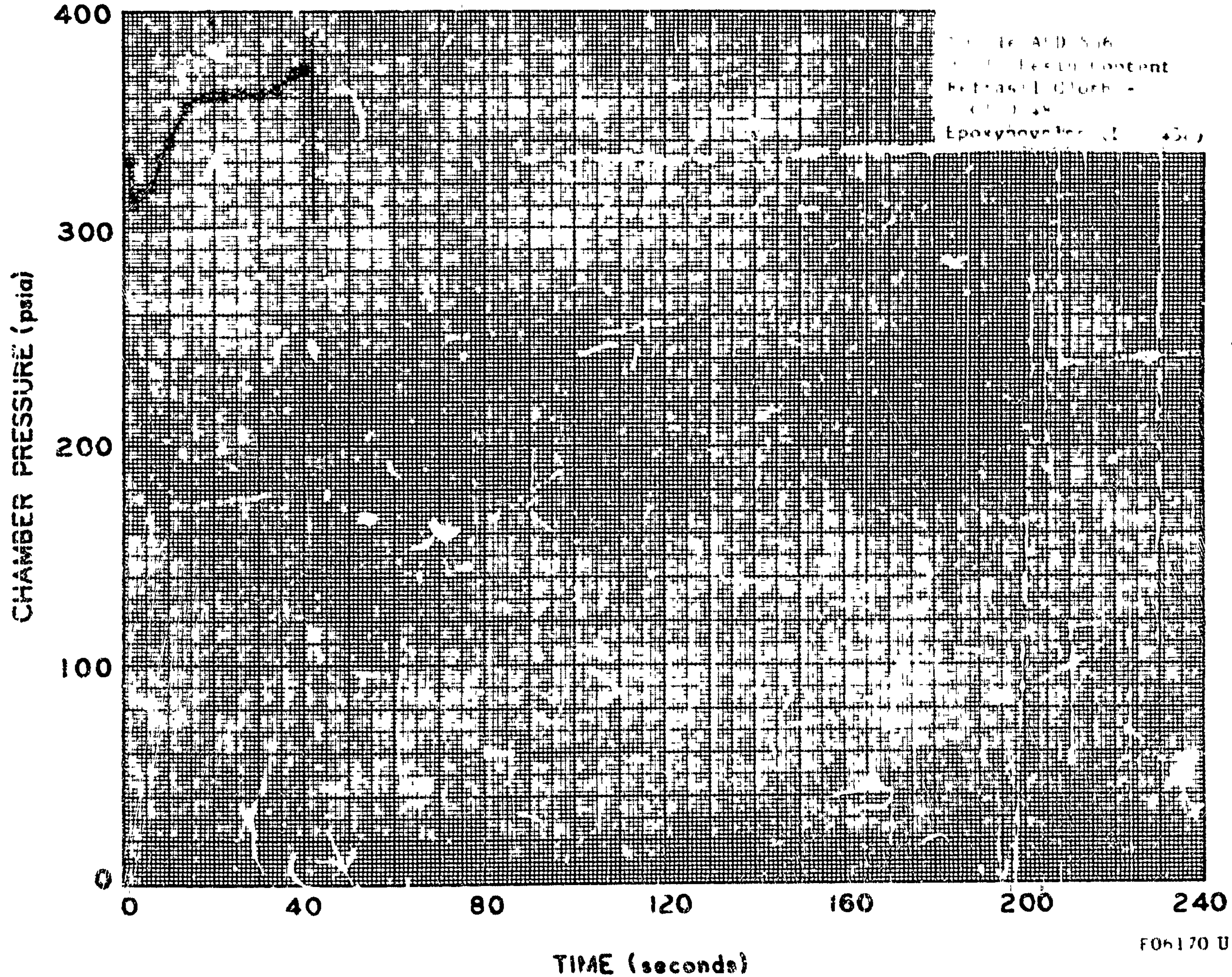

FIGURE . . . CHAMBER PRESSURE . . . TIME

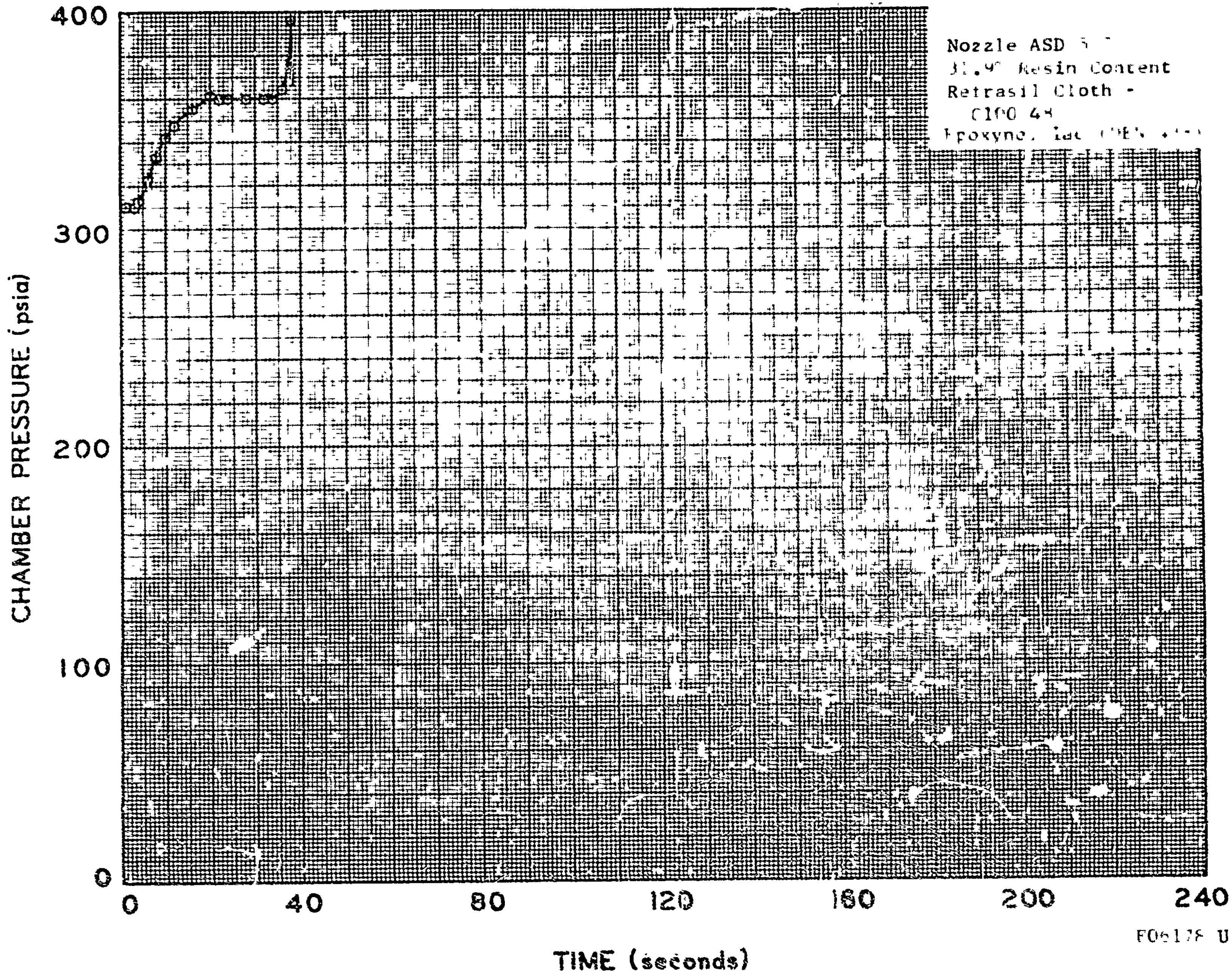

FIGURE 75. NOZZLE ASD 5°7; CHAMBER PRESSURE VERSUS TIME

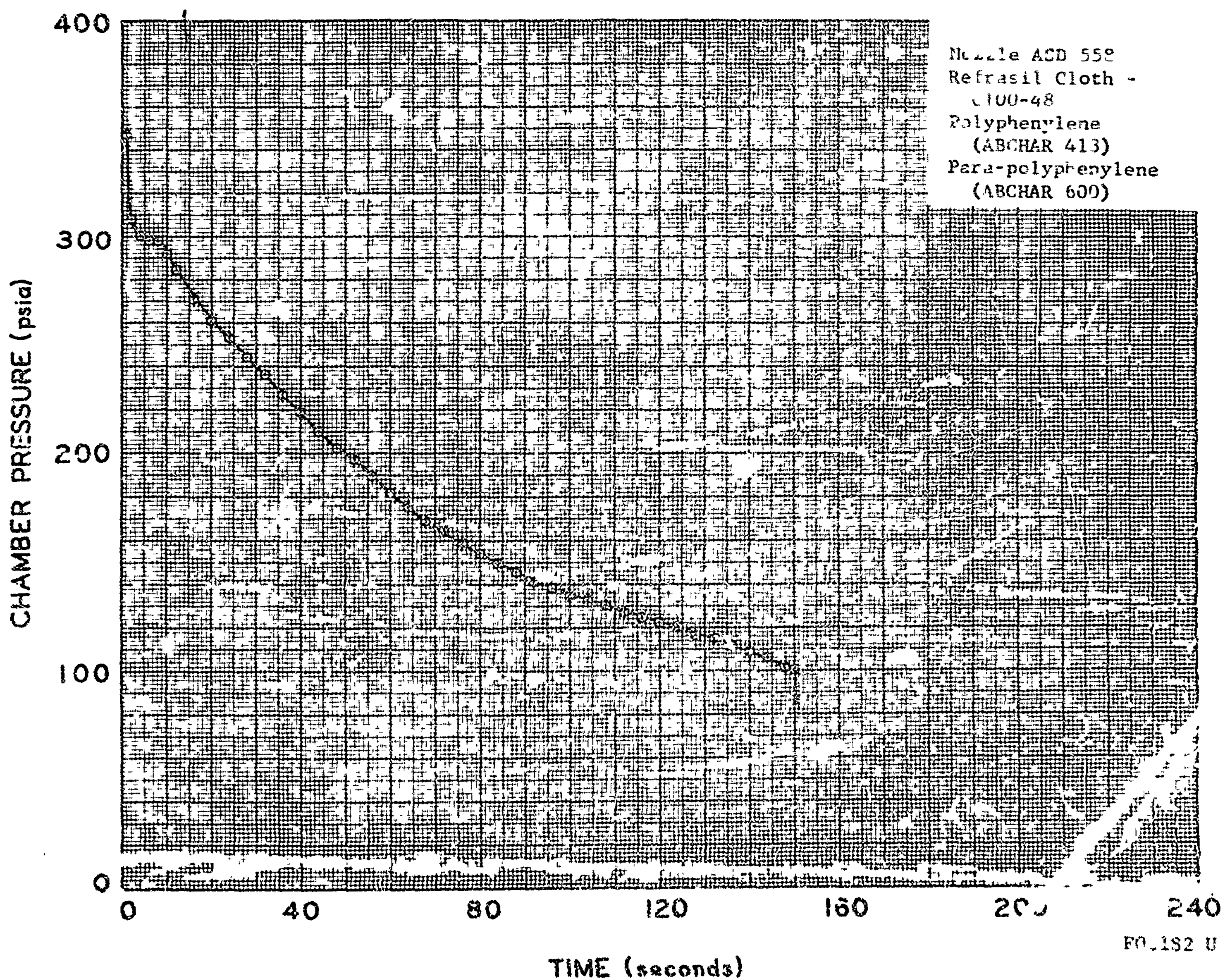

FIGURE 76 NOZZLE ASD 558; CHAMBER PRESSURE VERSUS TIME

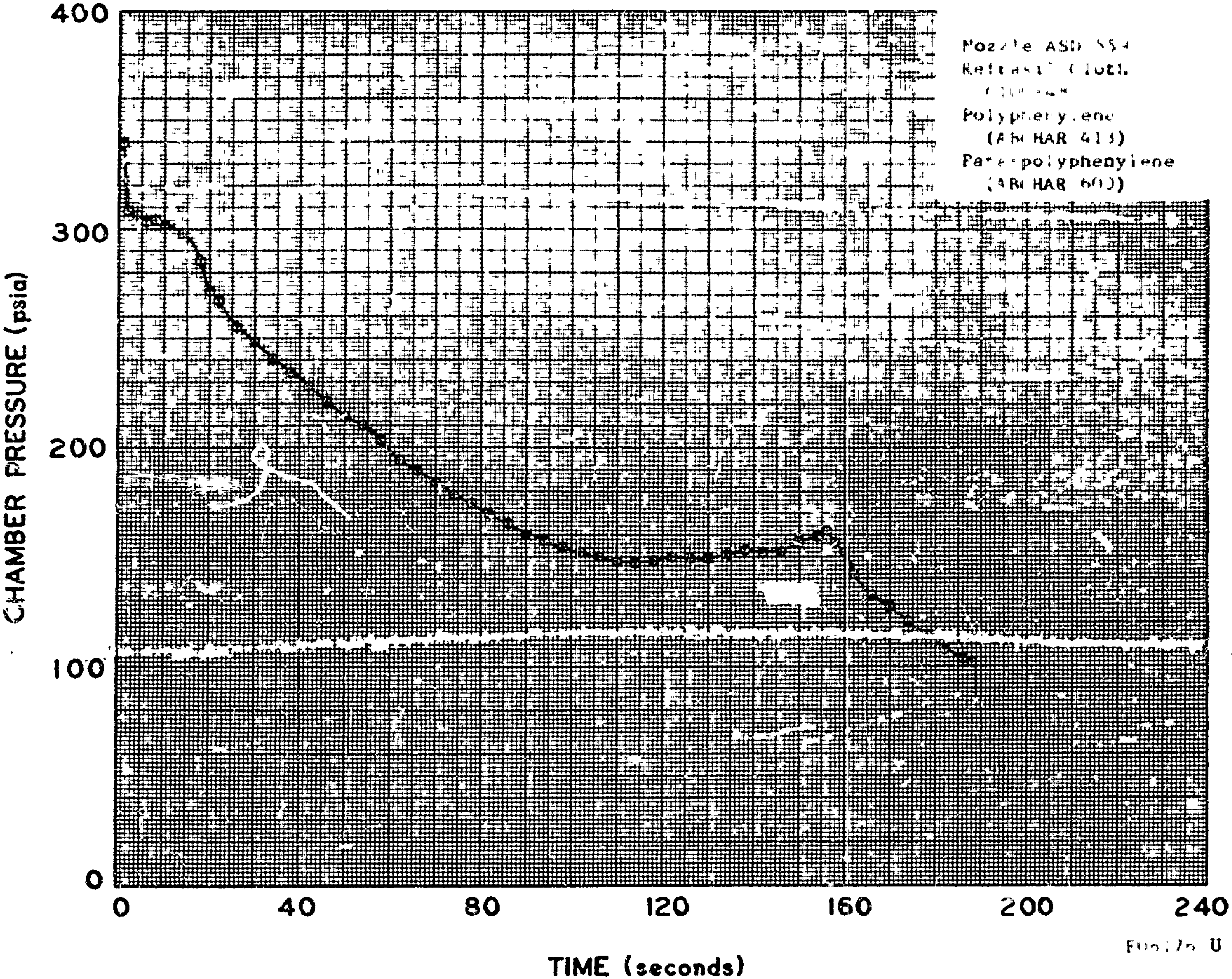

FIGURE 77. NOZZLE ASD 559; CHAMBER PRESSURE VERSUS TIME

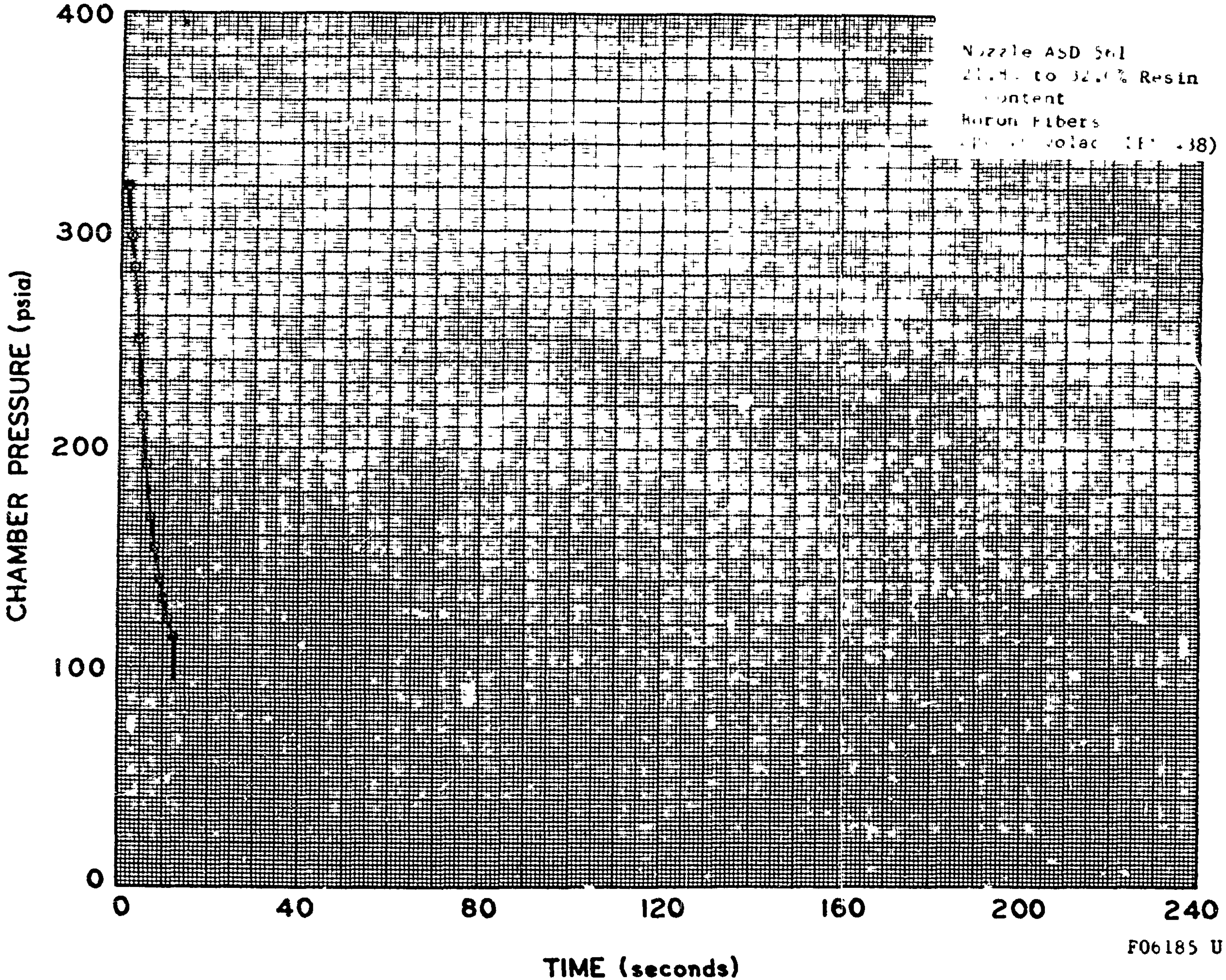

FIGURE 78. NOZZLE ASD 561; CHAMBER PRESSURE VERSUS TIME

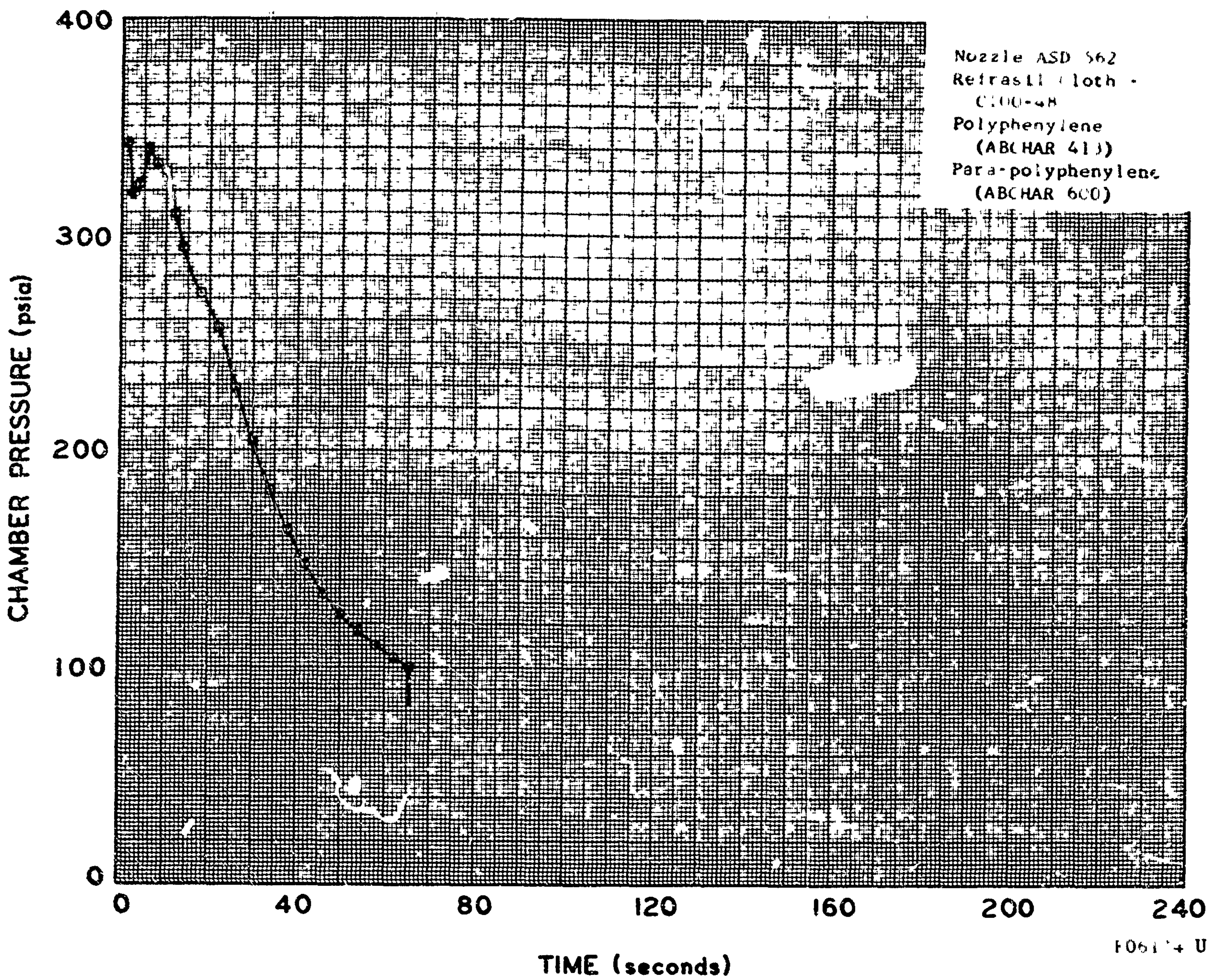

FIGURE 79 NOZZLE ASD 562 CHAMBER PRESSURE VERSUS TIME

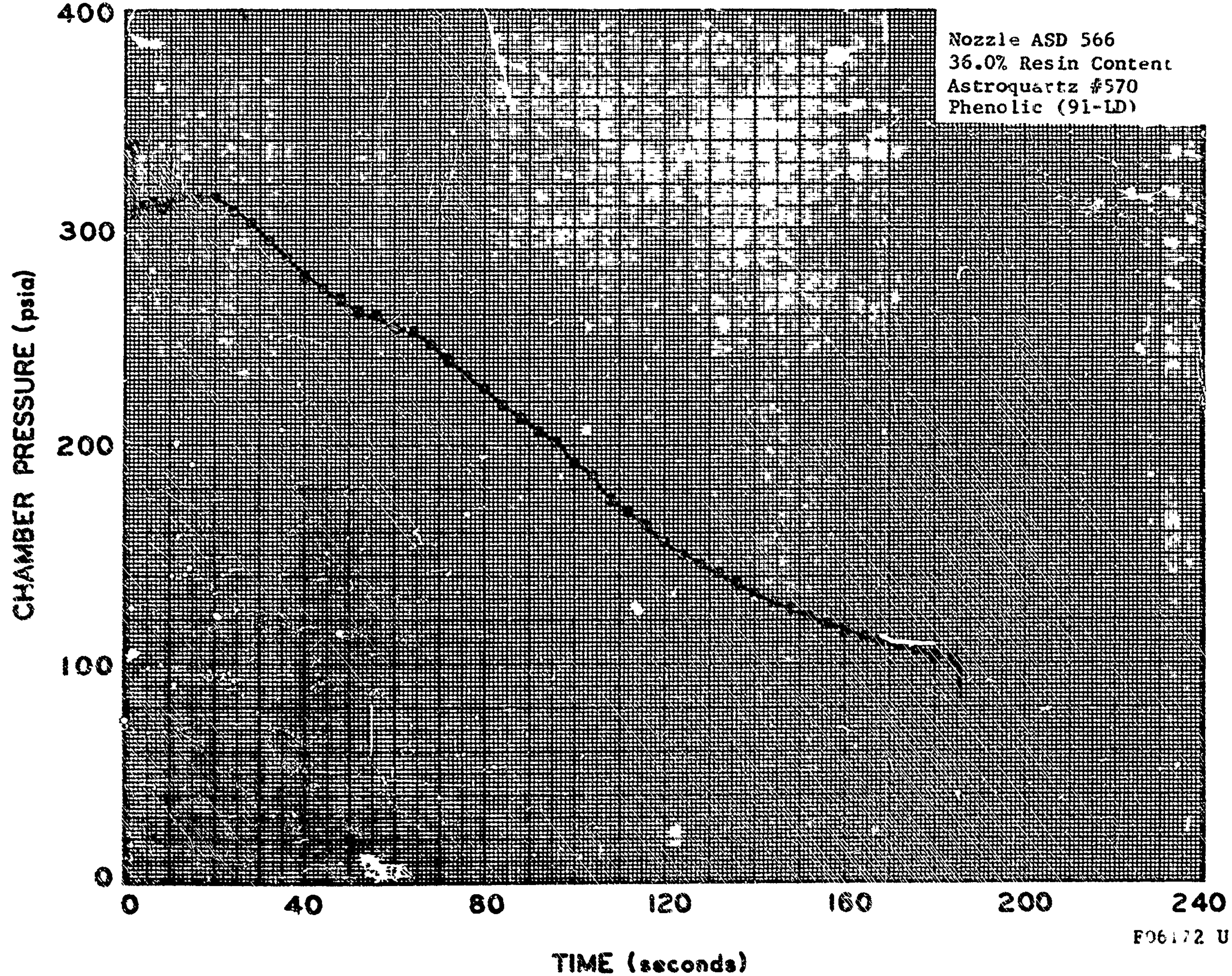

FIGURE 80. NOZZLE ASD 566; CHAMBER PRESSURE VERSUS TIME

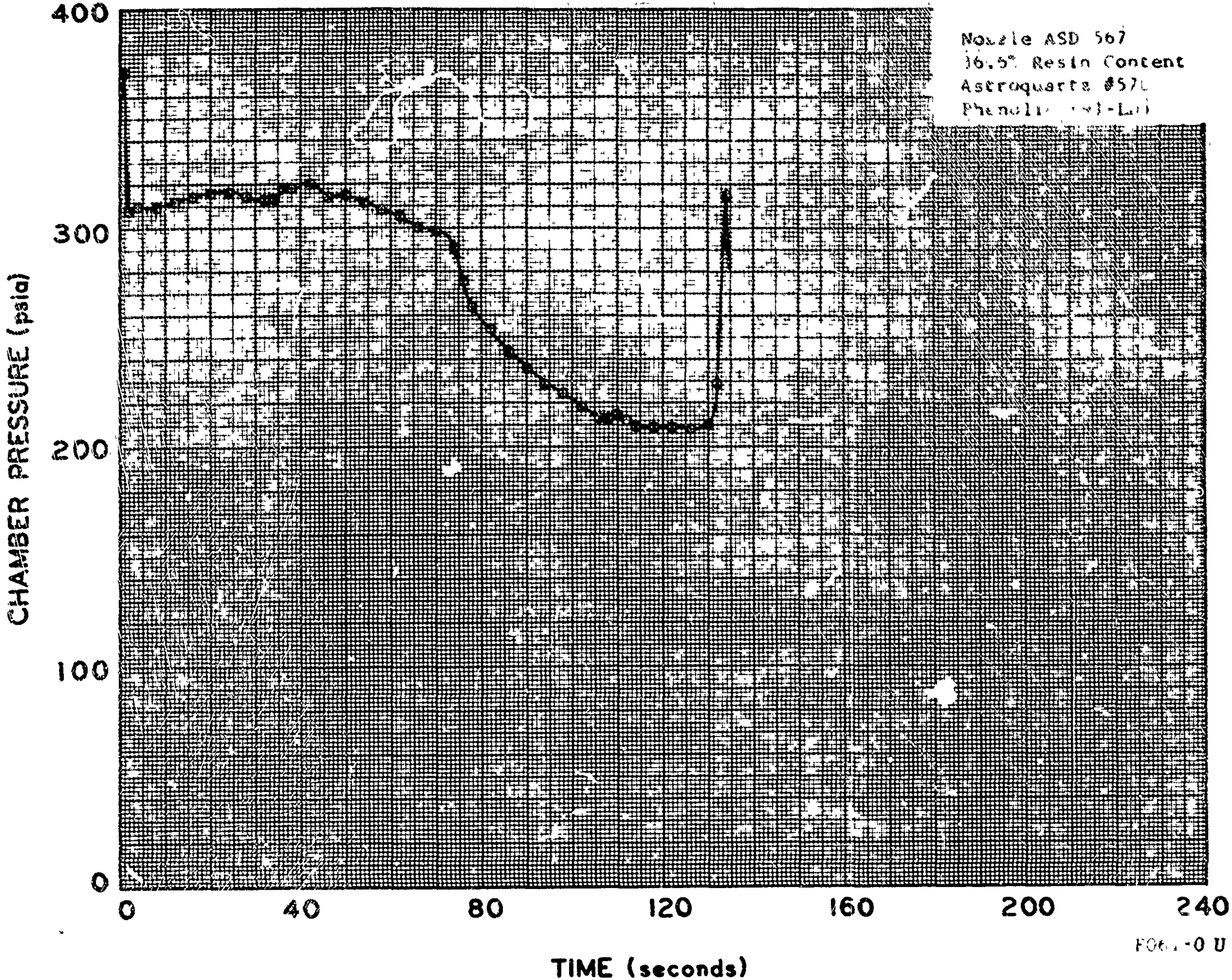

FIGURE 81. NOZZLE ASD 567; CHAMBER PRESSURE VERSUS TIME

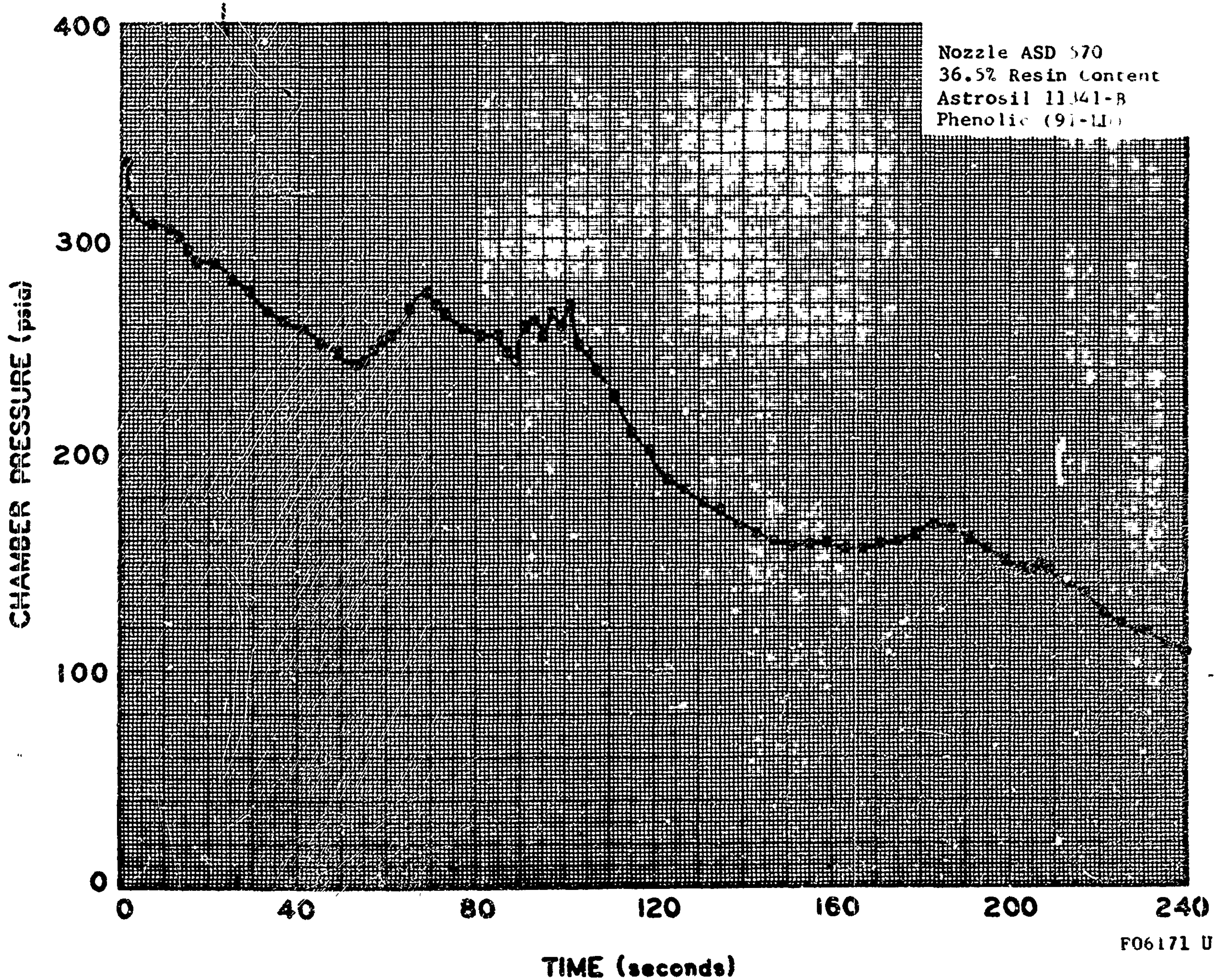

FIGURE 82. NOZZLE ASD 570; CHAMBER PRESSURE VERSUS TIME

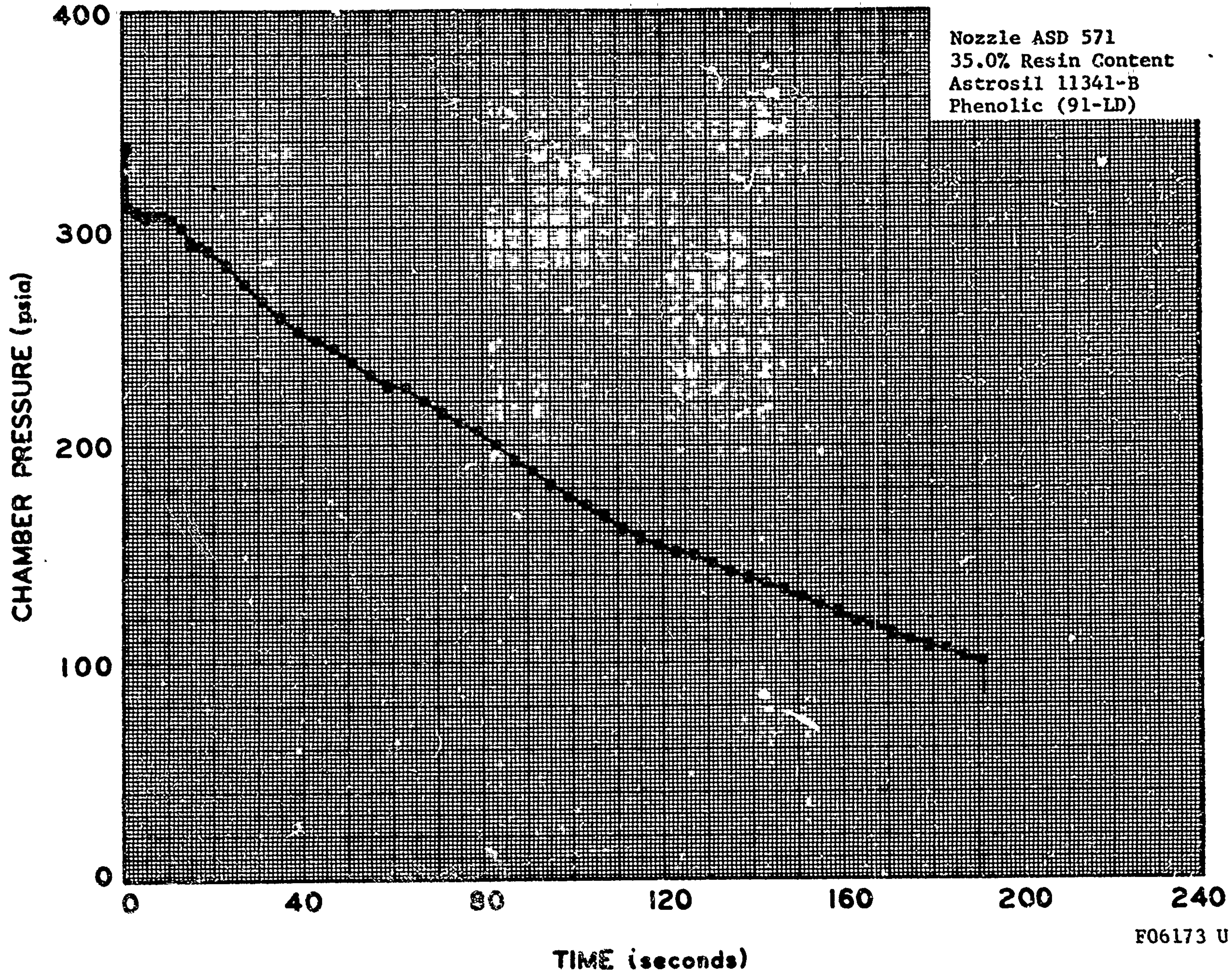

FIGURE 83. NOZZLE ASD 571, CHAMBER PRESSURE VERSUS TIME

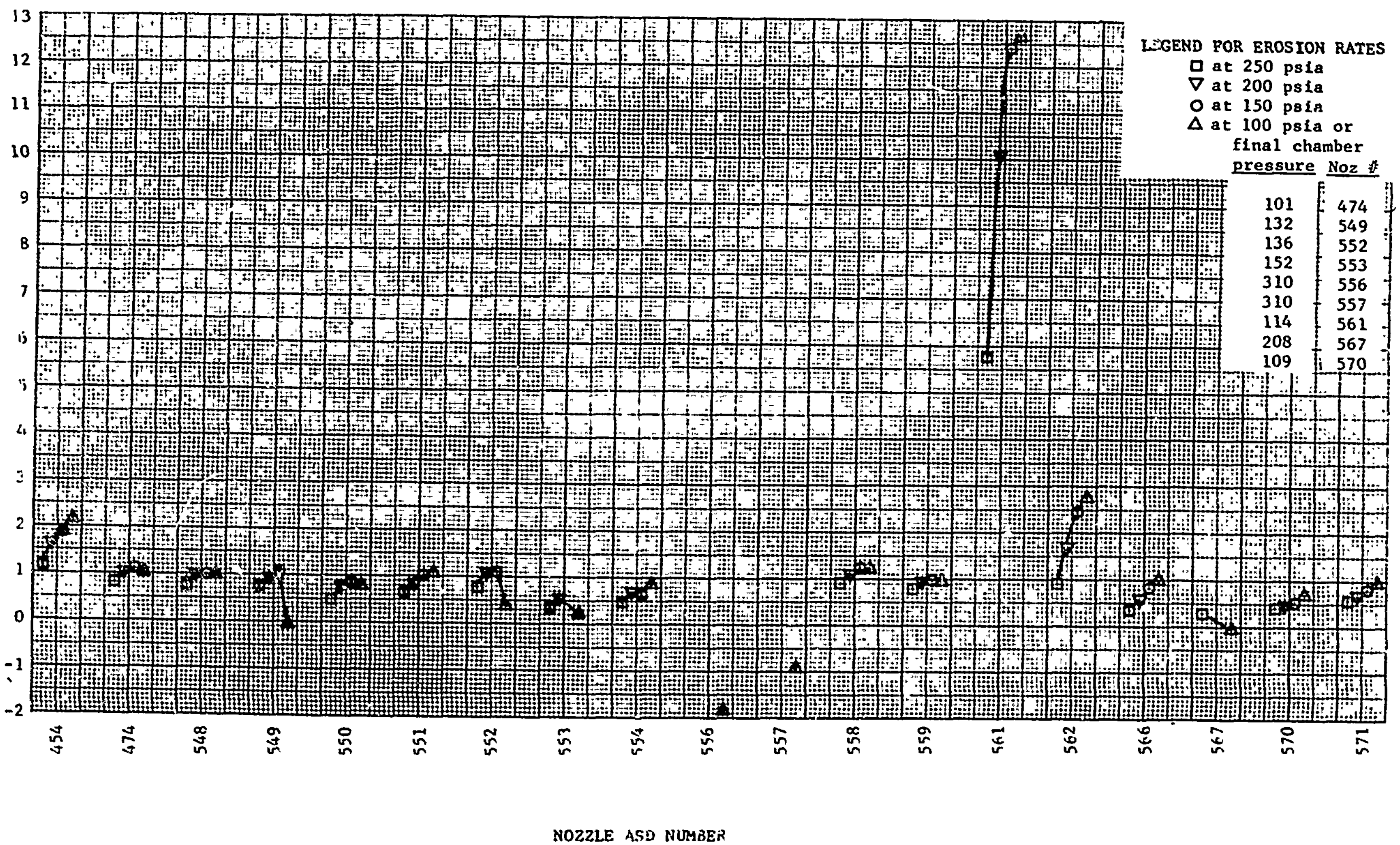

FIGURE 84. EROSION RATE VERSUS NOZZLE NUMBER, TEST SERIES NO. 5 LIQUID PROPELLANT

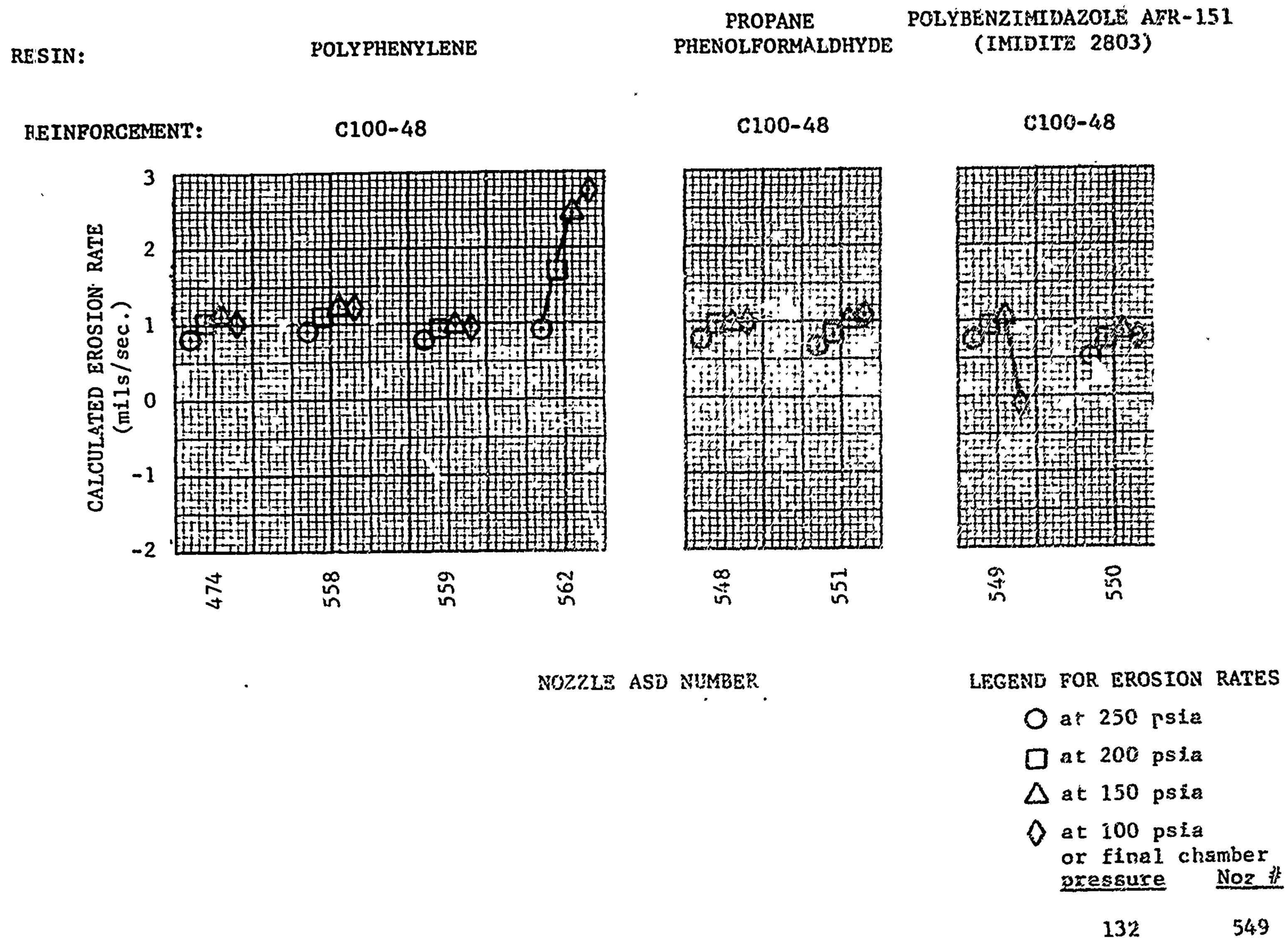

FIGURE 85 EROSION RATE COMPARISON, TEST SERIES 5, LIQUID PROPELLANT

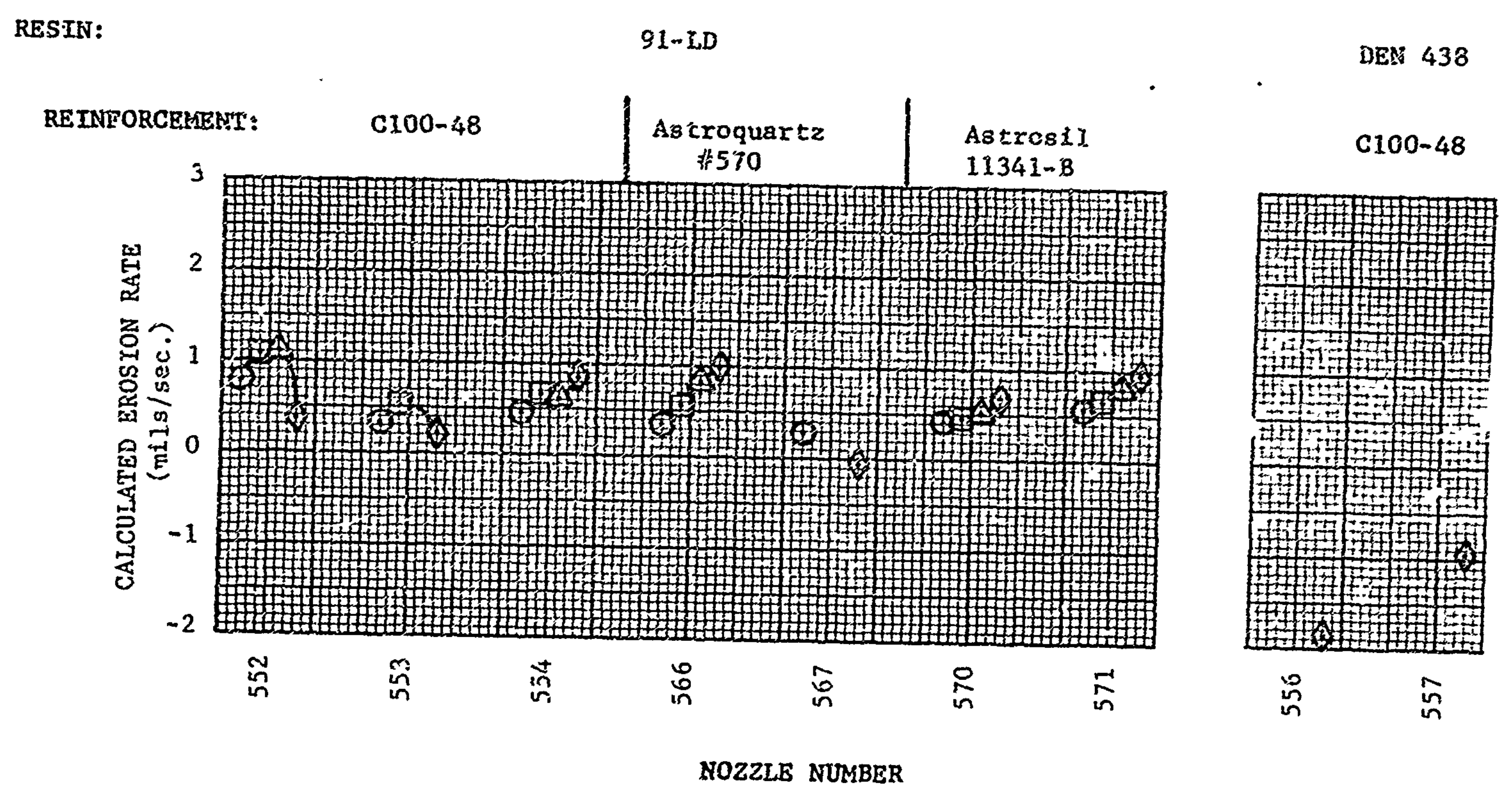

LEGEND FOR EROSION RATES:

○ at 250 psia

□ at 200 psia

△ at 150 psia

◇ at 100 psia or final chamber

pressure	Noz #
136	552
152	553
208	567
109	570
310	556
310	557

FIGURE 85. (CONT.) EROSION RATE COMPARISON, TEST SERIES 5, LIQUID PROPELLANT

NOZZLE NO. ASD-454

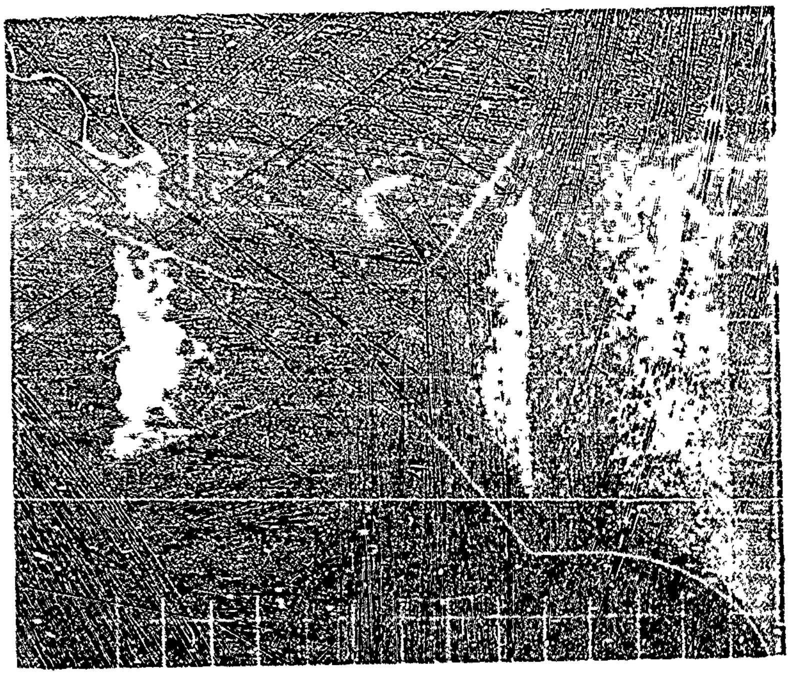

12 O'CLOCK

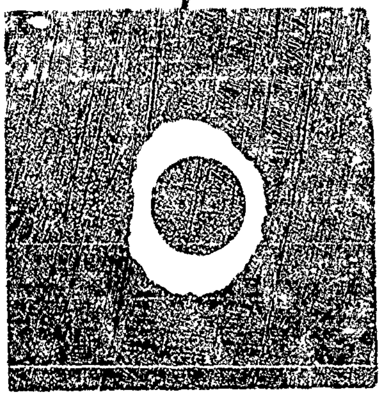

NOZZLE NO. ASD-474

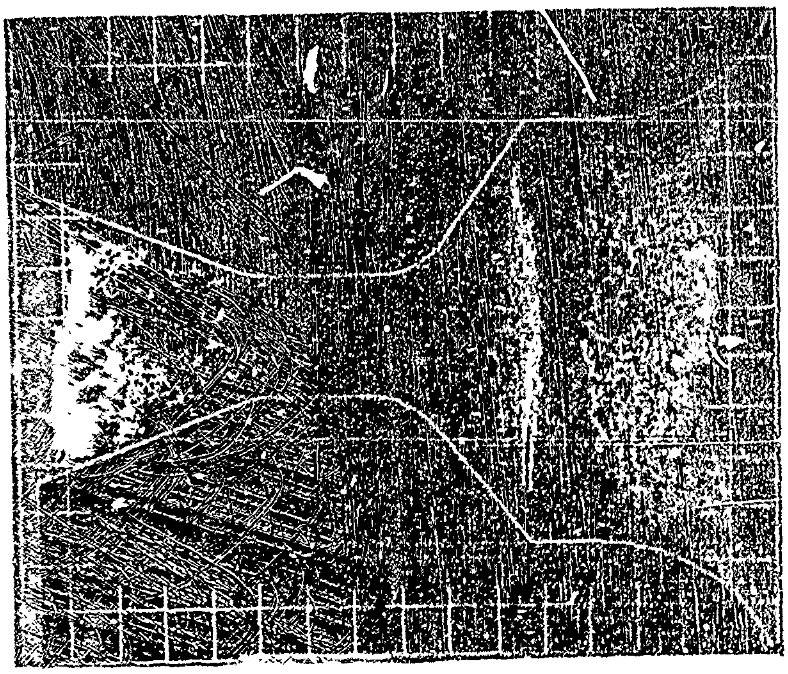

12 O'CLOCK

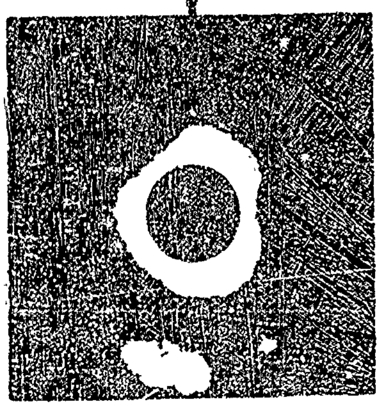

GRID SCALE
0.20 INCH

FIGURE 86. PROFILE AND AXIAL NOZZLE PHOTOGRAPHS

NOZZLE NO. ASD-548

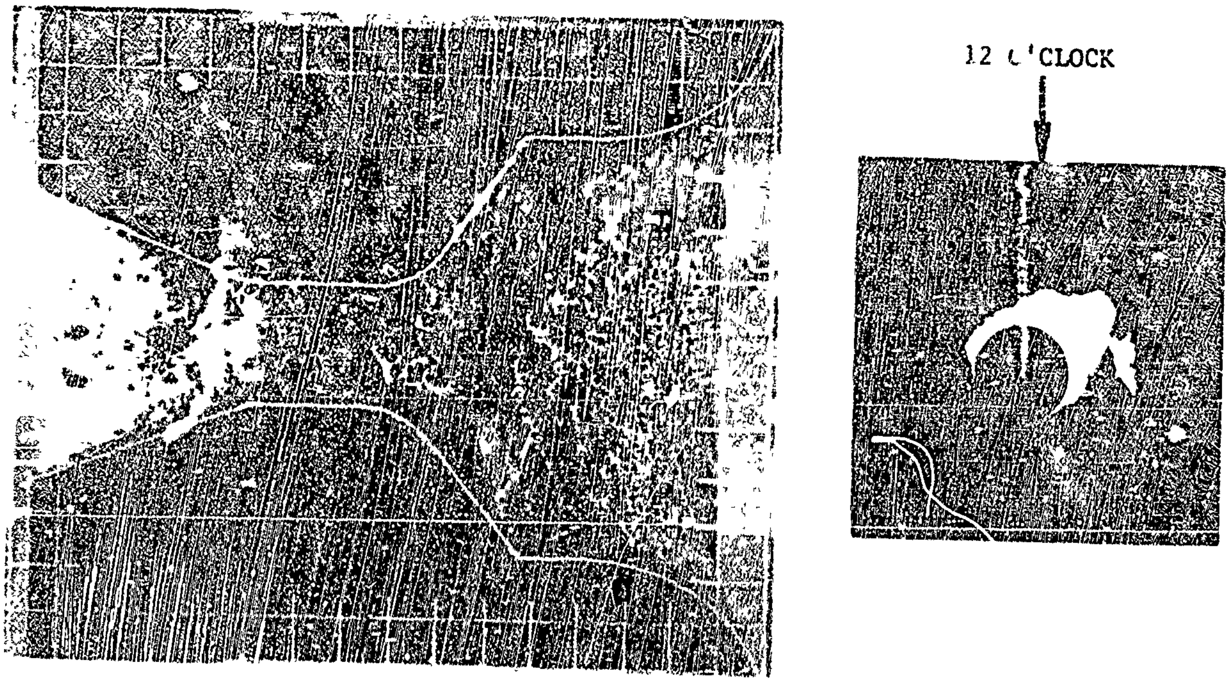

NOZZLE NO. ASD-549

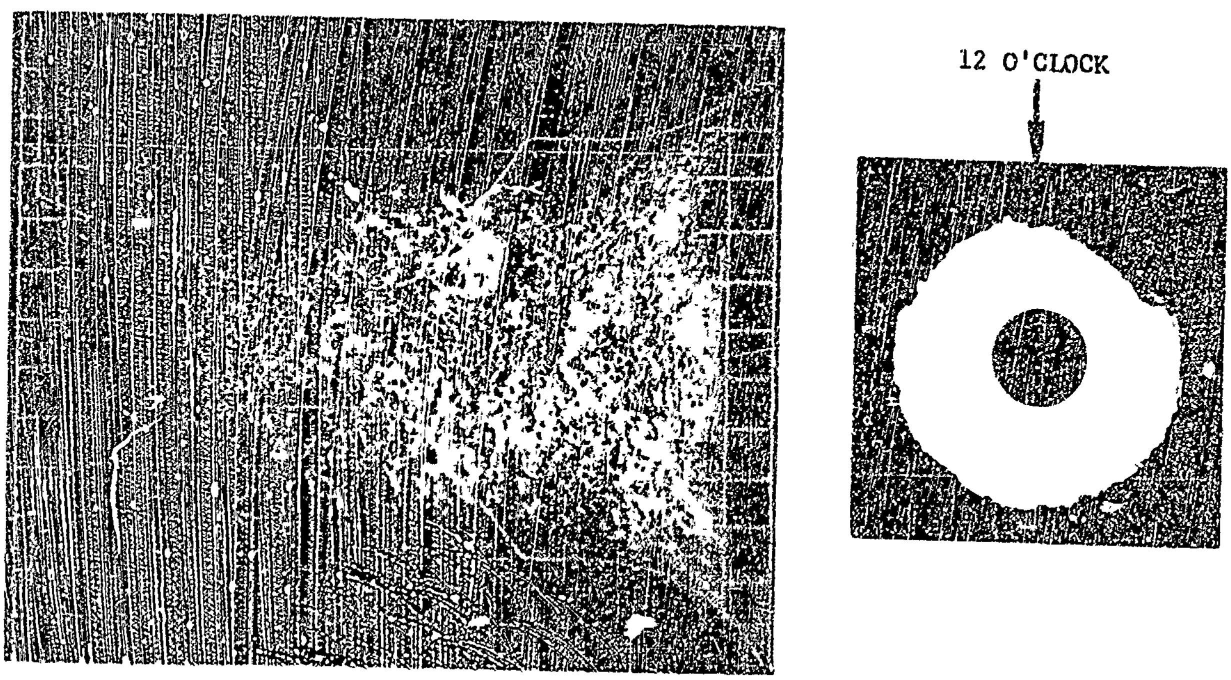

GRID SCALE
0.20 INCH

FIGURE 87. PROFILE AND AXIAL NOZZLE PHOTOGRAPHS

NOZZLE NO. ASD-550

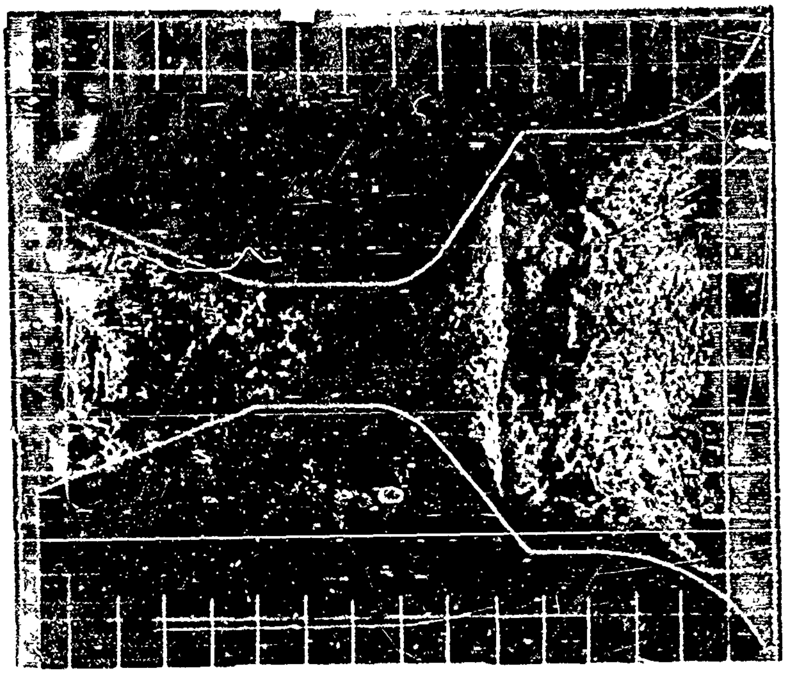

12 O'CLOCK

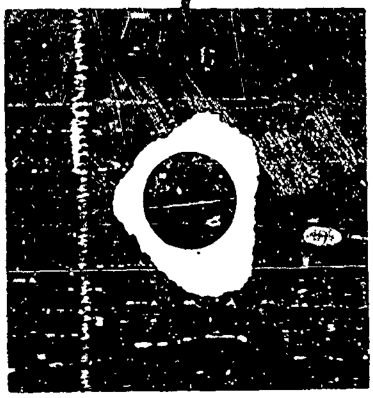

NOZZLE NO. ASD-551

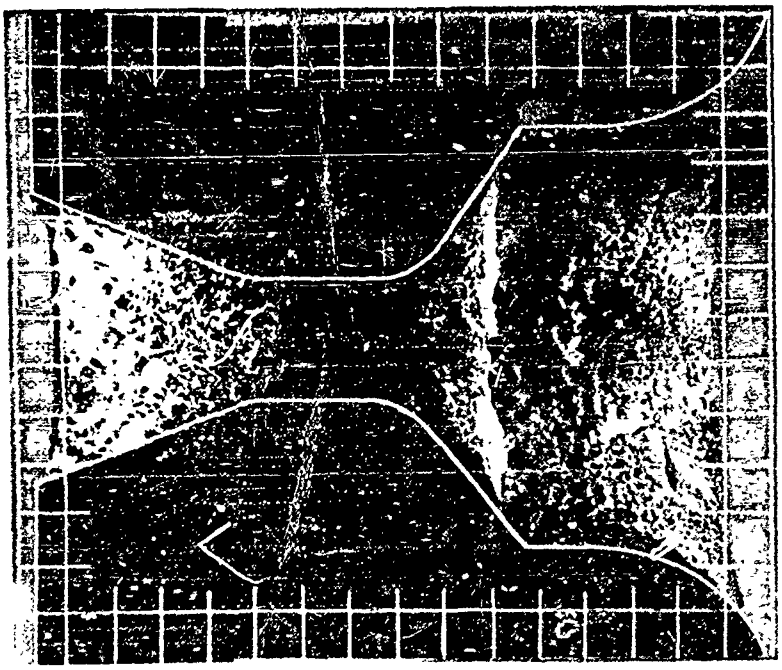

12 O'CLOCK

GRID SCALE
0.20 INCH

FIGURE 88. PROFILE AND AXIAL NOZZLE PHOTOGRAPHS

NOZZLE NO. ASD-552

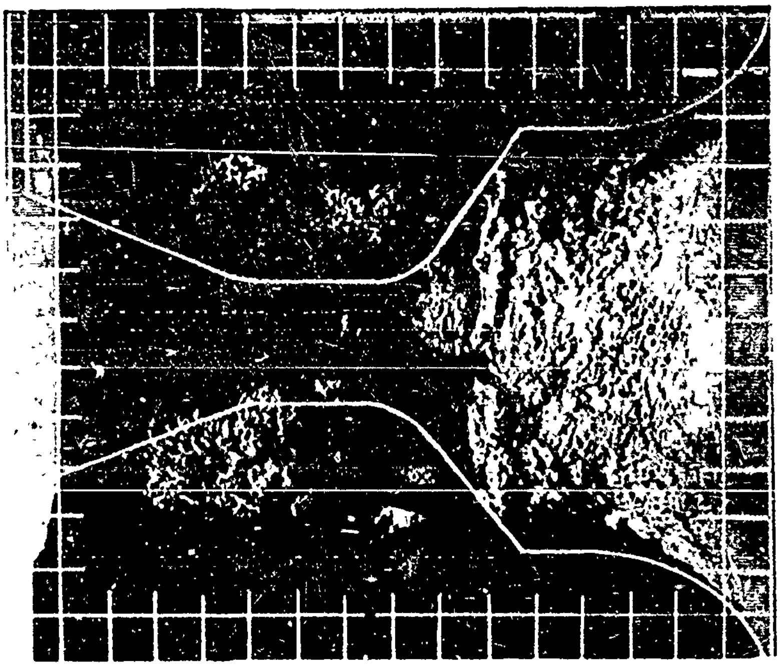

12 O'CLOCK

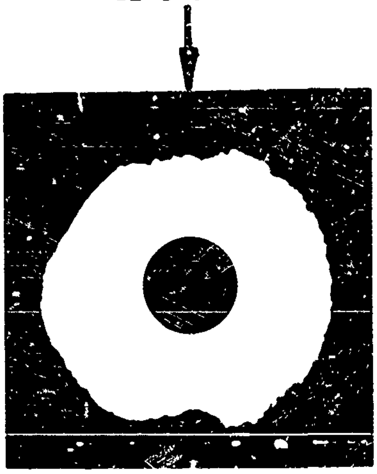

NOZZLE NO. ASD-553

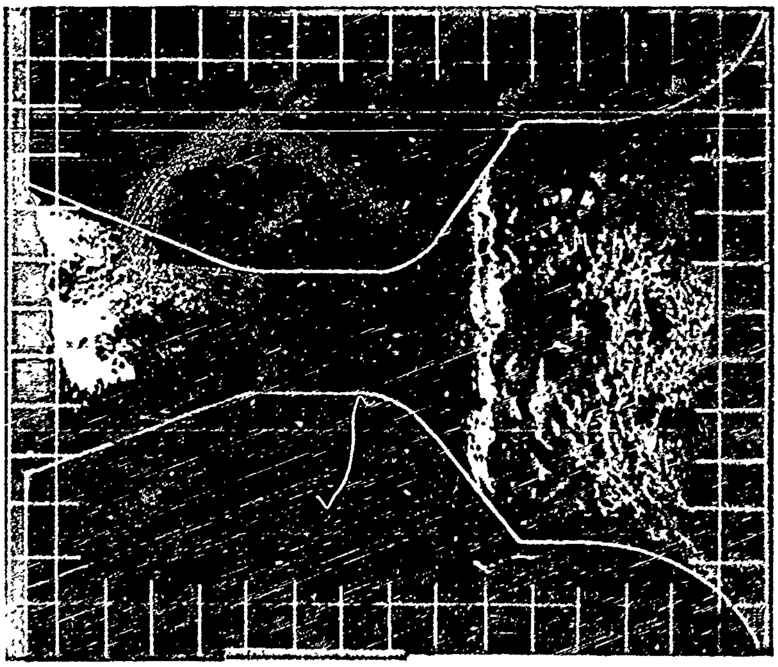

12 O'CLOCK

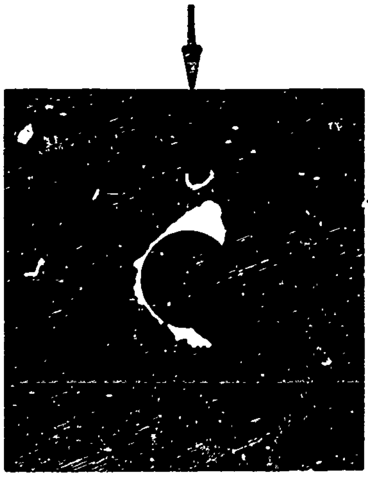

GRID SCALE
0.20 INCH

FIGURE 89. PROFILE AND AXIAL NOZZLE PHOTOGRAPHS

NOZZLE NO. ASD-554

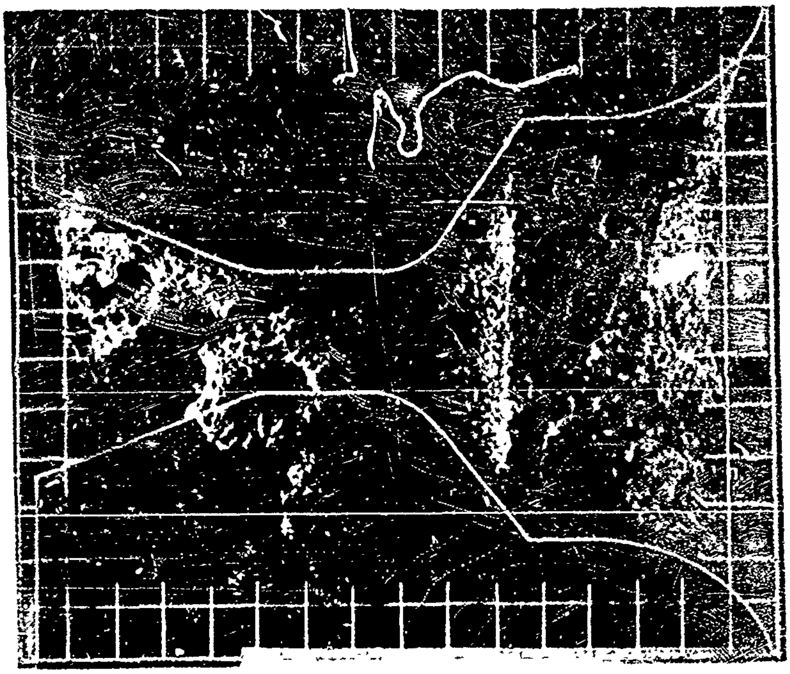

12 O'CLOCK

NOZZLE NO. ASD-556

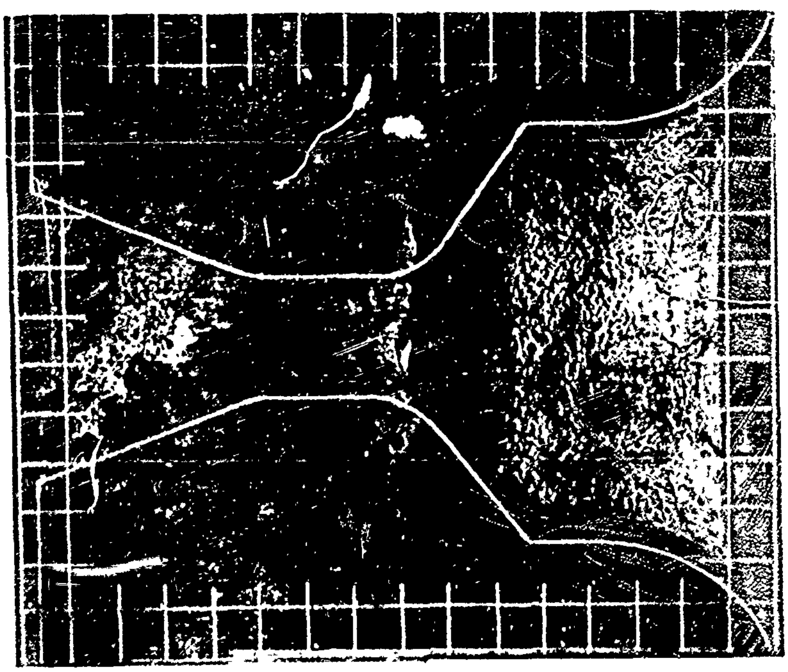

12 O'CLOCK

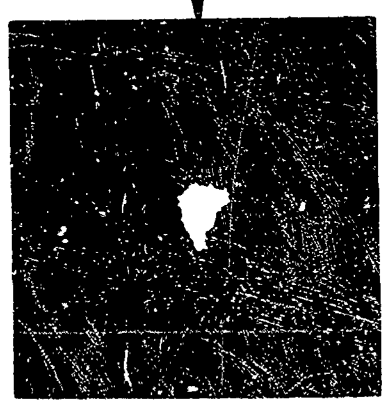

GRID SCALE
0.20 INCH

FIGURE 90. PROFILE AND AXIAL NOZZLE PHOTOGRAPHS

NOZZLE NO. ASD-557

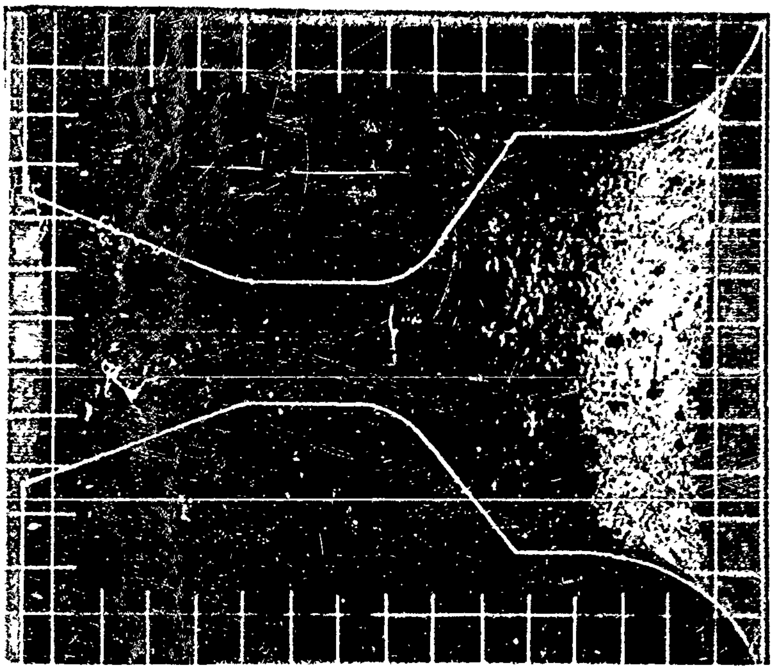

12 O'CLOCK

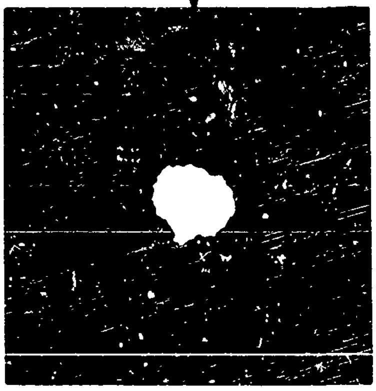

NOZZLE NO. ASD-558

12 O'CLOCK

GRID SCALE
0.20 INCH

FIGURE 91. PROFILE AND AXIAL NOZZLE PHOTOGRAPHS

NOZZLE NO. ASD-559

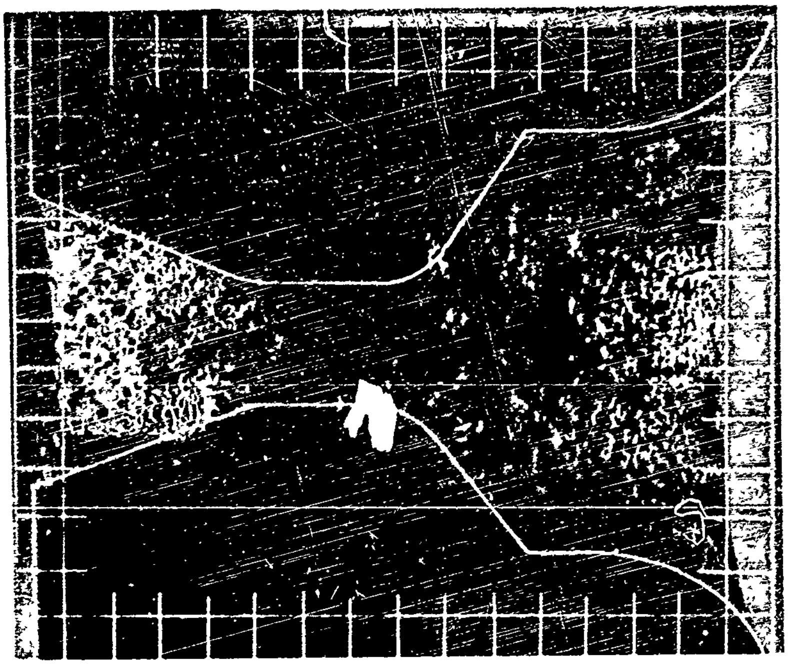

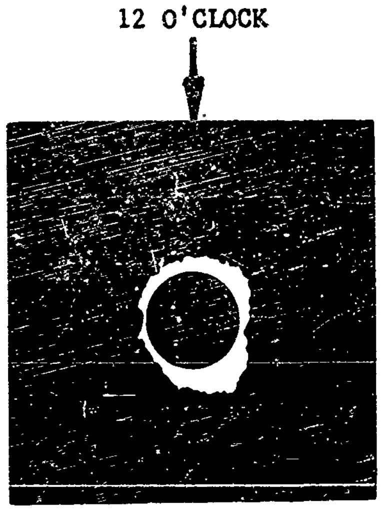

NOZZLE NO. ASD-561

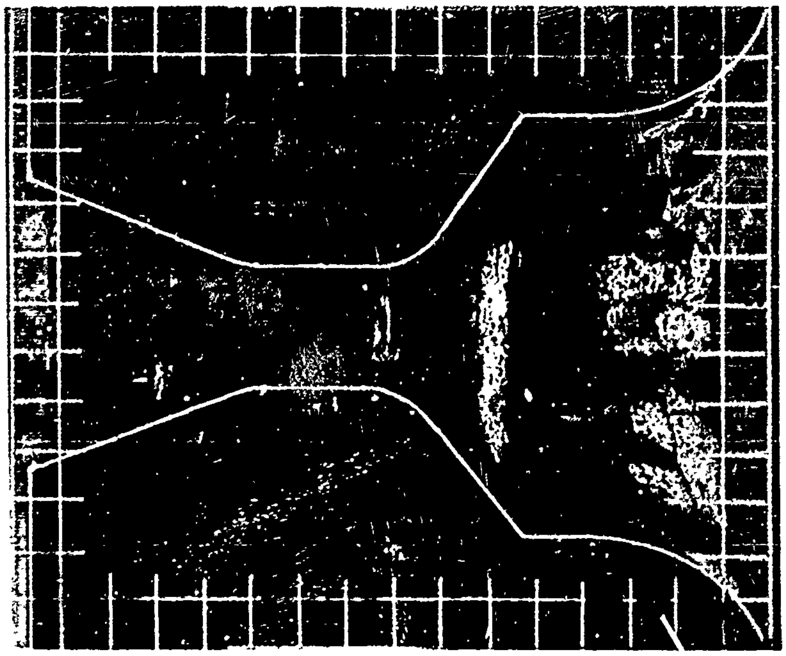

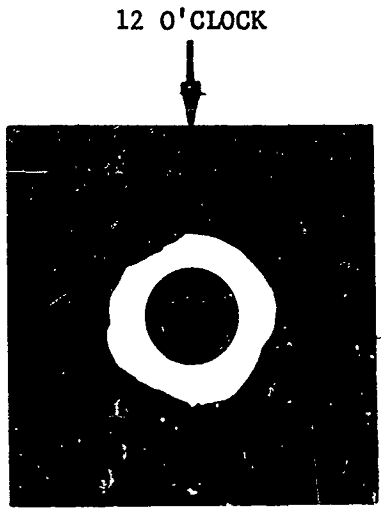

GRID SCALE
0.20 INCH

FIGURE 92. PROFILE AND AXIAL NOZZLE PHOTOGRAPHS

NOZZLE NO. ASD-562

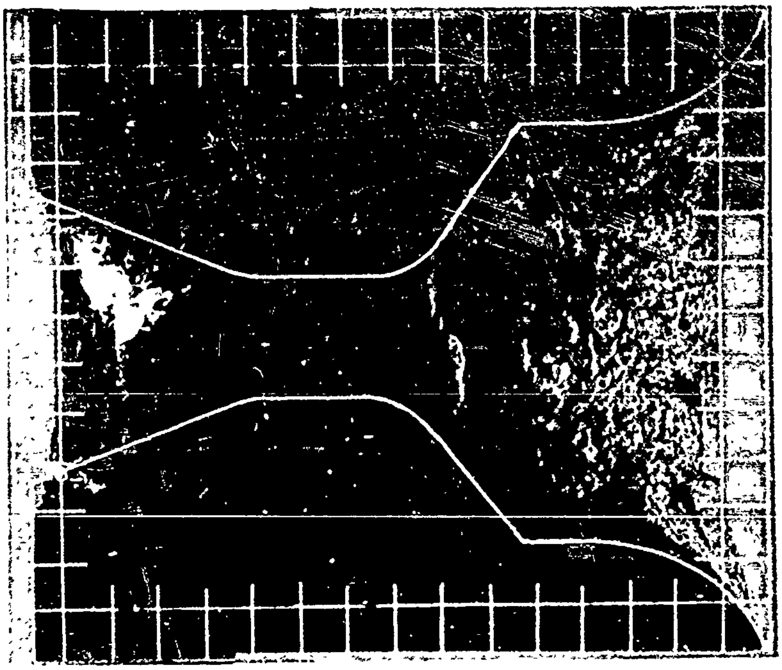

12 O'CLOCK

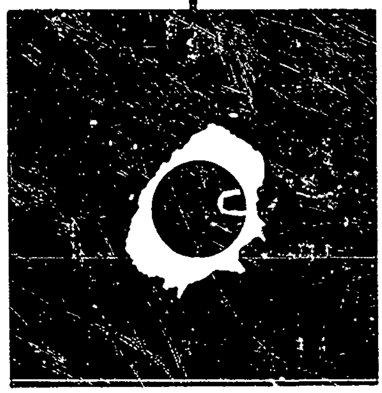

NOZZLE NO. ASD-566

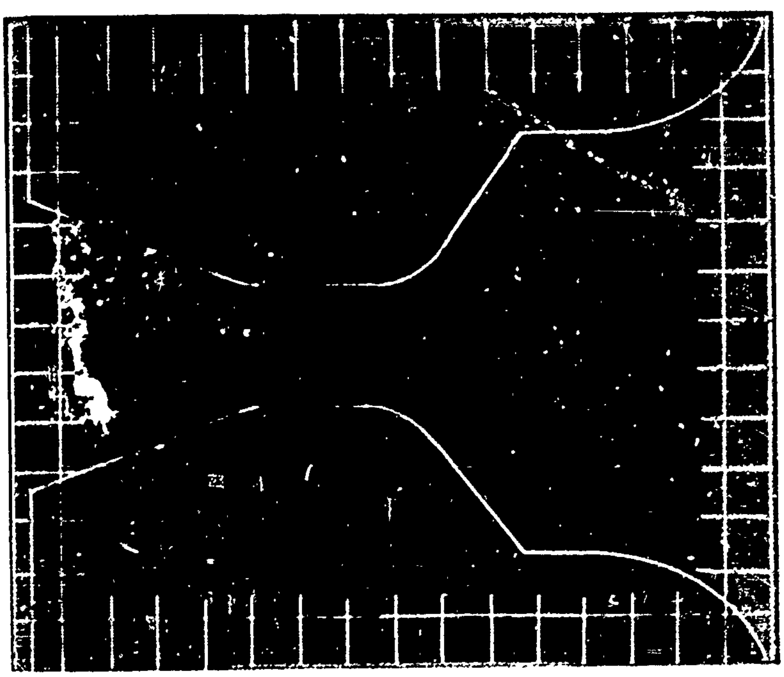

12 O'CLOCK

GRID SCALE
0.20 INCH

FIGURE 93. PROFILE AND AXIAL NOZZLE PHOTOGRAPHS

NOZZLE NO. ASD-567

12 O'CLOCK

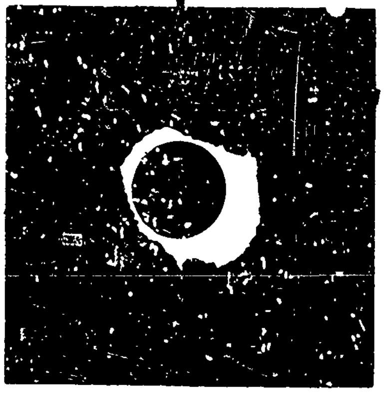

NOZZLE NO. ASD-570

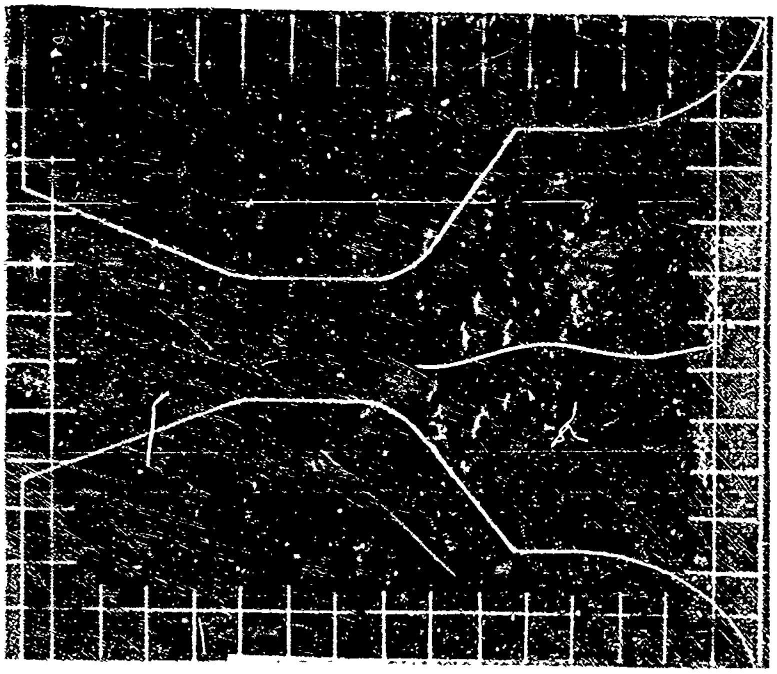

12 O'CLOCK

GRID SCALE
0.20 INCH

FIGURE 94. PROFILE AND AXIAL NOZZLE PHOTOGRAPHS

NOZZLE NO. ASD-571

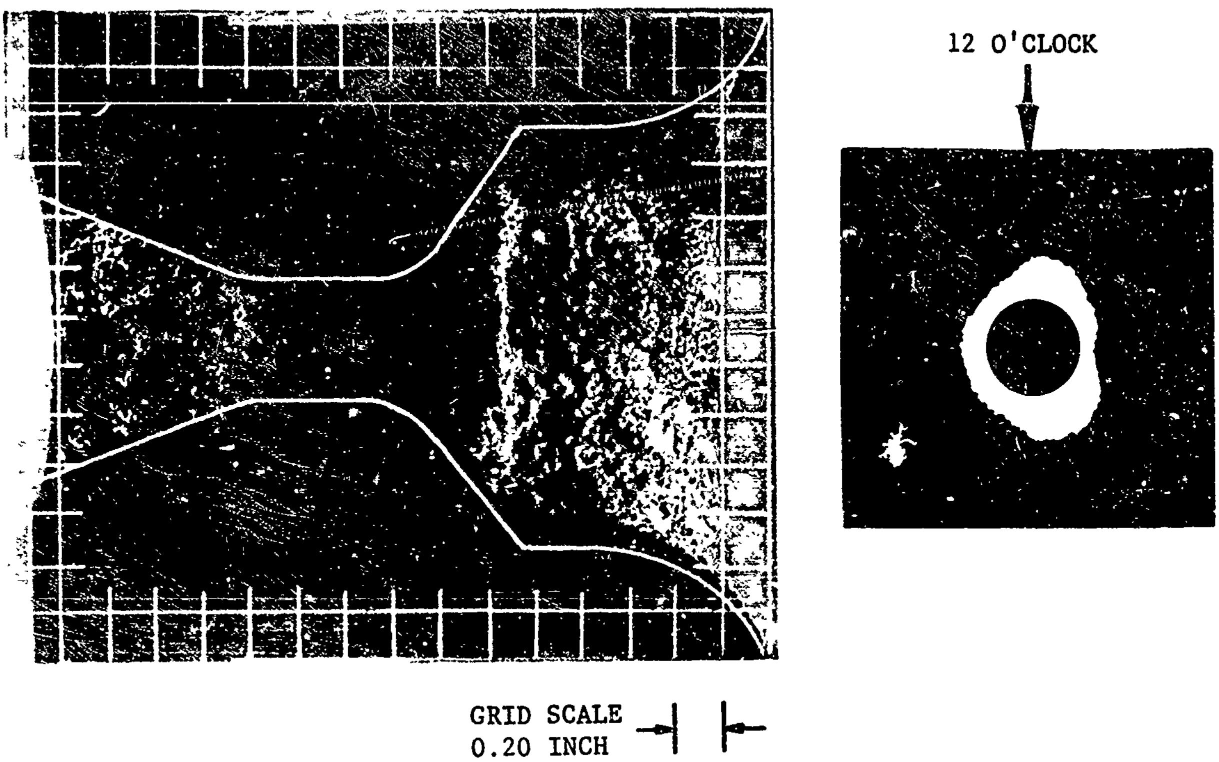

FIGURE 95. PROFILE AND AXIAL NOZZLE PHOTOGRAPHS

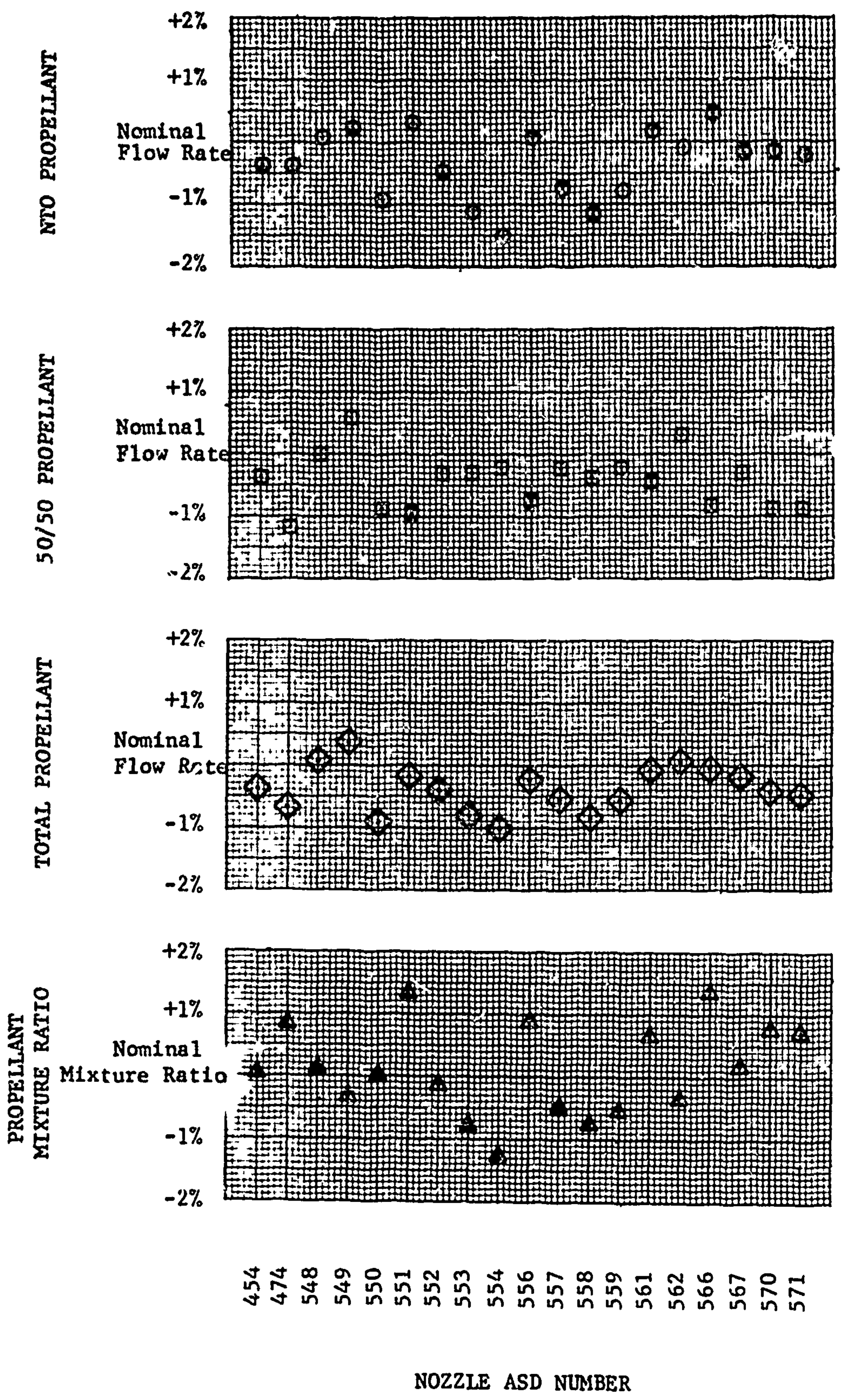

FIGURE 96. TEST TO TEST PROPELLANT FLOWRATE VARIATION FROM NOMINAL CONDITION

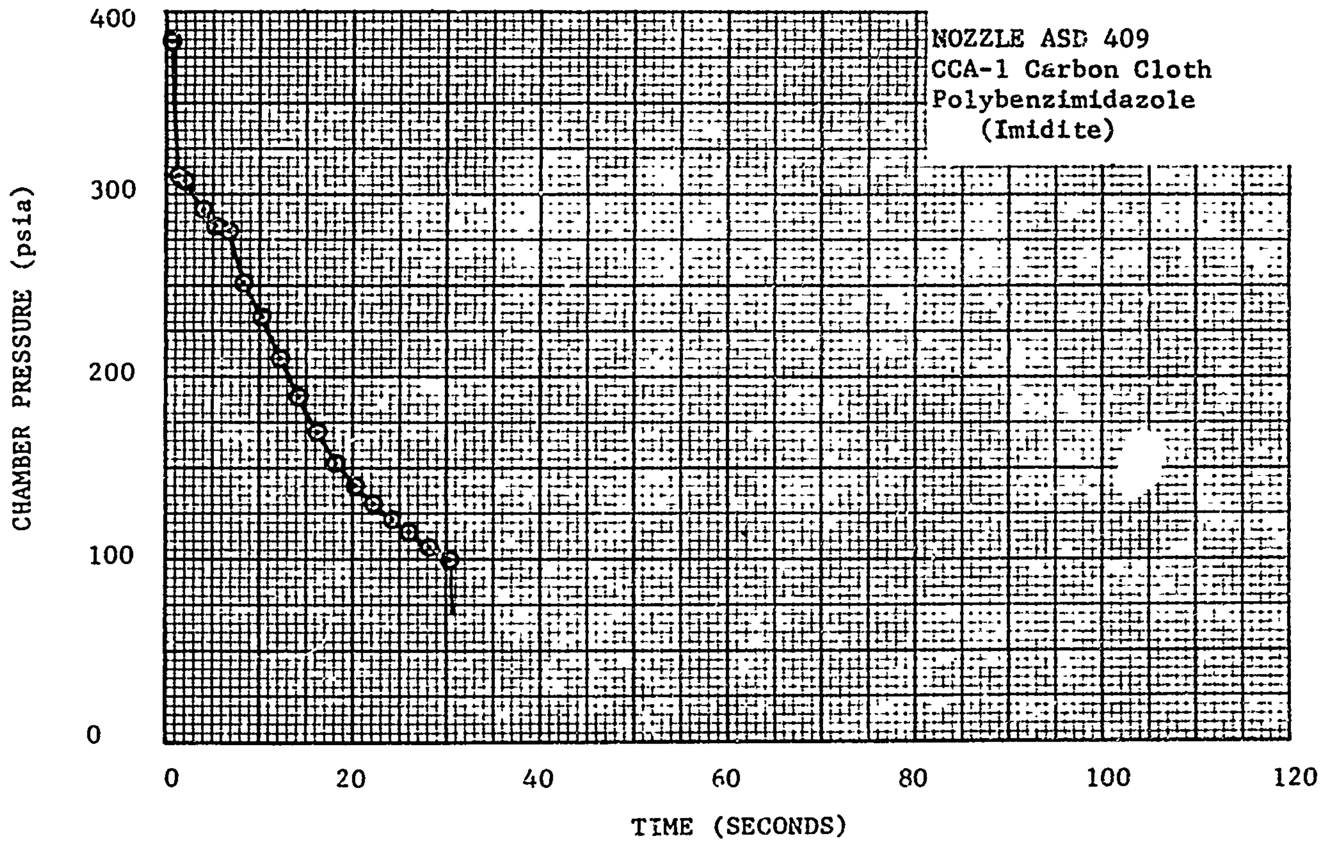

FIGURE 97. ASD NOZZLE 409 - CHAMBER PRESSURE VS. TIME

APPENDIX

HEAT TRANSFER STUDY

Determination of the Heat Transfer to the Throat of a Rocket Motor Using a Simulated Aluminized Solid Propellant and N_2O_4/50 percent Hydrazine - 50 percent UDMH-O/F = 1.6 Liquid Propellant.

1. INTRODUCTION

Heat transfer calculations have been performed to determine the throat heat flux in the rocket motor firings of Reference 1. These calculations were made using heat transfer analyses derived for smooth walled rocket motors. The results of these calculations will provide an estimation as to the actual heat flux existing in throat regions if the boundary layer mass addition rate can be specified. A discussion of the heat transfer analyses and results is presented below.

II. NOZZLE GEOMETRY

The nozzle geometry that was used in the heat transfer analyses is shown in Figure 98. This geometry is typical of nozzles used in Reference 1. A throat radius of curvature of 0.38 inch and throat diameter of 0.50 inch were used in the calculations.

III. NO-BLOWING CONVECTIVE HEAT TRANSFER COEFFICIENT

a. Simulation of Aluminized Solid Propellant

The throat convective heat transfer coefficient for the nozzle of Figure 98 using an aluminized solid propellant per Reference 1 was determined using a modified form of the equation derived by Bartz (Reference 2). The equation derived by Bartz for rocket nozzle application can be written as:

$$h = \frac{0.026}{(D_t)^{0.2}} \left(\frac{\mu^{0.2} C_p}{P_r^{\,0.6}}\right) \left(\frac{P_c g}{c^*}\right)^{0.8} \left(\frac{D_t}{r_c}\right)^{0.1} \left(\frac{A_t}{A}\right)^{0.9} \sigma \qquad (1)$$

where

h is the 'no-blowing,' smooth wall convective heat transfer coefficient ($Btu/in^2 sec^oF$)

D_t is the throat diameter (inches)

μ is the viscosity of the gas phase of the combustion products (lb/in. sec)

C_p is the specific heat of the combustion products at constant pressure (Btu/lb^oF)

P_r is the Prandtl number

P_c is the chamber pressure (psia)

r_c is the throat radius of curvature (inches)

C^* is the characteristic velocity (ft/sec)

$g = 32.2\ ft/sec^2$

$\frac{A_t}{A}$ is the area ratio at the point in question

and

$$\sigma = \left[\frac{1}{2}\left(\frac{T_w}{T_r}\right)\left(1 + \frac{\alpha-1}{2} m^2\right) + \frac{1}{2}\right]^{w/5-0.8} \left[1 + \frac{\alpha-1}{2} m^2\right]^{-w/5} \tag{2}$$

where

α is the gas phase ratio of specific heats

T_r is the recovery temperature (^oR)

T_w is the wall temperature (^oR)

$w \approx 0.6$

The expressions used in evaluating μ and P_r in Equation (1) as specified by Reference 2 are

$$\mu = 46.6 \times 10^{-10} (m_w)^{1/2} (T_r)^{0.6} \text{ (lb/in. sec)} \tag{3}$$

$$P_r = \frac{4\alpha}{9\alpha - 5} \tag{4}$$

The above method of evaluating the convective heat transfer coefficient for metalized propellants was employed in References 3, 4, and 5 and the theoretical thermal response compared very well with the experimental thermal data if the specific heat in Equation (1) was defined as:

$$C_p = \frac{H_{rec} - H_{wall}}{T_r - T_{wall}} \tag{5}$$

where

H_{rec} is the combustion products recovery enthalpy

H_{wall} is the enthalpy of the combustion products at the wall temperature

The specific heat at constant pressure as defined by Equation (5) represents the boundary layer average specific heat. This specific heat together with the chemical recovery temperature (defined below) are determined by performing a thermochemical analysis on the propellant formulation. Basically, this analysis assumes chemical equilibrium and uses the minimum free energy principle to determine the thermodynamic properties of the combustion products. To predict the specific heat and chemical recovery temperature at a nozzle throat the thermochemical analysis is applied (using the element weight fractions of the propellant) at (1) the nozzle chamber pressure and (2) the throat static pressure. Using the chamber thermodynamic properties and assuming isentropic nozzle flow, the throat stagnation enthalpy and static pressure are determined, i.e.,

$$\left(H_{stagnation}\right)_{chamber} = \left(H_{stagnation}\right)_{throat}$$

$$\frac{P^*}{P_{stagnation}} = \left(1 + \frac{\alpha - 1}{2}\right)^{-\frac{1}{\alpha - 1}}$$

Where α is the equilibrium specific heat ratio determined from the chamber thermochemical calculation.

Using the throat static pressure and the element weight fractions of the propellant a number of thermochemical calculations are made (assuming chemical equilibrium) at prescribed temperature levels to determine the combustion products' enthalpy versus temperature. The chemical recovery temperature at the throat is found at the temperature corresponding to the stagnation enthalpy. The enthalpy versus temperature results and recovery temperature are then used in Equation (5) to determine the boundary layer specific heat.

A plot of enthalpy versus temperature at the throat is shown in Figure 99 for the solid propellant. The step in enthalpy at 2330°K is produced by the solidification of Al_2O_3. The chemical recovery temperature is found to be 6090°R. Figure 100 is a plot of the boundary layer average specific heat at constant pressure as determined from Figure 99. The step in specific heat and enthalpy corresponding to the solidification of Al_2O_3 is unlikely; since specie diffusion and nonequilibrium chemistry will cause the solidification of Al_2O_3 to occur over a wide temperature. Therefore, the specific heat was assumed to vary with temperature as shown in Figure 100.

The total recovery temperature for turbulent flow may be expressed as (Reference 6):

$$C_p\,(T_{cr} - T_r = H_{cr} - H_r = \frac{V^2}{2gJ}\left(1 - \sqrt[3]{P_r}\right)$$

where

T_{cr} is the chemical recovery temperature

T_{T_r} is the total recovery temperature

V is the local velocity (sonic velocity in this case)

P_r is the Prandtl number.

Table I presents the properties used in Equations (1), (2), (3), and (4) to compute the throat convective heat transfer coefficient for the solid propellant. The results of these computations are shown in Figure 101 as throat convective heat transfer coefficient versus wall temperature. These results are applicable at the chamber pressure of 500 psia and a no-blowing - smooth walled nozzle contour. The effects of chamber pressure and blowing on the results of Figure 101 are discussed in paragraphs IV and V, respectively.

TABLE I

SOLID PROPELLANT PROPERTIES USED IN CONVECTIVE HEAT TRANSFER CALCULATIONS

Property	Value
D_t	0.50 inches
r_c	0.38 inches
T_r	6090°R
γ	1.192
P_c	500 psia
M_w	20.4
C_p	Figure 3

The throat radiative heat flux was found to be negligible with respect to the convective. For example, from Reference 7 the alumina cloud emissivity at 300 psia and a throat diameter of 0.50 inches is approximately 0.1. The cold wall radiative heat flux is then approximately 0.3 Btu/sec in^2 ($\dot{q}_{rad} \sim \epsilon \sigma T^4$). The convective heat flux for a wall temperature of 900°R is calculated, using Figure 101 and a total recovery temperature of 6070°R, to be 31 Btu/in^{2}sec.

b. N_2O_4/50% Hydrazine - 50% UDMH - O/F = 1.6 Liquid Propellant

In determining the throat convective heat transfer coefficient for the liquid propellant rocket motor of Reference 1 use was made of the experimental data presented in Reference 8. The test conditions and rocket motor parameters reported by JPL (Reference 8) and Reference 1 are listed in Table II.

TABLE II

TEST CONDITIONS AND ROCKET MOTOR PARAMETERS OF REFERENCES 8 AND 1

Definition of Condition Or Parameter	JPL (Reference 8)	Reference 1
Propellant	N_2O_4 - Hydrazine	N_2O_4 - Hydrazine
Chamber Pressure (PSIA)	301	300
Stagnation Temperature (°R)	4645	5760

TABLE II (Continued)

Definition of Condition Or Parameter	JPL (Reference 8)	Reference 1
C* (ft/sec)	5398	5627
Throat Diameter (inches)	3.2	0.50
Throat Radius of Curvature (inches)	3.2	0.38
Wall Temperature (^oR)	~900	Not specified
Throat Heat Flux ($Btu/in^2 sec$)	10.0	To be determined

Using the experimental data of JPL and Equation (1), the throat convective heat transfer coefficient of Reference 1 can be determined for a wall temperature of 900°R. That is,

$$\frac{h}{(8/T_r - T_w)_{JPL}} = \left[\frac{(D_t)_{JPL}}{D_t}\right]^{0.2}\left[\frac{\mu}{\mu_{JPL}}\right]^{0.2}\left[\frac{C^*_{JPL}}{C^*}\right]^{0.8}\left[\frac{(D_t/r_c)}{(D_t/r_c)_{JPL}}\right]^{0.1} \quad (6)$$

$$\text{and } \frac{\mu}{\mu_{JPL}} = \left(\frac{T_r}{T_{r_{JPL}}}\right)^{0.5}$$

Equation (6) assumes that $\sigma = \sigma_{JPL}$, $Pr = Pr_{JPL}$, $M_w = M_{w_{JPL}}$ and $C_p = C_{p_{JPL}}$. The validity of these assumptions is unknown as Reference 8 does not specify the O/F mixture used in the test. However, the difference in convective heat transfer produced by the σ, P_r, M_w and C_p dependency on O/F is negligible compared to errors resulting from strictly theoretical convective calculations.

From Equation (6) and Table II the throat convective heat transfer coefficient at a wall temperature of 900°R calculates to be 0.00390 $Btu/in^2 sec^oF$. The dependency of the coefficient on wall temperature was determined using Equation (2), the specific heat presented in Figure 102 γ= 1.225, and

$$\frac{h}{h_{@T_w = 900^oR}} = \frac{\sigma C_p}{(\sigma C_p)_{@T_w = 900^oR}}$$

The specific heat (Figure 102) and specific/heat ratio (γ) were obtained from Reference 9. The procedure used in Reference 9 in determining the specific heat was discussed in Paragraph IIa.

The throat convective heat transfer for the N_2O_4-/50% Hydrazine - 50% UDMH - O/F = 1.6 propellant and rocket motor conditions of Reference 1 are shown in Figure 103. The coefficients are applicable at a chamber pressure of 300 psia and a no-blowing-smooth walled nozzle contour. The total recovery temperature is calculated to be 5650°R. The convective heat flux for a wall temperature of 900°R is 19.6 Btu/in.^{2} sec using Figure 103 and T_r = 5650°R.

IV. CONVECTIVE HEAT TRANSFER DEPENDENCE ON CHAMBER PRESSURE

The effect of chamber pressure on the throat heat transfer coefficient was determined using Equation (1) and assuming that wall roughness and propellant mass flow remain constant. From Equation (1)

$$h \sim \left(\frac{1}{D_t}\right)^{0.2} \left(\frac{1}{T_r}\right)^{0.28} \left(P_c\right)^{0.8} C_p \tag{7}$$

Assuming constant mass flow and ratio of specific heats (γ):

$$\left[\frac{P_c D_t}{\sqrt{T_r}}\right]_o = \left[\frac{P_c D_t}{\sqrt{T_r}}\right]_I \tag{8}$$

Inserting Equation (8) into (7), the heat transfer coefficient at P_c = I is related to P_c = 0 by:

$$\phi = \left(\frac{h_I}{h_o}\right) = \underbrace{\left(\frac{T_{r_o}}{T_{r_I}}\right)^{0.33}}_{\sim 1.0} \left(\frac{P_{c_I}}{P_{c_o}}\right)^{0.9} \left(\frac{C_{p_I}}{C_{p_o}}\right) \tag{9}$$

The effect of C_p on chamber pressure was found from Reference 9 and Figure 99 for the liquid and solid propellant, respectively. Equation 9 is plotted in Figure 104 for the two propellants. The reference heat transfer coefficient (h_o) for the solid and liquid propellants are shown in Figure 101 and 103, respectively.

V. CONVECTIVE HEAT TRANSFER DEPENDENCE ON BOUNDARY LAYER INJECTION (BLOWING)

To determine the effect of boundary layer mass injection on the no-blowing heat transfer coefficients of Figure 101 and 103, it is suggested that the

analysis presented in Reference 5 be used. From Reference 5, the convective heat transfer coefficient with blowing can be expressed as:

$$\frac{h_B}{h_{B=0}} = \left(\frac{C_{P_m}}{C_{P_{B=0}}}\right)\left(\frac{C_f}{C_{f_{B=0}}}\right) \tag{10}$$

where:

C_p is the specific heat

C_F is the skin friction at the wall

and the subscripts are

B for blowing

B = 0 for no blowing

m for mixture

The ratio $C_f/C_{c_{B=0}}$ is determined from the expressions derived in Reference 10:

$$\frac{C_f}{C_{f_{B=0}}} = 1.0 - 0.335\,(B_1)^{0.414} \quad \text{for} \quad 0 < B_1 < 5$$

$$\frac{C_f}{C_{f_{B=0}}} = 1.2\,(B_1)^{-0.77} \quad \text{for} \quad 5 < B_1 < 100$$

where

$$B_1 = \frac{\rho_\omega V_\omega}{\rho_e U_e}$$

$\rho_\omega V_\omega$ is the injectant mass flow, and $\rho_e U_e$ is the mass flow at the outer edge of the boundary layer.

The specific heat with no blowing ($C_{P_{B=0}}$) is found from Equation (5).

However, the specific heat with blowing (mixture specific heat) is difficult

to obtain due to specie diffusion in the boundary layer. However, one approximate way as suggested in Reference 5 is to define C_{P_m} for the injectant - main stream mixture as

$$C_{P_m} = C_e^* C_{P_e} + \left(1 - C_e^* C_{P_c}\right)$$

where C_{P_e} and C_{P_c} are the specific heat of the free stream and coolant, respectively, and C_e^* is a proper reference composition. For laminar flow and low blowing rates, Reference 5 states that:

$$C_e^* = \frac{1}{2}\left(2 - C_{c_\omega}\right) \tag{11}$$

If it is assumed that the reference point is at the ou er edge of the laminar sublayer of the turbulent boundary layer then Equation (11) may be applicable to turbulent flow. C_{c_ω} of Equation (11) is:

$$C_{c_\omega} = \frac{B}{B + \mu\omega/\bar{\mu}^*} \tag{12}$$

where

$$B = \frac{\rho_\omega V_\omega}{\rho_e U_e (St)_B}$$

$(St)_B$ is the blowing Stanton number.

Use of Equation (12) requires that Le and $P_r = 1$. The reference viscosity (μ^*) in Equation (12) is determined from:

$$\mu^* = \mu_1 \left(\frac{T_r + T_\omega}{2T_r}\right)^{0.6}$$

where the subscript r denotes recovery.

VI. SUMMARY

The throat convective heat transfer coefficients for the simulated solid propellant at P_c = 500 psia and N_2O_4/50% Hydrazine - 50% UDMH - O/F = 1.6 liquid propellant at P_c = 300 psia are shown in Figures 101 and 103, respectively. These coefficients were calculated assuming a no blowing - smooth wall nozzle contour and using the test conditions presented in Reference 1. The calculations performed on the solid propellant employed the Bartz Equation (Reference 2); whereas, the liquid calculation used actual N_2O_4 - Hydrazine firing data (Reference 2) and the Bartz Equation to extrapolate to the desired test conditions. Chemical equilibrium was assumed for both propellants.

The effect of chamber pressure on the above convective heat transfer coefficients is presented in Figure 104. Figure 104 was constructed using the Bartz Equation and assuming chemical equilibrium.

An analysis is presented in Paragraph V to estimate the reduction in convective heat transfer that results from boundary layer mass injection (blowing). The analysis was obtained from Reference 5 and assumes unity Le and P_r. The effect of blowing on recovery temperature is neglected due to small throat velocities.

The effect of deposition, condensed phases of combustion product adhering to nozzle surface, on throat heat transfer is important for aluminized propellants if nozzle surface temperature is for any significant time below the melting point of Al_2O_3. Since ablators are employed as the flamefront material in the firings of Reference 1, the surface temperature will be high enough such that deposition can be neglected. However, phenomena effecting throat heat transfer that could not be included in the above analyses consist of (1) variable surface roughness and (2) irregular changes in nozzle contour. These phenomena are dependent on local chemical corrosion, sublimation, spallation, chunking, and mechanical erosion (wall shear) and may significantly increase wall heat flux. Therefore, care must be used in applying the above results to motor firings that have experienced either irregular surface regression or high surface regression rates in the throat and entrance sections of the nozzle.

The results obtained from the analyses performed in this section are summarized in Table III.

TABLE III

RESULTS OF HEAT TRANSFER ANALYSES PERFORMED
ON THE ROCKET MOTORS OF REFERENCE 1

Parameter	Simulated Solid Propellant	N_2O_4/50% Hydrazine-50% UDMH - O/F = 1.6
Chemical Recovery Temperature at Throat - ^oR	6090	5760
Total Recovery Temperature at Throat - ^oR	6070	5750
Convective Heat Transfer Coefficient at Throat (No blowing) - Btu/in.^{2}sec^{o}F	See Figure 101 (P_c = 500 psia)	See Figure 103 (P_c = 300 psia)
Convective Heat Transfer Dependence on Chamber Pressure	See Figure 104	See Figure 104
Cold Wall Convective Heat Flux at Throat (no blowing, Wall Temperature = 900^{o}R) - Btu/in.^{2}sec	31.2	19.6
Maximum Radiative Heat Flux at Throat from Combustion Products - Btu/in.^{2}sec	0.3	0.02

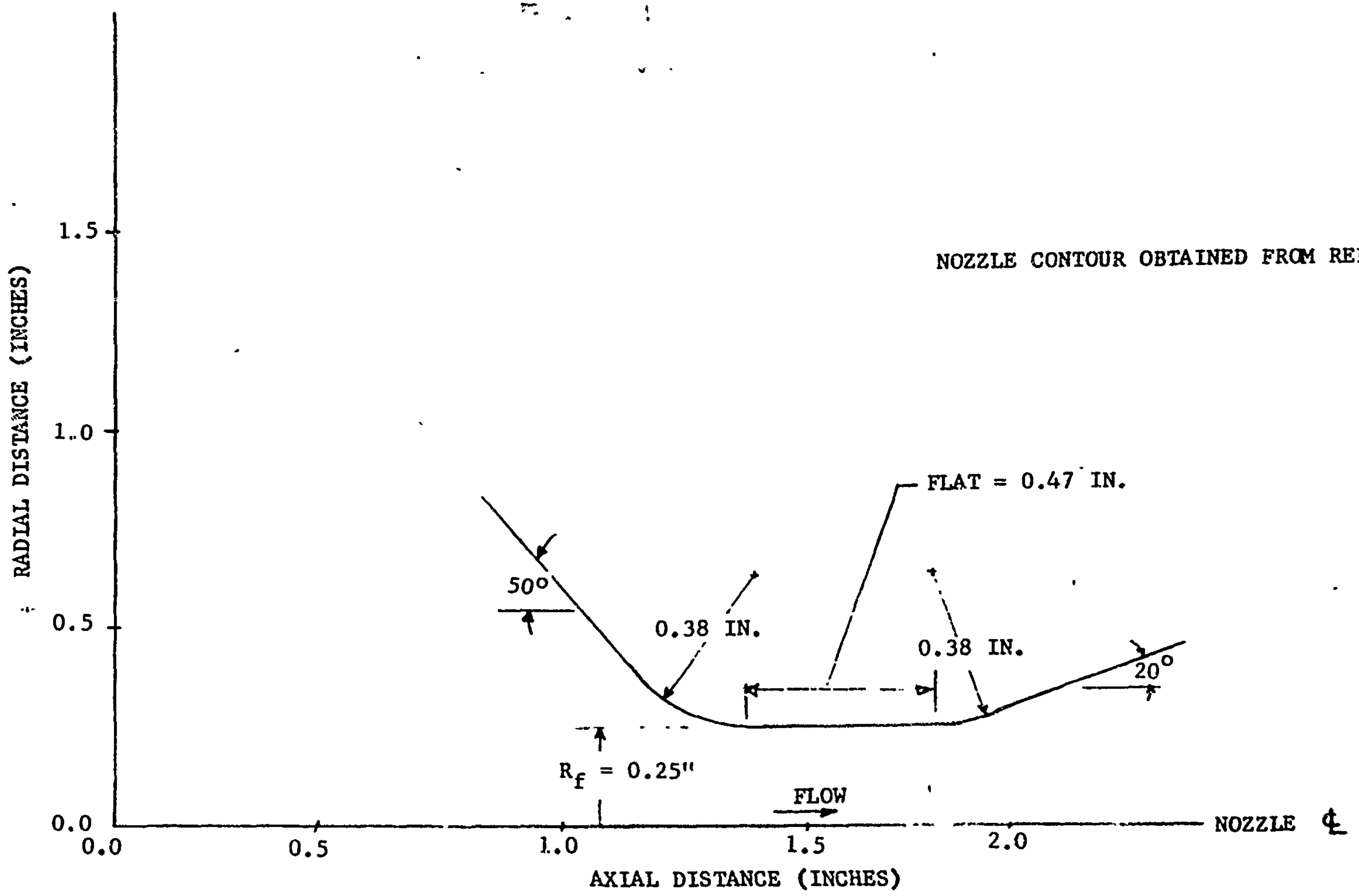

FIGURE 98. NOZZLE GEOMETRY USED IN HEAT TRANSFER CALCULATIONS

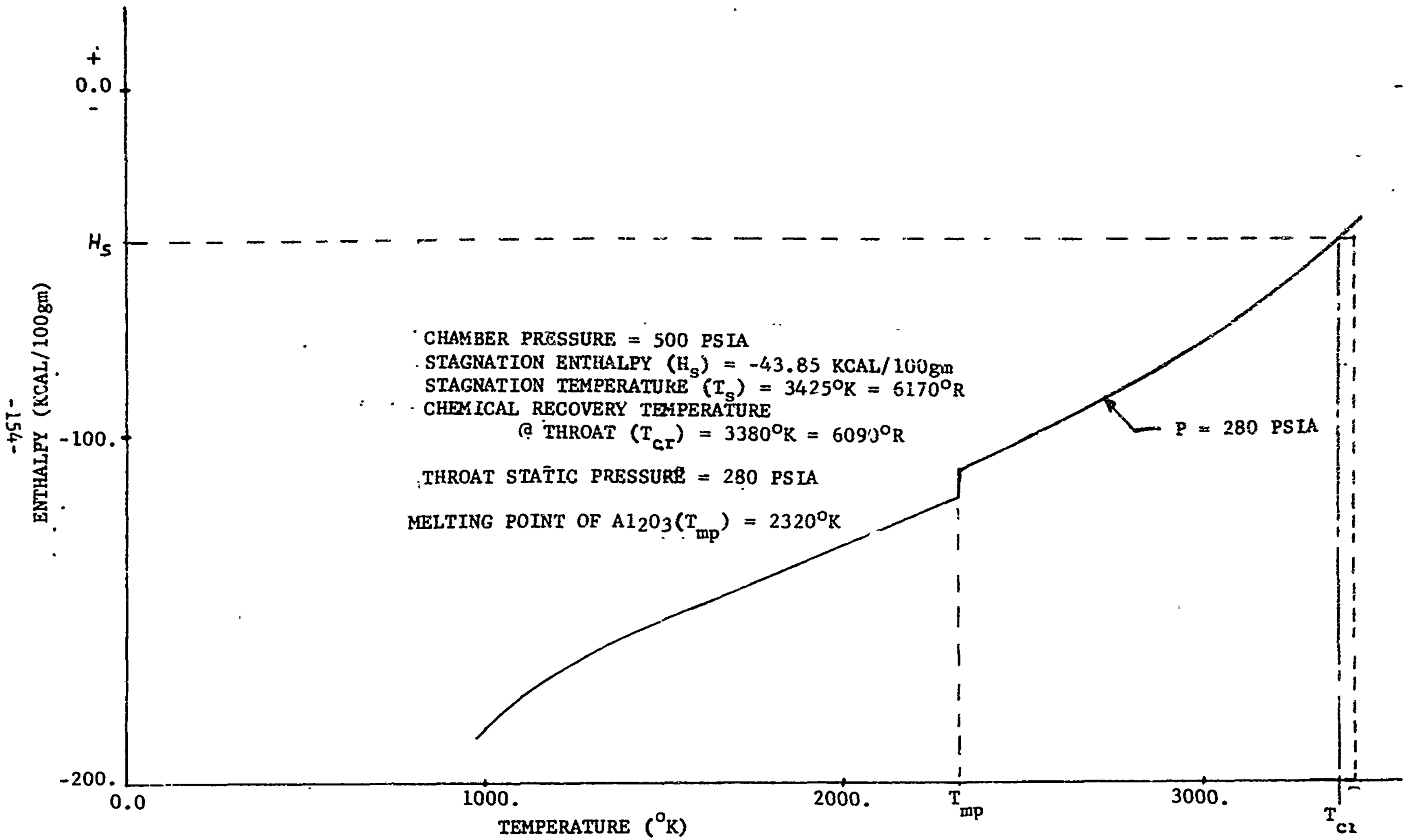

FIGURE 99. ENTHALPY VERSUS TEMPERATURE OF SOLID PROPELLANT COMBUSTION PRODUCTS AT THROAT STATIC PRESSURE

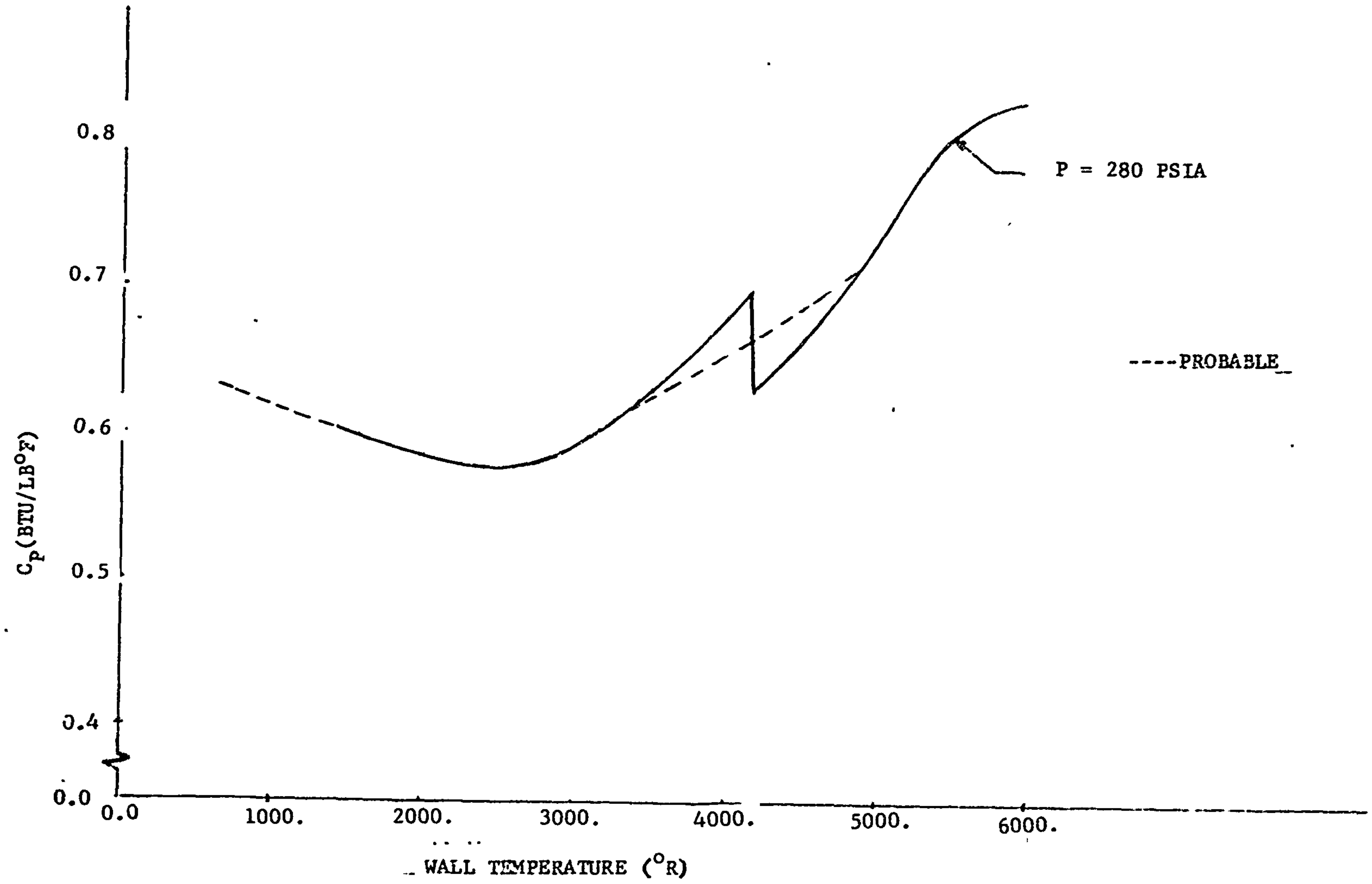

FIGURE 100. THROAT BOUNDARY LAYER AVERAGE SPECIFIC HEAT AT CONSTANT PRESSURE FOR SIMULATED ALUMINIZED SOLID PROPELLANT

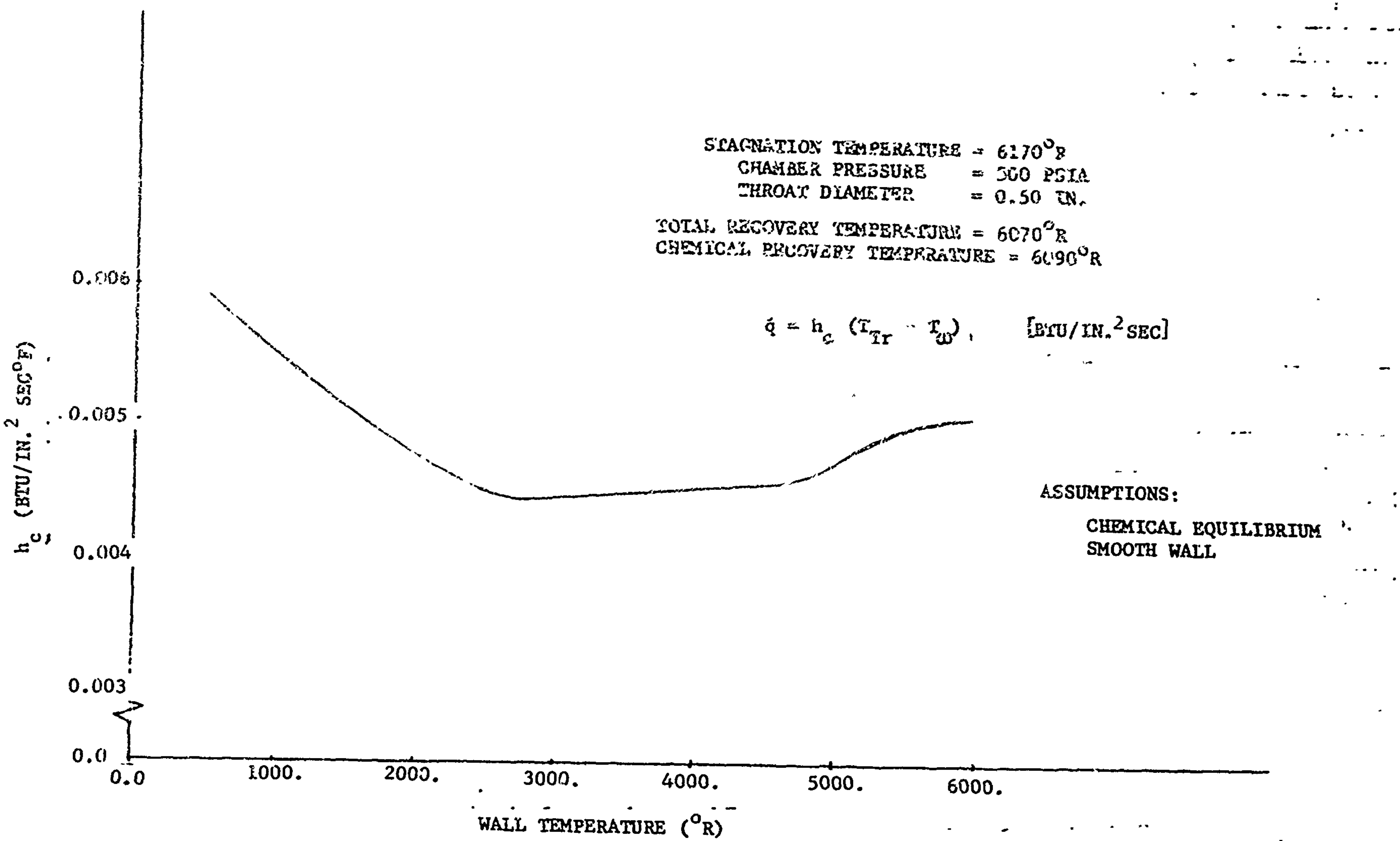

FIGURE 101. NO BLOWING THROAT CONVECTIVE HEAT TRANSFER COEFFICIENT FOR SIMULATED ALUMINIZED SOLID PROPELLANT

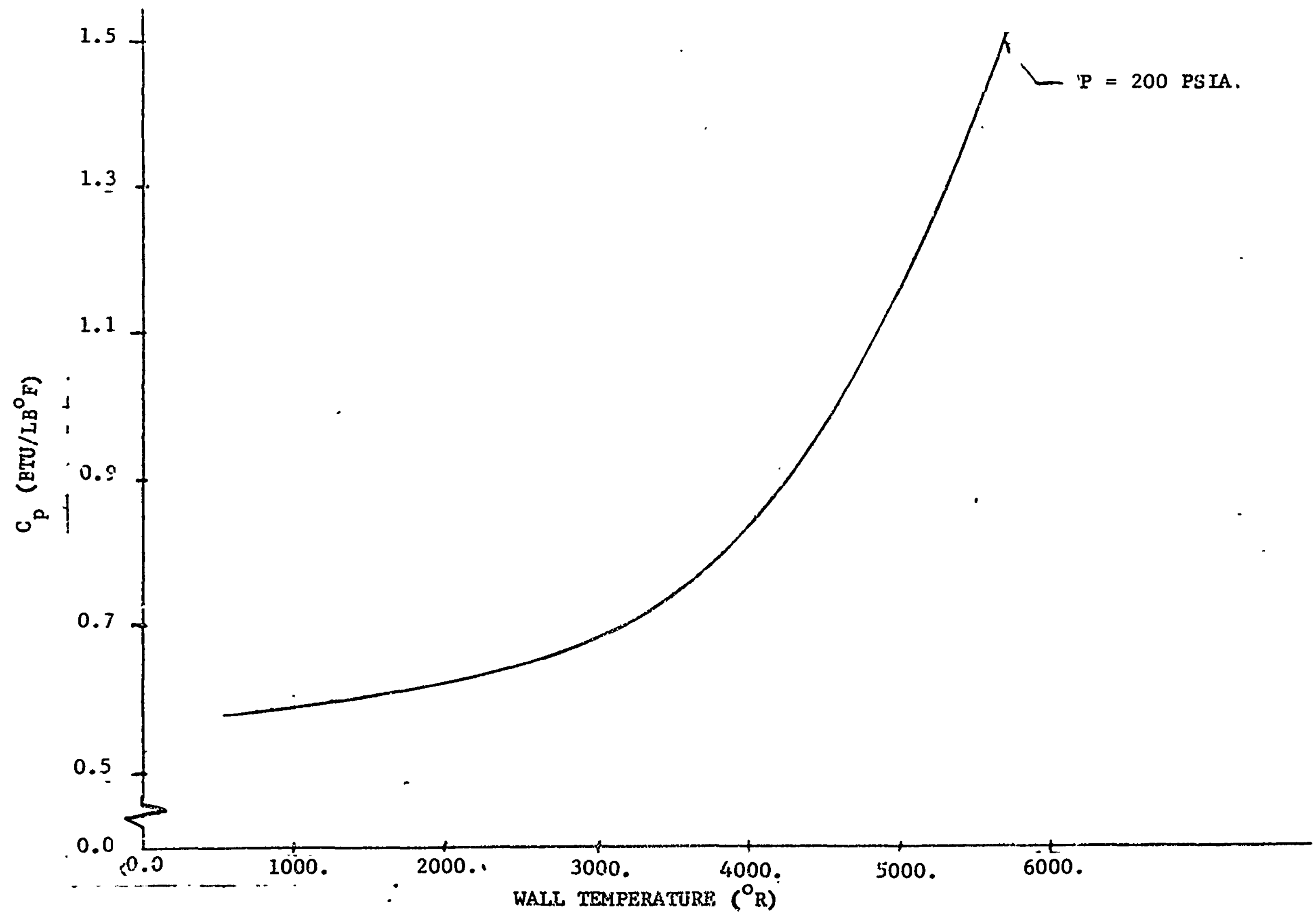

FIGURE 102. THROAT BOUNDARY LAYER AVERAGE SPECIFIC HEAT AT CONSTANT PRESSURE FOR N_2O_4/50-50 UDMH LIQUID PROPELLANT

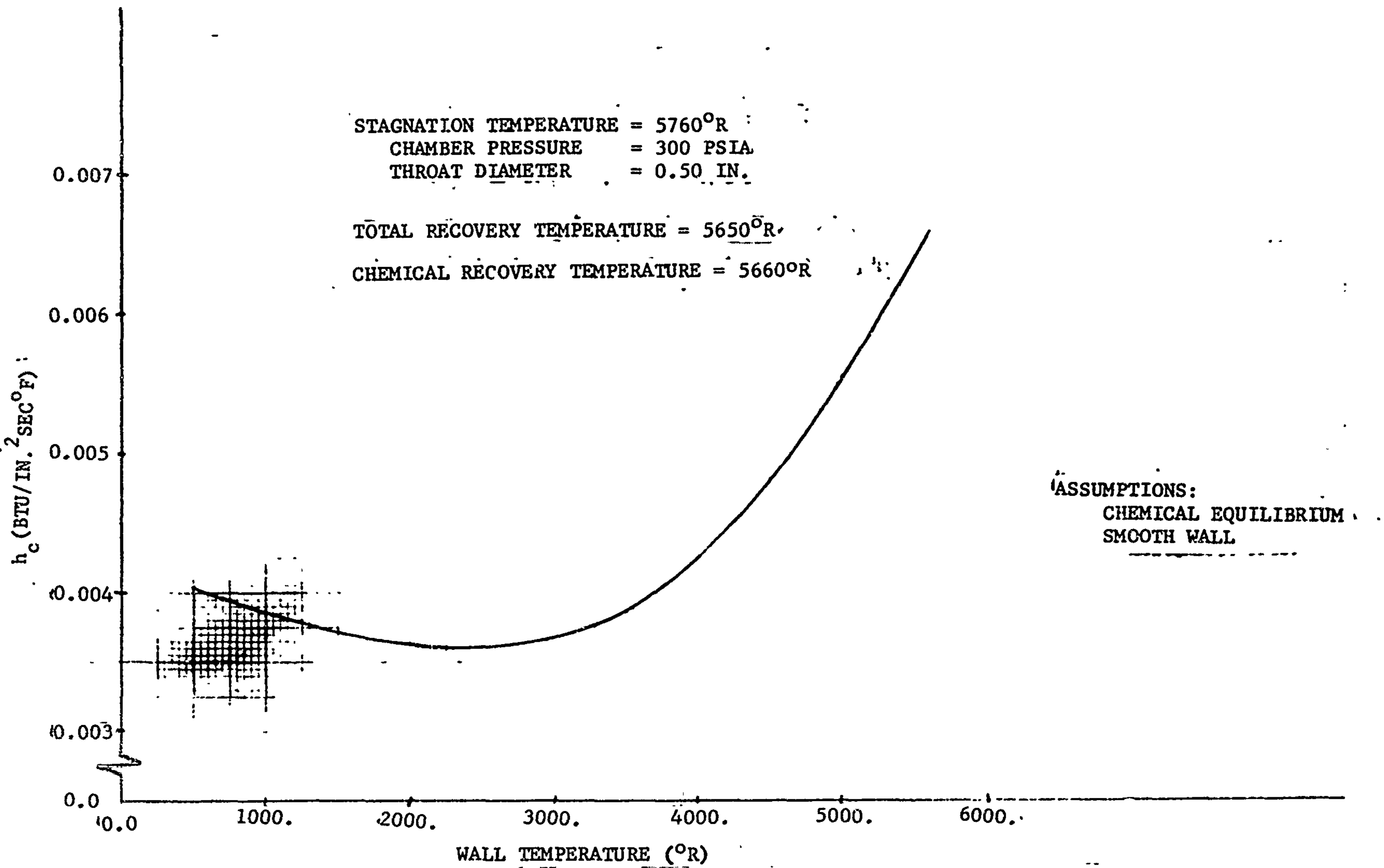

FIGURE 103. NO BLOWING THROAT CONVECTIVE HEAT TRANSFER COEFFICIENT FOR N_2O_4/50% HYDRAZINE - 50% UDMH - O/F = 1.6

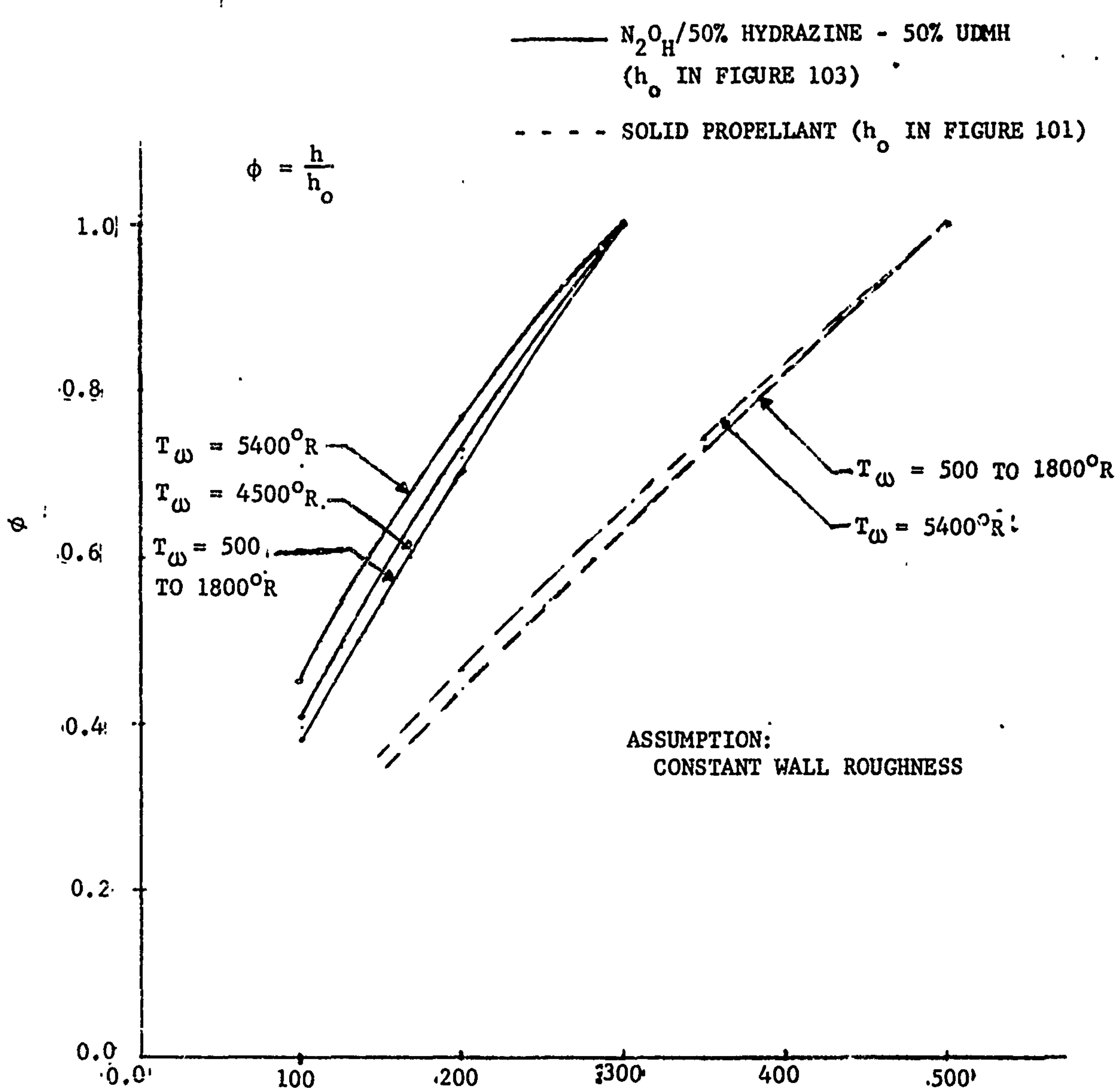

FIGURE 104. NO BLOWING CONVECTIVE HEAT TRANSFER COEFFICIENT DEPENDENCE ON CHAMBER PRESSURE

REFERENCES

1. Mayo, C. S., Ostrow, S. L., and Marcus, R. E., "Ablative Plastic Characterization in Simulated Motor Exhaust," Technical Report AFML-TR-65-245, Part I., Aeronutronic, Newport Beach, Calif., July 1965.

2. Bartz, D. R., "A Simple Equation for Rapid Estimation of Rocket Nozzle Convective Heat Transfer Coefficient," Jet Propulsion, January 1957.

3. Mitchell, R. L., et al., "An Investigation and Development of Film Protected-Convectively Cooled Nozzles," Second Quarterly Report, RPL-TDR-64-R4, Aeronutronic, Newport Beach, Calif., August 1964.

4. Armour, W. H., et al, "An Investigation of Feasibility Demonstration of Nozzles for Restartable Solid Rocket Motors, Second Quarterly Report, AFRPL-TDR-64-168, Philco Research Laboratory, Newport Beach, Calif., December 1964 (C).

5. Smallwood, W. L., et al, "Beryllium Erosion Corrosion Investigation for Solid Propellant Nozzles," First Quarterly Report AFRPL-TR-65-205, Aeronutronic, Newport Beach, Calif., November 1965 (C).

6. Eckert, E. R. G., and Drake, R. M., <u>Heat and Mass Transfer</u>, McGraw-Hill Book Co., New York, 1959.

7. Price, F. C., et al, "Internal Environment of Solid Rocket Nozzles," Final Report, Aeronutronic Report No. U-2709, July 1964.

8. Elliott, D. G., Bartz, D. R., and Silver, S., "Calculation of Turbulent Boundary Layer Growth and Heat Transfer in Axi-Symmetric Nozzles," TR No. 32-387, Jet Propulsion Laboratory, February 196 .

9. Moody, H. L., Blaes, H. M., and Saul, A. M., "The Behavior of Coated Refractory Metals in an N_2O_4/50-50 UDMH Thrust Chamber," Aeronutronic Engineering Note, January 1966.

10. Marxman, G. A., "Combustion in the Turbulent Boundary Layer on a Vaporizing Surface," Tenth Symposium on Combustion, pp 1337, The Combustion Institute, 1965.

UNCLASSIFIED

Security Classification

DOCUMENT CONTROL DATA - R&D

(Security classification of title, body of abstract and indexing annotation must be entered when the overall report is classified)

1. ORIGINATING ACTIVITY (Corporate author) Philco Corporation Aeronutronic Division Newport Beach, California 92663	2a. REPORT SECURITY CLASSIFICATION UNCLASSIFIED 2b. GROUP N/A

3. REPORT TITLE

Ablative Plastic Characterization in Simulated Motor Exhuast

4. DESCRIPTIVE NOTES (Type of report and inclusive dates)

Summary Report, 1 July 1965 to 1 September 1966

5. AUTHOR(S) (Last name, first name, initial)

Blaes, H. Shaw, J.
Mayo, C. S.
Ostrow, S. L.

6. REPORT DATE	7a. TOTAL NO. OF PAGES	7b. NO. OF REFS
October 1966	160	10

8a. CONTRACT OR GRANT NO. AF 33(615)-1632 b. PROJECT NO. 7340 c. Task No. 734001 d.	9a. ORIGINATOR'S REPORT NUMBER(S) AFML TR 65-245, Part II 9b. OTHER REPORT NO(S) (Any other numbers that may be assigned this report)

10. AVAILABILITY/LIMITATION NOTICES Each transmittal of this document outside the agencies of the U. S. Government must have prior approval of the Plastics and Composites Branch, MANC, Nonmetallic Materials Division, Air Force Materials Laboratory, Wright-Patterson AFB, Ohio 45433.

11. SUPPLEMENTARY NOTES	12. SPONSORING MILITARY ACTIVITY Air Force Materials Laboratory (MANC) Wright-Patterson AFB, Ohio

13 ABSTRACT New chemical compositions and physical constructions of ablative materials were exposed in a small scale, high temperature Aeronutronic solid propellant rocket motor simulator and a liquid propellant (nitrogen tetroxide - 50 percent hydrazine and 50 percent unsymmetrical dimethylhydrazine) combustion gas environment to determine the potential usefulness of these materials for hyperenvironmental conditions associated with current and future solid and liquid propellant motors.

Material erosion and thermal insulation characteristics of the research nozzles were evaluated by comparisons of chamber pressure versus time data, erosion and resin degradation rates, and visual photographic data.

This document is the second yearly summary technical report covering test series four and five, which included forty-nine (49) research nozzle specimens. Thirty (30) research nozzle specimens, comprising test series 4, were exposed to the exhaust environment of a simulated solid propellant having a flame temperature of 5800°F and being highly aluminized. Nineteen (19) nozzles, comprising test series 5, were exposed to the exhaust environment of a storable liquid propellant rocket motor that utilizes nitrogen tetroxide and the 50-50 hydrazine mixture.

Test results and specimen evaluations from test series 4 indicated that the Aeronutronic solid propellant simulator exhaust environment provided the specified exhaust environment with the required repeatable test screening characteristics to enable valid material evaluations.

Test results from test series 5 indicated that the specified nominal test conditions were met and enabled valid material evaluation.

DD FORM 1 JAN 64 1473

UNCLASSIFIED

Security Classification

UNCLASSIFIED
Security Classification

14. KEY WORDS	LINK A		LINK B		LINK C	
	ROLE	WT	ROLE	WT	ROLE	WT
Plastics Ablation Nozzle Materials Solid Propellant Motors Liquid Propellant Engines						

INSTRUCTIONS

1. ORIGINATING ACTIVITY: Enter the name and address of the contractor, subcontractor, grantee, Department of Defense activity or other organization *(corporate author)* issuing the report.

2a. REPORT SECURITY CLASSIFICATION: Enter the overall security classification of the report. Indicate whether "Restricted Data" is included. Marking is to be in accordance with appropriate security regulations.

2b. GROUP: Automatic downgrading is specified in DoD Directive 5200.10 and Armed Forces Industrial Manual. Enter the group number. Also, when applicable, show that optional markings have been used for Group 3 and Group 4 as authorized.

3. REPORT TITLE: Enter the complete report title in all capital letters. Titles in all cases should be unclassified. If a meaningful title cannot be selected without classification, show title classification in all capitals in parenthesis immediately following the title.

4. DESCRIPTIVE NOTES: If appropriate, enter the type of report, e.g., interim, progress, summary, annual, or final. Give the inclusive dates when a specific reporting period is covered.

5. AUTHOR(S): Enter the name(s) of author(s) as shown on or in the report. Enter last name, first name, middle initial. If military, show rank and branch of service. The name of the principal author is an absolute minimum requirement.

6. REPORT DATE: Enter the date of the report as day, month, year; or month, year. If more than one date appears on the report, use date of publication.

7a. TOTAL NUMBER OF PAGES: The total page count should follow normal pagination procedures, i.e., enter the number of pages containing information.

7b. NUMBER OF REFERENCES: Enter the total number of references cited in the report.

8a. CONTRACT OR GRANT NUMBER: If appropriate, enter the applicable number of the contract or grant under which the report was written.

8b, 8c, & 8d. PROJECT NUMBER: Enter the appropriate military department identification, such as project number, subproject number, system numbers, task number, etc.

9a. ORIGINATOR'S REPORT NUMBER(S): Enter the official report number by which the document will be identified and controlled by the originating activity. This number must be unique to this report.

9b. OTHER REPORT NUMBER(S): If the report has been assigned any other report numbers *(either by the originator or by the sponsor)*, also enter this number(s).

10. AVAILABILITY/LIMITATION NOTICES: Enter any limitations on further dissemination of the report, other than those imposed by security classification, using standard statements such as:

(1) "Qualified requesters may obtain copies of this report from DDC."

(2) "Foreign announcement and dissemination of this report by DDC is not authorized."

(3) "U. S. Government agencies may obtain copies of this report directly from DDC. Other qualified DDC users shall request through ________."

(4) "U. S. military agencies may obtain copies of this report directly from DDC. Other qualified users shall request through ________."

(5) "All distribution of this report is controlled. Qualified DDC users shall request through ________."

If the report has been furnished to the Office of Technical Services, Department of Commerce, for sale to the public, indicate this fact and enter the price, if known.

11. SUPPLEMENTARY NOTES. Use for additional explanatory notes.

12. SPONSORING MILITARY ACTIVITY: Enter the name of the departmental project office or laboratory sponsoring *(paying for)* the research and development. Include address.

13. ABSTRACT: Enter an abstract giving a brief and factual summary of the document indicative of the report, even though it may also appear elsewhere in the body of the technical report. If additional space is required, a continuation sheet shall be attached.

It is highly desirable that the abstract of classified reports be unclassified. Each paragraph of the abstract shall end with an indication of the military security classification of the information in the paragraph, represented as *(TS)*, *(S)*, *(C)* or *(U)*.

There is no limitation on the length of the abstract. However, the suggested length is from 150 to 225 words.

14. KEY WORDS: Key words are technically meaningful terms or short phrases that characterize a report and may be used as index entries for cataloging the report. Key words must be selected so that no security classification is required. Identifiers, such as equipment model designation, trade name, military project code name, geographic location, may be used as key words but will be followed by an indication of technical context. The assignment of links, rules, and weights is optional.

GPO 886-551

UNCLASSIFIED
Security Classification